TAMPEREEN TEKNILLINEN YLIOPISTO
TAMPERE UNIVERSITY OF TECHNOLOGY

Anssi Laukkanen

Microstructure Based Structure-Property Relationships for the Design of Thin Films and Composite Coatings by Multiscale Materials Modeling

Julkaisu 1597 • Publication 1597

Tampere 2018

Tampereen teknillinen yliopisto. Julkaisu 1597
Tampere University of Technology. Publication 1597

Anssi Laukkanen

Microstructure Based Structure-Property Relationships for the Design of Thin Films and Composite Coatings by Multiscale Materials Modeling

Thesis for the degree of Doctor of Science in Technology to be presented with due permission for public examination and criticism in Konetalo Building, Auditorium K1702, at Tampere University of Technology, on the 23rd of November 2018, at 12 noon.

Tampereen teknillinen yliopisto - Tampere University of Technology
Tampere 2018

Doctoral candidate: Anssi Laukkanen
Laboratory of Materials Science
Faculty of Engineering Sciences
Tampere University of Technology
Finland

Supervisor: Veli-Tapani Kuokkala, Professor
Laboratory of Materials Science
Faculty of Engineering Sciences
Tampere University of Technology
Finland

Pre-examiners: Zhiliang Zhang, Professor
Dept. of Structural Engineering
Norwegian University of Science and Technology
Norway

Lars-Erik Lindgren, Professor
Division of Solid and Material Mechanics
Luleå University of Technology
Sweden

Opponents: Renno Veinthal, Professor
Tallinn University of Technology
Estonia

Giovanni Bolelli, PhD
University of Modena and Reggio Emilia
Italy

ISBN 978-952-15-4257-2 (printed)
ISBN 978-952-15-4295-4 (PDF)
ISSN 1459-2045

Abstract

Integrated Computational Materials Engineering (ICME) is the next generation methodology for the discovery, development, and deployment of material solutions. ICME refers to tackling materials science and engineering problems by way of merging materials modeling exploiting High-Performance Computing (HPC), experimental and characterization activities, as well as data and its analytics in the solution process and utilizing this toolset to deliver better performing innovative material solutions faster. A crucial element in ICME is the application paradigms of multiscale materials modeling, such as the widely adopted Process-Structure-Properties-Performance (PSPP) approach. The PSPP construct itself is a common frame for experimentalists and modelers alike to convey materials problems from discovery to deployment in terms of the typical progression of how to develop a new material or material solution. To realize PSPP in practice for modeling, workflows are required. These workflows consist of interacting multiscale materials modeling objects, which are interfaced to support the solution of an ICME problem. Commonly, such workflows consist of multiscale models of material manufacturing (processing), digital representation of the following material structure, modeling the properties of the structure in question (for example engineering material properties), and evaluating the performance of the material solution that links the material to its application environment. The PSPP chain as such establishes causal relations from material processing all the way to its application performance. Since optimization-wise this is an imperfect construct, Material Informatics (MI) deals with managing and analyzing the data, ultimately targeting the solution of the coveted inverse problem, where a material is discovered and designed based on its performance requirements and optimized for example with respect to the affiliated costs. The goal is to deploy a material that satisfies the functionality requirements set for the product performance.

Applications of ICME began from the need for extreme performance, for example involving material solutions for aerospace applications. Another high end application involves surfaces and coatings for wear resistance and lubrication, engaging material challenges for example in transportation or highly abrasive environments such as mining applications. This is also the domain of the current work, i.e., how to systematically develop better wear resistant surfaces and coatings. The specific challenge is the development, implementation and validation of ICME workflows for microstructure founded design of coatings and thin films for improved wear resistance. Within this scope, the current work develops a multiscale framework for modeling the microstructure and surface topography of complex multiphase coating microstructures and thin films, employing means to model realistic material microstructural morphologies containing also a composite interface character. The behavior of thin solid coatings under sliding abrasive loading is studied, and the possibilities of utilizing Cohesive Zone Modeling (CZM) directly in the modeling of film rupture are established. Next, the focus turns toward the introduction of the

microstructural modeling of either thin or composite coating solutions, for which the computational methodologies are developed, implemented and validated. The analyzed cases consider primarily cemented carbide microstructures under abrasive tribological loading conditions. The computational methodology is developed further to increase realism with respect to modeling material interfaces, where Finite Element (FE) based models are interfaced to a Phase Field (PF) based modeling of rapid solidification microstructures as a result of material processing. After establishing a realistic enough description of the composite microstructure, the focus turns to introducing a modeling solution capable of addressing surface roughness and topography, in relation to other coating characteristics. This introduces a methodology enabling modeling of both the coating topography, its microstructure, interfaces with the bulk substrate, and the microstructure of the substrate itself. ICME workflows are discussed, outlined, and set up for the design of wear resistant surfaces utilizing the PSPP principle as a basis, considering especially the microstructure to product linkage in a bottom-up manner. The various use cases support the notion that ICME already provides added value to the solution of tribological problems and material related challenges by adding knowledge for solving problems otherwise difficult and costly to handle. Furthermore, the greatest impact and improved quality of results are obtained when both experimental and modeling approaches are used concurrently and not viewed as alternatives or competitors.

Preface

This study was carried out over gloriously numerous years in various projects at the VTT Technical Research Centre of Finland Ltd. The work would not have been possible without numerous national and international collaborations the author has had the priviledge of being exposed to over the years. First and foremost, the contributions of the researchers of VTT's materials modeling research group in its various incarnations, the "properTune" associated researchers across the board, and the numerous collaborators across VTT are appreciated and acknowledged. The "tug-of-wars" with Profs. Kenneth Holmberg, Kim Wallin and Veli-Tapani Kuokkala have been both extremely enjoyable and beneficial, let alone "fun" in the fullest meaning of the word. Much of the work was made possible by the DIMECC BSA and HYBRIDS programs, the financial support of the Finnish Funding Agency for Innovation (TEKES), the participating companies, and the VTT Technical Research Centre of Finland Ltd are acknowledged.

Support of family and friends has been superb over the years, Siiri and Sanna are acknowledged as the greatests co-authors this thesis work could possibly have had.

Espoo, June, 2018

Anssi Laukkanen

Contents

Abbreviations

AI	Artificial Intelligence
ALE	Augmented Lagrangian-Eulerian
BEM	Boundary Element Method
CG	Coarse Graining
CP	Crystal Plasticity
CSA	Concurrent Simulation Assisted
CZM	Cohesive Zone Modeling
DLC	Diamond-Like Carbon
FCC	Face Centered Cubic
FE	Finite Element
FIB	Focused Ion Beam
GND	Geometrically Necessary Dislocations
ICME	Integrated Computational Materials Engineering
HCF	High Cycle Fatigue
HPC	High-Performance Computing
HTC	High-Throughput Computing
MCA	Movable Cellular Automata
MD	Molecular Dynamics
MFP	Mean Free Path
MI	Material Informatics
ML	Machine Learning
PD	Peridynamics
PF	Phase Field
PSPP	Process-Structure-Properties-Performance

RVE	Representative Volume Element
SEM	Scanning Electron Microscope/Microscopy
SIF	Stress Intensity Factor
SPP	Structure-Properties-Performance
SVE	Statistical Volume Element
TS	Thermal Spray
TSL	Traction Separation Law
XFEM	Extended Finite Element Method

Nomenclature

Latin alphabet

a	crack length
E	elastic modulus
E'	stress state dependent elastic modulus
d	damage scalar
$\mathbf{f}$	body force vector
G_f	effective fracture energy
h	weight function
K	stress intensity factor
$\mathbf{t}$	traction vector
$\mathbf{u}$	displacement vector

Greek alphabet

α	damage rate parameter
δ	effective mixed-mode displacement
Ω	solution domain

List of Publications

This thesis is based on the work presented in the following five publications and included as Appendices I-V. References to related work by the author(s) but not included in the listed publications, as well as to some unpublished work, will also be made.

I Laukkanen, A., Holmberg, K., Ronkainen, H., and Wallin, K., "Cohesive Zone Modeling of Initiation and Propagation of Multiple Cracks in Hard Thin Surface Coatings," *Journal of ASTM International*, vol. 8, no. 1, pp. 1−21, 2011.

II Holmberg, K., Laukkanen, A., Ghabchi, A., Rombouts, M., Turunen, E., Waudby, R., Suhonen, T., Valtonen, K. and Sarlin, E., "Computational Modeling Based Wear Resistance Analysis of Thick Composite Coatings," *Tribology International*, vol. 72, pp. 13-30, 2014.

III Holmberg, K., Laukkanen, A., Turunen, E. and Laitinen, T., "Wear Resistance Optimisation of Composite Coatings by Computational Microstructural Modelling," *Surface and Coatings Technology*, vol. 247, pp. 1-13, 2014.

IV Laukkanen, A., Pinomaa, T., Holmberg, K. and Andersson, T., "Effective Interface Model for Design and Tailoring of WC-Co Microstructures," *Journal of Powder Metallurgy*, vol. 59, pp. 20-30, 2016.

V Laukkanen, A., Holmberg, K., Ronkainen, H., Stachowiak, G., Podsiadlo, P., Wolski, M., Gee, M., Gachot, C. and Li, L., "Topographical Orientation Effects on Surface Stresses Influencing on Wear in Sliding DLC Contacts, Part 2: Modeling and Simulations," *Wear*, vol. 388-389, pp. 18-28, 2017.

Author's Contribution

In Publication I, Anssi Laukkanen was the main researcher and author. He carried out the development and modeling work as well as the analysis of the results. Experimental reference data for validation was obtained from earlier published works of the research group.

In Publications II and III, Anssi Laukkanen was a co-author, with Kenneth Holmberg being the main author. Anssi Laukkanen carried out all the modeling, development, and analysis work associated with the microstructural modeling toolset. He was the main contributor to the respective sections of the manuscript.

In Publication IV, Anssi Laukkanen was the main researcher and author. He carried out the development and modeling work as well as the analysis of the results except for the phase field modeling, which was performed by Tatu Pinomaa. The phase field to finite elements interface was developed and implemented by Anssi Laukkanen.

In Publication V, Anssi Laukkanen was the main researcher and author. He carried out the development and modeling work and performed the analysis of the results together with Kenneth Holmberg. Experimental reference data for the validation was obtained from the previous publications of the research group.

All the authors provided invaluable comments and contributed to the completion of the respective publications.

1 Introduction

Materials science has always been at the forefront of exploiting modeling, and the surge in the numerical capabilities and HPC has resulted in a widespread adoption of computation and is pushing for the digitalization of the whole field. ICME is the next generation methodology for the discovery, development, and deployment of material solutions. Many if not most of the methodologies brought forth by ICME are not new themselves. Rather, the novelty is the introduction of numerical computation, data, and analytics to the solving of materials problems in parallel with the experimental work and empirical trials as a methodology of problem solving. The problems can range from the most difficult problem of material discovery to optimization and materials selection, or simply to better grasping of material affiliated problems and challenges in ever more demanding operational environments. The benefits are immediate, for example TMS (2013), TMS (2015) and MGI (2011), realize that the cycle of bringing new materials to the market can be shortened by at least a factor of two, and the same can be said for the affiliated R&D costs. ICME brings forth numerous new additions to the materials science or engineering toolset, such as the possibility to run virtual tests on materials, decipher causal relations systematically and in a controlled manner, and expand the design space far beyond the few prototypes or material test batches which can be actually manufactured physically. Of course, in order to walk the walk, ICME needs to be able to deliver impact to practical industry problems. At present, we are on the verge of the wider adoption of ICME, and it can be stated that computational materials research is here to stay. ICME is now gaining more traction from novel manufacturing technologies, Machine Learning (ML) techniques, and ultimately from the adoption of Artificial Intelligence (AI) in materials research and engineering (see TMS (2017)).

ICME refers to tackling materials science and engineering problems, such as the development and optimization of novel materials and solutions, by way of merging HPC, experimental work, characterization, data and analytics in the solution process and utilizing this toolset to establish better performing innovative material solutions faster. A crucial element in ICME is the application paradigms of multiscale materials modeling, such as the widely adopted PSPP approach. The identification of the PSPP concept and the widespread adoption of multiscale modeling was made in the landmark paper by Olsson (1997). The PSPP construct itself is a common framework for experimentalists and modelers alike to convey materials problems from discovery to deployment in terms of the typical progression of the development of a new material or material solution. To realize PSPP in practice for modeling, workflows and versatile toolsets are a necessity. These workflows consist of interacting multiscale materials modeling objects, which are interfaced to support the solution of an ICME problem. Commonly, such workflows consist of multiscale models of material manufacturing (processing), digital representation of the following structures, modeling of the properties of the structures in question

(for example engineering material properties), and evaluation of the performance of the material solution, which links the material to its application environment. An example of such a workflow on a general level for tribological problems is presented in Figure 1.1 together with traditional workflows approaching the problem solely by way of modeling or experimentation. The objective of ICME can be understood as an attempt to extract the best features from both experimental and modeling approaches so as to come up with an approach where both principally differing approaches are exploited with respect to their best characteristics. Experiments can be argued to suffer from the notion that defining and assessing relevant testing conditions with respect to the end product is troublesome, and full scale or prototype testing is slow and costly. Modifications to the solution are similarly difficult, since the interpretation of the test results is far from trivial and the number of iterations is very limited. Modeling again has its greatest hurdle in establishing whether the model captures the right physics, and how to proceed with its validation. Characterization requirements for multiscale material models can be extremely challenging and in many cases not even possible to meet directly. However, systematic understanding of the causal relations and running numerical trials on "what-if" scenarios is far cheaper than solving the problem experimentally. What the ICME proposes to do is to take the best from both worlds. The analysis of simpler laboratory scale tests is deepened by modeling the relevant physics, and multiscale models are exploited to bridge the findings to the product scale, limiting the number of prototypes and focusing the experiments on where their impact from a solution point of view is greatest. Similarly, virtual trials are introduced to investigate the influence of material design changes to the final product. The ICME approaches by convention adopted in the current work also aim to deepen the "physics-based" character of numerical modeling, in the current work primarily by explicitly incorporating material microstructure and micromechanical behavior.

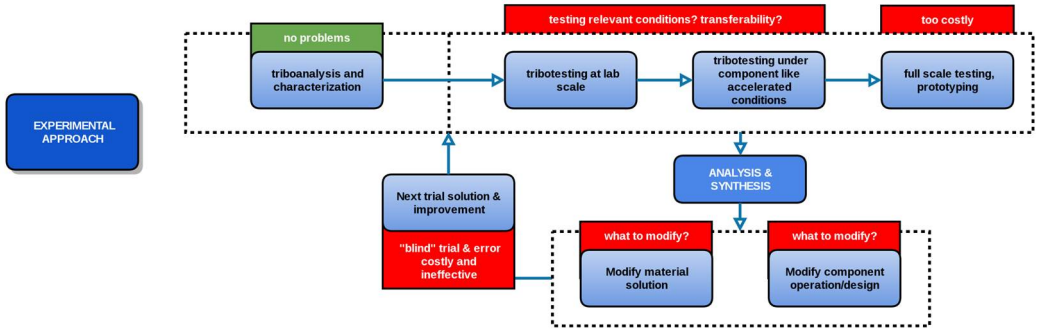

(a) Experiments driven approach

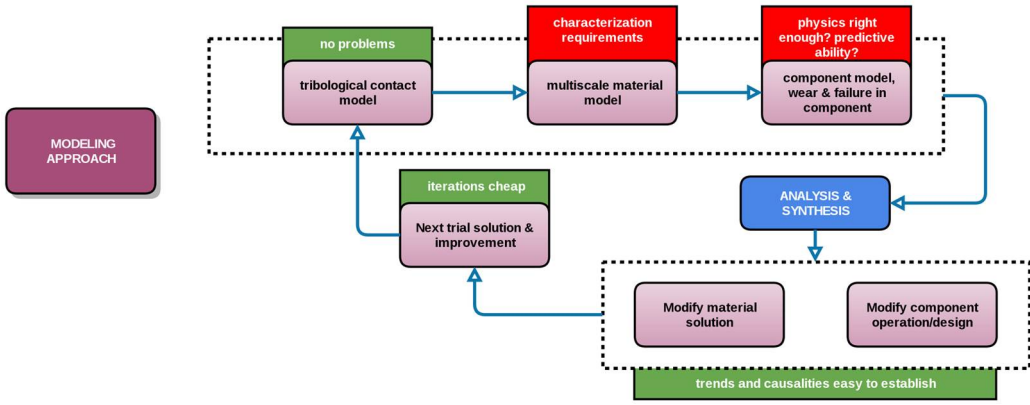

(b) Modeling driven approach

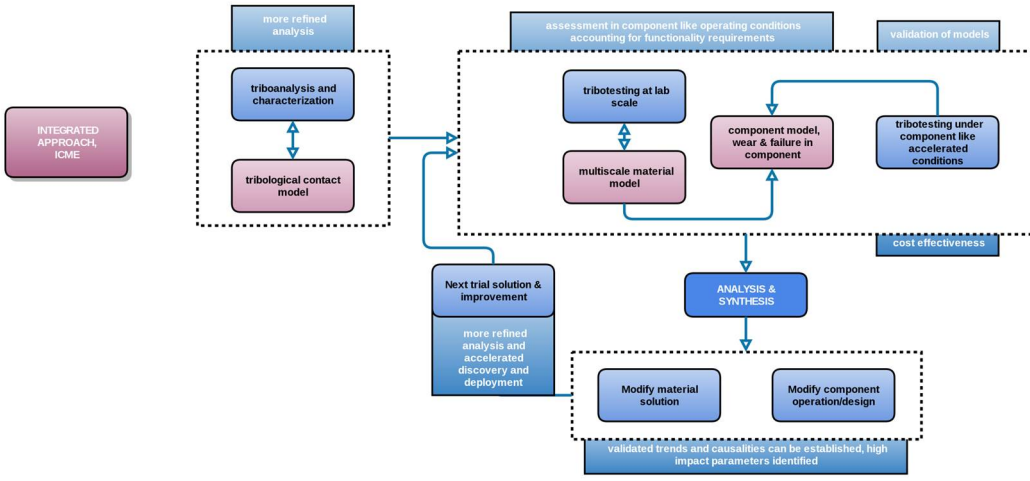

(c) ICME driven approach

Figure 1.1: Workflows for developing material solutions for tribological problems (Laukkanen (2016)).

In order for the ICME approach to be feasible and implementable in practical problem solving with a deadline, the toolsets need to be versatile and extensible. A practical challenge from the times before ICME when multiscale materials modeling was considered a complete solution by itself was that the development of a single modeling solution, bridging for example two spatial scales by way of considering only information transfer or homogenization, could take several years to develop, verify and validate to a limited extent. Thus, a prerequisite for ICME is the development of a modeling toolset, the step that typically can be acknowledged to be laborious and quite application domain specific. An example is presented in Figure 1.2. The toolset picked as an example already has elements of atomistic, microstructural and macroscale modeling, and as such the range of its applicability is vast. However, so is its degree of complexity and the identification of its capabilities and application ranges, let alone the not so-well known characteristics such as the propagation of errors in the modeling chain, making the application both complex and requiring extreme effort in its utilization and validation in practical problems. Upon establishing the usability of a certain subset of characteristics, the benefits and impact of ICME for that specific domain are within reach.

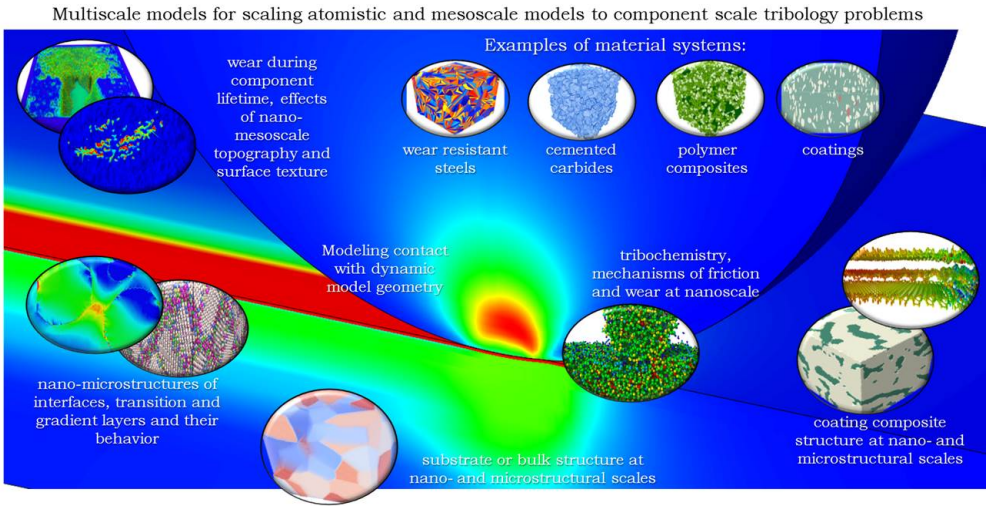

Figure 1.2: Multiscale materials modeling toolset for tribological problems (Laukkanen et al. (2017a)).

Multiscale materials modeling can be argued for many researches and practical problems to be divided into two often distinct regions. The most complex problem is bridging the atomistic information to the scale of the material nano-microstructure[1]. As a result, many so-called multiscale works focus on the atomistic end or then on the microstructural scales. In the former the typical model spatial sizes are in the range of tens of nm, while in the latter hundreds of μm are good indicating values. The emphasis of the current work is on the latter, and the focus is in developing modeling solutions where upscaling to the product scale and, for example, engineering bulk material properties can be envisioned and in many cases performed. As such, this field of multiscale modeling and application of ICME deals with microstructures and their behavior, especially in solid mechanical terms, typically referred to as micromechanics. A typical example of such a model is presented in

[1] or from discrete to continuous description

Figure 1.3, where a WC-Co cemented carbide microstructure is investigated with respect to its stress-strain response under compressive loading. The study of microstructures, their failure behavior, and the influence of both microstructural morphological parameters (for example size and shape distributions) as well as the general material behavior (for example the size dependencies and the evolution of damage) are of primary interest for micromechanical modeling.

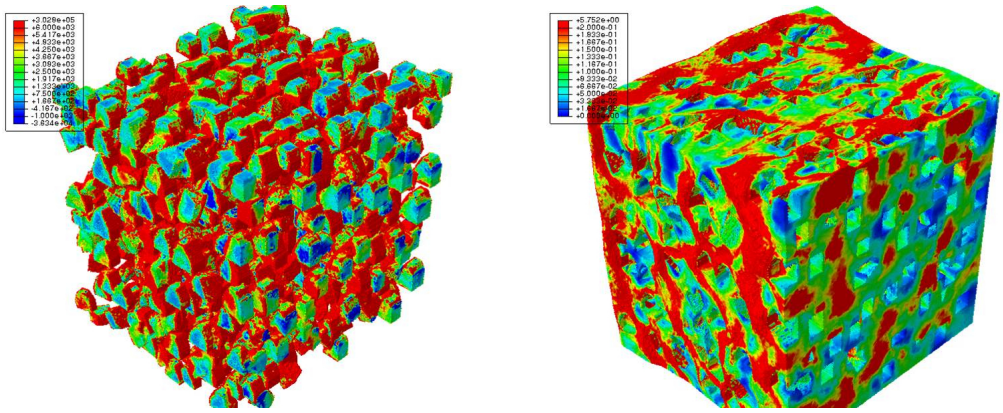

(a) First principal stress in the WC crystals **(b)** Equivalent plastic strain in the Co binder

Figure 1.3: Microstructural model of a WC-Co cemented carbide microstructure loaded in compression (Laukkanen et al. (2016a)).

The core objective of the current work is to contribute toward the development of ICME workflows for solving tribological problems involving the design and tailoring of respective material solutions. The focus is on the study of coated systems, either thin hard films or composite coatings, and the influence of various characteristics at the scale of the coating and the material microstructure with respect to resistance to wear. As such, the objective is to introduce methodologies to create models of microstructures and surface roughness to build models where the influence of these features and material behaviors can be studied. Since composites are typically hierarchical systems with various multiscale details, many of which are simplified during upscaling of both microstructure and behavior, going beyond ideal interface models is investigated. Significance with respect to failure and wear processes, i.e., steps toward microstructure scale modeling of damage is a necessary follow up in the quantification of the modeling results. The other objectives are to study the interaction of surface roughness with the other characteristics of coated systems directly, to investigate the possibilities of explicitly including surface topography and modeling its influence on the tribological contacts, and going beyond the effective surface roughness modeling. A crucial objective is also to take steps in the validation of computational models in order to qualify the methodologies and to establish future research needs and directions.

The thesis first establishes the Aims of the Research in Chapter 2. After that, the approaches adopted for modeling are presented in Chapter 3. This is followed by a presentation of the primary findings in Chapter 4. Chapters 5 and 6 discuss and summarize the thesis work. In Publication I, the behavior of thin solid coatings under sliding abrasive loading is studied and the capabilities of utilizing CZM directly in the modeling of film rupture are established. After that the focus turns toward the introduction of the

microstructural modeling capability to either thin or composite coating solutions, and the computational methodologies are developed, implemented and validated in Publications II and III. The analysis cases consider primarily cemented carbide microstructures under abrasive tribological loading conditions. The computational methodology is developed further to increase realism with respect to modeling material interfaces in Publication IV, where the FE based models are interfaced to a PF based modeling of rapid solidification microstructures as a result of material processing. After establishing a realistic enough description of a composite microstructure, the focus turns to introducing a modeling solution capable of addressing surface roughness and topography in relation to other coating characteristics. This is the subject area of Publication V, which introduces a methodology enabling the modeling of coating topography, its microstructure, interfaces to the bulk substrate, and the microstructure of the substrate itself. ICME workflows are discussed, outlined, and set up for the design of wear resistant surfaces utilizing the PSPP principle as a basis, considering especially the microstructure-to-product hierarchy in a bottom-up manner.

2 Aims of the Research

The aim of this work was to develop, apply, and initiate the validation of a microstructural and micromechanical modeling solution for thin films and composite coatings to support establishing ICME workflows for the design and optimization of wear resistant material solutions. The following research questions were stated:

1. Can the previously utilized fracture mechanical analysis means be extended by utilizing CZM and damage mechanical modeling to better model the wear resistance of coated surfaces?
2. Is microstructural and micromechanical multiscale modeling using FE applicable for solving the Structure-Properties-Performance (SPP) and PSPP tribological problems, and can it form a baseline for the design of better wear resistant surfaces and composite microstructures?
3. Is it possible to introduce interface modeling techniques to micromechanics, which could contribute to the further improvement of a physics-based modeling workflow?
4. Can explicit modeling of surface roughness and topography provide insights regarding its significance in comparison into the other coating design parameters (structure, defects, film thickness, substrate, etc.)?

These questions were addressed during the course of the work by way of developing computation modeling means and by applying them in the study of respective materials and behaviors. The thesis work focuses on the modeling side, although in practice the work was carried out in projects where experimental and characterization tasks were constantly carried out parallel with the modeling activities. Thus, the work also focuses heavily on applying modeling to problem solving instead of solely developing and implementing the computational means. In order to investigate means to model thin coating damage and failure, a study was carried out (Publication I) where CZM methods were utilized to investigate coating cracking under sliding abrasion and the possibilities of utilizing the derived damage metrics in the design of coatings. To carry out microstructural and micromechanical modeling, a toolset was developed and applied primarily for scratch test contacts with sliding abrasion (Publications II and III). The typical simplifications related to interface modeling were addressed by introducing an interface to PF based modeling of rapid solidification microstructures, and the findings were utilized to define more complex descriptions of cemented carbide composite interfaces and to assess the significance of this modeling approach (Publication IV). Finally, the influence of surface roughness was incorporated in the models by parametrically studying (based on characterization data) the impact of explicitly modeling surface roughness effects on the stress-strain response

of a Diamond-Like Carbon (DLC) coating during smooth-on-rough and rough-on-rough contacts (Publication V).

The scientific contributions of the thesis are as follows:

- The work produced a methodology for modeling thin film cohesive and adhesive failure utilizing the CZM methodology. The resulting methodology was utilized for studying and improving the thin film structures using design trials of multilayered and gradient coatings structures tailored to specific tribological contact conditions.
- The developed microstructural and micromechanical modeling approach and toolset for composites were applied to Thermal Spray (TS) WC-Co coatings, and a detailed evaluation of the microstructural characteristics critical for the avoidance of wear damage was performed. The findings act as a baseline and demonstration of how to develop new coating solutions for specific operational environments.
- The modeling solution enabling more detailed microstructure scale investigations of the coating hard phase-to-binder interface yielded a novel numerical methodology linking the thermodynamics based material processing models to microstructural property models.
- The effects of surface roughness as a design parameter of DLC coatings were quantified by the developed modeling approach, and its significance to the wear resistance of DLC coatings was demonstrated during model validation where correlation between the modeling and experiments was displayed.
- The methodologies and their implementations were found to be applicable as elements of ICME workflows describing the role of material micro- and mesostructures in the tribological performance of a particular material solution.

3 Materials Modeling

The objective of the current work is to enable the detailed modeling of wear resistant coated surfaces at the scale of their respective microstructures. Thus, different phases, their morphologies, anisotropies, defects, and surface characteristics such as roughness, as well as the ultimate evolution of these aspects due to material damage are the subject area of this study. These results contribute to producing materials design workflows forming the basis of ICME applications, as presented in Figure 3.1. These workflows are a core feature of the already classic PSPP approach and contribute to the solution of, for example, the structure-property problem, and as such are a critical element in pursuing computation driven material design methodologies. The current work addresses essentially the structure-to-performance stages by enabling the modeling of material properties based on the detailed representation of the microstructures, and further assessment of their performance under tribological loading conditions beyond simply evaluating the engineering material properties. In the current chapter, modeling of these structures is presented with respect to thin film structures, surface topography, and composite microstructures.

3.1 Modeling of thin films

The primary target of modeling thin films has commonly been to increase understanding of the conditions where a coating can fulfill its functional requirement of preventing the activation of a mechanism inducing wear. Approaches have often emphasized fracture mechanical approaches, such as in the classic works presented in Holmberg et al. (2003), where a fracture mechanical model was developed based on the crack density of a thin hard film and the input based on a numerical contact model. Similar approaches employing fracture mechanics have been utilized by several researchers for different coating systems, such as Li et al. (1997) for DLC coatings on hard material substrates, Nastani et al. (1999) for DLC coatings on a silicon substrate, and Diao et al. (1994) for TiN and Al_2O_3 coatings on hard material substrates. The latest developments in the fracture mechanical route can be stated to largely reside in a series of three papers: Holmberg et al. (2006a), Holmberg et al. (2006b), and Laukkanen et al. (2006). In these papers, the fracture mechanical methodology has been developed to include residual stresses as well as complex loadings and shapes and types of cracks in addition to considering the influence of material properties of the coating and the substrate.

3.1.1 Thin films (Publication I)

A common feature of the fracture mechanical route is the limitations of the underlying theory, i.e., the assumptions regarding the crack field type, size and shape that are

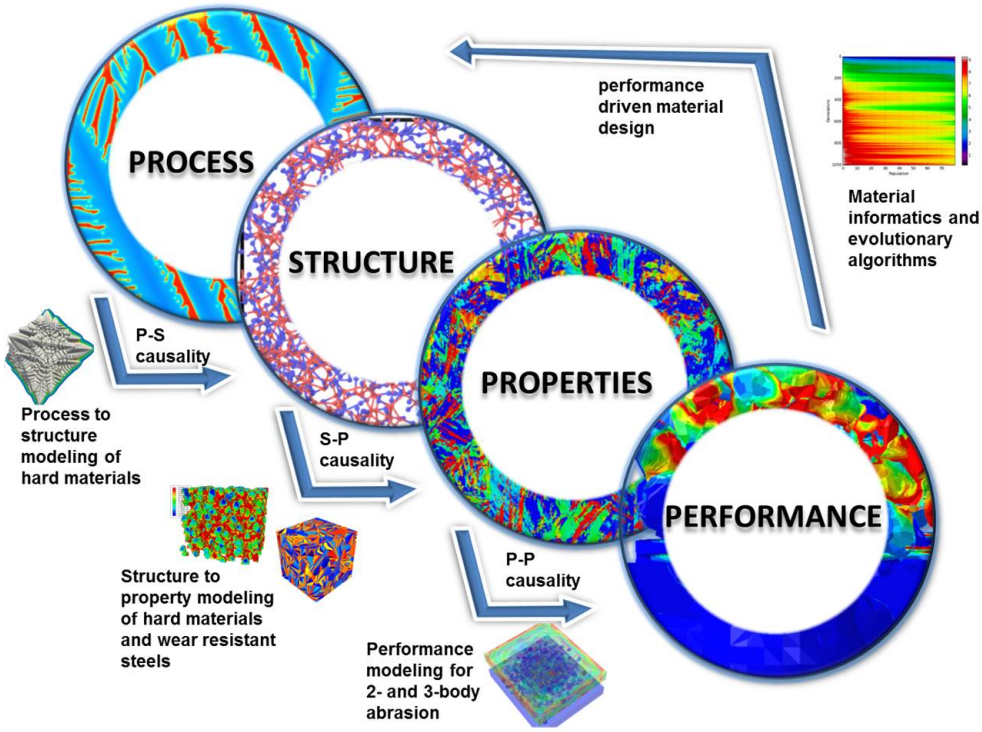

Figure 3.1: PSPP approach to ICME (Laukkanen et al. (2017a)).

required. Moreover, the treatment of multimaterial systems is somewhat limited in this kind of approach (see Laukkanen et al. (2006) for details). In Publication I, the previous work was revisited by exploiting the developments affiliated with CZM as well as the damage mechanical approaches to modeling failure initiation and propagation in coated systems, also taking advantage of the enhancements in the available HPC capabilities. The basis of CZM and its application in the microstructural scale still lies in the classic works of Dugdale (1960) and Barenblatt (1962). Consequently, the basis for the applicability of CZM to different types of cracking problems, including cohesive and adhesive crack problems, can be considered to exist. CZM is commonly applied over spatial scales although the underlying physics and basis for defining Traction Separation Law (TSL) behavior differ, and the atomistic scale arguments do not explicitly transform to larger scales. The present consensus, however, is that the principle is sound enough to be exploited. Similarly, mixed-mode loading conditions have been studied, for example by van den Bosch et al. (2006), which is a prerequisite for working with coated systems and having any possibility to track the relevant modes of failure.

The basic experimental problem setting is presented in Figure 3.2, i.e., a finite sliding and finite strain frictional contact with a plastically deforming substrate, utilizing an Augmented Lagrangian-Eulerian (ALE) formulation for better finite deformation performance. The cracking patterns as sketched in Figure 3.2 have been shown to be consistent (Holmberg et al. (2003), Holmberg et al. (2006a)) with experimental findings, as presented in Figure 3.3 for a TiN coating. The added feature of CZM is that it provides a more general modeling capability compared with the direct fracture mechanical approach, the

CZM tightly interacting with the solution of the contact problem and different material deformation behaviors.

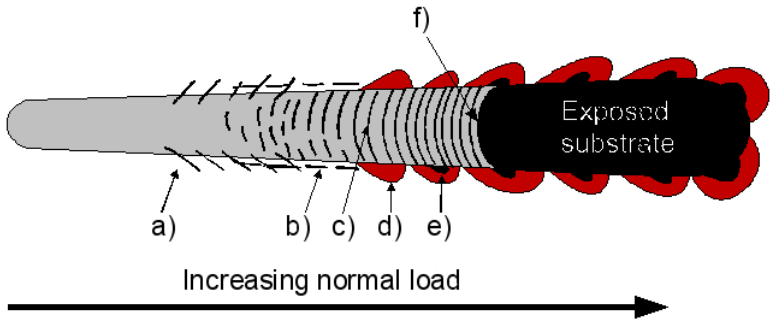

(a) Schematic representation of the studied cracking pattern for thin hard films in scratch testing: a) Angular cracks, b) parallel cracks, c) transverse (angled) cracks, d) coating chipping, e) coating spalling, and f) coating breakthrough.

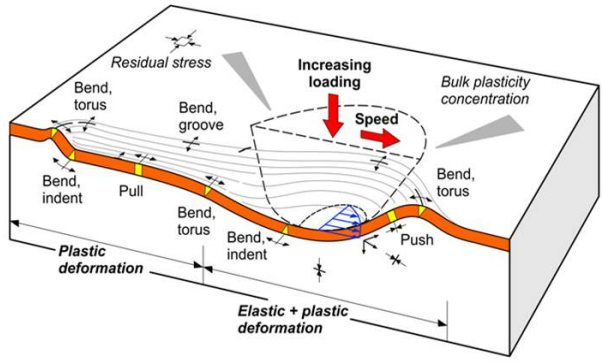

(b) Schematic representation of the different crack types and affiliated deformation mechanisms in a coated system.

Figure 3.2: Description of the mechanistic background in the cracking of thin hard films (Holmberg et al. (2006a)).

The input to a CZM is a TSL, and as such calibration of the failure model was carried out. The methodology developed by Laukkanen et al. (2006), which is based on a weight-function methodology having its basis on a Boundary Element Method (BEM) founded derivation of the actual weight functions, was applied. In the methodology, the Stress Intensity Factor (SIF) being computed is presented as

$$K^{(2)} = \frac{E'}{2K^{(1)}} \left[\int_{\Gamma} \mathbf{t}^{(2)} \frac{\partial \mathbf{u}^{(1)}}{\partial a} d\Gamma + \int_{\Omega} \mathbf{f}^{(2)} \frac{\partial \mathbf{u}^{(1)}}{\partial a} d\Omega \right], \tag{3.1}$$

where E' is the stress field dependent elastic modulus, (1) the weight function reference solution (and $K^{(1)}$ the respective SIF, generally under mixed mode conditions as in Laukkanen et al. (2006)), $\mathbf{u}$ the displacement vector, $\mathbf{t}$ the traction vector, $\mathbf{f}$ the body force vector, Ω the solution domain, $\Gamma = \partial\Omega$, and a the crack length parameter. The

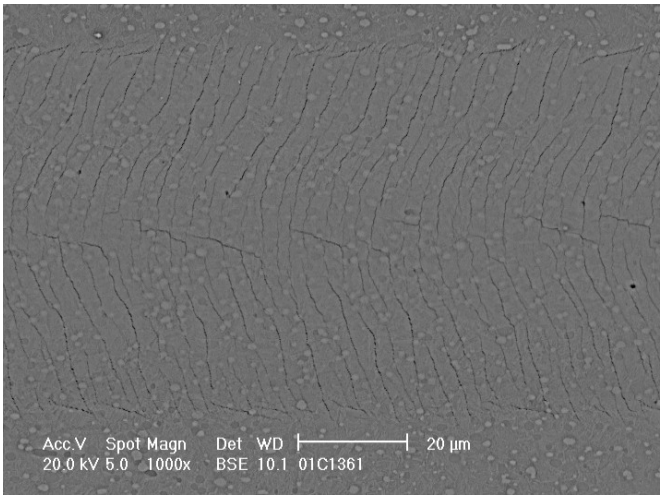

Figure 3.3: SEM image of crack patterns after scratch testing of a $2\mu m$ TiN coated surface, stylus movement from left to right (Holmberg et al. (2006a)).

weight function is given by

$$\mathbf{h} = \frac{E'}{2K^{(1)}} \frac{\partial \mathbf{u}^{(1)}}{\partial a} \tag{3.2}$$

which upon substitution to Equation 3.1 yields the weight function based expression for the evaluation of the SIF:

$$K^{(2)} = \int_{\Gamma} \mathbf{t}^{(2)} \mathbf{h} d\Gamma + \int_{\Omega} \mathbf{f}^{(2)} \mathbf{h} d\Omega. \tag{3.3}$$

Upon scratch testing and evaluation of the respective scratch test contacts by FE, the fracture toughnesses can be calculated for specific crack field types and for through coating cracks, which were utilized as a baseline for the fracture toughness in the current work (FE also introduces a substrate plasticity correction to the thin film stress state). The results are presented in Figure 3.4a. The FE modeling and the details are presented more thoroughly in Laukkanen et al. (2006) and Holmberg et al. (2009). The approach includes the effects of crack field orientation, crack density and crack location within the crack field, the loading conditions with respect to, for example, stress biaxiality and mode of loading. The calibration of the TSL was carried out based on the fracture toughness assessment, adapting an exponential TSL as a basis, where the damage is presented by

$$d = 1 - \frac{\delta_m^0}{\delta_m^{max}} \cdot \left(1 - \frac{1 - \exp\left(-\alpha \frac{\delta_m^{max} - \delta_m^0}{\delta_m^f - \delta_m^0} \right)}{1 - \exp\left(\alpha\right)} \right), \tag{3.4}$$

where α is the rate parameter for the damage evolution and $\delta_m^f - \delta_m^0$ is the difference between the effective mixed-mode displacement at failure and at the initiation of the damage. The chosen calibration approach is presented in detail in Laukkanen et al. (2011), but in short, it relies on considering the coating failure as brittle (fast evolution of damage through the coating or within a critical stress-strain field, selecting the extreme from Figure 3.4) and ensuring that the effective fracture energy is identical to the measured

fracture toughness, i.e.,

$$G_f = \int_{\delta_m^0}^{\delta_m^f} (1-d)t_i|^{d=0} d\delta. \tag{3.5}$$

Since no direct information regarding the adhesive failure or fracture toughness was available, other than the likely occurrence of adhesive failure once the through coating crack field propagates with greater density through the coating, identical TSL properties were utilized at the film-to-substrate interface as well.

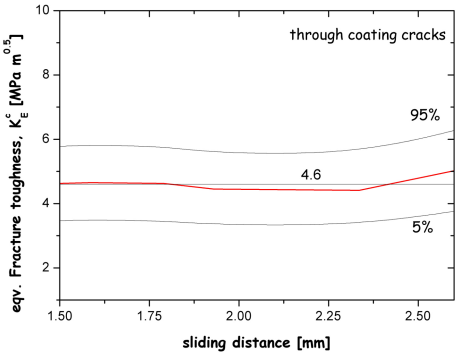

(a) Evaluation of through coating crack fracture toughnesses for a $2\mu m$ thick TiN coating from scratch tests.

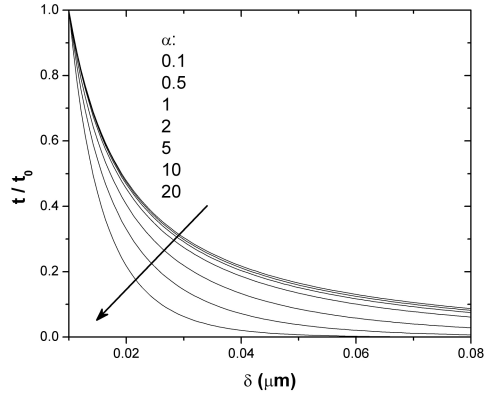

(b) CZM model and its TSL relationship with different parameters influencing the rate of decrease of cohesive traction.

Figure 3.4: Fracture toughness evaluation and its exploitation in establishing the TSL parameters for modeling the film fracture (Laukkanen et al. (2011)).

The FE approach did not rely on remeshing but rather retained the hexahedral mesh throughout the solution, and as a result the CZM was carried out by populating the element interfaces from the contacting region with cohesive zone elements. Examples of typical meshes and resolution of the stress fields are presented in Figure 3.5.

3.1.2 Surface topography (Publication V)

Publication I focused on considering film damage, while Publications II-IV dealt mostly with various aspects of coating microstructure. As a natural progression, the aim of Publication V was to address the influence of surface roughness. In particular, the emphasis was on developing the analysis and modeling methodologies in line with the microstructure scale modeling and to approach the surface roughness explicitly rather than by utilizing effective models. The interactions between the film, the substrate microstructure, the bond layer, and the other structures and surface topography could be investigated during the design of new coating solutions or when assessing the tribological performance of the films under differing operating conditions.

The evaluation of the contact behavior of rough surfaces has traditionally been approached by the so-called “effective” models, largely due to the complexities in both the analytical and numerical incorporation of the behavior of a rough surface in the modeling of the behavior of the tribological contact. This has been primarily due to the difficulties in

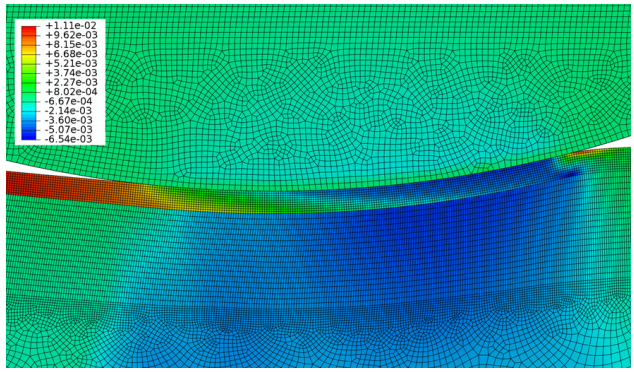

(a) First principal stress contours.

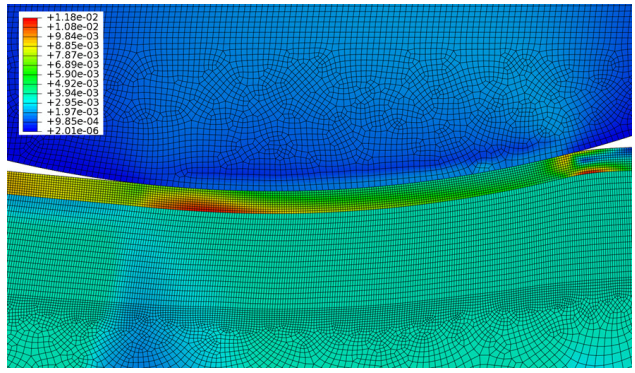

(b) Equivalent von Mises stress contours.

Figure 3.5: FE mesh and contact response for CZM of thin film scratch tests (Laukkanen et al. (2011)).

approaching the contact problem, and as such it is logical to approach it by way of numerical modeling. The present state-of-the-art is summarized in multiple sources, including for example Holmberg and Matthews (2009), where the complexities arising from the numerous parameters are acknowledged in making it difficult to outline a general theory or even methodology suited for coated surfaces. Although the significance of surface roughness has certainly been acknowledged, the simple models typically with an analytical origin have had difficulties in formulating a theory or model capable of merging the numerous parameters impacting the behavior of a coated system with those of surface roughness and topography. Such classic models, relying often on analytical simplifications of the rough contact problem to be able to approach the problem, have been presented for example by Greenwood and Williamson (1966), Halling (1975) and Halling et al. (1983). Following the possibilities to utilize numerical modeling in the realm of thin films as well, the use of computation in deriving roughness models has increased. Works have taken the next steps over classic works, and clear influences of surface roughness have been demonstrated, for example, by Kalin and Pogacnik (2013), Kucharski and Starzynski (2014) and Reichert et al. (2016). DLC coated surfaces have been studied, for example, by Jiang and Arnell (2000) and Xiao et al. (2016). These works can be stated to have taken the first steps in applying modeling to rough surface problems, although the approaches in a computational sense have been limited to simple models of surface contact where the

roughness has been discretized for example to a single asperity contacting a flat surface or a similar modeling outline. Typically these earlier works do not or can not include the other aspects of the system when considering the design of the coating microstructure (such as the gradient or multilayer character of the coating, bond layer, microstructure of the substrate, defects, etc.). In Publication V, a toolset was developed to include surface roughness and topography alongside the other studied characteristics of the coated system, to introduce a methodology where all these features are present at the microstructural scale of the tribological system.

The experimental details related to Publication V are presented in Holmberg et al. (2015). The details of the surface topography characterization technique and the fractal analysis procedures for surface characterization and its analysis are provided in Wolski et al. (2017). In order to be able to produce different types of representations of coated surfaces, a toolset was developed and implemented to support different methods and types of rough surface topographies, as presented in Figure 3.6. The basis of the approach is to support various typical sources of characterization input, such as different types of profilometry and topography data, or to simply generate surfaces based on mean values or statistical data, such as the R_a and R_z values. Following interfacing to experimental data, different surface representations are available, arranged by the ascending complexity of the surface representation:

- stochastic random walk surfaces: generation of surfaces based on random walk methods
- isotropic and anisotropic fractal surfaces: representation of the topography as a fractal surface
- Fourier series and spectra: use of series developments to describe the surface topography
- direct use of experimental data: reproducing the experimentally measured surface directly to the model

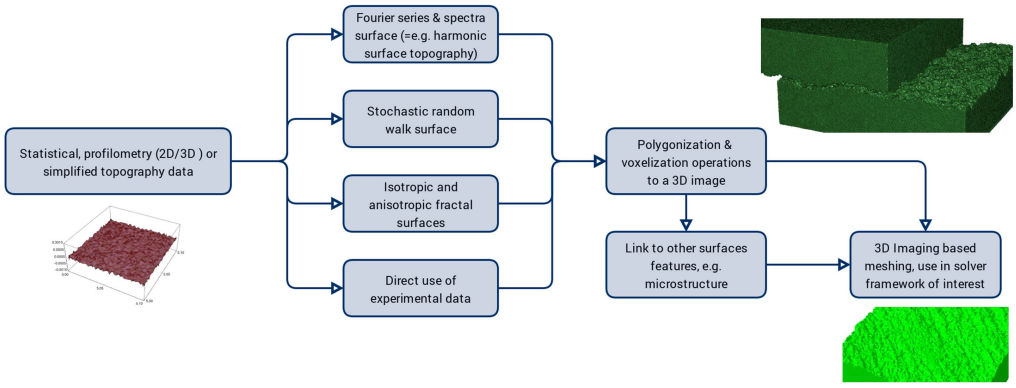

Figure 3.6: Toolset for modeling rough surfaces (Laukkanen et al. (2016b)).

The objective of supporting different ways to represent the surface roughness was essentially to both enable direct transfer of experimental measurements to the model of the surface, and also to enable parametric and systematic studies of the effects arising from the variation of surface roughness characterization parameters and methods. In Publication V, the coating system under study is a DLC coated steel substrate, typical of, for example, automotive applications. The surfaces were prepared with three surface finishes, resulting in different levels of surface roughness and consisting of the DLC surface layer, a CrCx and Cr bond layer, and an AISI52100 bearing steel substrate, as shown in Figure 3.7.

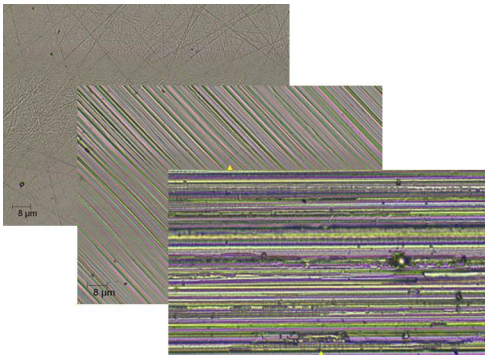

(a) Three different DLC coating surface finishes: smooth, average roughness, and rough surface

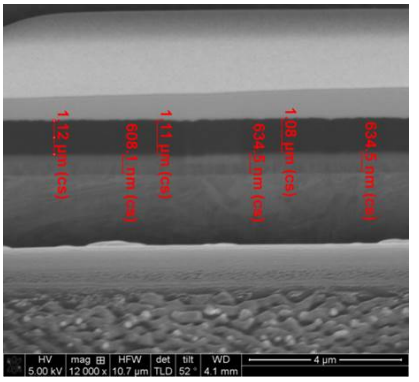

(b) FIB cross section of the coating

Figure 3.7: DLC coatings studied in Publication V (Laukkanen et al. (2017b)).

Examples of the generated surface roughnesses are presented in Figures 3.8 through 3.10. In Figure 3.8, a random walk surface prepared based on the analysis of surface topography measurement statistics is displayed, the surface being generated and merged with a representation of a Face Centered Cubic (FCC) like tessellated steel microstructure. In Figure 3.9, a similar system and a typical microscratch test diamond tip are introduced. The system studied in Publication V is presented in Figure 3.10 with respect to the material domain. In Figure 3.11, the FE mesh used for solving the contact problem is shown including the countersurface. The resolution of the microstructure of the bearing steel, the bond layer, and the DLC coating are visible in the figures.

3.2 Microstructural modeling of composite coatings

A central feature of composite coatings is their microstructure, which still today largely refers to the characteristics needed to produce a wear resistant surface against a particular loading. With the introduction of ICME, however, there is an obvious desire to develop systematic procedures for accomplishing that and, ultimately, optimizing tribological systems with respect to performance and cost. The focal area of this section is, then, the microstructural and micromechanical modeling of coated material solutions, especially considering the means for describing the material microstructure with the necessary level of detail. These coatings are typically labeled as “thick” composite coatings, i.e., the thickness can be in the range from 100 μm all the way up to 3 mm. The deposition methods consist of thermal spraying, laser cladding, and weld hardfacing, the current work focusing particularly on thermal spray and laser clad carbide coatings. Common

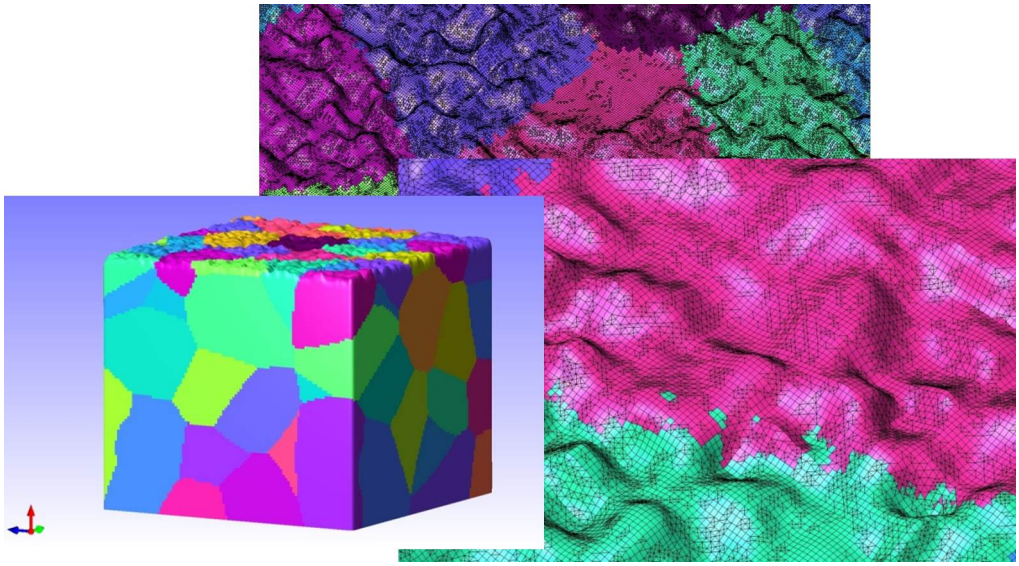

Figure 3.8: Model of a random walk surface topography and microstructural model of an FCC steel (Laukkanen et al. (2017b)).

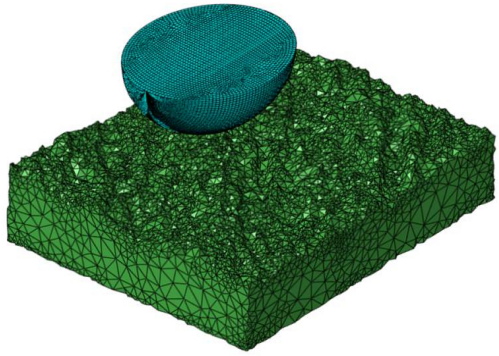

Figure 3.9: Microscratch test FE mesh of the surface topography and a diamond tip (Laukkanen et al. (2016b)).

examples of WC-Co coatings and the respective thermal spray processes, which contribute also to the experimental background of the current work, are presented in Turunen et al. (2006), Hannula et al. (2009), and Oksa et al. (2011).

The work in Publications II, III and IV contributes to the development of a toolset for modeling composite coating microstructures, as schematically presented in Figure 3.12. The toolset is divided into three separate larger modules focusing on the crystal and microstructure generation, modeling of the composite interface structures, and linkage to the process models, especially the PF models for linking to rapid solidification simulations. Starting from Figure 3.12a containing the crystal or composite constituent generation, the composite elements are introduced first either from a statistical basis or by interfacing

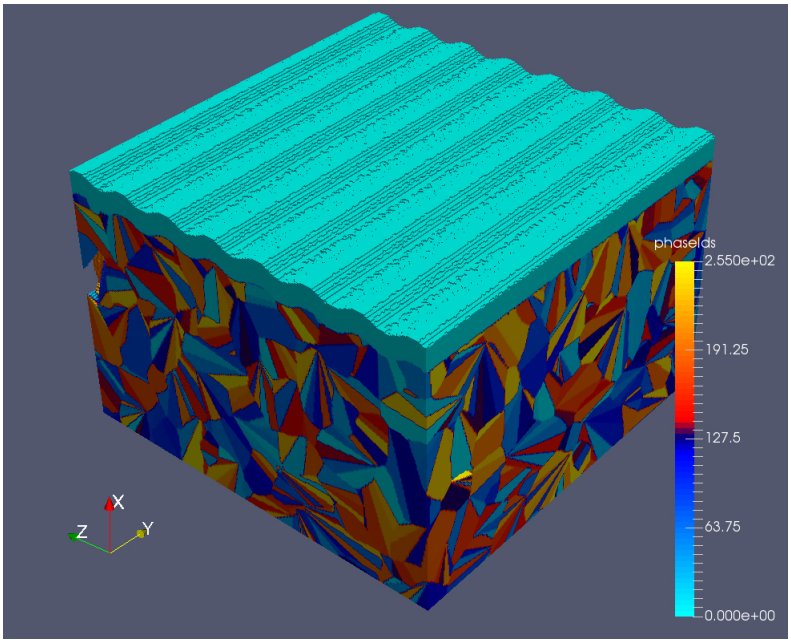

Figure 3.10: Anisotropic fractal surface multilayer DLC coating on a steel substrate modeled including its microstructure (Holmberg et al. (2018)).

directly with the characterization data using image based modeling techniques. Options are present to modify individual particles, fillers etc., for example to establish groups and libraries of specific different particles to be utilized in the subsequent generation of composite nano-microstructures. The next step is the generation of the microstructure, either by utilizing different random sequential assignment methods or by simulation driven methods. The former is usually associated with loose packings of multiple phases within the microstructure (of low overall filler volume fraction), while the latter can yield extremely dense composite microstructures (of high volume fraction). Following the generation of the microstructure, by default stored as a 3D image, voxelization and meshing routines yield the morphology that can be subjected to the physics of interest and solved using FE or other numerical means, such as various particle based methods. The approach for more detailed interface modeling is presented in Figure 3.12b. Two means similar to those for individual crystals are available, either using characterization data directly or linking to other numerical models such as those arising from the material processing. The approach enables the "parsing" of the characterization data or coarse-graining of PF or similar results as with individual crystals. After that, multilayered, gradient, etc. interfaces can be introduced with limitations imposed only by the resolution of the mesh, the data structure utilized, and the capabilities of the following solver to use this information. The interface typical of PF modeling is depicted in Figure 3.12c. The PF order parameter fields are parsed, the phase characteristics identified for further model generation for example using thermodynamical means, and the orientation fields directly introduced to initialize the microstructure for property and performance models.

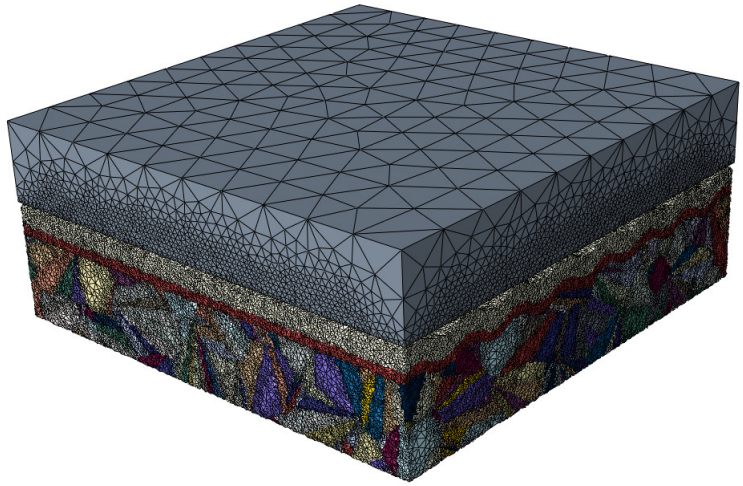

Figure 3.11: Mesh for a rough-on-smooth contact model of a multilayer DLC coating against a smooth DLC counter surface (Holmberg et al. (2018)).

3.2.1 Composite microstructures (Publications II, III and IV)

The modeling challenge and the source for the wear resistance of composite coatings lies in their complex microstructure, consisting of crystals (grains), fillers, etc., as well as of defects such as pores, cracks, and imperfect interfaces. The interfaces of the composites add another important element, which at present is still largely dealt with in a highly simplified manner not accounting for the true multiscale nature of the interfaces. Tribological contacts have not been widely studied in conjunction with composite microstructures, but for example the works by Dick and Cailletaud (2006) considering polycrystalline microstructures of steel under fretting like conditions, Chawla et al. (2006) in SiC-Al alloy, and Zhang et al. (2009) and Quey et al. (2011) on Ti-6-4 alloy surfaces should be mentioned. Work has been largely 2D due to the constraints associated with model generation, solving the tribological contact, and the type of the characterization data to name some of the challenges in working with microstructures. An example of work on a 3D structure has been presented by Wiederkehr et al. (2010) using a serial sectioning technique. For microstructural modeling in general, the chosen approach has largely been to work with SEM images, such as has been done by Langer et al. (2001) and Reid et al. (2008). Another aspect is the modeling of the actual wear damage, where the FE methods in general are typically at a disadvantage due to the common inabilities in the mesh adaptation in the generally applied Lagrangian formulations. Examples where the wear damage has been introduced explicitly are the Movable Cellular Automata (MCA) work of Österle et al. (2007), or the discrete methods such as Peridynamics (PD) in the work of Seleson et al. (2009). The discrete nature of these means enables the description of the moving boundary problem with greater ease than FE modeling, although this is typically met at the expense of the solution's accuracy and resolution in comparison to FE. Although FE is a little more challenging to apply with respect to the complexities of the problem, sliding abrasion problems have been solved for a thick coated system by Anwar et al. (2013), and a typical example of introducing cracking mechanisms is given by Mohd Tobi et al. (2013). These works do not account for the material microstructure directly or utilize truly physics-based fracture models, or to say the least, the solution

of the wear problem relies on more classic approaches such as wear laws and simple macroscale continuum criteria to introduce the material damage. Microstructural features such as pores and cracks have been introduced in Wiederkehr et al. (2010), Amsellem et al. (2008) and Beauvais et al. (2008). Furthermore, the microstructural characteristics described by the parameters such as the size, shape, and density of the reinforcing phase and the mechanical properties of the binding phase have been investigated by Hu et al. (2007), Pearson et al. (2009), and Zhang et al. (2009). Overall it can be stated that the models of composites are typically quite simplistic in terms of the microstructure and description of the failure mechanisms, and in general, the number of studies where the interaction of the microstructure and the tribological contact are introduced is limited, let alone approaches where the design of the tribosystem has been attempted.

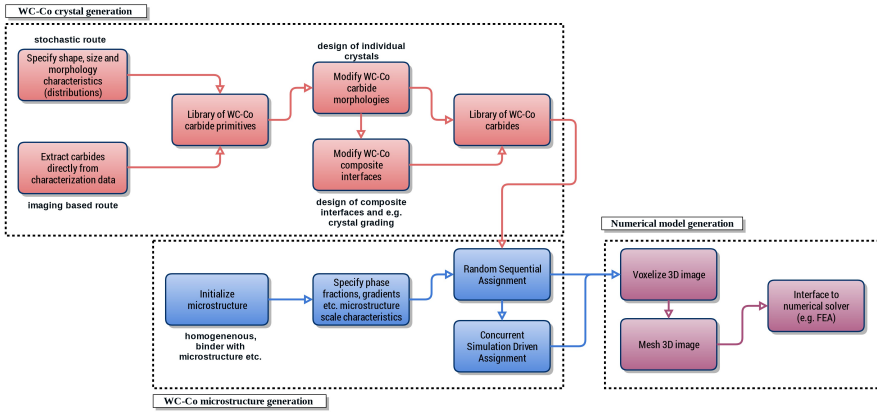

(a) Toolset module for modeling composite microstructures

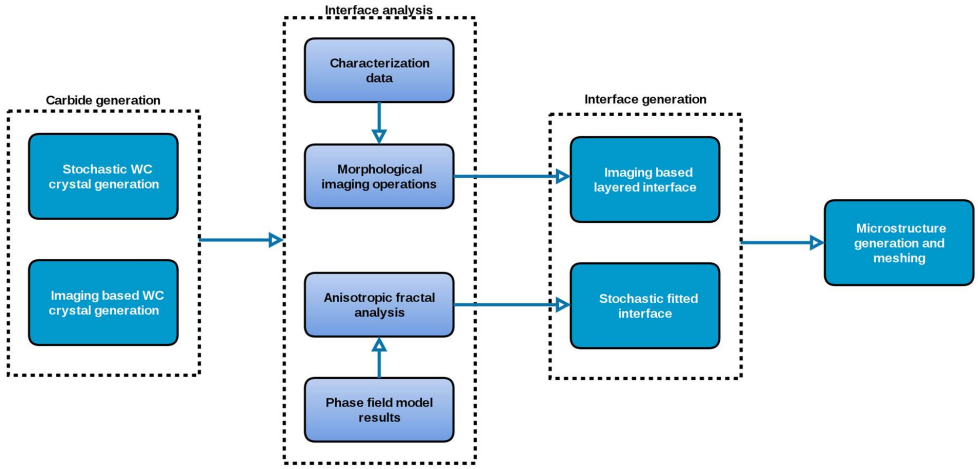

(b) Toolset module for modeling interfaces in composite microstructures

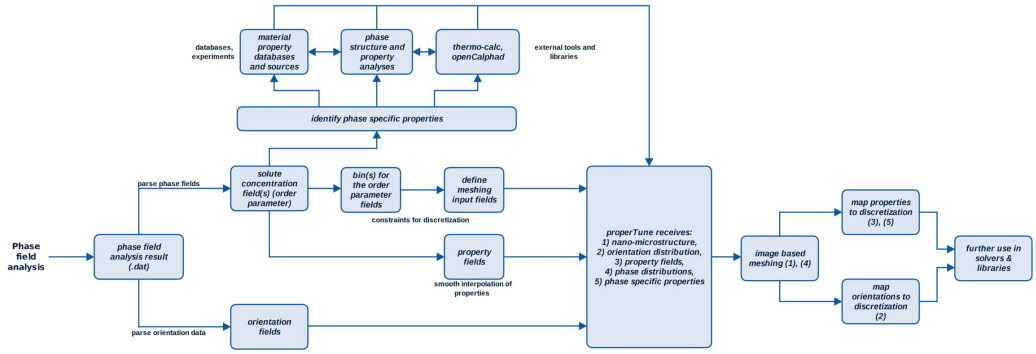

(c) Toolset module for linkage to rapid solidification modeling by PF and similar methodologies

Figure 3.12: General representation of the composite microstructure modeling toolset applied in the current work for WC-Co and similar hard materials (Laukkanen et al. (2016a)).

Publications II and III

The work carried out in Publications II and III focuses on the 3D and 2D modeling capabilities, both utilizing the imaging based and synthetic (or stochastic) modeling approaches. Typical models with respect to microstructure geometry concerning the 3D models of WC-Co microstructures are presented as examples in Figure 3.13 and 3.14. The two microstructures in Figure 3.13 were prepared using the methods presented in Figure 3.12 and by modifying the crystal size distribution to reflect the spread of grain sizes. The size of the Representative Volume Element (RVE) in both cases is 300 μm. A FE mesh of a WC-Co RVE is presented in Figure 3.14, demonstrating the typical resolution of the WC crystals embedded in the binding Co phase.

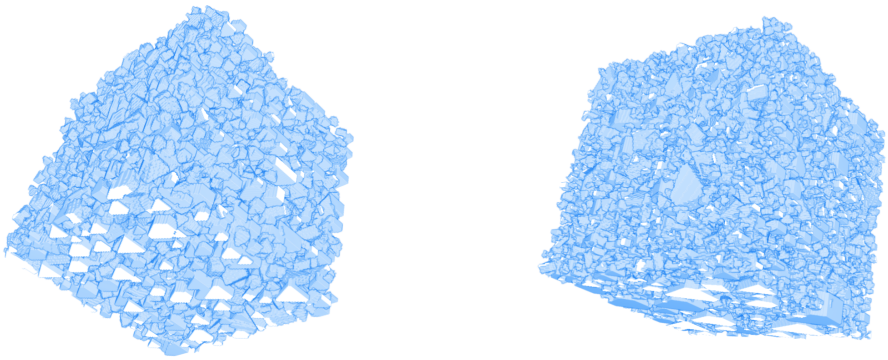

(a) Model of the WC-Co microstructure, "confined" crystal size distribution

(b) Model of the WC-Co microstructure, "spread" crystal size distribution

Figure 3.13: 3D Models of WC-Co microstructures (Laukkanen et al. (2016c)).

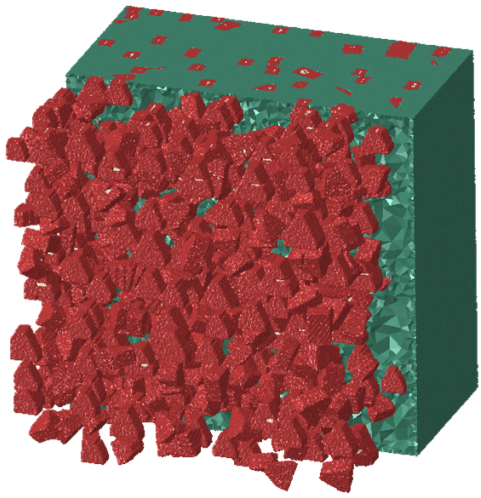

Figure 3.14: Cut of a WC-Co microstructure RVE mesh (Laukkanen et al. (2016c)).

In order to obtain the high WC fractions typical of common wear resistant microstructures,

whether manufactured by thermal spray, cladding or sintered, simulation driven packing routines, referred to as Concurrent Simulation Assisted (CSA) routines, are favored. Cross sectional details of RVEs are presented in Figure 3.15, demonstrating a microstructure during the microstructure generation process at the WC fractions of approximately 65% and 85%, respectively. The approach in CSA differs from the computational placement routines, which attempt to generate the structure by way of packing, stochastic geometry operations, and by identifying the possible locales from the microstructure where for example a carbide can be placed. In the developed CSA approach, the compaction of the microstructure from a loose randomly prepared sample is calculated explicitly by utilizing either a particle solver with a pair potential, or by way of a simplified FE contact solution. In both cases, very high packing fractions can be obtained to continue the further microstructure preparation operations.

Another approach utilized extensively is to generate models directly from the characterization data by employing image based modeling. An example of how the microstructural details can be resolved is presented in Figure 3.16. This is an example from a set of thermal sprayed WC-Co microstructures, which were modeled and their behavior studied in sliding abrasion, mostly utilizing two-dimensional models. As presented in more detail in Holmberg et al. (2014a), the procedure performs a segmentation and uses the image data directly to form a mesh. Various routines with differing treatments, especially to the phase boundaries, were established, including links to external libraries and meshers, especially for computing constrained triangulations[1]. In addition, it was found that the steps related to smoothing, filtering out for example the noise arising from the characterization, and post-processing of the microstructure to obtain the desired physical behavior such as individual deformation of carbides during the deformation process (a nano-microstructural feature not necessarily captured by the characterization but relevant in finite strain deformation processes) were common when preparing a microstructural model and included in the analysis workflow. Another example is a weld hardfacing coating with a martensitic binding microstructure and different carbide and boride hard particles presented in Figure 3.17. An outline of a sliding abrasion scratch test model is included, the details of the microstructure as captured by the FE models are shown, and the coating-to-substrate interface is included in the microstructural modeling. Another model, in this case 3D, of a scratch test of a WC-Ni laser cladded coating is presented in Figure 3.18 and has been studied in more detail by Suhonen et al. (2017). The scratch track following the computation of the tribological test contact is also shown. The microstructure has a large Mean Free Path (MFP) and the large fairly spherical carbides are present in a somewhat clustered form. Large pores are also present in the microstructure. The microstructural model can capture and match the features to a degree identifiable from the available characterization data.

[1] utilizing primarily Python Numpy and Scipy functionalities

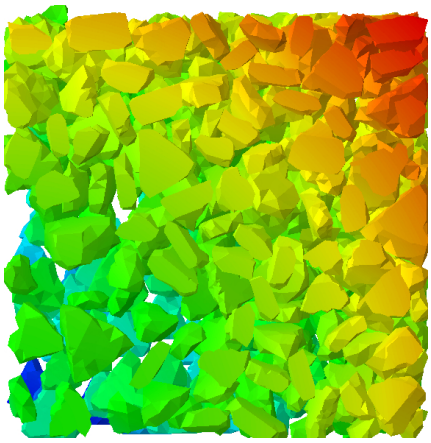

(a) CSA routine result in preparing a WC-Co microstructure, WC fraction approximately 65%.

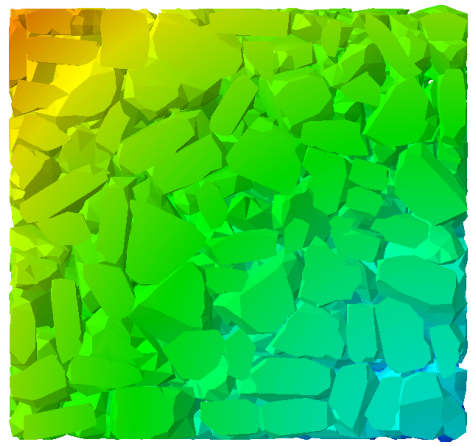

(b) CSA routine result in preparing a WC-Co microstructure, WC fraction approximately 85%.

Figure 3.15: Cross sections of the WC-Co microstructure following CSA packing

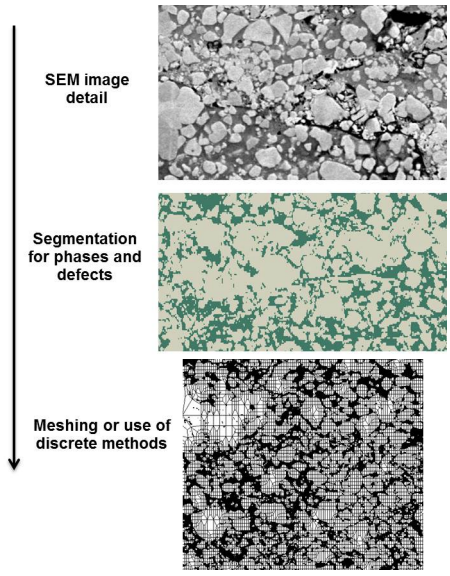

Figure 3.16: Detail of meshing output as a result of image based modeling of a WC-Co thermal spray coating (Holmberg et al. (2014a)).

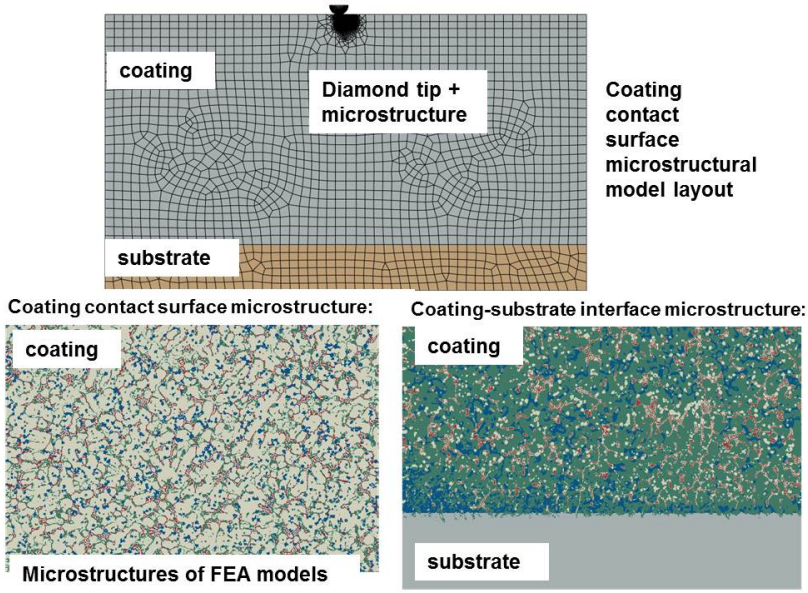

Figure 3.17: Weld hardfacing composite coating and a model of its micro-scratch testing (Suhonen et al. (2017)).

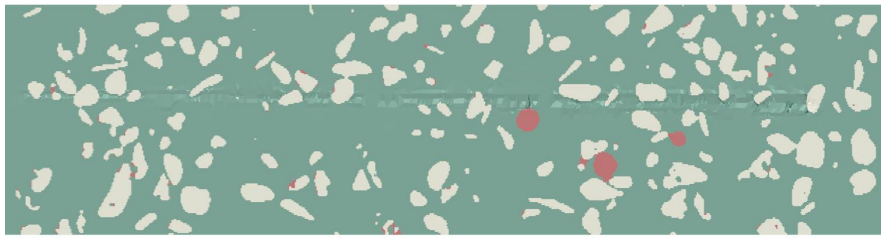

Figure 3.18: Laser cladded WC-Ni composite coating and a model of its micro-scratch testing (Suhonen et al. (2017)) (white = carbides, red = pores).

Publication IV

In Publications II and III, the composite structure was simplified with respect to interfaces, i.e., except for some analysis cases utilizing CZM to describe imperfect interfaces, with no further information about the interface character included in the models. In Publication IV, this aspect was taken under closer scrutiny to provide a basis for more complex interface models, which can, for example, arise from coarse-grained lower spatial scale treatments of the interface structures and interactions. This was found to be a characteristic lack in the present models of hard materials and tribological problems as a whole. However, from the experimental and material processing perspectives, the interfaces, interphases and overall the interactions within composite materials are far from ideal and defect free representations of common material models (for hard materials, see e.g. the experimental works of Turunen et al. (2006), Hannula et al. (2009) and Oksa et al. (2011)).

The approach selected in Publication IV was to extend the microstructural modeling capability to consider and model the interfaces of individual carbides as well, i.e., to create an interface region and/or, if necessary, further apply CZM and similar techniques to model imperfect cohesion/adhesion and its evolution with respect to the initiation and propagation of the damage within the material microstructure. The basics of the developed solution and its implementation are outlined in Figure 3.19. In essence, every composite constituent, typically a particle such as a carbide, can be treated as a multilayer, a graded structure, or a general subset of the microstructure itself in the 3D space surrounding the individual particle. This largely solves the problem of how to either incorporate an infinitesimal cohesive layer into each particle, or include an interphase of desired characteristics. It does not provide any added insight with respect to specifying the interface region material properties and behavior, but it does permit, for example, the direct specification of the respective behaviors on the basis of nanoindentation measurements. To further explore and extend the interface modeling capabilities, links to material processing modeling were pursued. In particular, since the microstructures of primary interest have been manufactured by rapid solidification processes, the PF modeling methodology as presented in more detail by Greenwood et al. (2018) and applied by Pinomaa et al. (2015) was adopted. By way of PF modeling, the solidification response, including WC dissolution during thermal spray and formation of further W-C-Co based phases such as the brittle W_2C semicarbide, the respective interphases can be captured and included in the FE based microstructural model appropriately. As such, the PF analysis results can directly act as an input to FE modeling, or the PF results can be further data mined to extract and process interface characteristics for further use in the FE interface models.

Another relevant way to add realism to the composite models is by incorporating various defects, such as cracks and pores. Secondary phases can be typically incorporated directly into the microstructure and be treated already with the methods presented above. The imaging based approaches can identify and include defect structures directly, but in addition, it was found that to better support the systematic study of defect structures in the microstructures, further stochastic means would be in order. This translates into implementing an ability to incorporate different defect types in desired fractions into microstructural regions of relevance with respect to the occurrence of a specific defect type. An example is presented in Figure 3.20 for a Cr_2O_3 coating, where thermal spray "splat" boundaries have been utilized to form a structure where the defects reside (these "splats" were generated in advance by way of sequentially packing ellipsoids). In this case, three defect types were generated by customizing the defect generation procedure

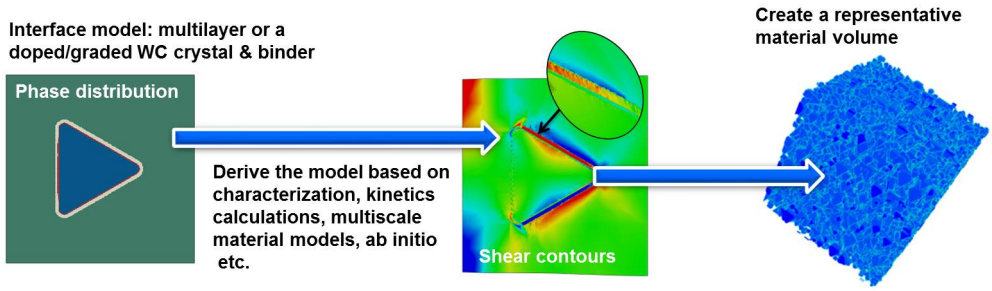

Figure 3.19: Schematic representation of the adopted interface modeling approach for hard material composite microstructures (Laukkanen et al. (2016c)).

to yield a structure mimicking the actual manufacturing process. Gas pores with a roughly unity aspect ratio were included in the structure directly, the "splat" boundary defects were incorporated by introducing a misfit between the "splat" boundaries, and sharp crack-like features were introduced to the interfaces by essentially "carving" out or detaching regions in the microstructural model. Subsequently, a defect containing a porous ceramic microstructure was generated and is easily modifiable to study, for example, the significance of certain defect types with respect to the strength or fracture properties of the material. The statistics necessary for the generation of the structure were extracted using image processing, as shown in more detail in Laukkanen et al. (2014).

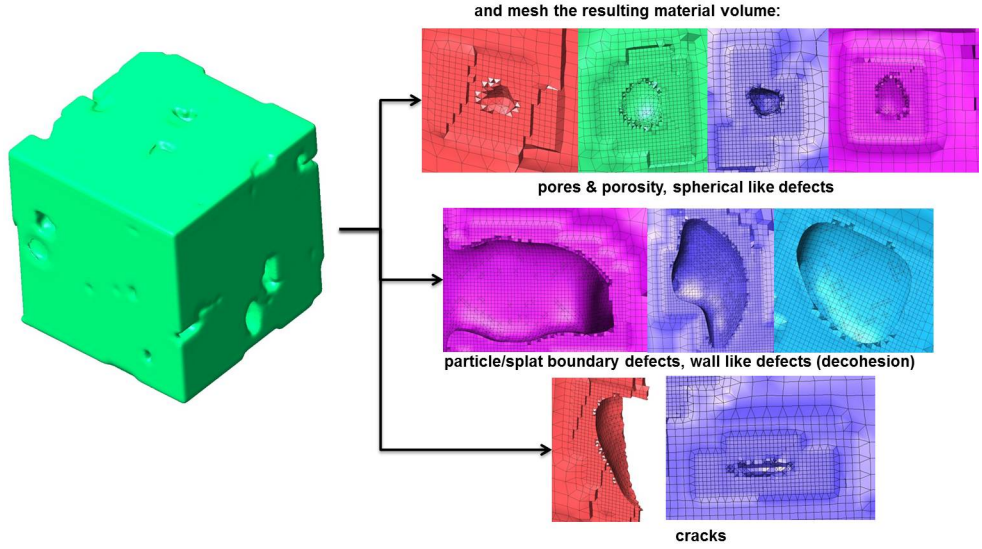

Figure 3.20: Synthetic defect containing model of Cr_2O_3 thermal spray coating (Laukkanen et al. (2014)).

4 Results

4.1 Failure of thin films (Publication I)

The CZM approach was utilized first to investigate whether the thin film cracking behavior could be reproduced by way of numerical modeling. The testcases were comparable to the TiN coating studied previously, for which extensive information about cracking behavior was available. Further details regarding material parameters and model parameterization are provided in Publication I. The first testcase presented in Figure 4.1 was used to evaluate the significance of the thin film parameters to cracking predictions. The experimental reference model of Figure 4.1a yielded a response where cracking from the trailing edge of the contact or from the film to the substrate interface was favored, overall matching the observed experimental behavior. Increased modulus of elasticity of the coating made the system stiffer to the applied scratch test contact and resulted in the delamination of the film from the substrate within the region under contact. Decreasing the modulus of elasticity eliminated the cracking density altogether, and investigation of the TSL response even implied no damage nucleation. The findings are indicative of the influence of the film properties onto cracking. However, as noted in the following section, further arguments need to be made with respect to the ability of the film to contribute to the load carrying capacity of the tribological system.

As one of the principal failure mechanisms, the damage evolution behavior at the film-to-substrate interface is presented in greater detail in Figure 4.2, essentially comprising a failure scenario where film adhesion is lost once the scratch test loading is large enough. The initiation took place from both the leading and trailing regions of the contact. Once initiated, the damage at the respective material point evolved and the interface crack also began to extend laterally. The two crack tips grew and merged during the progressing contact, forming a decohered interface where the crack size was roughly twenty times the coating thickess, indicating a complete loss of adhesion. The other prominent mechanism observed in the experiments was through coating cracking. A scratch test model displaying the progression of this form of cracking is presented in Figure 4.3. It is noted that the film exhibited initial damage when it was subjected to tensile stresses at the leading region of the contact, but this was only sufficient to initiate the damage. The through film cracking took place at the trailing region of the contact where the contact separated and the film was subjected to both tensile and bending stresses. In addition, on the basis of this observation, a trial of a multilayer coating better resistant to sliding abrasion was considered. The hypothesis was that a multilayer better smoothening the tensile stresses across the film thickness would offer improved toughness. The outcome is presented in Figure 4.3b, where it is observed that the damage introduced to the system significantly lessened, displaying a coupling between the multilayer coating's stress state, its adaptation to the tribocontact, and the respective damage exhibited by the film.

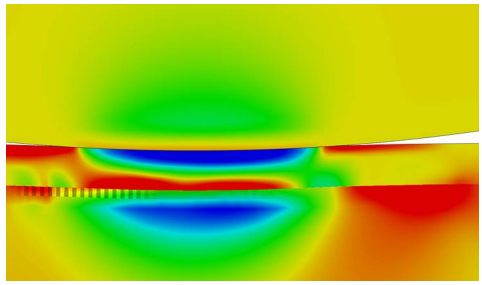

(a) 2 μm thick TiN film with $E = 200\ GPa$.

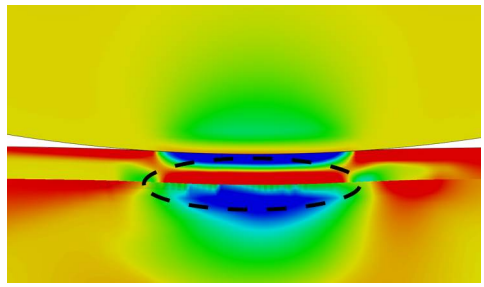

(b) 2 μm thick TiN film with $E = 500\ GPa$.

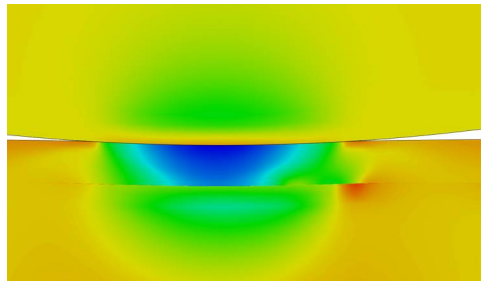

(c) 2 μm thick TiN film with $E = 100\ GPa$.

Figure 4.1: CZM modeling of the influence of the film modulus to the coating and the coating-to-substrate interface crack pattern, first principal stress contours (Laukkanen et al. (2011)).

The evolution of through coating damage is presented in Figure 4.4. It is observed that the crack initiation took place ahead of the contact due to finite strain and sliding effects and largely nucleated at the film-to-substrate interface, but the primary failure initiated from the surface at the trailing edge of the contact and was responsible for the through cracking of the film. Similarly, the graded multilayer film was only seen to exhibit minute damage in comparison to the homogeneous film, the shown result representing the final configuration of the homogeneous film at the point where complete failure had occurred. The previous results for through film and interface cracking were obtained by activating CZM only either at the film-to-substrate interface or through the film itself. A case where both were considered simultaneously, i.e., the whole system is filled with cohesive zone elements, is presented in Figure 4.5. It is observed that the interface and the through film cracking mechanisms interacted and actually, in comparison to solely through film cracking, the defect driving force was lessened to a degree where the failure took place

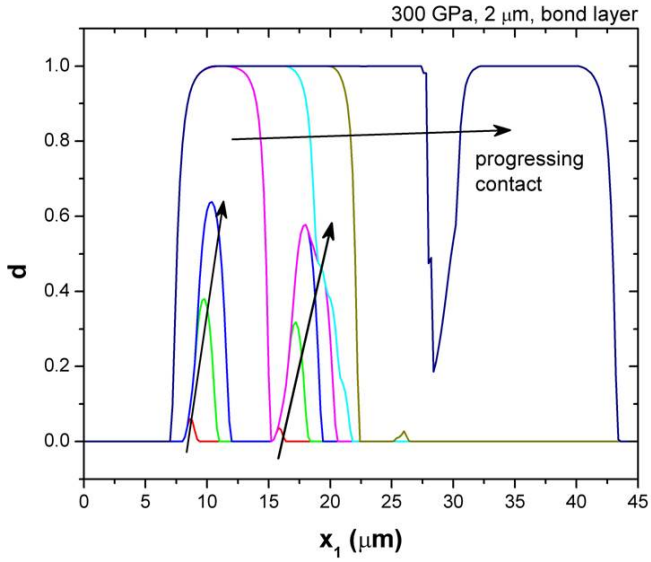

Figure 4.2: Initiation and propagation of the damage at the film-to-substrate interface during scratch testing, TiN $E = 300\ GPa$, film thickness 2 μm and the system contains a bond layer. x_1 is in the direction of sliding and positioned to the film-to-substrate interface (Laukkanen et al. (2011)).

also at the film-to-substrate interface, although the principal behavior with respect to the ultimate failure remained the same.

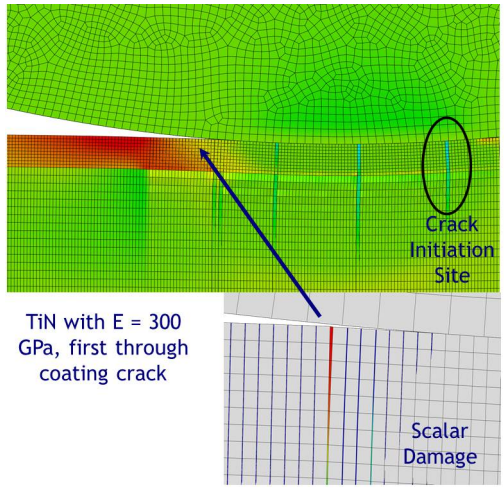

(a) First principal stress contours for through film cracking CZM and distribution of damage through the film at the location of the first through coating crack.

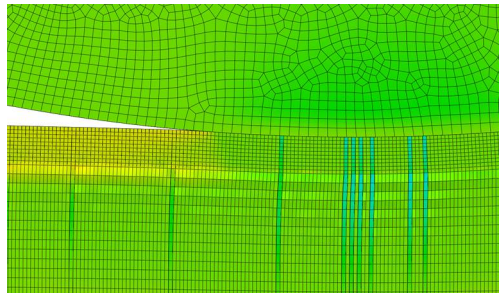

(b) First principal stress contours in a multilayer coating with through thickness material properties tailored according to the bulk film stress state.

Figure 4.3: CZM of through film cracking (Laukkanen et al. (2011)).

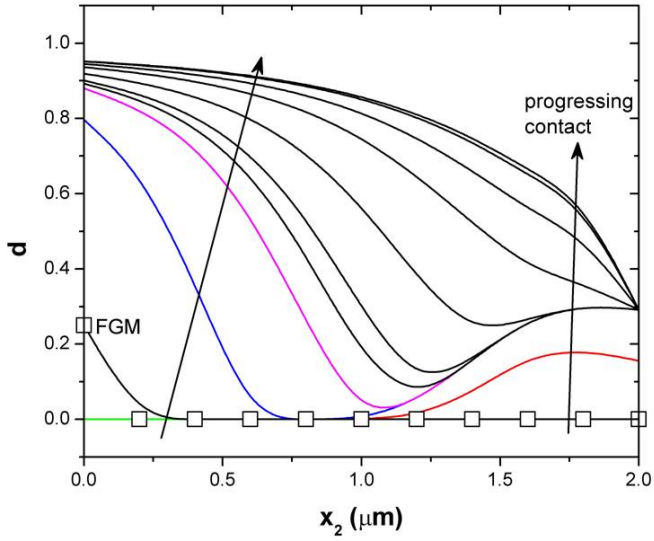

Figure 4.4: Evolution of the through film damage in TiN $E = 300\ GPa$, film thickness 2 μm. FGM refers to the multilayer system tailored according to the through film stress distribution. x_2 is the direction of the film thickness (Laukkanen et al. (2011)).

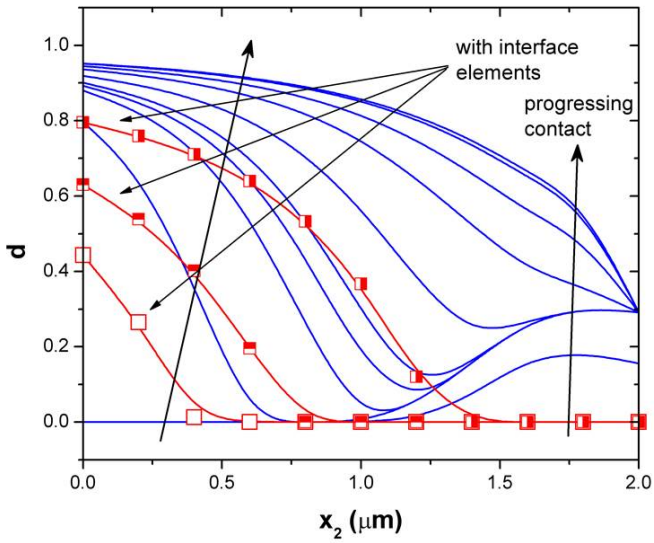

Figure 4.5: Evolution of both interface and through film damage in TiN $E = 300\ GPa$, film thickness 2 μm (Laukkanen et al. (2011)).

Different multilayer and graded film property profiles were considered in order to study their significance for the initiation and further propagation of the damage within the tribosystem. The influence on the initiation and propagation of through coating cracks is presented in Figure 4.6. For the reference, $E = 300\ GPa$ film was selected with a loading condition where the damage had nucleated but the film was not yet entirely broken to better demonstrate the influence of the film properties. Although the soft bond layer appeared feasible considering the lessened evolution of the damage near the defect initiation, in this case it was unable to support the film, which leads to the nucleation of a through coating crack if the load carrying capacity as expressed by the TSL behavior cannot be retained. The other film arrangements with multilayer like configurations were favored over a single layer film, as expected. In the "hard" film, the properties were graded toward a higher elasticity surface, and the benefits were apparent similarly to the case where the bond layer is introduced on its own. Introduction of a softer layer within the multilayer, i.e., the "discontinuous" film case, was also seen to improve the behavior. Overall, the results suggest rather simple and implementable ways to tailor the multilayer behavior for specific tribocontacts.

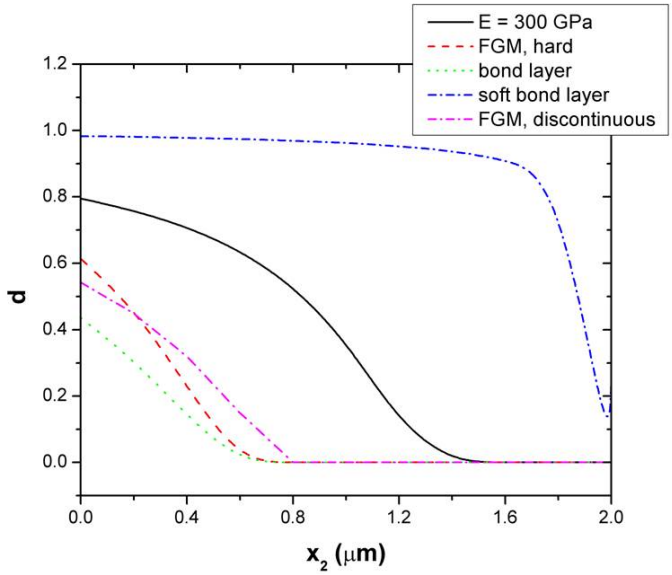

Figure 4.6: Influence of the graded film characteristics on the damage accumulation and further on the initiation of through film cracks (Laukkanen et al. (2011)).

The reference TiN model with CZM modeling of through film cracks was compared with the experimental crack field density results, as presented in Figure 4.7. The crack field densities obtained from the models as a function of scratch test sliding distance were close to the observed initiation of the crack field, and overall the comparison between the different models with $E = 300\ GPa$ and the experiment is promising.

In order to measure the damage exhibited by the different film arrangements relative to the load carrying capacity of the film, in the current case measured as the mean contact pressure at a specific loading condition, the sum of damage as exhibited by a specific model was extracted for different failure mechanisms. The findings are summarized in Figure 4.8. With respect to interface cracks, or adhesive failure, it is noted that an overall

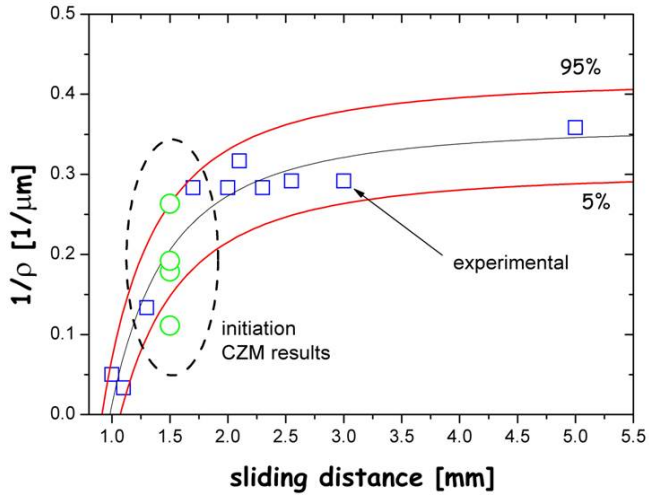

Figure 4.7: Comparison of experimental and modeled crack densities (Laukkanen et al. (2011)).

increase in the film stiffness loaded the interface ever more, leading to increased damage although obviously at the same time also increasing the load that the system is able to carry. For through film cracks, the differences caused in the film's ability to carry loads were smaller, and the examined gradient structures were superior to the other alternatives. Any loss in the TSL response for example due to the resulting softer bond layer can lead to a significantly greater rate of damage accumulation. Considering the further analysis cases where both principal failure mechanisms were active, again any loss in the cohesive or adhesive properties in terms of the TSL was very detrimental. The introduction of bond layers, arresting layers (where a softer layer is embedded in a multilayer) and graded layers resulted in an improvement leading to less film damage. The "hard" graded film had the best load carrying capacity-to-damage ratio, while the graded "softer" systems also decreased the rate of damage accumulation as long as the respective load carrying capacity was sufficient.

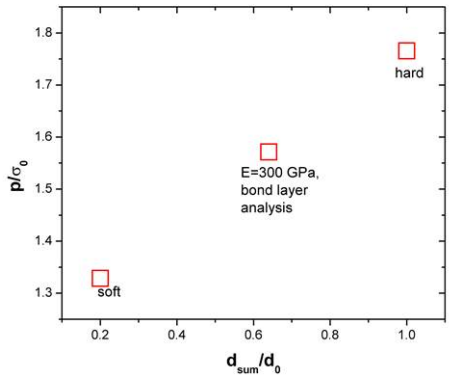

(a) Relationship between the sum of damage and the respective mean surface pressure for interface cracks.

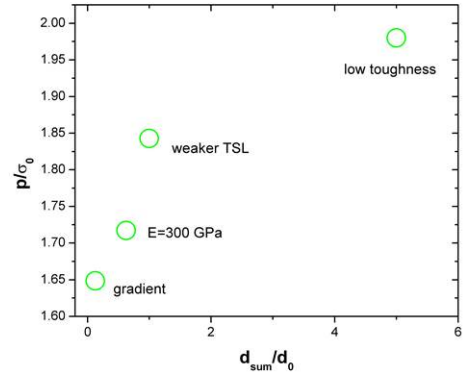

(b) Relationship between the sum of damage and the respective mean surface pressure for through film cracks.

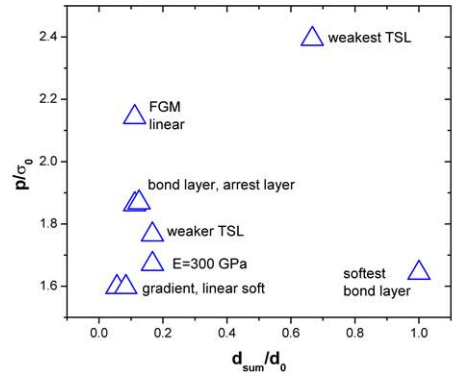

(c) Relationship between the sum of damage and the respective mean surface pressure for interface and through film cracks.

Figure 4.8: Summary of the load carrying capacity *vs.* damage of different multilayer film systems (Laukkanen et al. (2011)).

4.2 Composite microstructures under abrasive sliding (Publications II and III)

The behavior of various composite systems under sliding abrasion conditions, typically microscratch test contacts, were evaluated in Publications II and III. The case of applying the modeling tools to study the behavior of a WC-Co microstructure undergoing scratch testing is presented in Figure 4.9. The WC phase is presented in white, while the Co phase is shown in green. The stress-strain fields are typical for WC-Co microstructures. The carbides respond to the applied loading by developing a high stress state, which is transferred through the structure especially by carbide to carbide interactions when the MFP is small. Similarly, the response of the material to deformation arises primarily from the plastic straining taking place in the Co binder phase. The strains exhibited by the Co phase are large since the phase has to accommodate nearly all the deformations arising from the sliding scratch test contact. Various hard material microstructures and their response to microscratch testing are presented in Figure 4.10. In Figure 4.10a, a thermal spray processed WC-Co microstructure similar to Figure 4.9 is presented. In comparison to Figure 4.10b, which is a sintered structure, the influence of the somewhat greater Co binder content as well as the partial WC carbide dissolution (somewhat more rounded and larger carbides) are visible. In Figure 4.10c, a laser cladded WC-Ni microstructure contains very large carbides, influencing both the extensive deformation of the Ni binder as well as the stresses experienced by the WC grains. The TiC-Ni microstructure in Figure 4.10d contains a "skeleton" of TiC particles, which contributes positively to the ability of the microstructure to distribute the stresses to a greater volume. In Figure 4.10e, the carbide and boride containing an essentially martensitic matrix behaves in a more uniform manner compared to the hard materials with a softer binder phase, the contribution of harder particles being more contained due to the smaller internal mismatching of the microstructure.

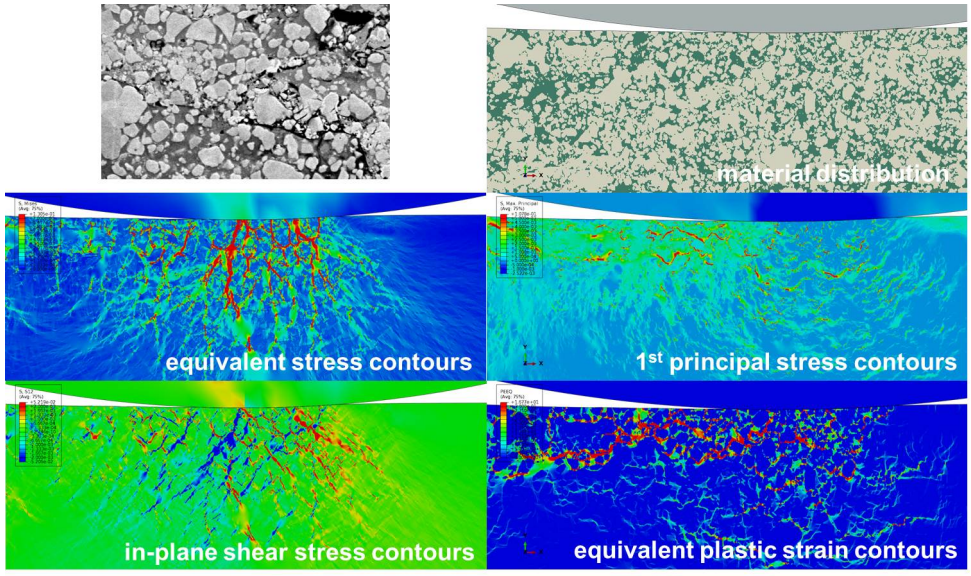

Figure 4.9: WC-Co microstructure undergoing scratch testing (tip movement from left to right) (Holmberg et al. (2014b)).

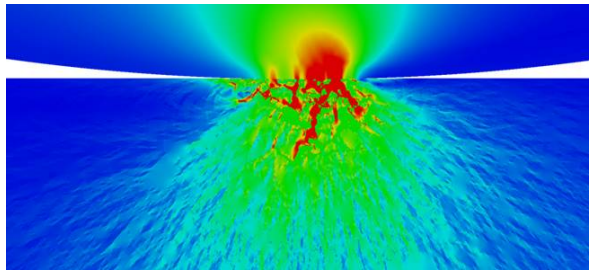

(a) Thermal spray WC-Co microstructure.

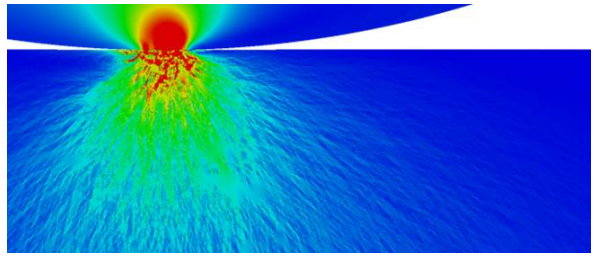

(b) Sintered WC-Co microstructure.

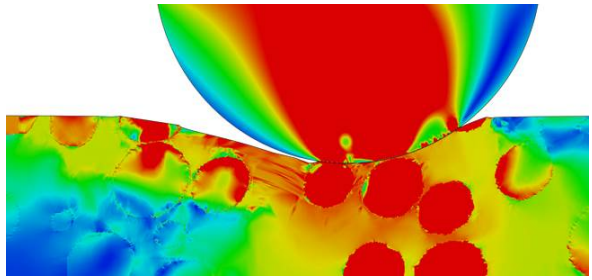

(c) Laser cladded WC-Ni microstructure

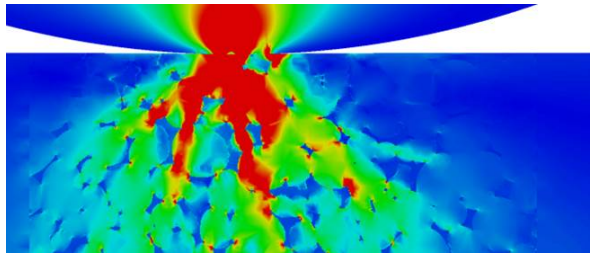

(d) Sintered TiC-Ni microstructure

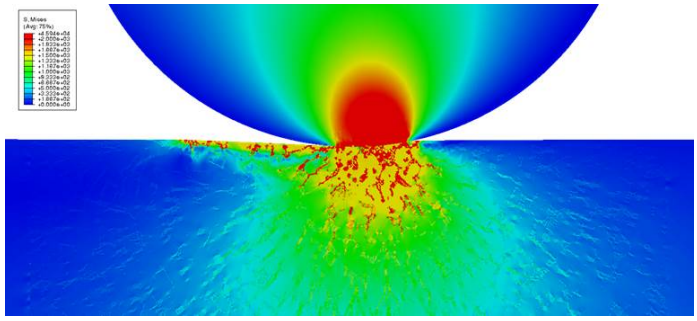

(e) Martensitic carbide and boride containing microstructure.

Figure 4.10: Scratch testing of various hard material microstructures (tip movement from left to right, contours represent equivalent von Mises stresses) (Holmberg et al. (2014b), Holmberg et al. (2014a), Suhonen et al. (2017)).

It can be identified that certain characteristics of hard material microstructures are responsible for many of the observed features of the stress-strain fields, as presented previously, for example in Figure 4.10. The primary characteristics are presented in Figures 4.11 and 4.12. The typical features deal with complex morphologies, locally small or large MFP or interactions between particles, or the available deformation mechanisms and pathways or channels within the hard material microstructure. As indicated in Figure 4.11, these features contribute to the locally elevated stresses in the WC phase, the interactions increasing the stress state within the clusters or arrays of carbides, the absence of deformation mechanisms due to the locally differing phase fractions relative to the microstructure average, and the regions where a low hard phase content enables extensive deformations due to the applied external loading. Furthermore, in Figure 4.12 the regions of maximum tensile stresses and respective plastic strains in the Co binder are highlighted in the tensile deformed region of the indentation outside the material volume undergoing compressive deformation, yielding more examples of the typical stress-strain response of hard material microstructures.

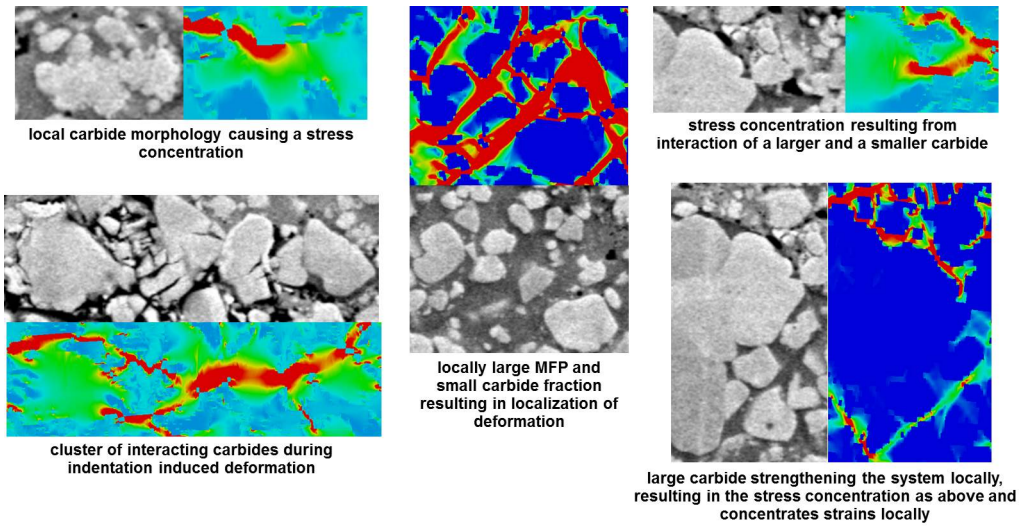

Figure 4.11: Details of the microstructure scale stress-strain behavior in a thermal sprayed WC-Co coating (Holmberg et al. (2014b)).

In addition to the above presented microstructural features, other characteristics such as the carbide size distribution and the tribological contact also influence the behavior of hard material microstructures, as presented in Figures 4.13 and 4.14. In Figure 4.13, WC-Co thermal spray microstructures have been modeled under indentation loading with different WC carbide size distributions. The WC sizes have been labeled as "conventional" ($\approx 1-3\mu m$), "microscale" ($\approx 1\mu m$), and "submicron" ($< 1\mu m$) with respect to the mean carbide size. The small contour plots present the microstructure and first principal stresses in the microstructure undergoing indentation loading, while the main figure displays the density of the fracture probability field evaluated as presented in Holmberg et al. (2014b). The utilized WC fracture model and its formulation are presented in detail in Wallin et al. (2008) and Wallin and Laukkanen (2006). The failure model accounts for the carbide size with respect to its propensity to initiate fracture, and the line graphs provide a homogenized representation of the outcome within the Statistical Volume

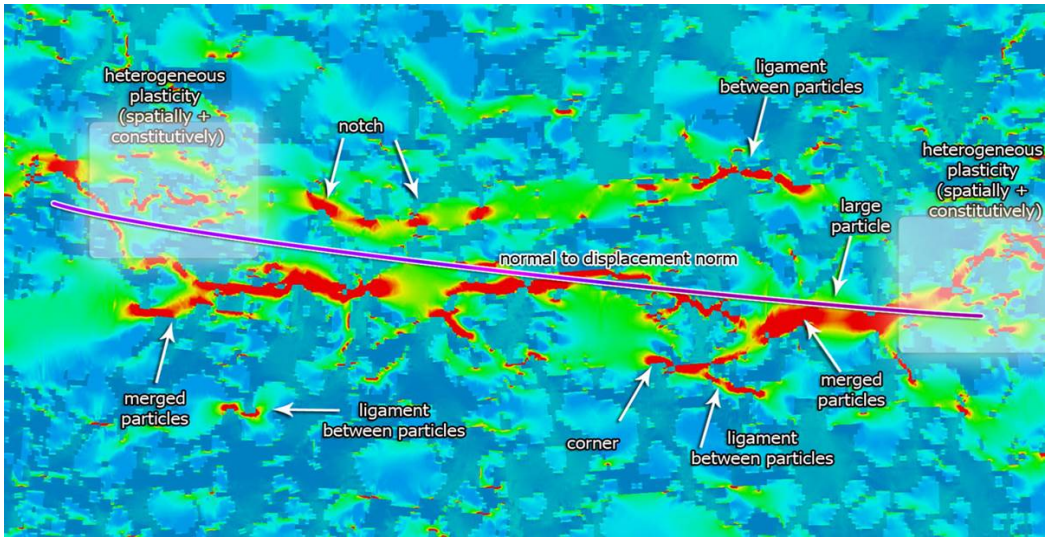

(a) Contours of first principal stress.

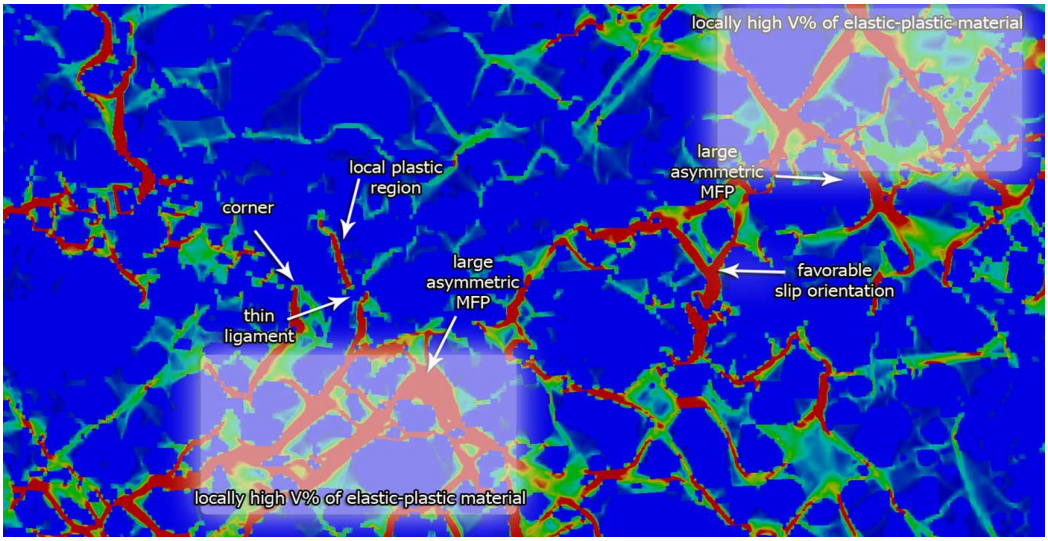

(b) Contours of equivalent plastic strain.

Figure 4.12: Stress-strain state in an imaging based model of the WC-Co microstructure undergoing loading by indentation (Holmberg et al. (2014b)).

Element (SVE). The first principal stress was utilized as the cleavage controlling stress. The results demonstrate that the conventional size distribution of carbides yielded the poorest response, as expected. However, the submicron size carbides did not provide the best results, as the microstructure containing on average micron sized carbides performed better. The explanation lies in the distribution of the tungsten carbides in the submicron size microstructure (so this could also be viewed as an MFP effect), where the smaller carbides were to some extent aggregated and the resulting clusters limited the possibilities of the binder to accommodate the externally applied deformation, resulting in local

stress gradients in the clustered carbide regions. This resulted in a somewhat poorer performance compared to the micronscale WC microstructure. Figure 4.14 presents an example of how the tribological contact size influences the behavior of the microstructure. The larger $200\mu m$ tip resulted in a rather smooth contact distributed over a larger fraction of the microstructure, while the smaller $20\mu m$ tip created a local stress-strain field and the WC-Co composite was no longer able to deform similarly when subjected to the applied loading, resulting in a locally elevated stress-strain state (under displacement controlled loading of comparable magnitude). The result is in many ways obvious from the computational point of view, but again something that is typically ignored or difficult to address when designing and assessing microstructures from a solely experimental perspective. Similar behavior under erosive contact against a composite microstructure is presented in Figure 4.15. The impact angle was 45°, the erosive particles making contact from left to right at the velocities of $15m/s$ and $50m/s$. At the lower velocity, a typical contact stress field was generated with trailing tensile stresses, and to a certain extent plastic deformation of the martensitic binder phase was also observed. However, beyond the surface deformation or strain hardening, no particular indications that would imply significant deterioration of the microstructure were present. At the higher velocity, however, the deformation was no longer contained in the immediate vicinity of the contact, and as a result, the carbides and borides of the structure began to develop large tensile stresses, particularly in the features of the structure that were complex in morphology. The martensitic microstructure collapsed locally, and indications that defects would initiate from the reinforcing particles and/or subsequently from shear localization within the binder also began to emerge. The differences arise from kinetic energy associated with the impact, the analysis is quasi-static with respect to the material domain so no rate dependencies or other dynamic effects influence the response.

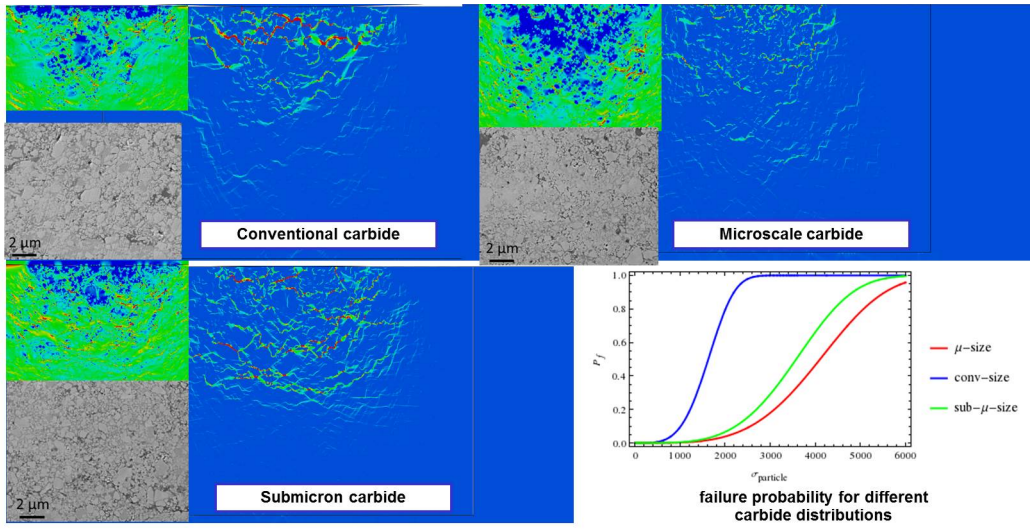

Figure 4.13: Three different WC carbide distributions and their influence on the stress-strain states (principal strain in small figures) and the coating failure probability (density in contours, mean in the line graph) under indentation loading (Holmberg et al. (2014b)).

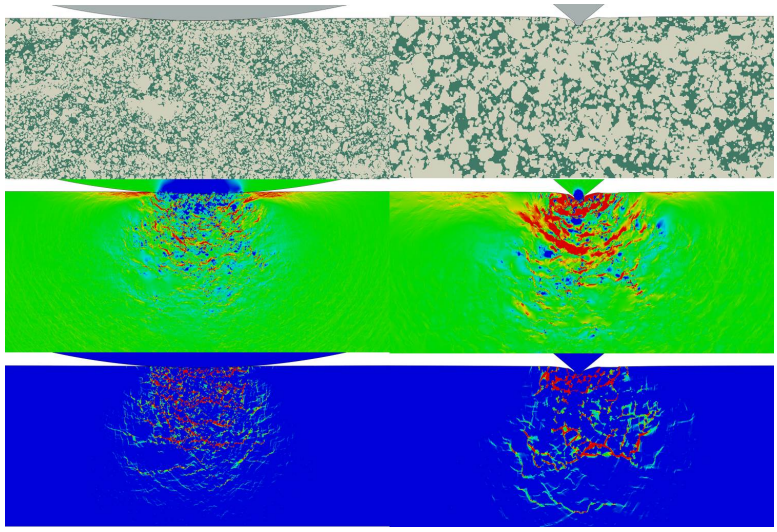

Figure 4.14: Influence of the applied tribological contact and its size scale on the stress-strain response: material distribution (top, the microstructures are both identical), contours of the first principal stress (middle) and contours of the equivalent plastic strain (bottom).

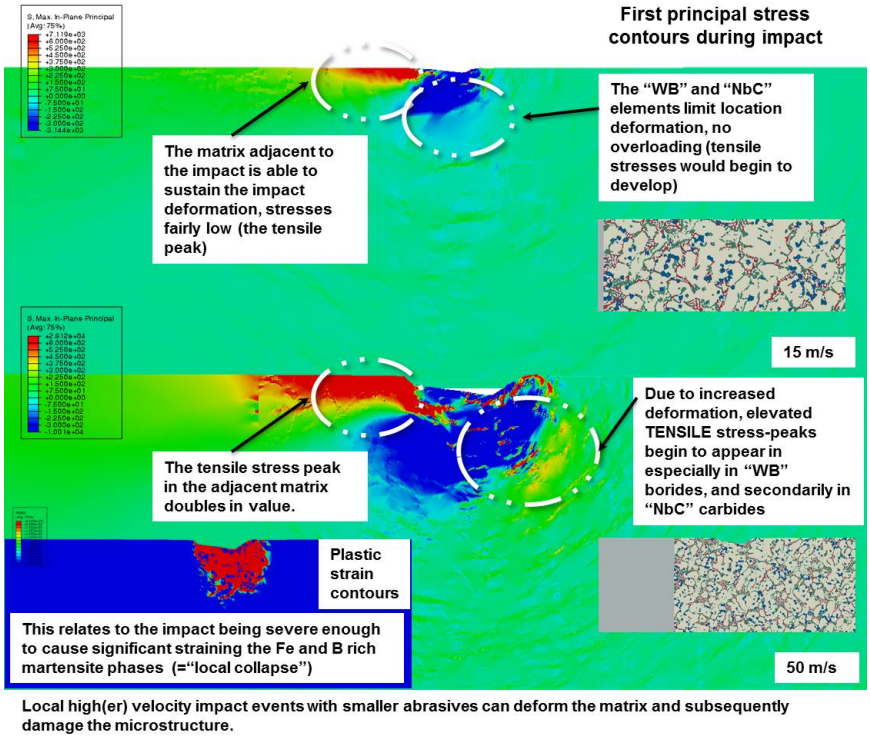

Figure 4.15: Influence of the erosive contact velocity on the response of a martensitic binder and carbide and boride composite microstructure (Suhonen et al. (2017)).

The nucleation, growth, and overall influence of the defects on the behavior of coatings and composite microstructures is depicted in the results presented in Figures 4.16 and 4.17. In Figure 4.16, the crack nucleation and propagation have been computed employing the Extended Finite Element Method (XFEM), as outlined in Holmberg et al. (2014a)). The benefit is the possibility of modeling both nucleation and propagation within the phases of the composite microstructure, although the computational cost is considerable. To lessen this cost, a submodel of a scratch test simulation was utilized to investigate the specifics of the defect evolution. The whole domain is specified as a possible source of defect nucleation utilizing a CZM approach. The mechanism depicted was such that the crack nucleated from an "oddly" shaped dissolved pair of carbides and also nearby from the Co binder and, in particular, the dissolved "throat" between the two carbides nucleated the defect. The crack evolved through the microstructure toward the surface, through both the binder and the carbides, occasionally arresting at the interfaces and finding easier ways for example by cracking adjacent carbides for further propagation. Similarly, local regions with high contents of Co acted as favored crack propagation pathways. Ultimately, the crack penetrated the surface interacting with the tensile stress field trailing the scratch test tip. The results in Figure 4.17 demonstrate the significance of thermal spray coating defects in the single phase Cr_2O_3 microstructure. The splat boundaries, cracks within the splat regions, and clusters or larger pores are seen to act as microstructure scale defects during tensile testing of the SVE.

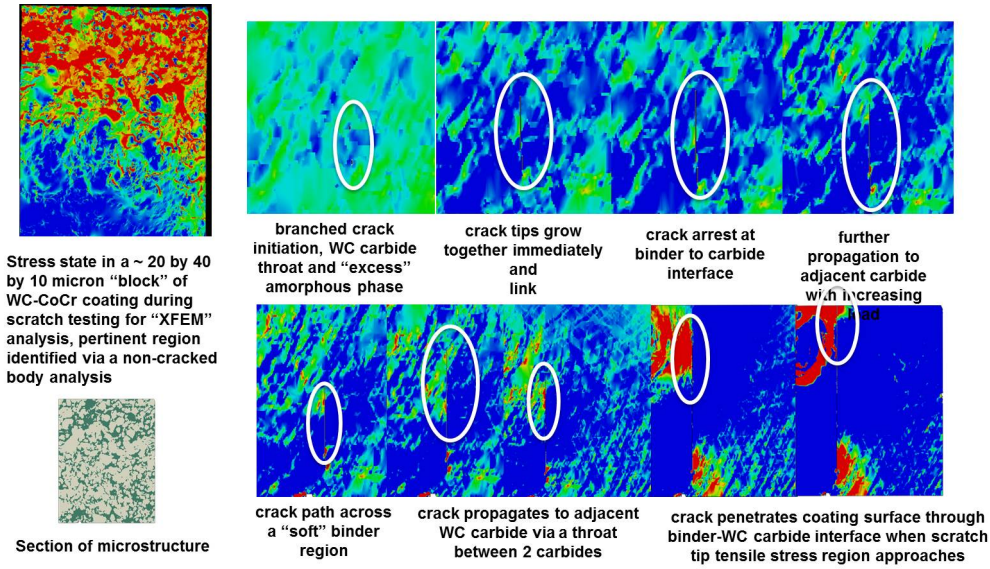

Figure 4.16: Sequence of crack initiation and growth through a WC-Co thermal spray coating (Holmberg et al. (2014a)).

In Figure 4.18, a set of analyses is presented where the behavior of different microstructures is evaluated statistically. The failure model as presented in Holmberg et al. (2014a) was utilized for the carbides along with the strain based criterion for the binder phase. This enabled the computation of the failure rate of, e.g., carbides with a specific stress state, which can be further utilized as an indicative wear rate in the comparison of different microstructures and their details over the SVE (failure rate within a specific feature of

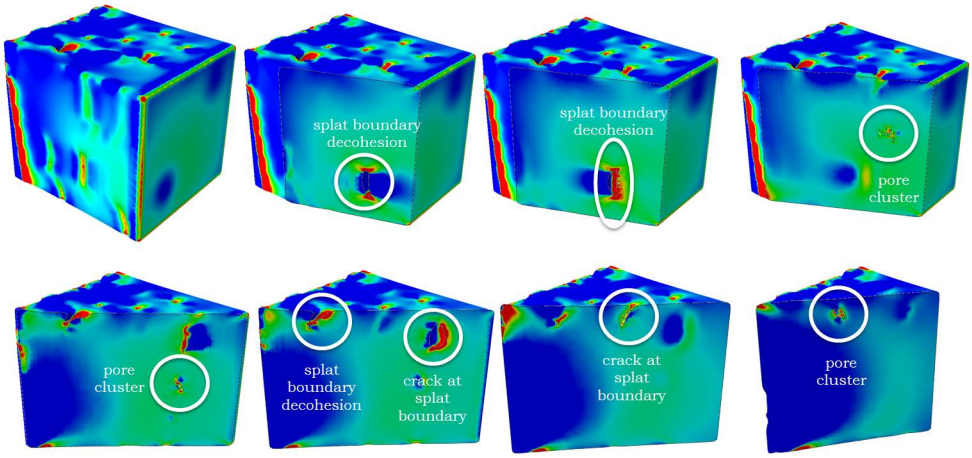

Figure 4.17: Influence of the microstructural defects in a Cr_2O_3 TS coating on the distribution of the first principal stress within the microstructure (Laukkanen et al. (2014)).

the microstructure). Comparison of the microstructural behavior and different load cases provides insight into the functionalities of the coatings in resisting the tribological contact. The first result in Figure 4.18a is the "reference" WC-CoCr coating studied already in many of the previous works with respect to its indentation and scratch test behavior. Upon investigating the microstructure scale behavior in more detail, it was observed that for the near surface microstructure the response of the microstructure was far from uniform. Large carbides appeared to exhibit greatest stresses making them prone to cleavage, followed by "sharp" features or corners of smaller carbides, while smaller carbides embedded more evenly with appropriate MFP in the Co binder exhibited the lowest stress state. The laser cladded WC-Ni coating of Figure 4.18b behaved similarly, although the scatter in the outcome of the studied contact case was greater, some carbides exhibiting greater loading than others. The scatter was investigated in more detail for the laser cladded system, and the results are presented in Figure 4.18c. The study constituted more contacts to obtain an estimate of the significance of the larger carbides and the exposed Ni based binder of the microstructure. The results demonstrated a size dependency, i.e., if the binder was exposed to the contact, the result was unfavorable to the microstructure, but if a large spherical WC carbide was contacted, the microstructure responded well to the imposed loading. WC-CoCr coatings with different WC size distributions are presented in Figure 4.18d with respect to the utilized failure metrics, showing better outcomes with microscale carbides. In Figure 4.18e, the findings with respect to the size of the contact are presented, showing the ability of a very small diamond tip to influence the response of the WC-CoCr microstructure and the outcome of the test. As a final note, an observation was made with respect to the different size carbide models and how this influences the load carrying capability of the coating, as presented in Figure 4.18f. The ability of the micronscale microstructure to support the applied loading to a greater degree over the other microstructures also transferred larger stresses to the WC-CoCr-substrate interface, where the submicron scale carbide microstructure was the best by this metric. This indicates that multiple criteria are necessary for the design of microstructures and that the activation of specific failure micromechanisms is an intricate process.

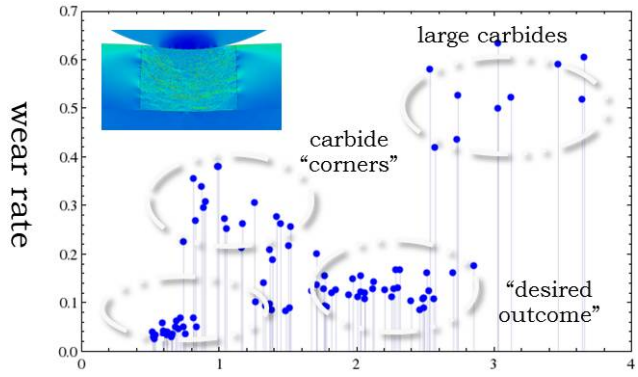

(a) WC-CoCr thermal spray coating undergoing indentation.

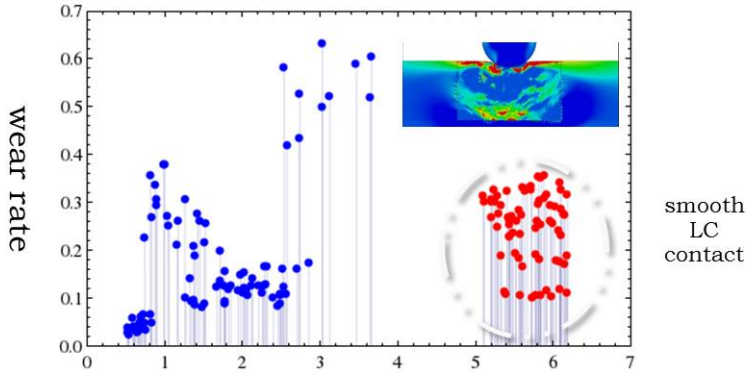

(b) WC-Ni laser cladded coating undergoing indentation.

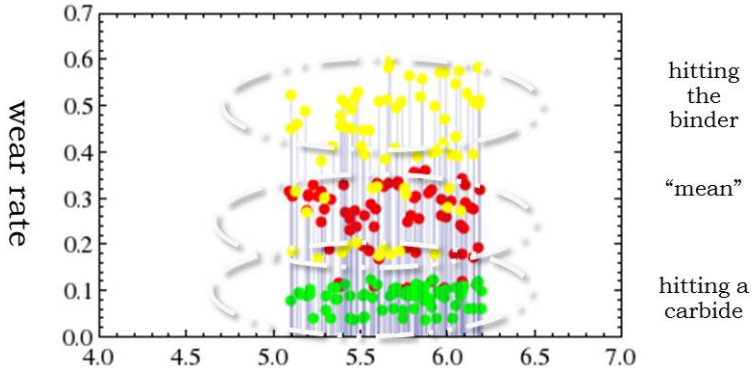

(c) WC-Ni laser cladded coating undergoing indentation in the different regions of the microstructure.

Figure 4.18: Comparison of the indicative wear rates for different hard material coatings under indentation.

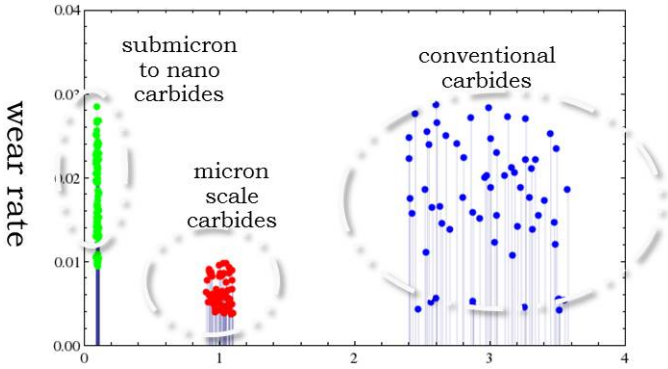

(d) WC-CoCr thermal spray coatings with different carbide size distributions undergoing indentation.

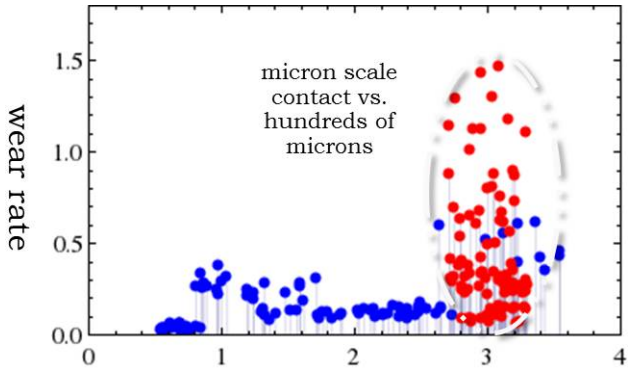

(e) WC-CoCr thermal spray coating undergoing indentation with different size indenter tips.

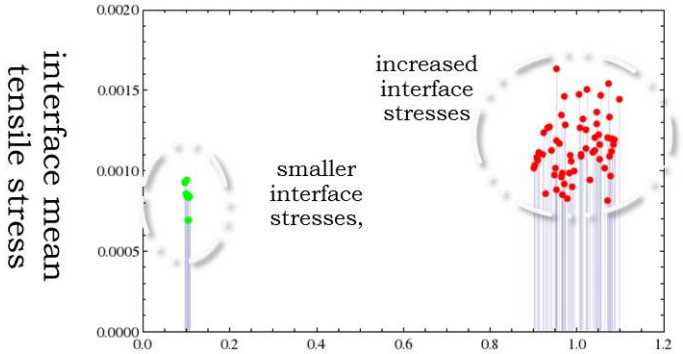

(f) Comparison of the coating-to-substrate interface first principal stress state for two WC-CoCr coatings with different carbide size distributions.

Figure 4.18: Comparison of the indicative wear rates for different hard material coatings under indentation.

4.3 Interfaces in hard material microstructures (Publication IV)

A more complex and realistic treatment of the phase interfaces in the WC-Co microstructures was the novel subject area of Publication IV. The workflow and typical outcome of the thermodynamical PF modeling of interfaces and subsequent FE modeling of the engineering material properties of an RVE are presented in Figure 4.19. Based on the PF modeling of the simplified rapid solidification microstructure, essentially the dissolution of the WC crystal and the formation of a semi-carbide at the WC-to-Co interface, an effective interface model (in this case a multilayered interface) was discretized and the outcome transferred to a three-dimensional RVE, and then utilized to compute the engineering material properties. Due to the differences in the interface composition, the model yielded differing mechanical response when subjected to virtual compressive testing.

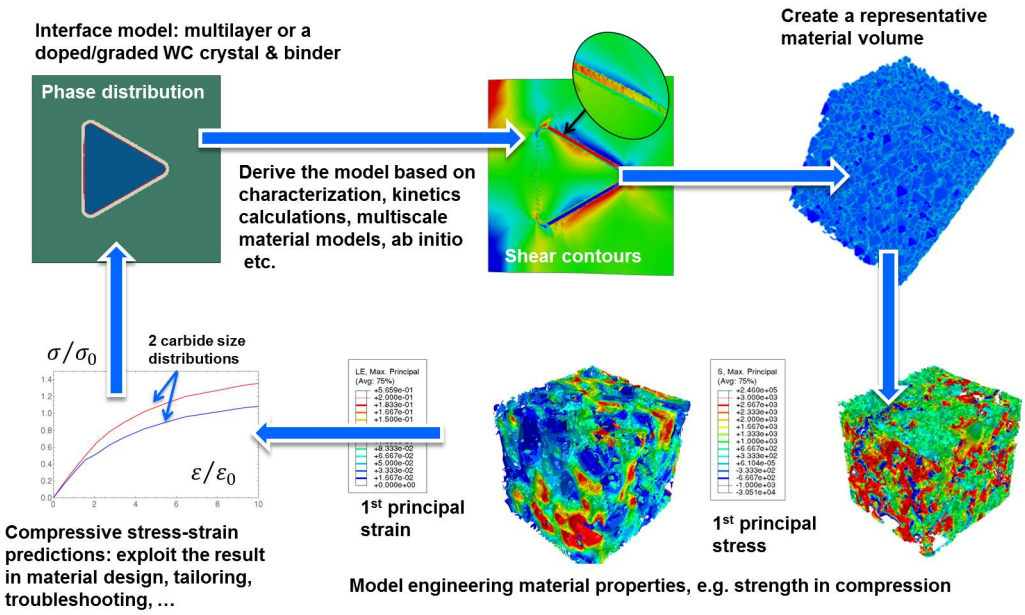

Figure 4.19: Workflow and results of creating an effective interface model for the WC-Co microstructure, and its engineering material properties obtained by linking PF and FE modeling (Laukkanen et al. (2016c)).

An imaging based model generalizing the application of the concept to a larger microstructure in a two-dimensional analysis is presented in Figure 4.20, where a WC-CoCr microstructure was used as an input to the PF model to study the effects of processing on the microstructure. Following the PF modeling of WC dissolution according to a TS relevant thermal cycle, the system was discretized into four phases for the evaluation of its mechanical properties by solute concentrations. Comparison of the analysis outcomes with and without the phases resulting from the dissolution of WC is presented in Figure 4.21. With respect to the distribution of stresses and the load carrying capacity, let alone the deformation mechanisms, the behavior was, as expected, significantly influenced by the incorporation of the brittle carbide phases. This was the result of the large enough phase fractions of the brittle phases in the current analysis case. A more detailed evaluation

of the differences is presented in Figure 4.22. Carbide dissolution influenced the stress state of the microstructure due to the resulting brittle carbide network. Similarly, the possibilities of the Co binder to exhibit "free" deformation were hindered, where regions with larger MFP remained unaffected.

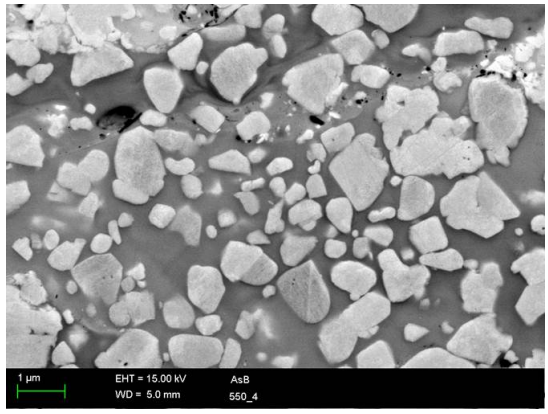

(a) Microstructure of a WC-CoCr thermal spray coating.

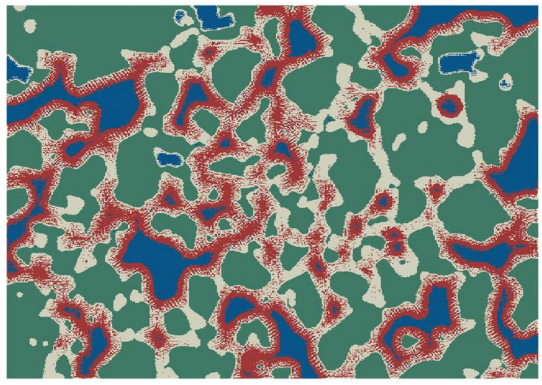

(b) PF simulation result following a thermal spray processing cycle.

Figure 4.20: PF simulation results of a WC-CoCr thermal spray coating (WC (green), Co (blue), and other carbide phases (gray and red)) (Laukkanen et al. (2016c)).

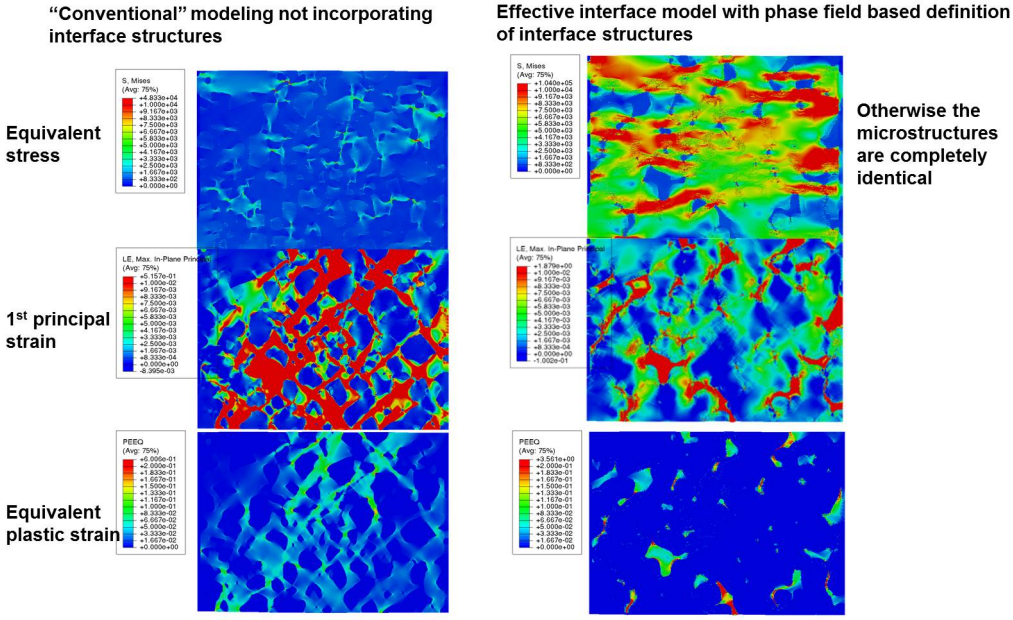

Figure 4.21: Comparison of the behavior of the model without and with interface phase structures (Laukkanen et al. (2016c)).

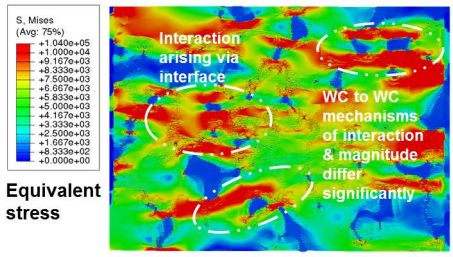

(a) Equivalent stress in the effective interface model of WC-CoCr.

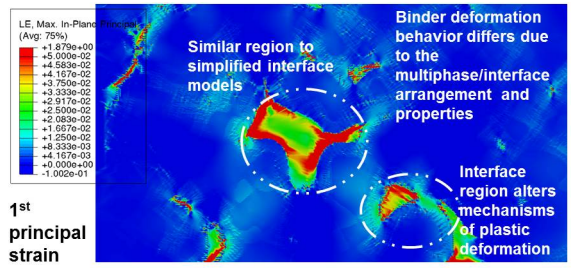

(b) First principal strain in the effective interface model of WC-CoCr.

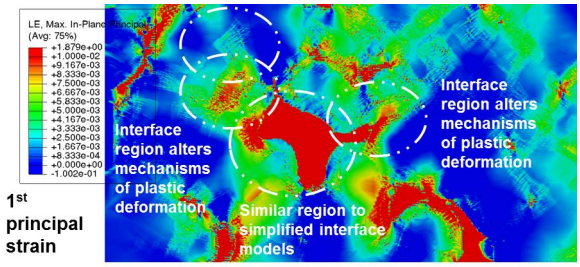

(c) Detail of the first principal strain in the effective interface model of WC-CoCr.

Figure 4.22: Influence of the effective interface modeling on the resulting stress-strain fields in the WC-CoCr microstructure (Laukkanen et al. (2016c)).

Utilization of the PF results in the modeling of three-dimensional RVEs was carried out and the results are presented in Figures 4.23 and 4.24 for the material behavior under mechanical loading. The interface stress fields were greatly influenced by the inclusion of interfaces, since the system is a TS microstructure with a fairly low WC fraction so that plastic deformation can still take place moderately freely within the binding phase. The influence of the rate of cooling is presented in Figure 4.24, showing that it influences the carbide dissolution and formation of the subsequent interphase microstructures. In addition, an "optimal" microstructure was extracted from the PF analysis results, containing a significant gradient around the WC crystal. The "optimality" was considered in such a manner that the interphase did not degrade the mechanical performance of the microstructure but somewhat improved it compared to the constant cooling rate models. On the other hand, neither did it negate the possibility of binder deformations taking place, which otherwise would result in an overall brittle microstructure. Compressive and impact wear behavior was also briefly addressed, with the results presented in Figure 4.25. In the microstructures, the crack nucleation took place primarily at the WC-to-binder interface region with some initiated microcracks propagating and linking, resulting in SVE scale macrocracks failing the entire computational domain. In impact loading with a ceramic ball, the dynamic loading resulted in the formation of a crushing zone and tensile cracks nucleating from the surrounding stress field. In addition, the fracture models as presented in Holmberg et al. (2014a) were applied to the WC-Co system to provisionally evaluate the toughness-strength dependency for the virtual microstructures, as summarized in Figure 4.25.

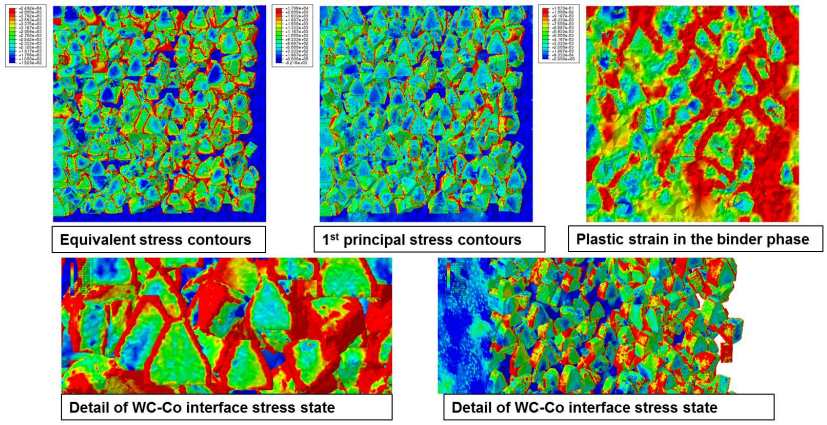

Figure 4.23: Three-dimensional WC microstructural RVE generated on the basis of the PF modeling of solidification and carbide dissolution (Laukkanen et al. (2016a)).

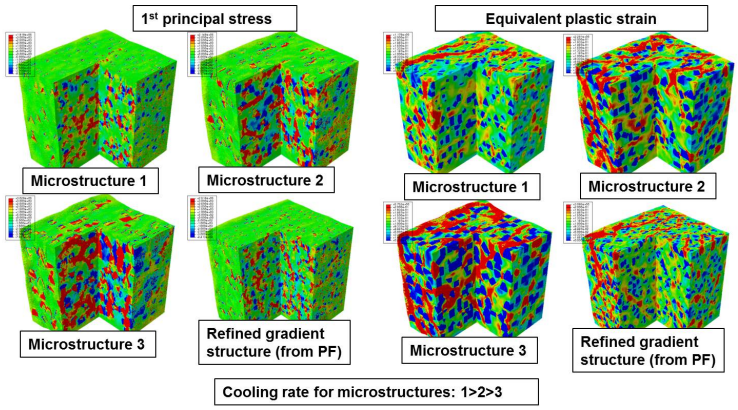

Figure 4.24: Different WC interfaces resulting from different cooling rates in the PF simultion (Laukkanen et al. (2016a)).

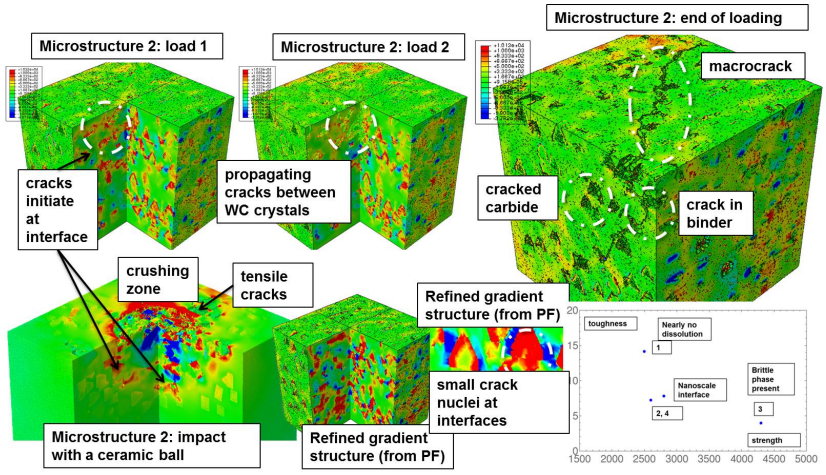

Figure 4.25: Failure behavior of the effective interface modeled WC-Co microstructures under compressive and impact loading (Laukkanen et al. (2016a)).

4.4 Surface roughness effects on coated surfaces (Publication V)

The topic of Publication V was to investigate the influence of surface roughness on thin film contacts. Both smooth-on-rough and rough-on-rough contacts were studied. The films were of DLC type as presented in Laukkanen et al. (2017b), Holmberg et al. (2015) and Wolski et al. (2017). Both anisotropic fractal surfaces and random walk surfaces were created on the basis of surface topography measurements. The first studied system is presented in Figure 4.26, where the results of a rough DLC surface sliding against a rough steel surface are presented. The contact conditions are of local asperity-against-asperity type, the surface area under contact being small, only 10-30% of the nominal contact area. The details of the stress state on the DLC surface are presented in Figure 4.27. A closer investigation of the DLC surfaces revealed that the influence of longer and shorter wavelength surface features was identifiable. The surface had a depression in it, which in Figure 4.27 is under compression, while the somewhat elevated region was subjected to tensile stresses. The small scale surface roughness, essentially the "random" noise present locally, was noted to affect the behavior within the larger features, which were actually grinding groove marks. The stress state magnitude was in the order of gigapascals, and an immediate overall observation is that the explicit incorporation of surface topography drastically influenced the contact analysis result.

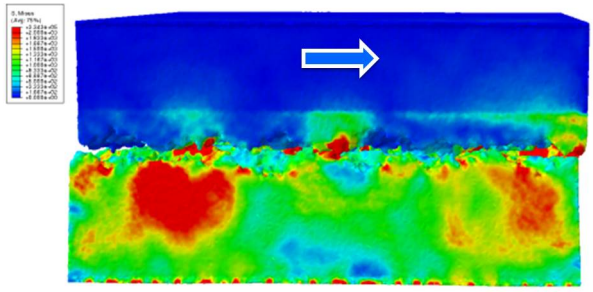

(a) Contours of equivalent stress.

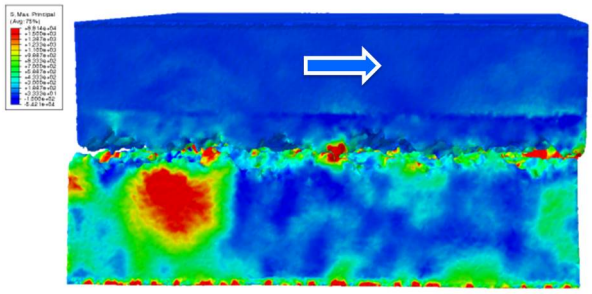

(b) Contours of first principal stress.

Figure 4.26: Modeling of a sliding rough-on-rough contact of steel against DLC (Laukkanen et al. (2017b)).

In addition to the most complex rough-on-rough contact scenario, somewhat simpler anisotropic fractal surfaces were generated and the sliding contact response computed against a smooth counterface at different orientations. The results for smooth, "average"

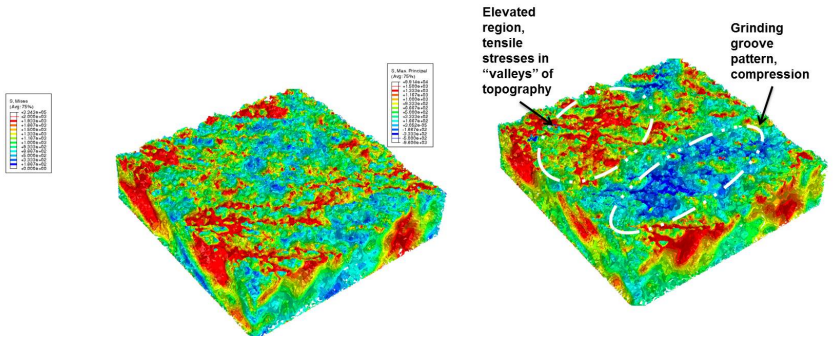

Figure 4.27: Stress state on rough DLC surface, equivalent stress (left) and first principal stress (right) (Laukkanen et al. (2017b)).

and rough surfaces, as defined in Laukkanen et al. (2017b), are presented in Figures 4.28 through 4.30 for different orientations of sliding relative to the anisotropic fractal surface grinding marks. First, the first principal stresses for all three surfaces are presented in Figure 4.28 for the case where the sliding contact takes place parallel to the grooves. It was observed that the stress field was influenced by the groove markings, the local fractal surface characteristics (higher order terms of the surface roughness), and the absolute magnitude of the surface roughness. It was also noted that the overall magnitude of roughness influenced the stress state and its distribution. For the smooth surface topography, the maxima of tensile stresses were produced within the scratch grooves between the asperities. For the average roughness, the asperity peak was under compressive stress, and the maxima of tensile stress were found at the sides of the asperity close to the region where the contact separated from the surface. The behavior was somewhat similar to that observed for the trailing region of the contact for ideally smooth surfaces. For the roughest surface, this behavior was even more amplified, i.e., the asperities resisted the deformation in the sliding direction parallel to the grooving, and significant tensile stresses arose within the asperity sides. As far as the magnitude of the stress state was concerned, the introduction of greater surface roughness yielded a greater magnitude of tensile stress, the reasons being the somewhat smaller contact area and the fact that bending stresses are also introduced. The stress state maximum increase is of the order of 50% from the smooth to rougher surfaces. The influence of the orientation of sliding is presented in Figure 4.29. With a 45° orientation, it was observed that the stress field was disturbed by the fact that sliding did not take place parallel to the groove marks. As a result, the first principal stresses remained similar or slightly decreased, the influence of the bending component increased, and the overall material volume under higher stresses decreased significantly. With the angle of sliding set to 90°, the behavior was again different. In this scenario, bending of the asperities remained quite unchanged, the stress state increased in value, but now the grinding grooves began to act like notches on the surface, yielding a new tensile stress peak around the roots of the multiple asperities. The distortion of the stress field can be seen as a positive characteristic as far as the tensile stress field is concerned, while the asperity roots acting as stress concentrations suggests another possible failure mechanism and that the behavior of rough surfaces can be highly dependent on the orientation of loading and sliding relative to the greater surface roughness anisotropies. It is apparent from Figure 4.30 that the behavior is also similar for average roughness surfaces. Since the stress state in the average roughness surfaces is,

at the 90° orientation, even greater than for the rough topography, this suggests that the dependencies between the different deformation mechanisms in relation to the surface topography can yield interactions resulting in a complex stress state, where the causal relations between the surface roughness, material properties, and coating thickness related parameters can be nontrivial.

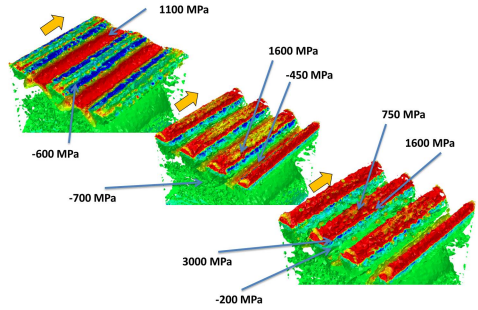

Figure 4.28: First principal stresses on the surface of a smooth, average, and rough DLC surface topographies (Laukkanen et al. (2017b)).

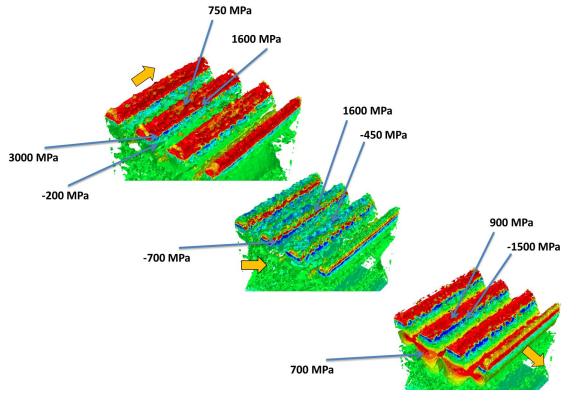

Figure 4.29: First principal stresses on the surface of a rough DLC surface topography at different angles of sliding (Laukkanen et al. (2017b)).

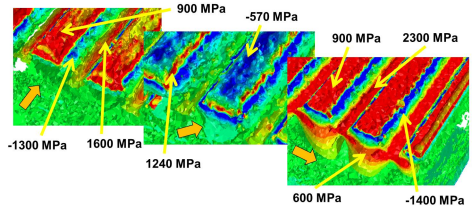

Figure 4.30: First principal stresses on the surface of an average roughness DLC surface topography at different angles of sliding (Laukkanen et al. (2017b)).

5 Discussion

The following sections address the primary results of Publications I-V. The developed methodologies and their implications to the understanding of the behavior and design of tribological systems affiliated with thin films and composite coatings are discussed. The ever critical validation activities are addressed briefly with respect to the main findings. A more detailed treatment of this topic of paramount importance is performed in the accompanying papers and affiliated experimental works, which largely focus on the development and application of the multiscale materials modeling methodologies. As closure, some general words regarding ICME in tribology are provided. Further discussion is provided on validation aspects. The scope of the research questions 1 and 4 are further discussed in Section 5.1, particularly Subsection 5.1.1 for the question 1 and Subsections 5.1.2 and 5.1.3 for the question 4. The research question 2 related to microstructural and micromechanical modeling is addressed in Section 5.2 and the research question 3 in Section 5.3.

5.1 Design of thin films

5.1.1 Optimizing coating-substrate systems

The results demonstrated foremost that tribological performance is a system property. In the current work, this was addressed by quantifying the behavior of different computational thin film designs both with respect to applied loading (used as a measure of load carrying capacity) and versus the damage that the specific loading condition introduces in the tribological system. The loading was selected in the current case to be representative of the reference coating developing its first through cracks, i.e., the initiation of damage to the degree that permanent failure can ensue. Since different cracking mechanisms can be introduced into TSL, albeit always with concerns whether the physically correct failure mechanisms can be captured, the basic failure mechanisms involving cohesion and adhesion as well as their implications to the material performance can be extracted. The results provided direct insight into how changes in the coating characteristics influence both the load carrying capacity and the damage accumulation in sliding abrasion contact conditions. The results indicated that greatly mismatching coating systems are to be avoided, i.e., systems containing both extremely hard and soft coatings or layers. Hard films suffered more easily from damage, while the softer ones avoided damage initiation but easily lost their load carrying capacity. Gradient and multilayer systems enable improvement of the film performance and optimization to particular contact conditions, as was indicated by the multilayer system tailored to match the stress distribution over the coating thickness, yielding a significant decrease in damage while still being able to carry the applied loading. In addition, even simple linear gradients within the multilayer, improving the top surface rigidity and matching the bond layer and/or substrate better,

were improvements over the homogeneous film. Moreover, the use of abruptly different bond layers to arrest the propagation of damage, or to build different damage containment mechanisms within the system, are apparent possibilities. Overall, although the number of parameters in a typical thin film system appears to be somewhat limited compared with those of a composite microstructure, a great degree of property variability can still be obtained by systematically tailoring the system to meet the requirements of a specific tribological loading scenario. Again, of course, the best use of the modeling framework and the identified trends is to begin considering multiple variables simultaneously and begin working toward global optimization of the tribosystem, which was still outside the scope of the present work but is an important future topic. A large hurdle also still exists in making the analysis means truly multiscale and to begin the incorporation of atomistic information into surface physics, chemistry, and interface behavior.

5.1.2 Influence of surface topography and orientation on friction and wear

The explicit introduction of the surface topography in modeling enables to study the interactions between the microstructure and the surface topography, including the microstructural behavior of the film, the entire coating solution, and the substrate material. Although the current work had significant experimental support all the way from the production of three different surface roughness DLC surfaces as outlined in Holmberg et al. (2015), it was established that similarly to microstructural modeling, a toolset enabling different ways of treating the surface data would be in order. Thus, the datasets can be statistically sampled to create further 3D representations of the surfaces, or, as in the present case, the possibility to use fractal data (Wolski et al. (2017)), and an anisotropic fractal approach can be utilized to describe the surface quality. This again has the merit that complex and realistic surface topographies can be systematically modeled and the fractal parameters and surface roughness systematically altered to investigate the dependencies between the surface character and the tribological surface performance. Since the methodologies link to the microstructural modeling toolset, the incorporation of features such as surface defects can be performed in a straightforward manner.

The observations of the stress-strain fields indicated that an orientation dependency exists. The dependencies can be interpreted in a straightforward manner by tracing the progression of the contact sliding across the roughness peaks and how the surface roughness "disturbs" the formation of the stress-strain fields in comparison to an ideal surface (particularly the grinding grooves which were prominent on the surfaces of the present study). This was particularly true for a contact sliding at a 45° angle relative to the grinding marks, when the contact differed most from the ideal, indicating possibilities for tailoring the surface texture and exploiting the surface topography to improve the wear resistance. The implications related to the microstructure-to-topography interactions are still largely beyond the scope of the current work, but are certainly a future topic of great importance in enhancing the exploitability of modeling. In addition, in the current cases, the isotropic fractal component was noted to be significant for the local stress-strain state (shorter wavelengths in the surface representation), although the principal behavior was dominated by the grinding grooves (longer wavelengths). Thus, these features are certainly not insignificant especially considering the nucleation of defects and if coating imperfections are included. Frictional effects are also expected, although the experimental results by Holmberg et al. (2015) do not provide a baseline for a more detailed assessment. With respect to the contact areas, the apparent contact areas in

different computed contacts were of the order of 15-30% of the nominal contact areas, which can be considered an expected number based on the classic works on rough-on-rough contacts, such as presented already by Bowden and Tabor (1950).

5.1.3 Interactions between surface roughness and coating wear performance

The fractal signatures were utilized in quantifying the surface roughness across several scales, the benefit of the methodology being the ability to include characteristics from the sub-micrometer range all the way to the millimeter scale depending on the respective experimental input. The signatures, particularly the anisotropic orientation texture and directionality, were found to be responsible for the observed stress-strain response. An interesting aspect for further work is the possibility of linking these structural and topographical parameters to the resulting contact response, i.e., the stress-strain fields. This necessitates the generation of further analysis cases, and their analysis in a data-centric manner due to the statistical nature of the output, especially if the isotropic fractal component has a greater influence. However, as the correlations are largely local, surface roughness arises as another parameter contributing to the local stress-strain fields critical to the tribological performance of thin films. A rough comparison of the contributions to the first principal stresses between the analysis cases indicates that in the studied DLC films, local roughness affiliated features influenced the outcome by $\leq 40\%$. This again is of an order which can certainly influence film performance, for example with respect to the initiation of cracking mechanisms, but somewhat smaller than the principal variables influencing the coating design such as the elasticity of the multilayers and film thickness. The differences in the stress states arising from the different surface roughnesses and orientations of the loading ranged overall from 20% all the way to 200%, particularly when comparing rough surfaces and a loading orientation not parallel or perpendicular to the anisotropic surface fractal. These differences can be largely understood by considering the surface "stiffness" relative to the loading orientation, also considering whether this yields a membrane or bending type of stress-strain response in the thin film. This also correlates with the observations of non-symmetric cracking patterns, the membrane like stress state induced by loading parallel to the grooves being able to yield an almost four times higher magnitude of stress compared to the perpendicular loading resulting in groove bending.

5.2 Design of composite coatings and microstructures

5.2.1 Microstructural modeling and wear resistance

The current work deals largely with wear resistance, i.e., it focuses on the features and characteristics of the microstructure considered attributable to wear behavior, but the actual cumulative wear process or the formation of large scale material defects are considered only to a limited extent. Thus, conclusions are drawn primarily focusing on the characteristics affecting the initiation stage of wear damage and cracking with respect to micromechanical processes. As such, wear is considered to be correlated with the formation of defects locally within the microstructure which, while operating at the respective spatial scales, can be attributed largely to local stress-strain conditions. Such arguments are, of course, supported by the work carried out in Publication I for thin films (CZM cracking modeling) and in Publication III for composite microstructures (CZM and XFEM modeling of composite coating failure). In any event, the interpretation of the

stress-strain fields in the assessment of the beneficiality or criticality of a certain material feature to wear needs to account for the respective micromechanisms of failure. Even if more complex and explicit criteria are utilized for the initiation and propagation of damage and defects in numerical models, the same argument applies and typically the formulations are similar as far as the physics based complexity and micromechanical background are concerned. Thus, the argumentation for drawing conclusions on the results with respect to wear performance is largely based on the understanding of the micromechanisms of failure and their continuous comparison with experimental observations. For example, for the composite coatings, it can be stated that the work carried out largely relies on the presentations of the failure mechanisms as shown in Figure 5.1. The principal failure mechanisms and implications arising from the stress-strain fields that are to be considered of relevance when interpreting the wear resistance are cracking of the brittle phase (carbide cracking), failure of the ductile binder, failure at composite interfaces, and initiation and growth of failure by way of pre-existing defects such as porosity and cracks. Also, the findings are inferred primarily from the causal relations between microstructure and the following material properties and wear resistance, more elaborate approaches to design and steps for their development are briefly addressed in Section 7.

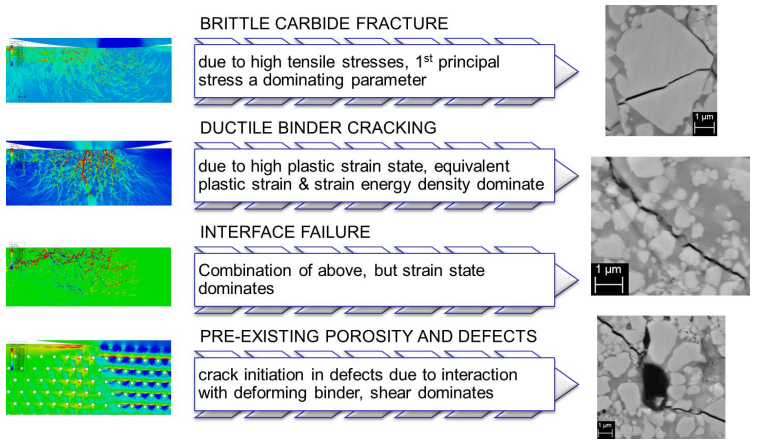

Figure 5.1: Basic failure mechanisms of hard material coating microstructures manufactured by TS (Holmberg et al. (2014a)).

According to such a micromechanistic assessment, the significance of the basic engineering material properties and coating microstructural parameters with respect to wear resistance was evaluated in Publication III, and is presented in Table 5.1. Since the design space of tribological systems in the spatial scale of material microstructures has been found to be extremely vast, it was construed that overall estimates could still be provided to yield guidelines regarding the significance and reasoning underlying the selection of certain key parameters for the kind of hard material composite systems studied in the current work. The outcome is grossly simplified in comparison to direct modeling results and their detailed analysis, and the parameters are by no means unique, but it does provide a baseline of how some of the typical engineering parameters associated with composite microstructure influence the outcome with respect to wear resistance. With respect to the binding matrix, the engineering property found to be of high relevance is the hardness as a measure of elastic stiffness and the material's ability to exhibit plastic deformation. The material solution specific tailoring of the binder properties relative to the hard phases is

one of the characteristic features to consider when designing a wear resistant coating, as long as the properties such as the phase fractions are simultaneously accounted for. The hardness of the reinforcing particles is another typical property considered critical to the wear resistance of coatings and essential for the basic requirement of producing a coating where the accumulation of plastic deformation and material damage are limited as a result of the cyclic loading appearing in a tribological contact environment. However, particle hardness is a key parameter when assessing how the microstructure functions during the tribological contact. Too large internal mismatches in the deformation exhibited by the system are likely to promote local modes of failure and the beneficial properties of individual phases may be lost. An argument can also be made regarding the excessive performance of the material solution due to the hard phase(s) and its contribution to the cost of the material solution. Particle size and MFP are crucial parameters, since they also contain information about the phase volume fractions according to the adopted definitions. Scale dependencies, such as those arising from nanostructural deformation or microstructural mechanisms (e.g. Geometrically Necessary Dislocations (GND)) in the microstructure of the binding phase) are outside the scope of the current work but a definite future topic of research. The prime parameters in this sense are the distribution and size of the hard phase relative to the tribological contact, the former deciding whether the surface is wear resistant enough and protected against cyclically induced damage, and the latter determining whether the scaling and distribution of the hard phase provides the surface with the necessary deformation mechanisms in the tribological application at hand. In this respect, tailoring of the particle size distribution and MFP leads to the same outcome, i.e., shielding of the binding material from tribological contact in the cases when it can induce damage in the respective phase while retaining deformability of the entire system to satisfy the requirements arising from the tribological contact (for example with respect to the load carrying capacity). The basic design of a tribological system can be argued to revolve around these two to some extent conflicting criteria. Particle size and MFP are variables that provide the means to adjust these interactions, influencing the particle-particle interactions along the way. Moreover, the strengthening effects arising from the nanostructures or complex metastable phases are to be kept in mind. Particle morphology is a characteristic influencing the microstructural layout on one hand by way of packing characteristics, but largely also due to the fact that complex morphologies would, based on the image based modeling results, appear to influence the defect initiation and further propagation considerably. Thus, one could argue that well defined and “primitive” morphologies are favored, although this may decrease the possibilities to obtain proper shielding of the binder and/or high volume fractions and packings when necessary. Again, morphology is only one of the geometric characteristics, the strength and toughness properties of a particular hard phase providing additional constraints or possibilities in terms of exploiting a certain hard material phase. Partly overlapping with the above is the role of the MFP in developing a wear resistant microstructure for a particular application. MFP is a somewhat better parameter compared to, e.g., phase fractions, since it includes behavior characteristics of both the hard and binding phases. The determination of a suitable MFP is typically a question of being able to utilize the surface protecting characteristics of the harder phase(s) by selecting an adequately small MFP value relative to the tribological contact. On the other hand, for hard material structures to be able to exhibit a good degree of deformability, it is often wise to attempt to obtain a MFP which is only as small as necessary for the particular purpose, i.e., to retain the maximum (or at least sufficient) toughness of the microstructure, while still having enough load carrying capacity (or “hardness”) to produce a strong enough surface to resist the plastic deformation. Cracks, defects, and clusters of particles (or aggregates of

Table 5.1: Effects of various coating characteristics on the wear resistance represented qualitatively (adopted from Holmberg et al. (2014a)).

	Effect on stresses	Effect on strain	Comment
Matrix elasticity	+	+	If matrix is able to experience plastic deformation
Matrix hardness	++++	+++++	If matrix is able to experience plastic deformation
Particle elasticity	+++++++	+	Assuming hard particles relative to binder
Particle hardness	+++	++	Assuming hard particles relative to binder
Particle size	+++	+++	Considering the range investigated[1]
Particle morphology	+++++	++++	Image based modeling based result
Particle clustering	++++++	++++++	Local effects
Mean free path	++++	++++	
Porosity	+++++	+++++	Local effects
Defects[2]	++++++++	+++++++	Local effects

fillers in general) commonly lead to a decrease in the surface wear resistance for obvious reasons of aggravating the local stress-strain state. In some cases, the clusters could be seen as small scale structures increasing the wear resistance, but typically clusters of WC carbides, for example, act more likely as a crack initiation site. Another scenario where for example a pore structure can be of benefit, in terms of the mechanical behavior, is the possibility to activate deformation mechanisms and in this way enable surface wear resistance to increase, a feature which could be within reach, considering tailoring of the microstructural functionalities for specific tribological contacts. Similarly, it can be readily stated that the current studied coating systems and tribological contacts are largely such that the crack initiation and propagation lead to an unacceptable loss of surface integrity. If wear cannot be avoided or steady cumulative wear is a design feature, the significance of the defect structures and overall anomalies in the microstructure would commonly decrease. However, this is again a matter of tailoring the microstructure to suit such behavior by, for example, ensuring adequate toughness by adjusting the binder properties, its distribution or other hierarchical structures, to provide adequate wear resistance to the material.

5.2.2 Stress-strain response of hard material composite microstructures

The main purpose of examining the microstructure scale stress-strain fields and their analysis is to bridge the gap between modeling and experimental observations of failure micromechanisms and to yield knowledge to facilitate the better designing of wear resistant tribological surfaces. The two principally differing hard material coatings of Publication

[1] where scale dependencies were studied in a limited manner
[2] cracks, porosity with high aspect ratio

II yielded examples of how the response of two surprisingly disparate tribological systems with respect to their microstructure can be evaluated. The laser cladded coating with large WC particles and a Ni based binder has a sliding wear performance similar to that of the WC-CoCr TS coating, but the microstructure morphology leaves the binder exposed. This is apparent when considering the material's low abrasion wear resistance, at which point the performance degrades compared to the TS coating with a greater hard phase fraction. However, for sliding contact this is not an issue with respect to the activation of failure mechanisms, as the WC particles in the soft Ni based binder reinforce the surface, yielding a coating which is both capable of load carrying and wear resistant under these conditions. The most critical mechanisms are those which activate plastic deformation and slip localization within the binder, i.e., a tribocontact where the local features can make a significant contact with the binder are critical with respect to binder straining and failure of the WC-to-Ni interface. However, for sliding contacts with larger contact areas, the microstructure and hard phase(s) can function as intended and provide an adequate tribological response. Moreover, under such optimal conditions for this microstructure, it was witnessed (and overall expected) that the frictional response of the coating is suitable for many applications, due to its smaller coefficient of friction in comparison with the TS WC-CoCr coating.

The WC-CoCr TS coating is in many respects similar to the sintered WC-Co structures, except for the somewhat smaller WC fraction and process dependent dissolution of WC to the binding material also influencing the carbide morphologies. The much smaller crystal size and the overall "characteristic size" of the microstructure, as well as the greater hard phase fraction in particular influence the behavior and response of the TS coating under abrasive loadings. The carbides also shield the binder from local contacts, which in most of the studied loading cases leads to a more balanced stress-strain response. However, the strain state of the binder phase can be very large locally in particular when the load carrying capacity of the coating is close and the significance of the defects and other locally abnormal features is greater than in the more "damage tolerant" laser cladded coating. One can argue that this is the result of the greater strengthening obtained by increasing the WC fraction and decreasing the MFP. This increases the overall strength of the system alongside the susceptibility of the microstructure to any local anomalies or features that adversely influence the local stress-strain state. On the other hand, due to the significance of the interfaces this offers increased possibilities for the development of novel hard material microstructures. Considering similar findings in published works, limited modeling studies exist for TS coatings, but some works have been performed for sintered structures explicitly introducing a composite microstructure. For TS coatings, one of the few similar works is that of Bolelli et al. (2015), who studied TS coatings under tribological conditions with 2D imaging based modeling. They identified inclusions responsible for crack initiation and studied the principal deformation mechanisms in microstructures having some similarity to the current work. Kim et al. (2006) utilized two-dimensional models to assess the behavior of simplified hard material microstructures. Their findings link the basic characteristics such carbide shape and microstructural contiguity to the mechanical properties. Saai et al. (2014) studied different WC-Co grades by defining respective RVEs and considering volume fractions and grain size, although only utilizing an elastic multiscale model. Herd et al. (2018) studied the fracture process and were able to reproduce behavior relevant to the current work, such as failure of "sharp" morphologies within the WC grain skeleton. The fatigue response of sintered systems has been studied by Ozden et al. (2016) and Ozden et al. (2015), continuing the earlier work by Chen et al. (2013), linking to the residual stress analyses presented by Kayser et al. (2017).

These works reproduce similar stress-strain response for the WC skeletonal sintered sharp microstructures, differing from the binder embedded WC crystals in TS coatings, but many of the features again affiliated with the stress-strain concentrations and binder responses can still be argued to have similarities. The importance of residual stresses, for example for High Cycle Fatigue (HCF), emerges as a topic for further consideration. Imaging based models of sintered structures have been created by Tkalich et al. (2017a) and used to evaluate the WC-Co hardmetal properties, manually outlining the grain geometries. This approach better identifies the individual WC grains, but does not consider the role of the binder in the sense of finite strain deformation. A tessellation approach was utilized by Tkalich et al. (2017b), which gives away some of the geometric details and morphology of the WC-Co microstructure, but as far as 3D modeling is concerned, it does provide a better basis for considering the interaction between the microstructural constituents and the composite behavior, as evidenced by the results of Tkalich et al. (2017b).

5.3 Interface models for composite microstructures

Treatment of interfaces is a major issue influencing the realism of composite hard material models. As an example, it was observed that imaging based models can in many cases be unrealistic, since the identification of hard-to-binding phase interfaces is not possible. Instead, the deformation is being transferred by clusters and skeleton structures of the hard phase rather than by individual carbides separated by nanometers or less of the binding phase. This influences particularly finite strain predictions, or in practice already limits the possibilities to even predict the stress-strain response beyond yield or to obtain representative yield values. In Publication IV, this was addressed by extending the toolset by linking to the PF modeling of solidification, subsequently capturing the interface structure of a WC-Co microstructure in more detail. The use of solute concentration data from PF enabled the derivation of an interphase region due to carbide dissolution resulting in complex solidification phase structures. Following the development of the toolset, this enables an increase in the design space of the modeling workflow by extending its capabilities toward material process modeling. Although not explored further in Publication IV, more complex property-performance combinations such as wear resistance can be studied with ease. The inclusion of interface characteristics was found to be very significant, although some of the examined cases were rather extreme, with a significant degree of carbide dissolution. However, the addition of the semi-carbide phase was found to drastically change most aspects of the deformation behavior of the hard material composite. The introduction of the carbide network and the dendritic skeleton structure impacts the basic mechanical behavior and, in addition, any further failure metrics, as evaluated for example in Publications II and III, would be significantly influenced. The solute creates a finite layer around the WC crystals, and typically these complex phases are observed to limit the deformability of the hard material and to degrade the TS coating properties. Neglecting the effects can lead to non-realistic modeling, while their inclusion provides a means to assess the possible detrimental characteristics and design manufacturing processes for the material to better meet its intended application requirements. Overall, it was found that interfacing to PF modeling provides an approach beyond the classic treatment of interfaces and removes one crude approximation due to the added physical aspects of the hard material microstructure.

5.4 Validation

Proper validation can be argued to be the greatest opportunity to accelerate the development of materials modeling solutions. In the following, some specific aspects of the validation of the present models are discussed, the experimental work being presented partly in the referenced separate publications.

5.4.1 Thin films

In Publication I, the validation was quite straightforward and fairly extensive. Relatively simple measurements were compared with the model, such as the scratch depth and width under progressively increasing loading. The models were found to be capable of accurately reproducing the experimental tests, and the baseline models were demonstrated to perform well. This was, however, a quite expected result based on the earlier similar work performed, for example, by Holmberg et al. (2006a) and Laukkanen et al. (2006). A more demanding trial was the utilization of the fracture toughness results to investigate whether the CZM methodology could in its present form reproduce the crack field density as observed in the experiments. The building of the model was largely directed so that the necessary degrees of freedom would be available to track the crack propagation through the thin film. Although the fracture toughness measurements are based on another methodology presented by Laukkanen et al. (2006) with its own validation steps, the CZM modeling was able to produce the experimentally measured scatterband of results for through coating cracking, which is also the most reliable and easily quantifiable experimental result. In addition, through coating cracking is the first coating failure mechanism observed in the experimental tests, although since the observations are often made only after the tests and crack geometries tend to be curved, etc., this has not always necessarily been so obvious. The interpretations regarding the tensile stress states at the trailing edge of the contact including both the membrane and bending stress states, however, yield a great deal of supporting data to that effect. In any event, this gives credence to the further simulations where the model is utilized more in a predictive manner and capabilities such as damage induced coupling leading to stress relaxation are introduced in the modeling approach. Recently, some supporting analyses for thin hard films and coatings have started to appear, also utilizing the CZM techniques, and some similarities can be argued to exist. Lofaj and Nemeth (2017) have observed similar cracking responses at the trailing edges of the contact in the nanoindentation analysis of a W-C coating on a steel substrate, utilizing a FE approach. Coating cracking and interfacial delamination have been considered by Xiao et al. (2015), and a similar fracture pattern demonstrating the interaction of the substrate and the thin film was found with respect to defect initiation. The significance of the substrate plasticity for the cracking behavior has been identified by Rehman et al. (2012), ending up with a suggestion of sufficient substrate strength relative to interface adhesion. A spallation like response has been assessed by Soulignac et al. (2013), where the effects on spallation and the significance of the interface roughness were assessed with respect to the interface damage in thermal barrier coatings. Overall these works demonstrate that the specific observations regarding failure behavior have similarities with respect to different coating systems, where the principal failure mechanisms and active deformation mechanisms are comparable.

With respect to modeling the contact of rough DLC surfaces, similar contact modeling approaches were utilized as before with respect to the scratch test contact. Of specific interest was whether the non-symmetric cracking pattern that was considered to be related to surface roughness orientation could be captured. Especially for the 45° loaded

"average" and "rough" surfaces, a cracking pattern was found to emerge only on the other side of the scratch, which was a clear observation of interest to study with rough contact models. The modeling results showed that a difference of approximately four times existed in the first principal stresses between the two sides of the scratch groove, an observation that is in line with the experimentally observed crack densities. In addition, the lowest stress state in the models was again observed for the 45° sliding direction, and the highest critical load recorded in the experiments matched this finding. However, overall the analysis of the results accounting for the experimental scatter and statistical nature of the modeling results complicates the evaluation, and in the future, for example, the creation of larger numerical data masses for the assessment is definitely recommendable.

5.4.2 Composite coatings and microstructures

In Publications II and III, the validation activities were pursued both quantitatively and qualitatively. The models were either indentations or scratch tests, and quantitative comparison showed a fair agreement between the microstructural models and experiments. Qualitatively, tests such as pin-on-disc and rubber wheel tests produced rankings which were comparable to the modeling results. The wear mechanisms could also be inferred and ranked based on the micromechanical modeling. The work in Publications II and III largely employed 2D modeling, which was a challenge for all validation activities, while at the time of preparing Publications IV and V, 3D approaches became available and are also hoped to significantly ease the validation activities in future works.

In Publication II, validation of the basic behavior regarding deformation and cracking behavior was pursued, despite the challenges arising from the 2D modeling. The indentation and scratch test response can be considered more quantitative, while for tests such as rubber wheel and pin-on-disk, qualitative assessment of the results against the modeled contact conditions was tested, i.e., whether observations concerning the ranking of the test cases and microstructures could be inferred from the microstructural model outcomes. Gross simplification of axisymmetricity was made in the comparisons when required, especially to be able to make a direct comparison with the indentation results. However, even such simplifications were deemed acceptable due to the overall importance of being able to perform any possible degree of validation. For the indentation of the WC-CoCr coatings, the computational results were approximately 20% off from the experimental mean value, a finding considered promising since in this case a more limited number of test cases was available for the comparison of modeling and experiments. For the laser cladded coating, the difference was <5%, most likely indicating that the microstructure is more approachable by the current modeling technique and that the larger dimensions also aided in the characterization tasks, further contributing to the input data quality. Regarding scratch testing, the values of the stress states for loading conditions comparable to the experimentally observed crack initiations were in line with the values obtained from the fracture toughness testing of the WC-CoCr coating (which was established analytically). These reference values are based on indentation fracture toughness measurements, although the degree of experimental scatter is also notable in these tests.

5.5 Development of ICME for tribology

The current work produced an abundance of experience related to the application of micromechanical modeling to tribological problems, which were all based on existing or

future practical applications. This yielded invaluable information regarding what kind of modeling functionalities and approaches actually add value and contribute to the solving of tribological challenges. Although the current work does focus on tribological problems, it is foreseen that the methodologies utilized, e.g., in generation of microstructural models, can easily see uses in the ICME realm beyond the scope of the current work, for example, in overall modeling of numerous mechanical phenomena at the scale of various material microstructures.

One clear notion was the necessity to develop a flexible and easily adaptable modeling methodology. Single analysis results are of definite value, but the most practical value of the work arose from the study of the trends related to a larger range of relevant parameters. This also aids the validation processes, since the limits of models and outright anomalies are easier to identify. In addition, the pairing of synthetic[3] and imaging based models was seen to be clearly beneficial. Even very simplistic modeling approaches were found to add value and produce results that supported the interpretation of the results of more complex and realistic models. The HPC requirements of many of the models are severe, i.e., computational cost is a limiting factor in utilizing the more complex workflows and with respect to inclusion of further material and more elaborate model information, but this is not foreseen as much of an issue due to ever greater access to computing hardware (the current work was performed utilizing in-house HPC capabilities). Although a future step is to develop better modifiable models and global optimization routines applicable to microstructures, at present one of the best approaches is to utilize parameterized synthetic models to investigate the causal relations between the structure, properties, and performance of materials. Since several synthetic approaches can produce quite realistic representations of the actual microstructural morphologies of materials, this approach is favored together with imaging based models that attempt to produce the best possible estimates for material behavior. A feature that has matured over the years and also within the toolset development of the current work is that model generation steps such as the development of the meshing solutions no longer occupy resources to the same degree as before, enabling more emphasis and effort to be placed on the refinement of describing the material features and behaviors.

A topic to consider further in the future is defects and their evolution. This means especially the development of micromechanical analysis capabilities where fully coupled treatment of defects is included. This, along with the somewhat easier weak discontinuity problem of complex phase-to-phase interfaces and interphases naturally makes the problem truly multiscale in nature in the pursuit of respective constitutive models and physics-based parameterizations. However, CZM, for example, lends itself to the development of damage models that can be generally applied to microstructural problems. The additional challenges are more likely to arise e.g. from the necessities of treating multiple material hierarchies, where approaches such as scale dependent crystal plasticity become necessary. In addition, implicit FE methods apply rather badly to moving interface and defect evolution problems involving strong discontinuities.

With respect to the development of microstructural modeling capabilities, the resolution of the present methodologies is largely sufficient, and the challenges deal with computational efficiency, definition of input parameters (especially small scale and with respect to interfaces), and how to effectively parallelize the computational approaches. In addition, new strategies are required for scale bridging, be they concurrent between macroscale and microscale, or merging the microscale and atomistic scales, current paradigms

[3]or stochastic

are insufficient and can degrade the quality of the numerical solutions. A common example is the errors and non-physical behavior in the solution arising from the coupling methodologies themselves.

Regarding ICME for hard material composite microstructures, the PSPP concept was deemed a workable overall structure for the microstructure design and for inferring the causalities leading to the material properties and tribological performance. The problem can be roughly divided into two as far as the approaches are concerned, i.e., working with the process modeling aspect or with the properties and performance arising as a result of a specific microstructural morphology and its behavior. The structure-to-properties problem is the most straightforward to solve, while the performance aspects already require a degree of refinement and modification as far as being able to, for example, resolve the tribological contacts with microstructural modeling and ensure that it is descriptive of the actual experimental conditions. Inclusion of the processing aspects is a great benefit, since it completes the digital workflow and design chain and provides a direct link to the alloy and manufacturing process design, which are crucial steps considering how one ends up with the microstructure and what its specific characteristics actually are. This again adds to the complexity of the workflow, since the process models tend to be either very simplistic or highly derived, even by themselves. All these efforts aim at grasping causalities, and while they are already capable of producing immense amounts of data, the exploitation of the data and its detailed analysis to work efficiently in a multi-dimensional design space are future challenges. Although even causal relations significantly improve the capability to design tribological material solutions, the vast design space that appears at every stage of the PSPP approach can only be tackled once methods such as ML and AI are introduced and integrated to manage and assess the data and yield global optimization capabilities.

6 Summary and Conclusions

In the following, the results of this thesis are briefly summarized and conclusions are drawn in reference to the research questions of the work presented in Chapter 2.

Summary

ICME with computational microstructural and micromechanical modeling offers new insights into the behavior and design of tribological systems and surfaces. Adoption of the principles of ICME, most importantly the concurrent utilization of experimental and modeling approaches, yields great amounts of data for solving tribological problems and, ultimately for the development of systematic design tools for tribological material solutions.

A key characteristic of the usability of a multiscale materials modeling toolset is versatility. In the current work, this first became obvious in the analysis of the imaging based modeling results, where establishing causal relations becomes much easier when the toolset provides support to models of varying complexity, in many cases even very simple and naive models of composite microstructures. Similarly, it is foreseen that the use of so-called "semi-synthetic," i.e., modifiable imaging based models blurring the division between synthetic and imaging models, will be of great use. In addition, it must be noted that most microstructural models are only usable in a single scale for the assessment of the properties, behavior, and performance of materials. Sophisticated methods to couple the models to the macroscale as well are still largely lacking, the traditional coupling methods typically inducing errors which become especially limiting when the material damage is included and the numerical solution becomes unable to capture the relevant physical behavior because of the multiscale approach.

The case specific optimization of a tribosystem is always seen as a viable option for material solutions in practise, since no single material or microstructure solution fits all possible application scenarios, especially if the material costs are considered as well. For example, for abrasive conditions in one of the studied cases the optimal solution for the microstructures was the MFP of $0.4\,\mu m$ and a crystal size of $0.3\,\mu m$ (WC-CoCr TS coating with high WC fraction), while for the sliding contact conditions several orders of magnitude larger crystals and MFP were also found to be applicable (WC-Ni laser cladded coating).

The use cases support the notion that ICME already provides added value to the solution of tribological problems and material related challenges by way of adding knowledge for problem solving which is difficult to obtain otherwise. The greatest impact and better quality results are obtained when both experimental and modeling approaches are used side by side and are not viewed as alternatives or competitors.

Conclusions

With respect to thin films and their modeling, the results of this thesis can be concluded as follows (research questions 1 and 4):

- The utilized CZM methodology using mixed-mode TSL was able to reproduce the experimentally observed cracking patterns for a $2\,\mu m$ TiN film, the primary mechanism being crack initiation and propagation at the trailing edge of the contact. Loss of adhesion at the interface takes place only after a substantial further increase in the applied loading.
- Various gradient and multilayer film simulations indicated possibilities to improve the film's performance against a progressively loaded sliding abrasive contact. Linear and especially progressive property gradients, when designed appropriately in relation to the bond layer and substrate properties, yielded reductions in the rate of damage accumulation while still retaining their load carrying capacity.
- As regards the property gradients, the simple nonlinear multilayer systems that even out the through coating stress gradients yielded the best simulated outcomes.
- The "macrotopography" of the studied rough DLC surfaces with anisotropic fractal patterns was found to dominate the contact response, the local features contributing less than $\leq 40\%$ to the stress state.
- Validation of the numerical modeling was successfully completed against the scratch shape and through coating crack density. For rough surfaces, the anisotropies in the cracking patterns were matched with the observations of local stress states arising from the surface topography.

With respect to the modeling of the composite microstructures of wear resistant coatings, the results can be concluded as follows. The typical mechanisms for crack initiation resulting in the failure of the investigated wear resistant microstructures were identified as (research question 2):

- brittle carbide fracture, with first principal stress or a related cleavage stress as the dominating failure parameters,
- ductile binder cracking, with equivalent plastic strain and strain energy as dominating failure parameters,
- interface failure, with strain state as the dominating failure parameter (in a mixed-mode loading context),
- cracking from pre-existing porosities and defects, with free surface associated shear and distortions as dominating failure parameters.

With respect to the characteristics of the microstructure influencing the wear resistance of a coating, the following ranking was established (research question 2):

- firstly, defects in the coating microstructure are of the highest importance as they can create detrimental local stress and strain concentrations,

- secondly, the presence of particle clusters is critical for the durability of the structure, particularly with respect to defect initiation and propagation,
- thirdly, the elasticity of the particles is of great importance with respect to shielding the surface,
- fourthly, binder hardness and particle morphology are of importance for the wear resistance,
- fifthly, particle size and MFP need to be considered, preferably concurrently, since the material solutions for tribological applications require understanding and designing of the tribosystem as a whole.

Regarding the computational strategies and ICME based methodologies, the findings of this work can be concluded as follows (research questions 2 and 3):

- The PSPP approach as a framework for the application of ICME proved an effective means for directing the exploitation of digitalization and integration of the experimental and modeling efforts.
- No single microstructural modeling strategy was found to be sufficient, but the most useful results and the best added value were obtained by experimenting with different approaches for individual microstructures, for example by running virtual "what-if" trials and experimentation.
- Introducing PF and interfacing it to FE was found to provide new means of defining interface models and creating a more realistic representation of the hard material microstructure. The outcome was found to be particularly significant with respect to the simulated stress-strain response of the studied cemented carbide microstructures, the introduced semi-carbide phase fundamentally altering the modeled composite material response.
- Validation activities require ever more work, and as the resolution and capabilities of modeling increase, so do the requirements and possibilities for the characterization and experimental approaches. Since computation of controlled laboratory experiments can in many cases be viewed as the best way to study and understand the tribological behavior of material solutions, this suggests that more emphasis be placed, for example, on in-situ techniques.
- The validation cases carried out in this thesis were quantitatively promising, ramping up the rate of model development.

7 Future Work

With respect to future work, the following topical areas were identified and are addressed briefly in the following sections.

Design methodologies for wear resistance

Current work established workflows and toolsets for evaluating the PSPP relationship related to tribological problems involving wear resistance. The physics-based workflows can be argued to yield significant information in terms of establishing the respective causal relationships. However, it is envisioned that relying on the HPC workflows will not be sufficient for design purposes due to the ever increasing complexity of the models when establishing better physical representativeness. As such, transition to High-Throughput Computing (HTC) becomes a necessity along with new optimization paradigms which will resort especially to the use of ML techniques as design tools. Physics-based and data-based models need to operate alongside to yield both accurate and fast-to-compute results to enable the propagation of the design process by exploiting AI technologies.

Single crystal behavior and polycrystalline microstructures

Current work utilized primarily top-down plasticity models to describe the deformation behavior of the binding and substrate phases. Also, no polycrystalline microstructures of the harder phases or coatings were incorporated beyond considering multilayered and gradient films. In order to be able to capture effects of orientation, texture and anisotropic plastic slip, Crystal Plasticity (CP) based approaches need to be utilized in describing the deformation processes. To capture scale dependencies which are crucial for designing hierarchical multiscale structures, non-local or gradient formulations become a necessity.

Coupled damage modeling, cumulative wear and smart concurrence

A major work item is the incorporation of material damage properly to micromechanical modeling approaches. The introduction of damage appears most viable when done within the context of CP modeling, at which point the interplays between plastic deformation mechanisms, microstructure scale damage and scale dependencies can be incorporated in similitude. This is one of the enablers for the capability to predict wear on part/product scale, i.e., cumulative wear over actual product and component lifetimes. Similarly, most of the presently available methods for concurrence are lacking, particularly the ones that have been traditionally applied within the confines of FE solvers. Newly developed means

with improved enriched variational formulations need to be introduced and matured to be HPC capable.

Merger of discrete and continuous solution methods

Although the necessity to push towards smoother integration of discrete and continuous analysis methods has been identified and pursued for a long while now, the capabilities necessary for tribological problems are still largely not available. This is apparent, on the other hand, in the challenges or inabilities facing the modeling of tribolayer formation, integration of lubrication and surface interactions, as well as in earlier referred to problems dealing with surface damage, wear, finite deformations and phase transformations. It can be argued that further efforts are required and a solution incorporating the best of both worlds or merger of both analysis capabilities has not yet materialized.

Multiscale modeling across atomistic and microstructural/meso scales

With respect to model coupling methodologies and concurrence in multiscale modeling the identified needs are in part mirrored already in the previous sections. However, what needs to be emphasized is the pursuit of atomistic and microstructure scale coupling in multiscale modeling. Solutions to problems such as providing microstructural models information about atomistic scale mechanisms of friction are still elusive, whether this consists of reactivity or mechanisms of lubrication between surfaces, or for example, phase transformations or surface transfer layer formation which again contributes to the surface interactions (as in the case of DLC). Although within individual modeling scales signs of progress can be argued to exist, effort still needs to be placed on Coarse Graining (CG) approaches. Especially, the exploitation of Molecular Dynamics (MD) findings and data to tackle surface behaviors at the scale of material microstructure is still lacking.

Micromechanical testing

Several sections in the current work, particularly the ones dealing with model validation aspects, identified challenges in obtaining direct microstructure scale information. Data that could be quantitatively and as directly as possible utilized for the aforementioned validation activities as well as to accelerate model development. Various characterization techniques ranging from atomistic to microstructure scale are swiftly becoming more commonplace, and similar progress can be identified regarding micromechanical testing. Testing employing material samples at relevant size scales or even single crystals or grains is bound to accelerate the development of microstructural and micromechanical material modeling capabilities. Thus, as a future work item pursuing ever tighter integration of advanced experimental and modeling techniques is seen to posses tremendeous potential.

Bibliography

"Materials genome initiative for global competitiveness," Tech. Rep., 2011.

"Integrated computational materials engineering (icme) - implementing icme in the aerospace, automotive and maritime industries," Tech. Rep., 2013.

"Modeling across scales: A roadmapping study for connecting materials models and simulations across length and time scales," Tech. Rep., 2015.

"Harnessing materials innovations to support next generation manufacturing technologies," Tech. Rep., 2017.

Amsellem, O., Madi, K., Borit, F., Jeulin, D., Guipont, V., Jeandin, M., Boller, E., and Pauchet, F., "Two-dimensional (2d) and three-dimensional (3d) analyses of plasma-sprayed alumina microstructures for finite-element simulation of young's modulus," *Journal of Materials Science*, vol. 43, no. 12, pp. 4091 – 4098, 2008.

Anwar, S., Axinte, D., and Becker, A., "Finite element modelling of abrasive waterjet milled footprints," *Journal of Materials Processing Technology*, vol. 213, no. 2, pp. 180 – 193, 2013.

Barenblatt, G., "The mathematical theory of equilibrium cracks in brittle fracture," *Advances Applied Mechanics*, vol. 7, pp. 55 – 129, 1962.

Beauvais, S., Guipont, V., Jeandin, M., Jeulin, D., Robisson, A., and Saenger, R., "Study of the porosity in plasma-sprayed alumina through an innovative three-dimensional simulation of the coating buildup," *Metallurgical and Materials Transactions A*, vol. 39, no. 11, pp. 2711 – 2724, 2008.

Bolelli, G., Candeli, A., Koivuluoto, H., Lusvarghi, L., Manfredini, T., Vuoristo, P. *et al.*, "Microstructure-based thermo-mechanical modelling of thermal spray coatings," *Materials & Design*, vol. 73, pp. 20 – 34, 2015.

Bowden, F. and Tabor, D., *The Friction and Lubrication of Solids.* Oxford University Press, 1950.

Chawla, N., Sidhu, R., and Ganesh, V., "Three-dimensional visualization and microstructure-based modeling of deformation in particle-reinforced composites," *Acta Materialia*, vol. 54, no. 6, pp. 1541 – 1548, 2006.

Chen, G., Ozden, U., Bezold, A., and Broeckmann, C., "A statistics based numerical investigation on the prediction of elasto-plastic behavior of wc – co hard metal," *Computational Materials Science*, vol. 80, pp. 96 – 103, 2013.

Diao, D., Kato, K., and Hayashi, K., "The maximum tensile stress on a hard coating under sliding friction," *Tribology International*, vol. 27, pp. 267 – 272, 1994.

Dick, T. and Cailletaud, G., "Fretting modelling with a crystal plasticity model of ti6al4v," *Computational Materials Science*, vol. 38, no. 1, pp. 113 – 125, 2006.

Dugdale, D., "Yielding of steel sheets containing slits," *Journal of the Mechanics and Physics of Solids*, vol. 8, pp. 100 – 104, 1960.

Greenwood, J. A. and Williamson, J., "Contact of nominally flat surfaces," *Proceedings of the Royal Society of London A*, vol. 295, pp. 300 – 319, 1966.

Greenwood, M., Shampur, K., Ofori-Opoku, N., Pinomaa, T., Wang, L., Gurevich, S., and Provatas, N., "Quantitative 3d phase field modelling of solidification using next-generation adaptive mesh refinement," *Computational Materials Science*, vol. 142, pp. 153 – 171, 2018.

Halling, J., "A contribution to the theory of mechanical wear," *Wear*, vol. 34, pp. 239 – 249, 1975.

Halling, J. *et al.*, "Toward a mechanical wear equation," *Journal of Lubrication Technology*, vol. 105, pp. 212 – 219, 1983.

Hannula, S.-P., Turunen, E., Koskinen, J., and Söderberg, O., "Processing of hybrid materials for components with improved life-time," *Current Applied Physics*, vol. 9, no. 3, pp. S160 – S166, 2009.

Herd, S., Wood, R., Wharton, J., and Higgs III, C., "Explicit fracture modelling of cemented tungsten carbide (wc-co) at the mesoscale," *Materials Science and Engineering A*, vol. 712, pp. 521 – 530, 2018.

Holmberg, K. and Matthews, A., *Coatings Tribology: Properties, Mechanisms, Techniques and Applications in Surface Engineering.* Elsevier, 2009, no. 56.

Holmberg, K., Laukkanen, A., Ronkainen, H., Wallin, K., and Varjus, S., "A model for stresses, crack generation and fracture toughness calculation in scratched tin-coated steel surfaces," *Wear*, vol. 254, no. 3-4, pp. 278 – 291, 2003.

Holmberg, K., Laukkanen, A., Ronkainen, H., Wallin, K., Varjus, S., and Koskinen, J., "Tribological contact analysis of a rigid ball sliding on a hard coated surface: Part i: Modelling stresses and strains," *Surface and Coatings Technology*, vol. 200, no. 12-13, pp. 3797 – 3809, 2006.

Holmberg, K., Laukkanen, A., Ronkainen, H., Wallin, K., Varjus, S., Koskinen, J. *et al.*, "Tribological contact analysis of a rigid ball sliding on a hard coated surface: Part ii: Material deformations, influence of coating thickness and young's modulus," *Surface and Coatings Technology*, vol. 200, no. 12-13, pp. 3810 – 3823, 2006.

Holmberg, K., Laukkanen, A., Ronkainen, H., and Wallin, K., "Surface stresses in coated steel surfaces – influence of a bond layer on surface fracture," *Tribology International*, vol. 42, pp. 137 – 148, 2009.

Holmberg, K., Laukkanen, A., Ghabchi, A., Rombouts, M., Turunen, E., Waudby, R., Suhonen, T., Valtonen, K., and Sarlin, E., "Computational modeling based wear resistance analysis of thick composite coatings," *Tribology International*, vol. 72, pp. 13 – 30, 2014.

Holmberg, K., Laukkanen, A., Turunen, E., and Laitinen, T., "Wear resistance optimization of composite coatings by computational microstructural modeling," *Surface and Coatings Technology*, vol. 247, pp. 1–13, 2014.

Holmberg, K., Laukkanen, A., Ronkainen, H., Waudby, R., Stachowiak, G., Wolski, M., Podsiadlo, P., Gee, M., Nunn, J., Gachot, C., and Li, L., "Topographical orientation effects on surface stresses influencing on wear in sliding dlc contacts, part 1: Experimental," *Wear*, vol. 330-331, pp. 3–22, 2015.

Holmberg, K., Laukkanen, A., and Hakala, T., "Coated surface wear resistance design by computational modelling," 4 2018.

Hu, J., Li, D., and Llewellyn, R., "Synergistic effects of microstructure and abrasion condition on abrasive wear of composites––a modeling study," *Wear*, vol. 263, no. 1-6, pp. 218–227, 2007.

Jiang, J. and Arnell, R., "The effect of substrate roughness on the wear of dlc coatings," *Wear*, vol. 239, pp. 1–9, 2000.

Kalin, M. and Pogacnik, A., "Criteria and properties of the asperity peaks on 3d engineering surfaces," *Wear*, vol. 308, pp. 95–104, 2013.

Kayser, W., Bezold, A., and Broeckmann, C., "Simulation of residual stresses in cemented carbides," *International Journal of Refractory Metals and Hard Materials*, vol. 63, pp. 55–62, 2017.

Kim, C.-S., Massa, T., and Rohner, G., "Modeling the relationship between microstructural features and the strength of wc–co composites," *International Journal of Refractory Metals and Hard Materials*, vol. 24, no. 1-2, pp. 89–100, 2006.

Kucharski, S. and Starzynski, G., "Study of contact of rough surfaces: Modeling and experiment," *Wear*, vol. 311, pp. 167–179, 2014.

Langer, S., Fuller, E., and Carter, W., "Oof: an image-based finite element analysis of material microstructures," *Computational Sciences and Engineering*, vol. 3, pp. 15–23, 2001.

Laukkanen, A., "Integrated computational materials engineering for design and tailoring of wear resistant material solutions," ser. Nordtrib. VTT Technical Research Centre of Finland Ltd, Jun. 2016.

Laukkanen, A., Holmberg, K., Koskinen, J., Ronkainen, H., Wallin, K., and Varjus, S., "Tribological contact analysis of a rigid ball sliding on a hard coated surface, part iii: Fracture toughness calculation and influence of residual stresses," *Surface and Coatings Technology*, vol. 200, no. 12-13, 2006.

Laukkanen, A., Holmberg, K., Ronkainen, H., and Wallin, K., "Cohesive zone modeling of initiation and propagation of multiple cracks in hard thin surface coatings," *Journal of ASTM International*, vol. 8, no. 1, pp. 1–21, 2011.

Laukkanen, A., Varis, T., Suhonen, T., Metsäjoki, J., Andersson, T., and Laitinen, T., "Multiscale modeling of microstructural defects and influence on mechanical properties and wear resistance of thermal spray coatings," 2014, p. 6.

Laukkanen, A., Oksa, M., Pohjanne, P., and Holmberg, K., "Multiscale modeling of degradation and lifetime of thin hard coated material systems," ser. EERA Annual Conference 2016, 2016.

Laukkanen, A., Pinomaa, T., Andersson, T., Paajanen, A., Holmberg, K., and Lindroos, T., "Multiscale interface model for design of nano-microstructures in hard materials," ser. WorldPM2016. EPMA, 2016.

Laukkanen, A., Pinomaa, T., Holmberg, K., and Andersson, T., "Effective interface model for design and tailoring of wc-co microstructures," *Journal of Powder Metallurgy*, vol. 59, pp. 20 – 30, 2016.

Laukkanen, A., Holmberg, K., Ronkainen, H., Stachowiak, G., Podsiadlo, P., Wolski, M., Gee, M., Gachot, C., and Li, L., "Topographical orientation effects on surface stresses influencing on wear in sliding dlc contacts, part 2: Modeling and simulations," *Wear*, vol. 388-389, pp. 18 – 28, 2017.

Laukkanen, A., Pinomaa, T., Andersson, T., Lindroos, M., Suhonen, T., and Holmberg, K., "Icme in design of hard materials and substitution of critical raw materials," ser. TMS ICME. The Minerals, Metals and Materials Society, May 2017.

Li, K., Diao, D., and Bhushan, B., "Fracture mechanics of thin amorphous carbon films in nanoindentation," *Acta Materialia*, vol. 45, pp. 4453 – 4461, 1997.

Lofaj, F. and Nemeth, D., "Multiple cohesive cracking during nanoindentation in a hard w-c coating/steel substrate system by fem," *Journal of the European Ceramic Society*, vol. 37, no. 14, pp. 4379 – 4388, 2017.

Mohd Tobi, A., Shipway, P., and Leen, S., "Finite element modelling of brittle fracture of thick coatings under normal and tangential loading," *Tribology International*, vol. 58, pp. 29 – 39, 2013.

Nastani, M., Kodali, P., K., W., Embury, R., and Raj, Y., "Fracture toughness of diamondlike carbon coatings," *Journal of Materials Research*, vol. 14, pp. 2173 – 2180, 1999.

Oksa, M., Turunen, E., Suhonen, T., Varis, T., and Hannula, S.-P., "Optimization and characterization of high velocity oxy-fuel sprayed coatings: Techniques, materials, and applications," *Coatings*, vol. 1, pp. 17 – 52, 2011.

Olsson, G., "Designing a new material world," *Science*, vol. 288, no. 5468, pp. 993 – 998, 1997.

Österle, W., Kloss, H., Urban, I., and Dmitriev, A., "Towards a better understanding of brake friction materials," *Wear*, vol. 263, no. 7-12, pp. 1189 – 1201, 2007.

Ozden, U., Mingard, K., Zivcec, M., Bezold, A., and Broeckmann, C., "Mesoscopical finite element simulation of fatigue crack propagation in wc/co-hardmetal," *International Journal of Refractory Metals and Hard Materials*, vol. 49, pp. 261 – 267, 2015.

Ozden, U., Jiang, K., Bezold, A., and Broeckmann, C., "Evaluation of fatigue crack growth performance in different hardmetal grades based on finite element simulation," *Procedia Structural Integrity*, vol. 2, pp. 648 – 655, 6 2016.

Pearson, J., Zikry, M., and Wahl, K., "Computational design of thin-film nanocomposite coatings for optimized stress and velocity accommodation response," *Wear*, vol. 267, no. 5-8, pp. 1137 – 1145, 2009.

Pinomaa, T., Laukkanen, A., Gurevich, S., and Provatas, N., "Phase field analysis of solidification structures and interface composition in wc – co hard metals." EPMA, 2015, p. 6.

Quey, R., Dawson, P., and Barbe, F., "Large-scale 3d random polycrystals for the finite element method: Generation, meshing and remeshing," *Computer Methods in Applied Mechanics and Engineering*, vol. 200, no. 17-20, pp. 1729 – 1745, 2011.

Rehman, H., Ahmed, F., Schmid, C., Schaufler, J., and Durst, K., "Study on the deformation mechanics of hard brittle coatings on ductile substrates using in-situ tensile testing and cohesive zone fem modeling," *Surface and Coatings Technology*, vol. 207, pp. 163 – 169, 2012.

Reichert, S., Lorentz, B., Heldmaier, S., and Albers, A., "Wear simulation in non-lubricated and mixed lubricated contacts taking into account the microscale roughess," *Tribology International*, vol. 100, pp. 272 – 279, 2016.

Reid, A., Langer, S., Lua, R., Coffman, V., Haan, S.-I., and Garcia, E., "Image-based finite element mesh construction for material microstructures," *Computational Materials Science*, vol. 43, no. 4, pp. 989 – 999, 2008.

Saai, A., Svenum, I.-H., Kane, P., Friis, J., and Berstad, T., "Multi-scale modeling of wc-co drill bits material with density functional theory and crystal elasticity model," *Procedia Materials Science*, vol. 3, pp. 640 – 645, 2014.

Seleson, P., Parks, M., Gunzburger, M., and Lehoucq, R., "Peridynamics as an upscaling of molecular dynamics," *Multiscale Modeling and Simulation*, vol. 8, no. 1, pp. 204 – 227, 2009.

Soulignac, R., Maurel, V., Remy, L., and Köster, A., "Cohesive zone modelling of thermal barrier coatings interfacial properties based on three-dimensional observations and mechanical testing," *Surface and Coatings Technology*, vol. 237, pp. 95 – 104, 2013.

Suhonen, T., Laukkanen, A., Andersson, T., Cheney, J., and Sordelet, D., "Modeling the effect of microstructure on impact and abrasion wear performance of novel fe-based mmc coatings," 2017.

Tkalich, D., Cailletaud, G., Yastrebov, V., and Kane, P., "A micromechanical constitutive modeling of wc hardmetals using finite-element and uniform field models," *Mechanics of Materials*, vol. 105, pp. 166 – 187, 2017.

Tkalich, D., Yastrebov, V., Cailletaud, G., and Kane, P., "Multiscale modeling of cemented tungsten carbide in hard rock drilling," *International Journal of Solids and Structures*, vol. 128, pp. 282 – 295, 2017.

Turunen, E., Varis, T., Gustafsson, T. E., Koskinen, J., Fält, T., and Hannula, S.-P., "Parameter optimization of hvof sprayed nanostructured alumina and alumina – nickel composite coatings," *Surface and Coatings Technology*, vol. 200, no. 16-17, pp. 4987 – 4994, 2006.

van den Bosch, M., Scheurs, P., and Geers, M., "An improved description of the exponential xu and needleman cohesive zone law for mixed-mode decohesion," *Engineering Fracture Mechanics*, vol. 73, pp. 1220–1234, 2006.

Wallin, K. and Laukkanen, A., "Aspects of cleavage fracture initiation–relative influence of stress and strain," *Fatigue & Fracture of Engineering Materials & Structures*, vol. 29, no. 9-10, pp. 788–798, 2006.

Wallin, K., Laukkanen, A. *et al.*, "New developments of the wallin, saario, törrönen cleavage fracture model," *Engineering Fracture Mechanics*, vol. 75, no. 11, pp. 3367–3377, 2008.

Wiederkehr, T., Klusemann, B., Gies, D., Muller, H., and Svendsen, B., "An image morphing method for 3d reconstruction and fe-analysis of pore networks in thermal spray coatings," *Computational Materials Science*, vol. 47, no. 4, pp. 881–889, 2010.

Wolski, M., Podsiadlo, P., Stachowiak, G., Holmberg, K., Laukkanen, A., Ronkainen, H., Gee, M., Nunn, J., Gachot, C., and Li, L., "Multiscale characterisation of 3d surface topography of dlc coated and uncoated surfaces by directional blanket covering (dbc) method," *Wear*, vol. 388-389, pp. 47–56, 2017.

Xiao, Y., Shi, W., and Luo, J., "Indentation for evaluating cracking and delamination of thin coatings using finite element analysis," *Vacuum*, vol. 122 Part A, pp. 17–30, 2015.

Xiao, Y., Shi, W., Han, Z., Luo, J., and Xu, L., "Residual stress and its effect on failure in a dlc coating on a steel substrate with rough surfaces," *Diamond and Related Materials*, vol. 66, pp. 23–35, 2016.

Zhang, M., McDowell, D., and Neu, R., "Microstructure sensitivity of fretting fatigue based on computational crystal plasticity," *Tribology International*, vol. 42, no. 9, pp. 1286–1296, 2009.

Publications

Publication I

Laukkanen, A., Holmberg, K., Ronkainen, H., and Wallin, K., "Cohesive Zone Modeling of Initiation and Propagation of Multiple Cracks in Hard Thin Surface Coatings," *Journal of ASTM International*.

Publication II

Holmberg, K., Laukkanen, A., Ghabchi, A., Rombouts, M., Turunen, E., Waudby, R., Suhonen, T., Valtonen, K. and Sarlin, E., "Computational Modeling Based Wear Resistance Analysis of Thick Composite Coatings," *Tribology International*.

Tribology International 72 (2014) 13–30

Contents lists available at ScienceDirect

Tribology International

journal homepage: www.elsevier.com/locate/triboint

Computational modelling based wear resistance analysis of thick composite coatings

K. Holmberg [a,*], A. Laukkanen [a], A. Ghabchi [a,1], M. Rombouts [b], E. Turunen [a], R. Waudby [a], T. Suhonen [a], K. Valtonen [c], E. Sarlin [c]

[a] VTT Technical Research Centre of Finland, Espoo, PO Box 1000, FI-02044 VTT, Finland
[b] VITO, Vlaamse Instelling voor Technologisch Onderzoek, Mol, Belguim
[c] Tampere University of Technology, Tampere, Finland

ARTICLE INFO

Article history:
Received 22 October 2013
Received in revised form
27 November 2013
Accepted 1 December 2013
Available online 12 December 2013

Keywords:
Modelling
Wear
Composite coatings

ABSTRACT

A computational modelling and simulation approach was developed and applied for wear resistance analysis of composite coatings. Three new numerical finite element models were developed to include microstructural properties of typical thick thermal spray and laser cladded metal matrix coatings. The first was an ideal synthetic defect free material model, the second an advanced synthetic model containing defects and the third an image based real model. A thermal spray WC-CoCr coating and a laser cladded WC-NiCrBSi coating were characterised and the information obtained of their microstructure and properties was used for computational stress and strain simulations. The simulations were carried out for a set of indentation and scratch test contact conditions. Wear related features were validated empirically by abrasive rubber wheel testing and sliding contact pin-on-disk testing in dry conditions. Features like high local curvature, notches, abnormally large particles, thin ligament or throat-like structures of a specific material phase, clusters of interlinked carbides or high local fraction of a specific material phase had a great impact on the resulting stress state and wear resistance of the coating. The composite structures of the coatings offered a 2 to 50 times lower abrasive wear and more than four orders of magnitude lower sliding wear rate compared to the reference steel surface.

1. Introduction

Wear is taking place at the top surface of products, components and tools. The wear resistance requirements are thus focused especially on the surface properties. Advanced surface engineering offers many possibilities to modify the properties of surfaces to become more wear resistant, e.g. by surface treatments, deposition of thin layers or processing of thick surface coatings [1].

Thin coatings, like physical vapour deposition (PVD) and chemical vapour deposition (CVD) coatings, are excellent in many tribological applications and today largely in use. However, they may be vulnerable especially in harsh, high load and high temperature conditions due to both material and structural limitations originating from their tiny thickness, which is typically in the range of 1–3 μm and even less. The use of thick composite coatings is another solution to tailor surface properties of the component. Typical processing methods for thick coatings are thermal spraying and powder cladding, either as welded overlays or laser fused layers. These methods offer a flexible route to produce unique composite-structured, rather thick coatings, in a typical thickness range of 150 μm–3 mm, on a substrate material selected according to other criteria, like price, extent of alloying elements and other additives, mechanical strength and low weight [2–4].

Over the last decades a myriad of hybrid coating materials suitable for thick coatings – mainly mixtures and composites of ceramics, metals and polymers – has been developed. Entirely new possibilities for developing high-performance materials have, however, opened up in the 2000s, with the development of new manufacturing methods, widespread adoption of nanotechnology, and more in-depth understanding through new process diagnostics and higher modelling capacity [5–8]. Particle-reinforced composite materials consisting of a metal matrix and hard dispersed particles offer a potential solution for increased wear resistance demands. An improvement in wear properties is often counterbalanced by the deterioration of other properties, such as impact resistance or corrosion resistance. It is important to tailor and optimise the material for the particular application, taking all the requirements into consideration [8–10].

Computational modelling and simulation of deformations in a material due to surface loading, and calculations of stress and

* Corresponding author. Tel.: +358 40 544 2285; fax: +358 20 722 7069.
E-mail address: kenneth.holmberg@vtt.fi (K. Holmberg).
[1] Present affiliation. The Boeing Company, Seattle, WA, USA

0301-679X/$ - see front matter © 2013 Elsevier Ltd. All rights reserved.
http://dx.doi.org/10.1016/j.triboint.2013.12.001

strain in loaded contacts is a research approach that is rapidly developing today. Modelling and simulation of a tribocontact helps to understand the mechanisms that result in plastic deformation, surface cracking, wear particle formation and continuous wear. The numerical simulations can be carried out on various dimensional scale levels, from nano size to macro size, by using software representing the material structure from atomic and even sub-atomic to continuum macro and component level [11–14].

The material modelling and simulation approach has been used in contact mechanics [15] and in fracture mechanics of structures [16]. The same FEM-based approach has successfully been used for improved understanding of the wear process of a sliding contact with one of the surfaces coated by a thin surface coating [1,17–24]. Precise measurements of the elastic and the plastic response of the coating and substrate system, and measurements of the contact geometry made it possible to simulate stress and strain conditions, deformations, to calculate fracture behaviour and to evaluate the wear performance of thin, homogenous, coated surfaces and the effect of influencing material and operational parameters.

Thin hard coatings, such as PDV and CVD deposited coatings, can be modelled as a surface layer system, in which both the coating and the substrate material are considered as homogenous and in which the interaction between the coating and the substrate material, as well as the geometrical characteristics, are crucial for the wear behaviour [1,19].

Thick composite coatings, such as the thermal spray and laser cladded coatings, need to be modelled in terms of their complex composite microstructure, including grains, pores, cracks and various phases in the matrix, in order to achieve representative stress and deformation simulations that correlate with the real situations. Composite surface structures of materials such as cast iron, WC-Ni alloys, metal matrix composites and PVD nano-composites have been modelled mainly with the two-dimensional (2D) finite element method (FEM) and with analytical models [25–29]. Microstructural models are more precise representations of the material microstructure and they have been developed based on three-dimensional (3D) FEM modelling for e.g. polycrystalline, SiC–Al alloy and Ti6Al4V alloy surfaces [30–34].

Microstructural models developed for representing real materials have been generated by numerical techniques based on image analysis of cross section images obtained by scanning electron microscopy (SEM) or light optical microscopy (LOM) [35,36,13]. A 3D microstructural representation can be generated in a similar way, but by taking microscopy images of several layers below the surface. Wiederkehr et al. [37] took LOM images from 15 parallel cross sections below the surface, exposed by polishing, with an average inter-distance of 4 μm, and they used an FEM based image morphing method for producing a 3D microstructural material model of a thermal spray surface with pores and cracks.

The modelling of the wear process, in which material is detached from the contact surfaces and interacts in the dynamic triboprocess between the two moving surfaces, needs other kinds of modelling techniques, such as the movable cellular automata (MCA) methods used by Österle et al. [38]. Additionally finite elements can be applied by considering cracking mechanisms like in the work by Mohd Tobi et al. [39] when applied to thick coatings, or by considering material abrasion, like in the work by Anwar et al. [40]. Discrete methods overall provide several advantages for the modelling of material failure and removal processes, as has been demonstrated in the peridynamics approach by Seleson et al. [41].

Both 2D and 3D microstructure modelling and simulation methods have been demonstrated for characterising the mechanical properties of alumina, metallic FeCrBSi and TiC/Cu coatings with pores and cracks [37,42,43]. Based on empirical experience, it is known that size, shape and spatial arrangement and orientation of pores and cracks have a strong influence on the material properties of thermal spray coatings [2,4]. Since the pores can add material flexibility and stop crack growth, the porosity is not always detrimental. Other microstructural material parameters that need to be optimised in a composite coating for a favourable tribological surface behaviour, in addition to the pore-related parameters, are the size, shape, density and spacing of the reinforced particles, the interfacial bond strength and the binder mechanical properties [27,29,33].

Modelling the response of thick composite coatings and their behaviour, including explicitly their microstructure, falls within the scope of mesoscopic analysis methods. In the current context, the most stringent additional requirement set to the modelling methods is the need to treat the weak and strong discontinuities of the coating microstructure, which can be performed by incorporating suitable tailored finite elements and extended finite element methods. Finite element methods with properly developed meshing strategies can be applied for microstructure modelling, but strong discontinuities and their evolution within the microstructure commonly require a more refined approach, such as extended finite element methods.

The aim with this article is to present how computational FEM models can be developed for the purpose of estimating wear resistance of composite thick coatings. The developed models are used for stress and strain simulations of thermal spray WC-CoCr and laser cladding WC-NiCrBSi coatings. The wear resistance analysis is based on microlevel finite element modelling as well as empirical indentation testing, scratch testing, rubber wheel abrasion testing and pin-on-disk tribotesting for model validation.

2. Methodology

In this computational modelling and simulation study we use the so called PSPP (processing–structure–properties–performance) approach modified after Olsson [11] and illustrated in Fig. 1. The following three links need to be modelled to achieve a holistic model for the wear performance of a surface:

(1) the interaction between the wear process and the material properties of the surface,
(2) the interactions between the material properties and the microstructure, and
(3) the interactions between and the microstructure and the surface manufacturing process.

It is often too complex to build a computational model covering the whole PSPP range with today′s knowledge. Thus is it more adequate to use a step by step modelling strategy. We have previously demonstrated how the properties can be linked by FEM modelling to wear performance for tribological contacts with

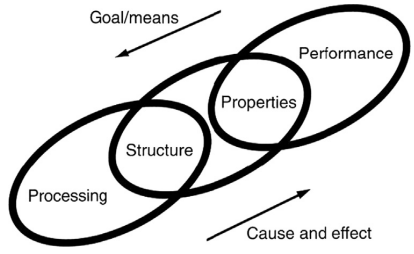

Fig. 1. The PSPP approach links tribological design performance criteria to surface properties, microstructure and coating processing.

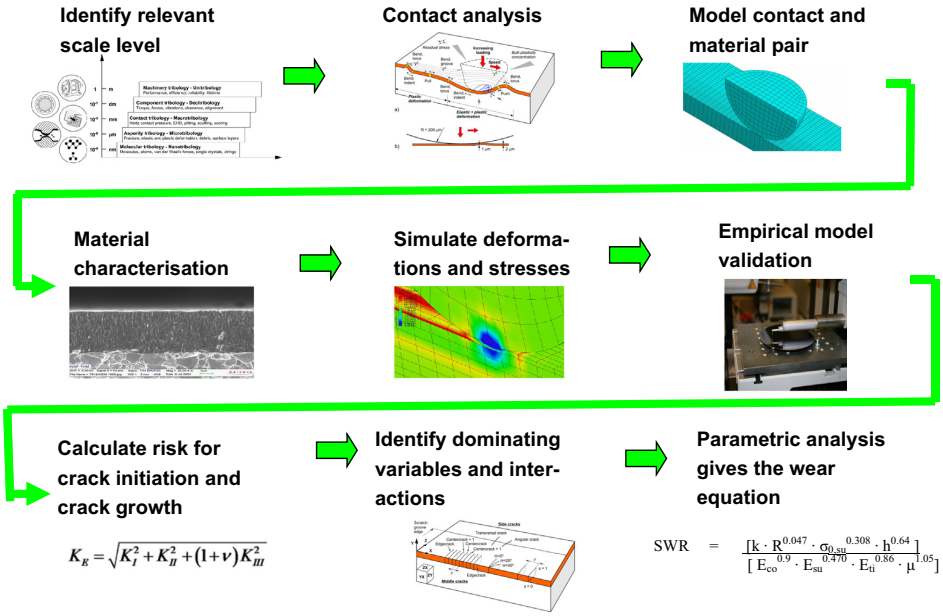

Fig. 2. Methodology for surface coating optimisation with regard to optimal wear resistance based on computational material modelling and loading response simulation.

components coated by thin homogenous PVD and CVD coatings [19]. However, composite coatings like thermal spray and laser cladded coatings are not homogenous and so there is a need to include the microstructure in the material model and thus cover the SPP range. The calculated loading conditions can then be compared with the strength of the material and the risk for deformation, cracking, fracture and wear can be estimated. The simulations show the interaction between the different influencing parameters and help to find the dominating parameters to be optimised.

The computational modelling and simulation approach is fairly laborious and requires a good fundamental understanding of the materials and phenomena to be modelled. However, when an effective model has been developed, the information is very generic and can be used for different applications. A basic requirement is always that the validity of the model must be tested by comparing the results with those of a relevant empirical test.

The computational modelling and simulation approach includes several steps, which combine tribocontact analysis, software development, material characterisation, empirical testing and numerical analysis. The methodology to develop an accurate and generic equation for optimisation of the wear resistance can be characterised by the following steps shown in Fig. 2:

1) Identify the relevant dimensional scale level for the tribocontact to be optimised.
2) Analyse the contact conditions and identify possible influencing variables and parameters.
3) Construct the contact and material model by e.g. FEM or molecular dynamics techniques.
4) Determine the relevant material properties of the material pair, e.g. by macro, micro or nano level material characterisation.
5) Carry out computer simulations for the chosen material pairs and contact conditions, to show the prevailing stresses, strains and deformations.
6) Validate the model by comparing the simulated results with the results of empirical measurements in similar contact conditions.
7) Calculate the tendency for crack initiation and crack growth that results in material detachment based on e.g. fracture mechanics for tough and brittle materials.
8) Identify the dominating variables with respect to critical local stress and strain peaks that may exceed the material capacity.
9) Carry out parametric analysis of the dominating variables, to show their weight and interaction and formulate the surface wear resistance equation, its limits of validity and accuracy.

A wear resistance equation that can be developed according to the above methodology is typically limited to some contact mechanism conditions like severe abrasive wear, mild sliding wear, impact fatigue wear etc. The equation can cover a large range of material, geometry and energy variables. Simulations can be done to explore the risk for surface failure and wear in various conditions. A first stage equation, like the one shown in Fig. 2, does not show the accumulated wear process nor predict the lifetime with regard to wear for components. It quantifies the risk for initiation of surface failure resulting in wear and can be expressed as the surface wear resistance (SWR). It is a tool that can be used by designers for improved surface material selection and robust tribological design of machine components [14].

We have previously carried out and reported all the steps in coated surface computational modelling and simulation that were shown in Fig. 2 for thin, homogenous, coated surfaces like TiN and DLC [14,19–21,23,24,44]. In this article we will report the steps from (1) to (6) for thick composite thermal spray WC-CoCr and laser cladded WC-NiCrBSi coatings. Work on the steps (7) to (9) is currently in progress and will be reported separately later. The software developed for this purpose according to the methodology described above is named VTT ProperTune™.

3. Materials and characterisation

The coated surfaces modelled and studied in this work with respect to their wear resistance were two typical thick composite coatings, namely a thermal spray WC-CoCr coating and a laser cladded WC-NiCrBSi coating. A representative of the two coating structures is shown in Figs. 4a and 5a.

The thermal spray coating was deposited by using a high velocity oxygen fuel (HVOF) system with hydrogen as the fuel gas. The coating structure consists of densely packed splats with a typical splat thickness of 5 to 20 μm and splat diameter of 10 to 50 μm. The structure includes randomly distributed cracks, voids and pores. The metal CoCr matrix surrounds the hard WC particles and includes local decarburized zones, as shown in Fig. 4a.

The metal matrix material of the laser cladded coating was a nickel based alloy with Cr, B and Si as alloying elements.

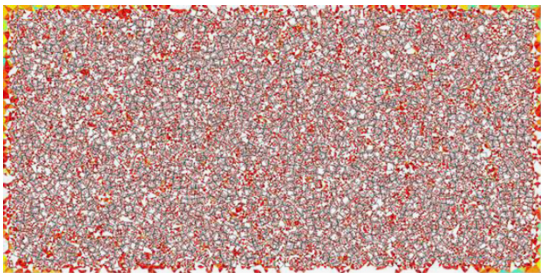

Fig. 3. Microstructural FEM mesh of the ideal synthetic defect-free model representing a typical WC-CoCr coating, colouring representing element shape metrics overlaid on top of the microstructural geometry.

As a strengthening phase, 50% spherical, fused tungsten carbide powder with a particle size between 45 and 106 μm was added. Laser cladding was performed with a fibre-coupled 3 kW diode laser and a coaxial cladding nozzle. The coating structure comprises spherical WC particles in the metallic NiCrBSi matrix (Fig. 5a) and includes only minor defects.

Both coatings were deposited on AISI 1018 steel substrates that were grit-blasted with 590–710 μm alumina particles followed by ultrasonic cleaning in a bath of acetone.

In order to get accurate input values for the models there was a need to determine the mechanical properties of the surface material on a macro scale level but also to determine very detailed micro scale properties of the two composite structures. Often it was quite a challenge to determine accurate micro scale properties. In some cases, when there was no suitable measurement method available, values from literature were used.

The material data for the structure and the properties of the two coatings are found in Table 1. In addition is the material data for the used carbon steel reference material given. This is used as a reference to compare the tribological performance of the composite coatings with, in Section 8.

4. Composite coating modelling

Three fundamentally different finite element model generation routines were developed and adopted and are presented in detail below. They are:

(i) an ideal synthetic defect-free material model,
(ii) an advanced synthetic material model containing defects, and
(iii) a real image based material model.

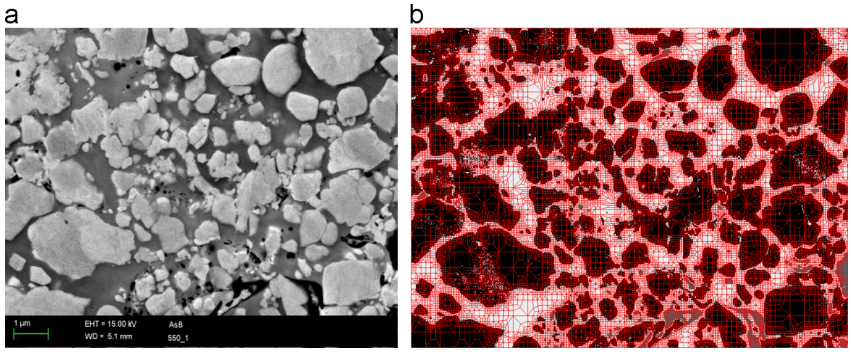

Fig. 4. Microstructure of the WC-CoCr coating from (a) an SEM image and (b) the real model FEM mesh of the same structure.

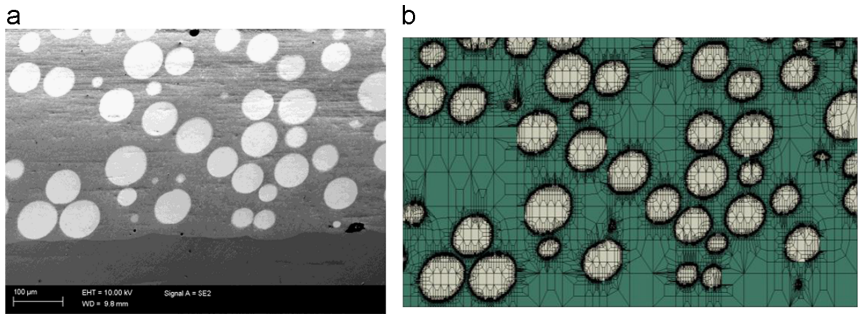

Fig. 5. Microstructure of the WC-NiCrBSi coating from (a) a SEM image and (b) the real model FEM mesh of the same structure.

Table 1
Material structure data and mechanical properties.

	Symbol (unit)	Reference steel AISI1018	Thermal spray coating WC-CoCr	Laser cladded coating WC-NiCrBSi
Structure				
Carbide size	d (μm)	–	1–3	45–125
Mean free path	MFP (μm)	–	0.70	50
Defect density	(%)	–	<1	<0.1
Carbide aspect ratio	(−)	–	0.5	~1
Macro properties				
Coating thickness	h (mm)	–	430	420
Hardness	H (MPa)	2000	11 960[a] 13 150[b]	6500
Elastic modulus	E (GPa)	250	300[a] 280[b]	240[d]
Yield strength, compressive	σ_y (MPa)	390	5 370[c]	2780[d]
Poisson's ratio	ν (−)	0.3[d]	0.25[d]	0.28[d]
Fracture toughness	K_{Ic} (MPa $m^{0.5}$)	55[d]	6.7[a] 6.1[b]	11[d]
Surface roughness, after processing	Ra (μm)	6	6	22 (parallel) 25 (perpendicular)
Surface roughness, after polishing	Ra (μm)	0.02	0.1	0.1
Micro properties [d]				
WC hardness	H (MPa)	–	33 800[a]	30 000
WC elastic modulus	E (GPa)	–	625[a]	450
WC Poisson's ratio	V (−)	–	0.22	0.22
Binder hardness	H (MPa)	–	6500	5410
Binder elastic modulus	E (GPa)	–	220	220
Binder yield strength, compressive	σ_y (MPa)	–	2800	2350
Binder Poisson's ratio	V (−)	–	0.3	0.3
Counter surface [d]		**Al_2O_3 ball in pin-on-disk test**	**SiO_2 grains in rubber wheel test**	
Hardness	H (MPa)	19 600	1200	
Elastic modulus	E (GPa)	380	70	

[a] Measured from the surface.
[b] Measured from cross-section.
[c] Value measured with instrumented indentation data.
[d] Literature values.

These definitions reflect how the local microstructure was simplified and the model was generated for numerical modelling and simulation purposes.

We used three different models to study the coatings because they each gave a set of results that was complementary to the others. The synthetic material models were useful for the understanding of the generic material behaviour under loading, and for the identification of critical and dominating parameters in relation to wear. The ideal synthetic defect-free model was efficient to investigate generic material parameters as they appear in ideal structures as a base line, while the advanced synthetic model was efficient to investigate the effects and interactions related to defects and pores in the material. The real image based model gave a detailed and accurate insight in the material behaviour of the specific coating structures investigated, both on micro and macro scale, and the model gave very precise information about deformations, stresses and strains as they appear in these materials under specific loading.

4.1. Synthetic and real image based material models

4.1.1. The synthetic material models

The synthetic models are based on a mathematical description of the actual microstructure. They comprise the evaluation and quantification of microstructural features and their distributions such as reinforcement particle size, shape and density and further utilising the determined properties via statistical and stochastic means. Often this includes for example tessellation approaches in either two or three dimensions, in order to derive either simplified aggregate-type of models, or mesoscopic sub-models for component-and-characterisation-type solution domains.

Synthetic models can be based on either polygonal or voxel/pixel representations of the phase geometry, or a combination of both. The most common synthetic approach is to apply various tessellation techniques for the generation of the grain geometry, as is typically applied for materials like polycrystals. Synthetic aggregate generation methodologies based on Voronoi tessellation have been presented by e.g. Fritzen et al. [45] and Quey et al. [34] for analyses involving primarily metallic materials. The reason for applying somewhat different routes for constructing the numerical models lies in the possibilities to use them for the extraction of results of different nature.

The *ideal synthetic models* are fairly crude approximations of actual micro- and nanostructures, but they have the desirable property of limiting the number of structure controlling variables. Thus, the simple synthetic models can provide answers and interpretations on the very basic structural properties, such as shape, dimension, mean free path and orientation of particles within the composite structure. Extraction of trends on, for example, the particle mean stress state, the stress state of the particle corner-to-binder interface, or mean binder strain state in between particles is fairly straightforward. Example of our developed synthetic WC-CoCr model is presented in Fig. 3.

The *advanced synthetic models* are more realistic by combining various tessellation routines with actual structural features like

porosity, voids and pre-existing cracks. As such, synthetic models can be used for the studies on relationships like the effect of the porosity and its distribution on the fracture mechanical performance of the composite material. Many such aspects are difficult to tackle even with real models, due to problems related to the specimen preparation.

4.1.2. The real image based material models

Real image based models are based on a segmentation of nano- and microstructural features directly on the basis of, for example, electron microscopy imaging. The scanning electron microscopy images are post-processed and the phase distribution is extracted for discretisation for the finite element solution. For building of the numerical finite element model, various approaches are available. They are either directly based on voxel/pixel based meshing or on the extraction of isosurfaces by way-approaches such as the marching cubes method presented by Wang [46]. The resulting surfaces and volumes are treated as geometry entities in a FEM analysis and are identical to synthetic mesoscopic models.

A representative pixel-based meshing strategy for segmented structures was presented in OOF2 [47], where a penalty approach was used in an adaptive manner to end in a representable mesh of different phase regions. Voxel based approaches rely, for example, on the application of marching cubes like methods, like in the work by Chawla et al. [31] on SiC composites, where a serial sectioning approach combined with a marching cubes algorithm was used for the extraction of the geometry of a 3D multiphase microstructure. Examples of our developed real WC-CoCr model is presented in Fig. 4b and of the real WC-NiCrBSi model in Fig. 5b.

The real models provide the best approximation of the actual material property distribution, and handle nearly arbitrary particle shapes, such as joined and overlapping carbides, resulting from the thermal spray process.

4.2. The model generation

4.2.1. Ideal synthetic model

The process of generating the ideal synthetic model is demonstrated as a flow chart in Fig. 6. The structure was generated by using a purpose-build Python library, which interfaces to the continuum finite element software utilised in the present investigation. The process described in Fig. 6 builds instances of various properties related to the synthetic structure, focusing greatly on the geometric topology of the thermal spray coating. The resulting structure is an output intended for a finite element solver via a separate interface.

In the generation of the ideal model, the first decision lied in the selection of an appropriate geometry primitive addition of the WC particle to the model, which in the first place was assumed to contain solely the binder material. The material properties of this carbide particle are deduced, such as its size, aspect ratio and orientation. The particle geometry was further generalised by the use of statistical and stochastic means, like by modifying the particle to resemble a polyline-defined structure over a simplistic geometry primitive. The spatial arrangement of the particle was deduced in a similar manner, whether it be ordered or statistical, and in addition, the local carbide volumetric concentration was used for estimating the local particle density on the basis of the mean free path or the particle-to-binding-material fraction.

The computational analyses were carried out in a high-performance computing environment for various composite coating morphological features such as mean-free path, carbide size, geometry and stochastic features. The degrees-of-freedom count for the model was typically in the range of 100k–1M.

4.2.2. Advanced synthetic model

When generating the advanced synthetic model, without the above referred simplifications, a somewhat different procedure was adopted. The properties of the synthetic, or advanced synthetic model, contain essentially further microstructural details and their statistical description as well as possible defects. This procedure is presented in Fig. 7.

The procedure is quite specific to the thermal spray coatings studied in the current work, and it initiates the introduction of splat boundaries. An elliptic Voronoi type process was adopted to tessellate the material domain by splats, the splat definition being either deterministic or statistical in nature. Likewise, non-melts were considered over splats. Each splat was tessellated further to generate the sub-structure, the actual local carbide distribution geometry. Furthermore, strong discontinuities such as pores and cracks were introduced, as well as weak discontinuities such as splat boundary interfaces or cohesive regions which differ from those of the parent materials.

The analyses were carried out with different porosity fraction and defect containing, initiating and propagating scenarios using various cohesive zone based failure criteria and parameterisations, using measured coating fracture toughness values as an input for

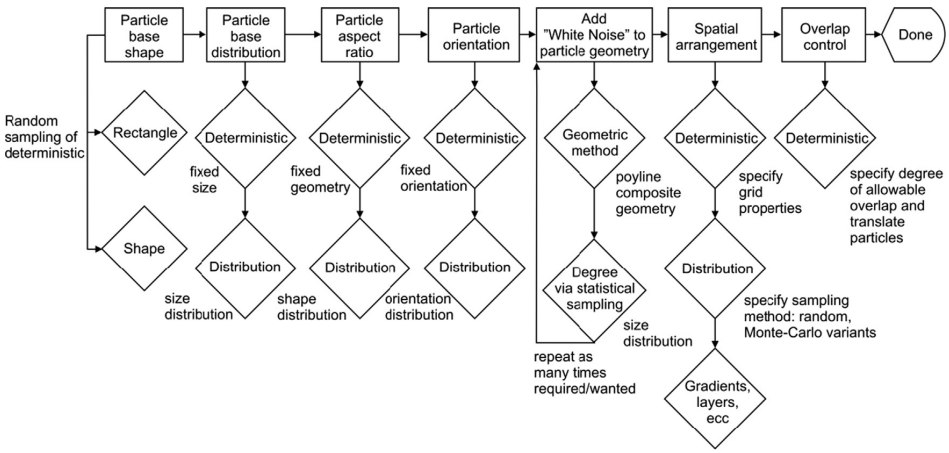

Fig. 6. The model generation procedure used for the generation of the ideal synthetic model.

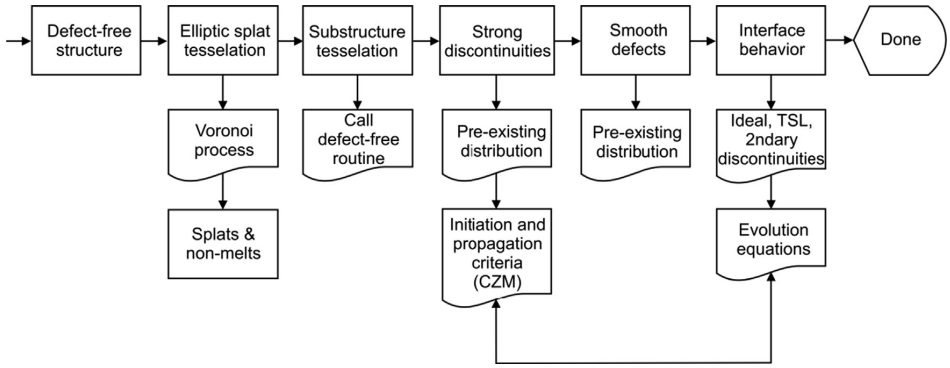

Fig. 7. The model generation procedure used for the generation of the advanced synthetic model containing defects.

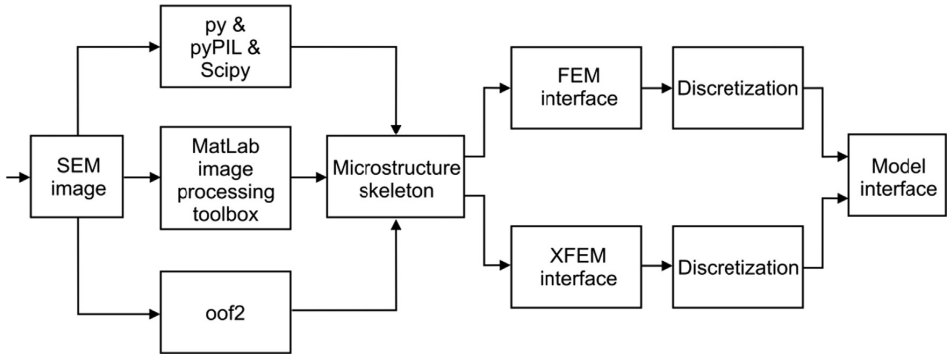

Fig. 8. The model generation procedure used for the generation of the real image based model.

the traction-separation laws. The degrees-of-freedom count for the model was typically in the range of 100k–4M.

4.2.3. Real image based model

The real image based model generation process is described in Fig. 8. The basis for the real model was a high-resolution SEM image. A sufficiently large material plane was needed to be processed with a sufficiently high image resolution to capture both a sufficient volume of material at application-relevant size scale and the local microstructural geometry. This process was performed by subjecting a SEM image that was post-processed into a grayscale image for supporting the image processing, to image processing tools for building of a segmented microstructure and for identification of the material distribution which were free meshed using a penalty approach. The constitutive behaviour of the individual phases was considered isotropic, either linear-elastic or elastic–plastic depending on its deformation behaviour.

The analyses were carried out for numerous different high-resolution SEM images of the coatings to investigate the micro-structural response in a statistical setting. The degrees-of-freedom count for the model was typically in the range of 1–10M.

5. Contact conditions

When composite coatings are used in practical applications, the loaded contact is typically on a macroscale with dimensions expressed in millimetres, while the composite material structure has a matrix including hard particles, pores, voids and cracks of micrometer dimensions. The relevant dimensional scales, on which these wear phenomena were studied, were on a macro scale for the entire counter body and on a micro and nano scale for the composite coating structure, as shown in Fig. 9.

The contact conditions modelled were those of an indentation and scratch test. The indenting and scratching counter bodies were represented by a spherical 200 μm radius diamond tip. The inert tip material simplifies the modelling of the contact process as adhesive material interaction is minor and phenomena like generation of surface layers can be neglected. In scratch test the tip was sliding with increasing load over a flat surface. The modelled countersurfaces were the two about half mm thick composite coatings.

Three effects are important to consider in modelling with regard to the failure behaviour of the surface in a scratch test: (i) the ploughing of the spherical tip stylus resulting in elastic and plastic deformation of the metal matrix, (ii) the sliding of the stylus on the coating resulting in friction, and (iii) as a result of this there is a pulling force on the coating behind the contact, resulting in tensile stresses and fracturing.

The complex stress field in the surface is a result of the following four effects:

1) Friction force. The friction force between the sliding stylus and the coating generates compressive stresses in front of the stylus, originating from the pushing action, and tensile stresses behind the tip, originated from the pulling.
2) Macro-geometry changes. The elastic and plastic deformations are spherical indent, groove and torus shaped. They result in stretching and compressing of the coating. The stresses arising are both compressive and tensile.

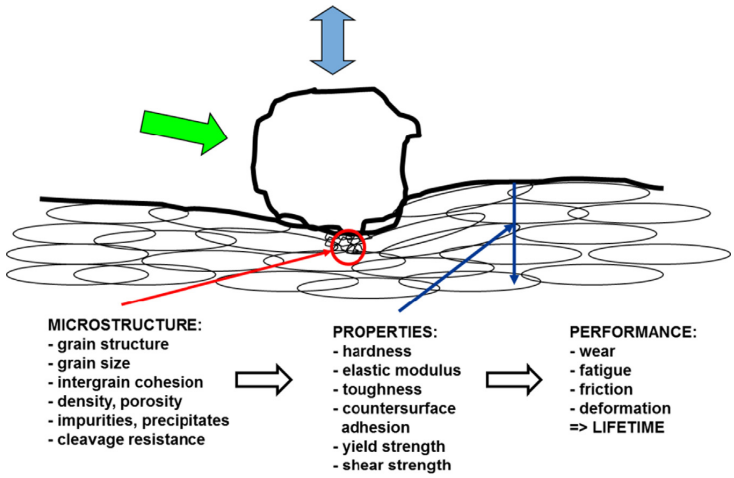

Fig. 9. Loading and sliding conditions in the studied thermal spray coated surface and microstructure and property parameters that influence on wear performance.

3) Micro-geometry change. The hard carbide particles, and defects like pores, voids and cracks, result in discontinuities of the surface properties. This results in high stresses at the borders between the material phases with different properties. The micro scale results are affected by the local material distribution and its microstructural morphology, which translates into local non-linear property mismatching and interaction between hard particles and the binder material.

The above described contact conditions and sliding process were simulated by the computer models. The following parameters were used in the calculations of the stress and strain distributions in the models:

- Scratch test parameters: The sliding distance is 10 mm and the load increases linearly from 5 N pre-load before sliding to 50 N at 10 mm sliding distance. The sliding velocity is not included in the models, i.e. the models are time independent.
- Sliding stylus (Rockwell C): The radius of the spherical tip is 200 μm, the material is diamond, the elastic modulus is 1140 GPa, the hardness is 80 Gpa, the Poisson′s ratio is 0.07, and the roughness is considered ideally smooth.
- Coatings: The structures and properties of the thermal spray WC-CoCr and laser cladded WC-NiCrBSi coatings are defined Table 1.

The plastic penetration of indenters in indentation and scratch testing did not exceed 1/10th of the coating thickness and therefore the substrate does not have any active role in the wear process and thus are its characteristics not in detail described in this study [48].

6. Stress and strain simulations

6.1. Synthetic model stress and strain simulations in indentation

In general a composite structure, even an ordered one with simple geometrically primitive carbides, in a loaded contact behaves in a very different manner compared to a common continuum analysis of the same contact problem. The simple ideal synthetic model simulation results in Fig. 10 are a clear representation of such behaviour, where the normally continuous region of compressive stresses is affected by the presence of reinforcing carbides. As a result of nonlinear material property mismatching between the binder and the carbides the particle edges and corners are seen to develop a high local tensile stress state. This state is dependent on the relative location of the carbide in relation to the indenting tip.

A simple ordered structure, here represented by the ideal synthetic model, was reduced to two variables characterising an elementary lattice (centered rectangular Bravais lattice in two dimensions) and the carbides in it, namely the mean free path (MFP) between the carbides and the carbide size. The elementary primitive for the WC particles is an even rectangle. The effect of the MFP and the carbide size, ranging from conventional micro size to nano size, on near-carbide state of stress and strain is presented in Figs. 11 and 12.

The type of deformation in the studied contact is dependent on the MFP, and for a fixed carbide to binder fraction also on the particle size. For conventional large carbides and larger MFP the binder can deform quite freely and the strengthening caused by the carbides is small. Clear evidence of shear in a two-dimensional setting is seen. As the MFP decreases, the deformation is forced laterally to the binder between the carbides and vertically the flow of binder between the carbides is fairly weak. A two dimensional state of deformation can meet an external imposed boundary condition with smaller equivalent strains than a one dimensional one, and as such, for a decreasing MFP the strain state exhibited by the binder increases, when measured by the equivalent strain.

Similar effects are noted for decreasing carbide size when the volumetric fraction of carbides and binder remains constant. A distinct difference is the increased carbide-to-carbide interaction, which acts to increase the binder strain state, and can be stated to affect the transition towards a state of more confined one dimensional like deformation. Such effects are also desirable since they reflect the strengthening of the structure by the addition of WC particles.

The mechanism of strengthening is well illustrated in Fig. 11 again as a function of MFP and carbide particle size. While the state of deformation changes as a result of increasing particle-to-particle interaction as a function of MFP and particle size, the system is noted to experience higher carbide stresses. The stress state increases also within the binder. For conventional particle sizes it is seen that for a large MFP the stress state, and as such the

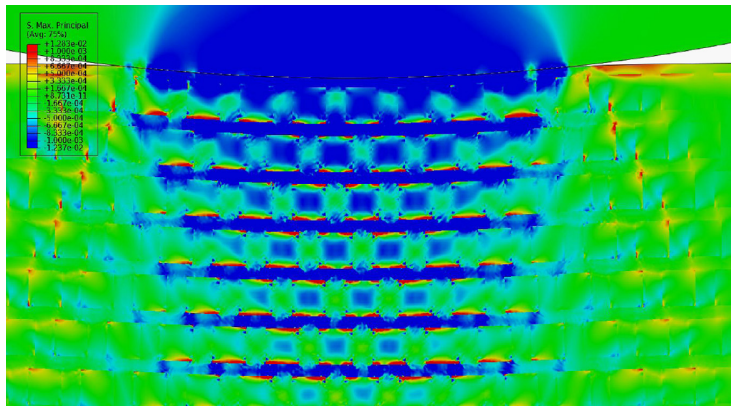

Fig. 10. Simulation of first principal stresses in an indentation contact by the ideal synthetic model.

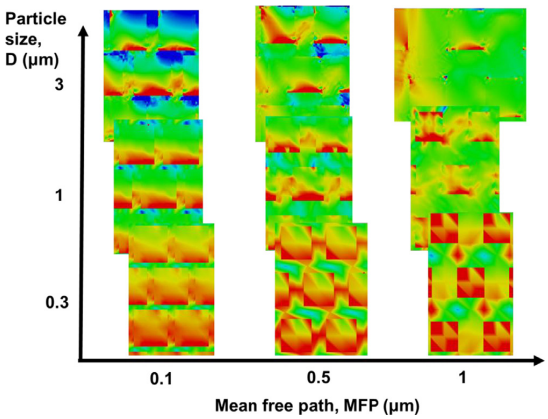

Fig. 11. Simulations of first principal stresses under an indentation contact by the ideal synthetic model for three particle sizes and three mean free paths. The image dimensions are scaled to show the carbides at about equal size to better visualise the stress fields.

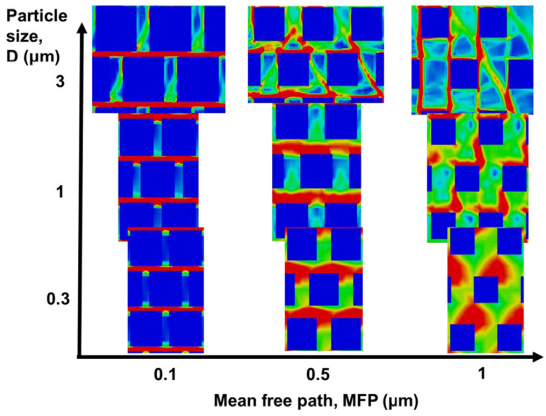

Fig. 12. Simulations of material strains under an indentation contact by the ideal synthetic model for three particle sizes and three mean free paths. The image dimensions are scaled to show the carbides at about equal size to better visualise the strain fields.

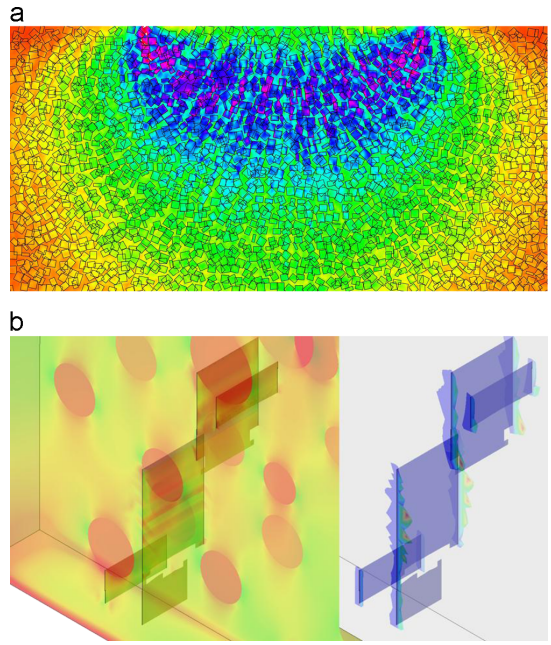

Fig. 13. (a) The distribution of first principal stress in an indentation contact utilising the advanced synthetic model for the WC-CoCr coating. (b) Initiated cracks in the laser cladded WC-NiCrBSi coating simulated by use of the advanced synthetic model: crack initiation and propagation in the microstructure (left), and details of the crack field shape (right).

strengthening caused by the carbides in a Dirichlet type boundary value problem, is fairly non-existent. The carbide state hardly differs from the state of the binder matrix material.

The decrease of MFP brings forth an increase in the near-particle edge stress state, but stress gradients within the particles themselves can still be observed. The decrease of particle size from micro-size and to nano-size changes the way the particles are stressed, i.e. their internal stress state. The decrease of MFP acts in a similar manner with few exceptions explained below. The decrease of particle size is seen to homogenise the intra-carbide stress state, although for example at the micro-size range there are

still notable gradients within the particles, but the stress state is increased from those in the conventional, several microns, size range.

The nano-size range is demonstrated to yield an even more uniform state of stress, and it is also seen that the state of stress within the binder increases as a result of particle interaction, which was in Fig. 12 seen as a transition in binder deformation. The nano range of carbides displays the most uniform states, but the binder is under a more stringent and confined stress–strain state in comparison to the other studied cases.

For very small MFP:s and nano-size carbides, it is seen that the system tends again towards a somewhat more uniform state of stress when the intra carbide stress gradients appear to dissipate. This suggests a slight change in the mechanism of strengthening, the system appearing to behave almost as a layered composite when the binder deformation is confined to a lateral direction and the particles interact strongly with each other.

Thus, a decrease in the MFP and the particle size support a greater strengthening effect, but simple minimisation is not straightforward optimal for all applications, since it leads to an elimination of mechanisms of deformation and can decrease the degree of strengthening. This can lead to a decrease in fracture properties of the structure, such as the fracture toughness. Furthermore, the performance component is strongly affected by the presence of pores and cracks, and a more lenient structure in terms of stress–strain state exhibits less potential conditions for void and crack growth, and the material toughness is as well lower under such conditions.

A complete exploitation of the performance of single phases and their interfaces by increasing the system strength does also pose requirements for toughness of both the cohesion of the microstructural elements and their interfaces, and these need to be accounted for when considering the optimisation of a certain structure and tailoring a coating.

6.2. Advanced synthetic model stress simulations in indentation

The advanced synthetic model yields results that are controlled by the statistical properties of the microstructure, as presented in Fig. 13 for the WC-CoCr and WC-NiCrBSi coatings. It is seen that the structure does not contain the detailed features of the real models, but on the other hand, the distinct effects of microstructure statistic are clearly visible.

In Fig. 13a results for indentation of WC-CoCr coating are presented, illustrating the heterogeneous first principal stress distribution as arising from the statistical properties related to carbide size, location and orientation. The homogenisation effect present in simple synthetic models is visible when comparing to earlier findings of Section 6.1. The advanced synthetic model emphasises the importance of local microstructural features such as carbide size and mean-free path.

An analysis of indentation of the WC-NiCrBSi coating containing initiating and propagating defects is presented in Fig. 13b. Idealised carbide morphology is utilised in a statistical setting with respect to the spatial arrangement. Cracks initiate and propagate following an XFEM treatment of the resulting displacement discontinuities. In Fig. 13b on the left the principal stress distribution along with the defects is shown, and on the right level sets of individual cracks are highlighted to display the individual cracks. Cracks propagate following a fracture toughness based criterion typically initiating at the stress concentrations present at carbide to binder interfaces due to elastic and plastic mismatch in mechanical properties. In the current indentation type loading configuration, cracks propagate through the coating driven by the tensile stresses present in the coating, especially since the fracture criterion is simplified and based on mode I fracture toughness neglecting any mixed-mode contributions.

6.3. Real model stress and strain simulations for WC-CoCr in scratch test

The stress and strain fields are highly affected when the computations include microstructural features compared to macro-contact level calculations, as shown in Fig. 14. In the figure the scratch test tip crosses from a macro scale homogeneous domain to an embedded block of composite microstructure. In the macro scale analysis the stress field is uniform and displays common features identified to belong to a two body contact simulation.

The real model analysis results differ in the sense that the local structure of the WC-CoCr coating affects the stress distribution, resulting in a response which does not compare with the macro scale contact analysis, but gives a principally different result. The coating structure of the real model is behaving as a statistical sample of the actual microstructure, i.e. being a statistical volume element.

As such the microstructure, not its average or homogenised response, affects the outcome and performance at the scratch test contact scale. In addition to the local nature of the stress field in the real model, it is also noteworthy, although not necessarily clearly evident, that the peak values, in terms of von Mises stresses, are higher in the real model than the average stresses in the macro scale model. This can be expected considering the nature of material discontinuity in the composite structure.

Results obtained from using the real model for the WC-CoCr coating are presented in Fig. 15 for first principal stresses.

The local micro scale nature of the results and the impact of the composite structure are emphasised in the determination of how

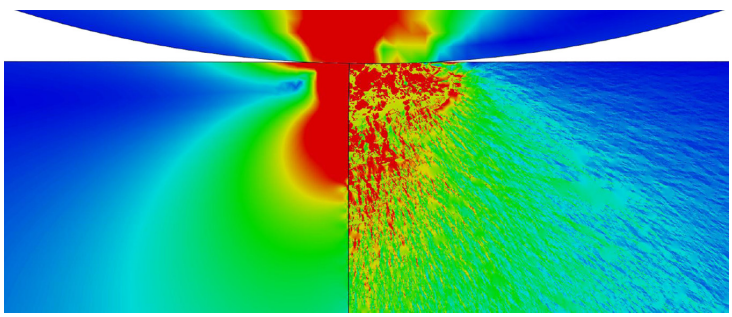

Fig. 14. First principal stresses in a contact with a spherical diamond tip sliding on a thermal spray WC-CoCr coated surface as calculated with macro dimensions (on the left) and with microstructural features (on the right).

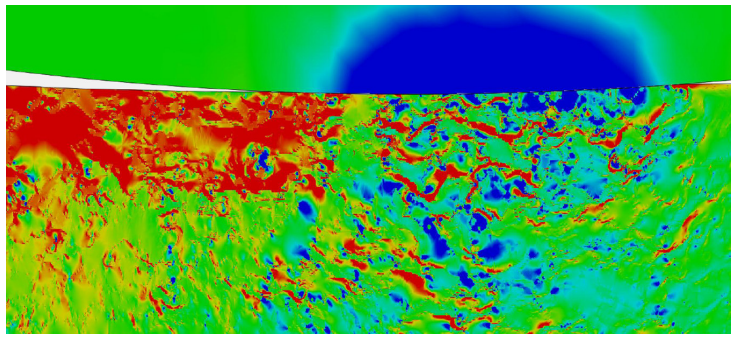

Fig. 15. First principal stresses in a thermal spray WC-CoCr coating undergoing scratch test surface loading. The stress maximum is ~7.5 GPa. The stress distribution highlights the mismatch between the WC particles and the CoCr binder properties, as well as local micro scale geometric features of the WC particles. The tip is sliding from the left to the right.

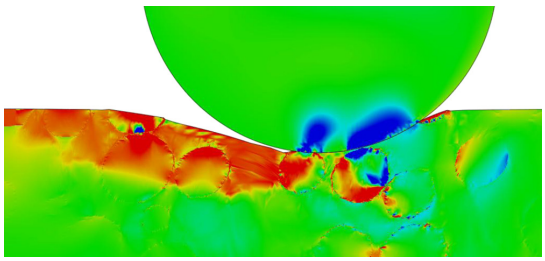

Fig. 16. First principal stresses in a laser cladded WC-NiCrBSi coating undergoing scratch test loading. The strain maximum is ~0.2. The primary mechanism of deformation is NiCrBSi plasticity amidst the carbide structure. The tip is sliding from the left to the right.

a specific nano- or microstructure responds to an applied external state of loading. Although the nano- and microstructure do play havoc on the stress–strain fields if compared to macro scale continuum analysis results, certain similarities can be identified, if comparing for example to previous work reported by Holmberg et al. [20,21] and Laukkanen et al. [23].

The material regions undergoing principally tensile and compressive states of stress are still visible. The area immediately beneath the scratch test tip and within the contacting region experiences a compressive state, while the region trailing the contact undergoes a tensile stress state. However, although the macro scale state driving the material response towards these principal states can easily be identified, the local response is also affected by the nano- and microstructure topology, as shown in Fig. 15.

6.4. Real model stress simulations for WC-NiCrBSi coating in scratch test

The first principal stress state of a WC-NiCrBSi laser cladded coating is presented in Fig. 16 by applying the developed real model. The situation is quite different from the WC-CoCr thermal spray coating in terms of microstructural features, since the size scale of the WC particles is several orders larger than those in the thermal spray coating and in their shape the spherical feature dominates. The carbide size is comparable to the size of the tip used in the actual contact, and the MFP of the microstructure is similarly in a completely different scale, as shown in Fig. 16.

As shown in Fig. 16 the tip is in direct contact with only a couple of WC particles, and the total particle count of the model can be easily identified. The coating in this sense is comparable in many respects to the simple synthetic model presented earlier.

The stress–strain state is greatly affected by the behaviour of the binder, since at the scale of the microstructure the WC particles are surrounded by it and locally the large MFP permits the binder to deform with limited interference by the carbides. The mismatch in the stress state between different phases is smaller, and the distribution of stress is more homogeneous. The particles experience tensile stress particularly if they are in direct contact with the loading tip. Plastic flow occurs within the binder with fair ease.

7. Model validation and wear testing

It is important in computational material modelling and simulation to include empirical validation of the computational results. This is the only way to assure that the model reflects the reality. The validation is typically done step by step and on different levels starting from very simple contacts and surface interactions and continuing all the way to real component testing.

In this study we have chosen to validate the computational results by the following empirical methods:

1) Deformability by indentation.
2) Crack behaviour by scratch test.
3) Abrasive wear in rubber wheel test.
4) Sliding wear and friction in pin-on-disk test.

A very simple first validation test for the material model was to check if the model deforms in a similar way as a sample of the material in an indentation test where an indenter was pressed some micrometres into the surface. The elastic and plastic response to loading was recorded and compared to computer simulated results. Initiation of first cracks was recorded and compared to locations of tensile stress peaks in the simulations.

The scratch test adds to the testing the tangential load on the surface and is thus closer to the loading conditions in a tribological sliding contact. In scratch test deformations were compared to simulated deformations and the crack behaviour was clearly demonstrated in the scratch groove by the development of the cracking at increasing load. The crack pattern was compared to stress and strain pattern from the simulations.

The validation of computational results by tribotesting with continuous contacts producing accumulated wear products is much more complex and not so straight forward. However, well controlled tests like rubber wheel test for abrasive wear and

Table 2
Results of the empirical validation, tribotesting and from numerical modelling (*in italic*).

Performance	Symbol (unit)	Reference steel AISI1018	Thermal spray coating WC-CoCr	Laser cladded coating WC-NiCrBSi
Indentation				
1. Total deformation as indentation depth at 3 N	h (μm)	6.65 (± 0.83)	3.8[a] (± 0.25) 3.5[b] (± 0.20)	4.7[a] (± 0.18)
—post load release	h (μm)	6.31 (± 0.88)	3.0[a] (± 0.79) 2.9[b] (± 0.70)	4.2[a] (± 0.16)
2. Total deformation as indentation depth at 3 N from the model	h (μm)	*NA*	*2.7*	*4.6*
3. Crack initiation by indentation	Load for crack initiation (N)	NA	125[a] (± 6)	[c]
4. Crack growth by indentation	Indentation fracture toughness K_{Ci}	55	6.7[a] (± 0.57) 6.1[b] (± 0.55)	11 [d]
Scratch test				
5. Crack initiation by μ-scratch test[a]	L_{CA} (N)	1.25 (± 0.22)	13 (± 2.9)	1 (± 1)
	L_{CSC} (N)	–	20 (± 2.7)	25 (± 6)
	L_{CD} (N) [e]	7.38 (± 0.08)	30 (± 3.0)	50 (± 5)
6. Average tensile stress in scratch test from model	ref load 10 N	*NA*	0.8 (at 10 N)	0.2 (at 10 N)
	σ (GPa)/L_{CA}	*NA*	1.3 (at 13 N)	0.07 (at 1 N)
	σ (GPa)/L_{CSC}	*NA*	2.1 (at 20 N)	0.24 (at 25 N)
	σ (GPa)/L_{CD}[e]	*NA*	3.0 (at 30 N)	0.42 (at 50 N)
Rubber wheel abrasion test				
7. Abrasive wear volume loss in rubber wheel test	(mm^3/min)	9.4	0.2	4.2
Pin-on-disk test				
8. Sliding wear rate in PoD for Al_2O_3 pin (ball) and disk	K_{pin} (10^{-6} mm^3/N m)	0.3	3.2	1.2
	K_{disk} (10^{-6} mm^3/N m)	250	< 0.02	< 0.02
9. Friction in PoD vs Al_2O_3 pin (ball)	μ (−)	0.48	0.75	0.41

[a] Measured from the surface.
[b] Measured from cross-section.
[c] No suitable method available due to the large carbides and small mean free path that does not give enough surface for measurements.
[d] Literature value.
[e] L_{CA} is load at which the first angular cracks become visible; L_{CSC} is the load at which the first semi-circular cracks in the grove become visible; L_{CD} is the load at which the first delamination as removal of material flakes from the surface becomes visible.

pin-on-disk test for sliding wear were very useful. They showed qualitative and quantitative wear behaviour in these specific contact conditions and trends in wear performance when changing influencing test and material parameters. This was compared to simulated surface strength performance.

Indentation testing was done with a Rockwell C 200 μm radius diamond tip for the material deformation validation shown in Table 2. Tests were repeated 10 times for the coated samples and 5 times for the AISI 1018 sample. This was done due to concerns regarding the relative mechanical heterogeneity of the coated samples relative to the more homogeneous steel. The critical crack initiation load was detected from the loading part of the load-indentation depth curve as a jump where load does not increase, but indentation depth seems to advance [49]. This load value correlates to the moment where the major corner cracks are initiated [50,51].

Scratch testing procedures were based on the European Standard EN 1071-3. This is developed for the testing of thin ceramic coatings. However, the methodology seems relevant to thick carbide coatings too [4]. A linearly increasing, progressive normal load was applied to the sample with a Rockwell C diamond tip. The minimum and maximum normal forces applied in the tests were 0.10 N and 50 N, respectively. The initial normal force was 0.03 N. The scratch length was 5 mm and the scratch speed was 10 mm/min. The scratch tests were performed in a laboratory air of 22 ± 1 °C temperature and 50 ± 5% relative humidity [4,52,53]. The scatter in the results for the composite heterogeneous thermal spray and laser cladding coatings is seen in the deviation values in Table 2. The mechanisms behind this are in detail discussed in [56,57].

Rubber wheel sand abrasion tests were done according to ASTM G65 standard, where samples were forced against a rubber wheel in dry conditions with standard surface roughness at a static normal force of 45 N. Silicon oxide particles with an average size of 250 μm and a mass flow of 235 g/min were used. The sliding velocity was 1.86 m/s and test time was 30 min for all samples. Tests were done twice for all samples and the average mass loss during the tests was measured [54].

Pin-on-disk (PoD) testing was carried out according to standard ASTM G99. The rotating samples had a sliding velocity of 0.1 m/s against an alumina ball with a 10 mm diameter. A normal force of 10 N was applied. The sliding time was 2 h. However, the tests with the steel sample disks were shorter as high wear was obtained early on, whilst developing a stable coefficient of sliding friction. Tests were repeated three times for all samples and the wear rates were calculated accordingly [1,55].

Wear images of the thermal spray and laser cladded worn surfaces as well as the worn surfaces of the alumina pin after pin-on-disk testing are shown in Fig. 17a, b, d and e after 120 min sliding, and of the steel disk worn surface and its corresponding alumina ball counter surface in Fig. 17c and f after 41 min of sliding. Summary of validation and tribotesting results are in Table 2.

8. Discussion

8.1. Computational modelling approach

In this work we used the PSPP methodology for presenting both the computational and experimental data systematically in four categories: processing, structure, properties and performance. This methodology supports the systematic data collection that the computational modelling requires. The computational modelling and simulations in this study covered the links from the coating microstructure to the tribological performance while the link to processing of the coating will be reported separately.

The collecting of relevant input data for the material model of the thick coatings turned out to be not so easy. The processing data

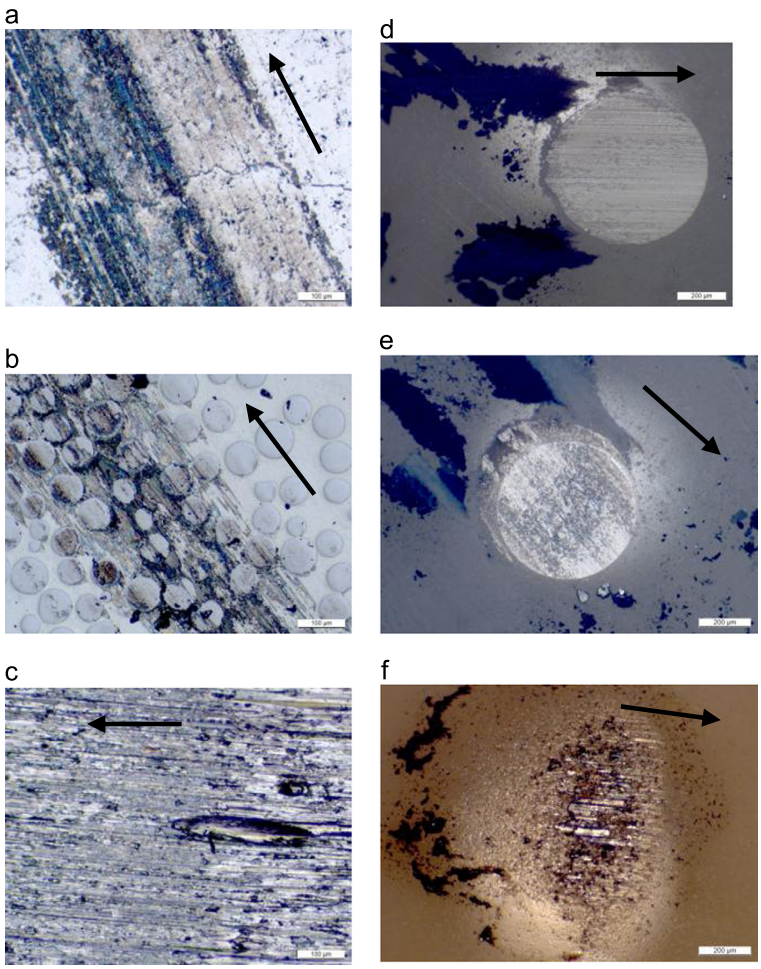

Fig. 17. Images of worn surfaces from pin-on-disk testing of the (a) thermal spray WC-CoCr coating, (b) the laser cladded WC-NiCrBSi coating, (c) the steel surface, and from the ceramic Al_2O_3 pin countersurfaces (d), (e) and (f), respectively. The arrows show the sliding directions of the counter surfaces.

and the structural data was fairly straight forward to measure with state-of-art techniques. In some cases, when we lacked suitable measuring methods, we needed to rely on data from the literature. The large size of the carbide particles in the matrix caused problems with the generation of reliable data from the performance tests (Table 2), especially for the laser cladded coatings.

However, this approach made it easier to overview the whole and very large set of measured or extracted input material data to the model, as well as the simulated performance data and the experimental data for the validation. There is a clear need to further develop and at some stage to standardise the PSPP methodological structure and also to develop some of the measurement techniques needed for generating microstructural data for composite materials that are relevant for their tribological evaluation.

8.2. The model development and simulations

The methodology developed for synthetic models which can capture the statistical and morphological features of the coating microstructures is novel. The adopted approach is general, i.e. the possibilities for controlling and tailoring the structures are numerous and primarily limited only by the available and obtainable statistical information about the microstructures in question. Numerous directly microstructure founded real models have been derived, and their use in this sense has become a commonplace routine. The combination of both synthetic and real models enables one to better understand the dependencies and causal relations between microstructural features and stress–strain fields, as well as the role of different micromechanisms responsible for material properties and component performance.

The synthetic models can, for the most part, be treated with common free meshing algorithms. Some of the more complex meshing scenarios involving stochastic procedures in the generation of the microstructure can only be tackled by routines applicable to actual real microstructural models. In the cases available solutions for generating meshes for real microstructural input were adapted, refined and further developed for the coatings under study. This was done particularly to address mesh phase boundary feature preservation issues in the thermal spray coatings.

Steps were taken towards simulating the behaviour of the coatings also in a performance limiting manner, focusing particularly on

effects of defects. Application of homogenisation methods to extract macroscale properties is often adequate, but performance limiting micromechanisms can be approached only if the actual mechanisms themself are modelled in the component setting of interest. The use of state-of-the-art finite element techniques, XFEM in particular, appears quite capable in being able to handle the numerics of the fracture mechanical problem in a case where the phase distributions are quite challenging.

8.3. Model validation by empirical testing

The direct validation of the models was done by comparing material behaviour in indentation and scratch testing. These contact conditions with an inert and rigid diamond tip are simplified to such a degree that a direct quantitative comparison was possible. The level of computational modelling is not yet advanced enough to allow direct quantitative validation in the more complex abrasive rubber wheel and sliding pin-on-disk test conditions. These two methods are included to show the link to real tribological accumulated wear contacts by more general qualitative evaluation of the tribological behaviour.

The empirical data from the laboratory testing is shown in Table 2. Deformability data from indentation and cracking information in scratch testing extracted from the numerical simulations is also shown for comparison. In addition to the two studied thick composite coatings is similar data shown for a steel surface as a well-known reference material.

In indentation with 3 N load on the laser cladded coating was the plastic indentation depth 4.7 μm while it was 4.6 μm as calculated from the model and shows very good agreement (1 and 2 in Table 2). For the thermal spray coating were the similar values 3.5–3.8 μm and 2.7 μm, respectively, and show a fair agreement. The reason for the lower level of agreement may be due to the more complex and oriented structure in thermal sprayed coatings which is seen from the lower post load release values. The softness of the steel surface is reflected by the higher 6.65 μm indentation depth value.

Indentation test was also used for observing the cracking behaviour and both the crack initiation loads as well as the fracture toughness indicating the crack growth are of interest. Crack initiation load and fracture toughness was measured for the thermal spray coating but no value of the crack initiation load for the laser cladded coating could be obtained (3 and 4 in Table 2). The reason is that there was not enough free surface to enable accurate measurements with the used technique due to the large carbides and the small mean free path. The higher fracture toughness of the reference steel is observed.

The scratch test was used to compare how the critical loads for initiation of the studied three cracking patterns correlate with the calculated average tensile stresses at the same locations on the surface (5 and 6 in Table 2). The first angular and circular cracks and delamination occur at 13, 20 and 30 N load for the thermal spray coating and the calculated average stresses at the same locations would be 1.3, 2.1 and 3.0 GPa. This shows that a tensile stress of above 1.3 GPa is needed at the surface at the groove edge to form the first cracks but more than 2.1 GPa is needed at the surface in the bottom of the groove. The reason is that the circular cracks are generated in the bottom of the groove where the concave geometry hinders crack generation while the angular cracks and delamination occurs at the convex groove edge where the geometry and its local curvature due to deformation promotes crack generation.

The laser cladded coating (5 and 6 in Table 2) showed a very early first angular crack at 1 N load with calculated maximum average tensile stress value at that location of only 0.07 GPa. A load of 50 N was on the other hand needed for the generation of the first delamination. The generated average tensile stress at the same reference load of 10 N and at the same location was more than four times higher for the thermal spray coating.

The empirical crack initiation load data from scratch test and the calculated average tensile stresses from the model based computational simulations are compared in Fig. 18. The crack initiation load values correspond to four different cracking types. The values both for thermal spray and laser cladded coatings follow almost a straight line indicating a very good correlation between the model simulations and the experimental results. The lines also show how the thermal spray coating generate much higher tensile stresses at the same surface loading compared to the laser cladded coating. Surface cracking is on the other hand appearing earlier at higher loads for the thermal spray coating.

The results from the rubber wheel tests show, as expected, a very good wear resistance of the thermal spray coating (7 in Table 2), a fair wear resistance of the laser cladded coating and the poorest wear resistance of the reference steel surface.

On the other hand, in the pin-on-disk dry sliding conditions (8 and 9 in Table 2) the thermal spray coating showed a very high coefficient of friction, $\mu=0.75$, and high wear of the alumina ball counter surface while the laser cladded and reference steel surfaces had a lower coefficient of friction, $\mu=0.41–0.48$, and did not cause so much wear to the alumina ball counter surface. The wear rate of both composite coatings was very low, below the measurement limit of the instrument, while it was very high for the steel surface.

The high friction and wear in the thermal spray coating vs the ceramic Al_2O_3 pin is explained by a very severe contact situation with a hard pin sliding and scratching against hard and sharp small carbide particles in the metallic matrix. The contact situation is less severe for the laser cladded coating sliding vs the ceramic pin since in this case particles form larger and smoother circular areas on the sliding surface, which easier can carry the load and offer lower shear. Some material transfer on the coated surface was observed. With the steel surface sliding in the same conditions against the ceramic pin was steel material transfer to the ceramic pin surface observed and after some sliding cycles the contact was actually steel sliding against a steel layer on the ball. This is also reflected by the friction and wear values.

A comparison of the wear test results with the results of the indentation experiments shows a mild correlation with hardness, or the plastic deformability of the surface in question. The fracture toughness of the reference steel was superior to that of the coated

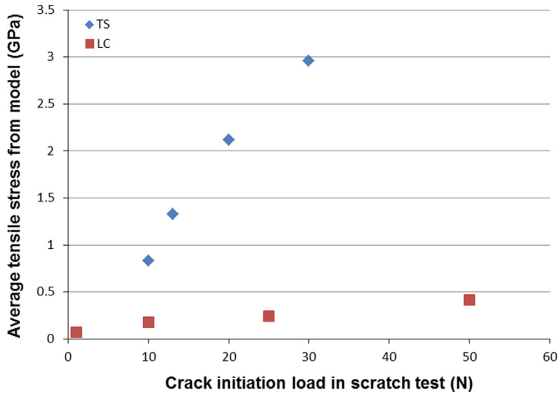

Fig. 18. Calculated average tensile stresses from model based simulations as a function of crack initiation load for four different crack types (see point 6 in Table 2) from empirical scratch testing. Data is shown for the thermal spray (TS) and the laser cladded (LC) coatings.

surfaces, and does not directly correlate or has an inverse relationship with the wear rates. A comparison of the wear results with the scratch test results similarly suggests that the tribologically beneficial properties of the thermal spray coating result from a high fraction of high modulus reinforcement particles, which results in extremely high local peak tensile stresses identified to correspond with the scratch test critical loads.

A feature in tribological problems which frequently is neglected in modelling efforts is the effect of surface roughness on the results. Also in our current work the surfaces have been assumed to be ideally smooth. Justification for this idealisation in the current work arises from observations made about the dominating role of the local WC phase distribution. The local microstructural features influence the stress–strain fields far more than the overall contact mechanics and geometry of the problem. As such, it is reasonable to argue that surface roughness values of the order measured in the current work have far smaller influence on the overall coating behaviour than its microstructure. However, it must be noted that with respect to performance related measures surface roughness will in many cases most likely play a case specific role and needs to be addressed in future works. This concern particularly defect initiation related coating performance.

The model validation methods applied showed good correlation between the numerical simulation results and the indentation tests with regard to loading response of the surfaces. The corresponding correlation showed fair agreement in scratch testing. For pin-on-disk and rubber wheel abrasion test there was a qualitatively explainable material behaviour supported by the quantitative results.

8.4. Simulated surface stresses, deformations and strains on macro and micro scale

The prime purpose of the numerical modelling was to bridge the gap between macroscopic findings and results obtained by applying the various synthetic and image based modelling techniques. The experimental findings of Section 7 were linked to numerical results of Sections 6.3 and 6.4, which provide the most accurate description of material behaviour by the use of the image based models. The discussion below is based on a detailed analysis of the complete set of computational stress and strain simulations carried out in comparison with the results from the empirical testing.

The behaviour of the reference steel, although not computationally evaluated, is considered to result from properties common to such materials, i.e. the mechanisms of plastic deformation during a sliding contact process, which is fundamentally different from the wear processes that caused the deterioration of the coated surfaces. The reference steel is assumed to have been subject to local plastic deformation during the various wear related experiments, and as a result of this, to the initiation of surface failure.

8.4.1. Laser cladded coatings

The assessment of the behaviour of the laser cladded coating, and findings discussed above on the basis of the real model based results, suggests that the large spherical tungsten carbide particles, which are scarce in density, dominate the behaviour of the coating by leading to a partially exposed binder. The abrasive wear resistance is actually somewhat poor, especially in comparison with the thermal spray coating, and of the same order as that of the reference steel, while the sliding wear performance is similar to that of the thermal spray coating.

The results that represent the abrasion resistance of the laser cladded coating are apparent in the real model analysis results, and indicate that the tendency for plastic deformation in the binder is a significant wear resistance issue, which is related to the exposed binder. The binder may locally directly be affected by the wear process, and the binder is worn while the WC particles to great extent remain intact, and hence the probable mechanism for their removal is the loss of the binder support.

For sliding wear conditions, the situation is somewhat different. The numerical analyses indicate that the reinforcement particles, albeit being large in size, and the soft binder that is greatly exposed, are more than capable to reinforce the surface by improving its load carrying capacity. In an optimal setting between the two sliding surfaces, the coated surface responds to the contact pressure though the carbides that carry the load in an elastic manner, and the stress state remains at a sufficiently low level not to transmit significant plastic deformation to the more compliant binder material. This can be expected for macro scale contacts. In real contacts with asperities and actual surface roughness, the material loading response can be assumed to occur mainly locally on micro scale in an average sense. The counter surface is able to reach the deforming regions of the coating, either directly or through greater contact pressures via the interface to carbides. This initiates the wear process by binder failure and carbide–binder interface failure (Fig. 17b and e).

The possibility of direct particle failure cannot be excluded, as this was observed especially in the scratch tests, in conditions favourable to particle crushing due to the steep loading gradient and the high final load level. For moderate loading, a significant contributing load-carrying mechanism is one where the WC particles face the contact stresses and this is comparable to friction results in pin-on-disk testing. In sliding contact against an alumina ball the laser cladded coating exhibited a lower coefficient of friction than the thermal spray coating, and this suggests a microstructural influence arising from the spherical carbides. Thus, as long as the wear conditions are favourable and the contact pressures are controlled with respect to carbide fraction and density, the laser cladded coating can perform with satisfaction.

8.4.2. Thermal spray coating

The thermal spray coating is fundamentally different in its layout in comparison to the laser cladded coating. In terms of real model results the thermal spray coating can be considered an extreme of decreasing the mean-free-path and increasing the particle fraction. The surface design of the coating relies on a high carbide fraction and the purpose of the substrate, as suggested by numerical real model analyses, is from a mechanical performance standpoint to offer mechanisms for deformation. As a result, the structure of the coating is resistant against both abrasive and sliding wear since the volume of WC reinforcement particles is able to endure very high stress states without significant failure (Fig. 17a and d).

It is likely that local micro scale forms of failure, such as interface decohesion or initial cracks or pores, are made milder to some extent by the ductile binder. In terms of the ability of the binder to deform and strain harden, the local binder strains are the sole mechanism of deformation present in this kind of coating structure. Due to the heterogeneity of the thermal spray coating structure, no clear cracking mechanism or path is available, but rather the local micro scale conditions are dominating. This behaviour is strongly influenced by the statistical properties of the composite structure.

The particle-to-binder effective elastic modulus has been tailored by experience to correlate with the composite structure in the first place. The risks with such a structure lie in how it tolerates defects. If local high stresses are present, any defect with even a minute size can become critical and lead to the initiation of a microscopic crack. This is indicated by the fairly low fracture toughness measured for the thermal spray coating, which is, however,

a very expected value. Thus, one of the features of an optimal coating is a defect distribution, with regard to size and shape, which is in compliance with the distribution of material within the microstructure. Defects in microstructural hot-spots, such as throats between particles, singular like carbide shapes, areas with imperfect mixing from a phase fraction standpoint etc., need to be avoided. Otherwise, the coating toughness is affected, resulting either in carbide fracture or deformation concentration within a local region of the binder.

The control of the interface properties, as well as the control of the secondary phases, is of great importance. The higher the WC particle fraction is, the less tolerance there is for internal defects on any scale. The design of a coating needs to weigh in the requirements, preferably on a component case basis, set to its microstructure, whether for example a lower modulus structure with larger MFP:s, and greater tolerance for defects, is acceptable, or whether extreme resistance to abrasion is required with small MFP:s and a high carbide fraction.

Thermal spray coatings seem to exhibit optimal microstructures that are case specific against a certain form of failure or wear process. An optimal system needs to retain its ability to deform as influenced by the binder fraction, structural morphologies and brittle phases, but it also need to withstand the relevant failure mechanisms, which in terms of wear resistance largely depends on the WC particles. The optimal microstructure is depending on the dimensional scale and the actual application. Going to any extreme e.g. in particle size distribution is not a solution to yield a multi-purpose coating. The thermal spray coating is sensitive to any local variation in the WC properties or to the introduction of secondary structures, since the extremely high local stresses increase the probability of initiating cracks on the microstructural size scale.

9. Conclusions

In this study we use a PSPP based approach for wear resistance evaluation based on computational modelling and simulation and on empirical validation. The developed software according to this methodology is named VTT ProperTune™. The method is used for evaluation of the wear resistance and for improved understanding of the macro and micro scale surface fracture and deformation mechanisms of thermal spray WC-CoCr and laser cladded WC-NiCrBSi composite coatings, with AISI 1018 steel as a reference material. We conclude the following:

1) The PSPP structure turned out to be a logical and good systematic frame for computational modeling based wear studies over multi-scale levels from macro to micro and nano level.
2) Three material models were developed for composite thick coatings: (i) an ideal synthetic defect-free material model, (ii) an advanced synthetic material model containing defects, and (iii) a real image-based material model.
3) The ideal synthetic material model was useful for the understanding of the generic material behaviour under loading, and for the identification of critical and dominating parameters in relation to wear and parameter interactions.
4) The image-based real finite element model was useful for the investigation of specific material structures, both on macro and micro level, and the model gave very precise quantitative information about deformations, stresses and strains in real materials at specific loading conditions.
5) In composite coatings, the tensile stresses are driven by similar features of nano- and microstructure as observed on macro scale. High local curvature, notches, abnormally large particles, thin ligament or throat-like structures of a specific material phase, clusters of inter-linked carbides or high local fraction of a specific material phase have a great impact on the resulting stress state.
6) The composite coatings studied showed about 2 to 50 times lower wear in abrasive conditions and more than four orders of magnitude lower wear rate in sliding conditions than that of the reference steel. The thermal spray WC-CoCr coating is fundamentally different in its layout in comparison with the laser cladded WC-NiCrBSi coating. In the laser cladded coating, the mismatch in the stress state between different phases is smaller, and the distribution of stress is more homogenous than it is in the thermal spray coating.
7) With regard to short mean free path and high hard particle fraction, the thermal spray coating can be considered as an extreme microstructure. The coating system is resistant towards both abrasive and sliding wear since the amount of tungsten carbide reinforced particles enables the composite coating to accommodate very high stresses without significant failure. The influence of defects, such as interface decohesion or initial cracks or pores, is mitigated by the ability of the ductile binder to deform and strain harden. Due to the heterogeneity of the structure, no clear macro scale failure mechanism or fracture path occurs, but rather the micro scale microstructural conditions are dominating.
8) With very small mean free path and small submicron-size carbides, the coating system tends towards a more uniform state of stress as the intra carbide stress gradients seem to dissipate. In the studied case of a mean free path of 0.4 μm and grain size of 0.3 μm was optimal with regard to surface strength.
9) Based on this analysis can the following general recommendations for composite coating design for wear resistant applications be formulated:
   a. For abrasive wear conditions with high contact pressures is a thermal spray microstructure, like in the current study, beneficial since it gives high strength and can withstand high local surface scratching without failure. However, the counter surface may be prone to wear especially at larger grain size.
   b. For sliding wear conditions at lower contact pressures is a laser cladded microstructure, like in the current study, beneficial since the spherical hard particles can carry the load, give low friction and do not cause wear of the countersurface. A thermal spray coating with small carbide size may also give good tribological performance.
10) The applied model validation methods showed a good correlation between the numerical simulation results and the empirical results when comparing the indentation depth of the surfaces. The correlation was in fair agreement when comparing the numerical simulation results with the crack initiation in scratch testing. There was a qualitatively logically explainable material behaviour supported by the quantitative results from the rubber wheel and pin-on-disk tests.

The study showed that computational material modelling and wear simulation brings additional value to the empirical testing, in the form of better and deeper understanding of the basic material and contact mechanisms and the parameter interactions in relation to the wear resistance of surfaces in tribological contacts. This forms a platform for further systematic surface design and performance optimisation.

Acknowledgements

This study was carried out in the Matera project MOTRICOT – Model based tribologically optimised thick multimaterial coated

surfaces. The financial support of Tekes – the Finnish Funding Agency for Technology and Innovation; The Institute for the Promotion of Innovation by Science and Technology of Flanders (IWT); the participating industrial companies Omco, Metso and Ruukki and the VTT Technical Research Centre of Finland is gratefully acknowledged. We are thankful for the detailed critical comments and improvement suggestions received from our colleague Peter Andersson when checking the final text. The support from the Center for Thermal Spray Research at Stony Brook University, USA to A. Ghabchi is gratefully acknowledged.

References

[1] Holmberg K, Matthews A. Coatings tribology: properties, mechanisms, techniques and applications in surface engineering. Elsevier tribology and interface engineering series no. 56. 2nd ed. Amsterdam, The Netherlands: Elsevier; 2009.
[2] Davis JR, editor. Handbook of thermal spray technology. Ohio, USA: ASM International; 2004.
[3] Jeandin MA. Socratic approach to surface modification: the example of thermal spray. In: Proceedings of the 24th international conference on surface modification technologies, Dresden, Germany; 7–9.9; 2010. p. 3–20.
[4] Ghabchi A. Wear resistant carbide-based thermal sprayed coatings: process, properties, mechanical degradation and wear. PhD thesis. Stony Brook University, New York, USA. VTT Science no. 29. Technical Research Centre of Finland, Espoo, Finland; 2013.
[5] Sampath S, Jiang X, Kulkarni A, Matejicek J, Gilmore DL, Neiser RA. Development of process maps for plasma spray: case study for molybdenum. Mater Sci Eng A 2003;348:54–66.
[6] Vaidya A, Streibl T, Li L, Sampath S, Kovarik O, Greenlaw R. An integrated study of thermal spray process – structure – property correlations: a case study for plasma sprayed molybdenum coatings. Mater Sci Eng A 2005;403:191–204 (3A).
[7] Turunen E. Diagnostic tools for HVOF process optimization. PhD thesis. VTT Publication no. 583. VTT Technical Research Centre of Finland, Espoo, Finland; 2005.
[8] Turunen E. Custom-made materials for demanding conditions. Espoo, Finland: VTT Impulse, VTT Technical Research Centre of Finland; 2011; 26–31.
[9] Hannula S-P, Turunen E, Koskinen J, Söderberg O. Processing of hybrid materials for components with improved lifetime. Curr Appl Phys 2009;9: 160–6.
[10] Ghabchi A, Rombouts M, Holmberg K, Persoons R. Microstructure and failure modes during scratch testing of laser cladded WC-NiCrBSi coatings with spherical and angular carbides. Tribol.—Mater. Surf. Interfaces 2013;7 (1):13–20.
[11] Olsson GB. Designing a new material world. Science 1997;288(5468):993–8.
[12] Elalem K, Li DY, Anderson MJ, Chiovelli S. Modeling abrasive wear of homogeneous and heterogeneous materials. In: Totten GE, Wills DK, Feldmann D, editors. Hydraulic failure analysis: fluids, components, and systems effects. ASTM STP 1339. West Conshohocken, PA, USA: American Society for Testing Materials; 2001.
[13] Gupta M, Nylen P. Design of low thermal conductivity thermal barrier coatings by finite element modelling. In: Sudarshan TS, Beyer E, Berger LM, editors. Surface modification technologies XXIV, proceedings 24th international conference on surface modification technologies, Dresden, Germany, 7–9.9; 2010. p. 353–65.
[14] Holmberg K, Laukkanen A. Wear models. In: Bruce R, editor. Handbook on lubrication and tribology, vol. II: theory and design. 2nd ed.. New York, USA: CRC Press; 2012. p. 13–1–21.
[15] Wriggers P. Computational contact mechanics. Chichester, UK: John Wiley & Sons; 2002.
[16] Andersson TL. Fracture mechanics. Fundamentals and applications. 3rd ed.. London, UK: CRC Press LLC; 2005.
[17] Gong ZQ, Komvopoulos K. Mechanical and thermomechanical elastic–plastic contact analysis of layered media with pattered surfaces. J Tribol Trans ASME 2004;126:9–17.
[18] Gong ZQ, Komvopoulos K. Surface cracking in elastic–plastic multi-layered media due to repeated sliding contact. J Tribol Trans. ASME 2004;126: 655–663.
[19] Holmberg K, Laukkanen A, Ronkainen H, Wallin K, Varjus S. A model for stresses, crack generation and fracture toughness calculation in scratched TiN-coated steel surfaces. Wear 2003;254:278–91.
[20] Holmberg K, Laukkanen A, Ronkainen H, Wallin K, Varjus S, Koskinen J. Tribological contact analysis of a rigid ball sliding on a hard coated surface, part I: modelling stresses and strains. Surf Coatings Technol 2006;200: 3793–809.
[21] Holmberg K, Laukkanen A, Ronkainen H, Wallin K, Varjus S, Koskinen J. Tribological contact analysis of a rigid ball sliding on a hard coated surface, part II: material deformations, influence of coating thickness and Young's modulus. Surf Coatings Technol 2006;200:3810–23.
[22] Holmberg K, Matthews A. Coatings tribology: properties, techniques and applications in surface engineering. Elsevier tribology series, vol. 28. The Netherlands: Elsevier Science B.V.; 1994; 442.
[23] Laukkanen A, Holmberg K, Koskinen J, Ronkainen H, Wallin K, Varjus S. Tribological contact analysis of a rigid ball sliding on a hard coated surface, part III: fracture toughness calculation and influence of residual stresses. Surf Coatings Technol 2006;200:3824–44.
[24] Laukkanen A, Holmberg K, Ronkainen H, Wallin K. Cohesive zone modeling of initiation and propagation of multiple cracks in hard thin surface coatings. J ASTM Int 2010;8(1):1–21.
[25] Colaco R, Vilar R. A model for the abrasive wear of metallic matrix particle-reinforced materials. Wear 2003;245:625–34.
[26] Hu J, Li DY, Llewellyn R. Computational investigation of microstructural effects on abrasive wear of composite materials. Wear 2005;259:6–17.
[27] Hu J, Li DY, Llewellyn R. Synergistic effects of microstructure and abrasion conditions on abrasive wear of composites—a modeling study. Wear 2007;263: 218–27.
[28] Ben Tkaya M, Mezilin S, El Mansori M, Zahouani H. On some tribological effects of graphite nodules in wear mechanism of SG cast iron: finite element and experimental analysis. Wear 2009;267:535–9.
[29] Pearson JD, Zikry MA, Wahl K. Computational design of thin-film nanocomposite coatings for optimized stress and velocity accommodation response. Wear 2009;267:1137–45.
[30] Dick T, Cailletaud G. Fretting modelling with a crystal plasticity model of Ti6Al4V. Comput Mater Sci 2006;38:113–25.
[31] Chawla N, Sidhu RS, Ganesh VV. Three-dimensional visualisation and microstructure-based modelling of deformation in particle-reinforced composites. Acta Mater 2006;54:1541–8.
[32] Tan Y, Longtin J, Sampath S, Wang H. Effect of starting microstructure on thermal properties of as-sprayed and thermally exposed plasma sprayed YSZ coatings. J Am Ceram Soc 2009;92(3):710–6.
[33] Zhang M, McDowell DL, Neu RW. Microstructure sensitivity of fretting fatigue based on computational crystal plasticity. Tribol Int 2009;42:1286–96.
[34] Quey R, Dawson PR, Barbe F. Large-scale 3D random polycrystals for the finite element method: generation, meshing and remeshing. Comput Methods Appl Mech Eng 2011;200:1729–45.
[35] Lagner SA, Fuller ER, Carter WC. OOF: an image-based finite-element analysis of material microstructures. Comput Sci Eng 2001 May/June: 15–23.
[36] Reid ACE, Langer SA, Lua RC, Coffman VR, Haan SI, Garcia RE. Image-based finite-element mesh construction for material microstructures. Comput Mater Sci 2008;43:989–99.
[37] Wiederkehr T, Kluserman B, Gies B, Müller H, Svendsen B. An image morphing method for 3D reconstruction and FE-analysis of pore networks in thermal spray coatings. Comput Mater Sci 2010;47:881–9.
[38] Österle W, Kloss H, Urban I, Dmitriev AI. Towards a better understanding of brake friction materials. Wear 2007;263:1189–201.
[39] Mohd Tobi AL, Shipway PH, Leen SB. Finite element modelling of brittle fracture of thick coatings under normal and tangential loading. Tribol. Int. 2013;58:29–39.
[40] Anwar S, Axinte DA, Becker AA. Finite element modelling of abrasive waterjet milled footprints. J Mater Process Technol 2013;213:180–93.
[41] Seleson P, Parks ML, Gunzburger M, Lehoucq RB. Peridynamics as an upscaling of molecular dynamics. Multiscale Model Simul 2009;8(1):204–27.
[42] Amsellem O, Madi K, Borit F, Jeulin D, Guipont V, Jeandin M, Boller E, Pauchet F. Two-dimensional (2D) and three-dimensional (3D) analyses of plasma-sprayed alumina microstructures for finite-element simulation of Young's modulus. J Mater Sci 2008;43:4091–8.
[43] Beauvais S, Guipont V, Jeandin M, Jeulin D, Robisson A, Saenger R. Study of the porosity in plasma-sprayed alumina through an innovative three-dimensional simulation of the coating buildup. Metall Mater Trans 2008;39A: 2711–24.
[44] Holmberg K, Ronkainen H, Laukkanen A, Wallin K. Friction and wear of coated surfaces—scales, modelling and simulation of tribomechnisms. Surf Coatings Technol 2007;202:1034–49.
[45] Fritzen F, Böhlke T, Schnack E. Periodic three-dimensional mesh generation for crystalline aggregates based on Voroni tessellations. Comput Mech 2009;43: 701–13.
[46] Wang W, Liu XJ, Liu K. FEM analysis on multibidy interaction process in three body friction geometry with rough surface. Tribology, 6; 2012; 59–66.
[47] OOF2. Finite element analysis of microstructures. National Institute of Standards and Technology. ⟨http://www.ctcms.nist.gov/oof⟩; 4.1.2013.
[48] Hay JL, Pharr GM. Instrumented indentation testing. ASM handbook 2000;8: 232–43.
[49] Suhonen T, Varis T, Turunen E, Liu X, Ge Y, Söderberg O, Hannula S-P. The effect of microstructure on mechanical properties of HVOF sprayed WC-CoCr composite coatings. Tribologia Finnish J Tribol 2009;28:14–28.
[50] EN ISO 14923. Thermal spraying—characterization and testing of thermally sprayed coatings. European Standard, CEN Management Centre, Brussels, Belgium; 2003.
[51] Lan H, Venkatesh TA. Determination of the elastic and plastic properties of materials through instrumented indentation with reduced sensitivity. Acta Mater 2007;55(6):2025–41.
[52] EN 1071-3. Advanced technical ceramics – methods of test for ceramic coatings – Part 3: Determination of adhesion and other mechanical failure modes by a scratch test. European Standard, CEN Management Centre, Brussels, Belgium; 2005.

[53] Jennett NM, Owen-Jones S. The scratch test: calibration, verification and the use of a certified reference material. Measurement Good Practice Guide no. 54, National Physical Laboratory, Teddington, UK; 2002.
[54] ASTM G65. Standard test method for measuring abrasion using the dry sand/rubber wheel apparatus. West Conshohocken, PA, USA: ASTM International; 2010.
[55] ASTM G99. Standard test method for wear testing with a pin-on-disk apparatus. West Conshohocken, PA, USA: ASTM International; 2004.
[56] Ghabchi A, Varis T, Turunen E, Suhonen T, Liu X, Hannula SP. Behavior of HVOF WC-10Co4Cr coatings with different carbide size in fine and coarse particle abrasion. J Therm Spray Technol 2010;19:368–77.
[57] Ghabchi A, Holmberg K, Varis T, Sampath S., Damage mechanisms and cracking of thermal sprayed WC-CoCr coating under scratch test. Submitted to Wear; November 2013.

Publication III

Holmberg, K., Laukkanen, A., Turunen, E. and Laitinen, T., "Wear Resistance Optimisation of Composite Coatings by Computational Microstructural Modelling," *Surface and Coatings Technology.*

Surface & Coatings Technology 247 (2014) 1–13

Contents lists available at ScienceDirect

Surface & Coatings Technology

journal homepage: www.elsevier.com/locate/surfcoat

Wear resistance optimisation of composite coatings by computational microstructural modelling

Kenneth Holmberg *, Anssi Laukkanen, Erja Turunen, Tarja Laitinen

VTT Technical Research Centre of Finland, P.O. Box 1000, FI-02044 VTT Espoo, Finland

ARTICLE INFO

Article history:
Received 13 December 2013
Accepted in revised form 8 February 2014
Available online 15 February 2014

Keywords:
Modelling
Wear mechanisms
Composite coatings
Thermal spray

ABSTRACT

The wear resistance of components can be changed remarkably by surface coatings. New processing methods offer many possibilities to tailor the wear resistance of surfaces to match design criteria. Computational modelling and simulation is a systematic approach to optimise the wear performance. Modelling of physical surface phenomena can be carried out on all spatial scale levels, from sub-atomic one to macrolevel and for the various stages in material development, from material processing to structures, properties and performance. The interactions between the coating matrix, the reinforced particles, degraded material phases and defects like pores, cracks and voids are of crucial importance for the wear performance of composite coatings. This has been modelled by synthetic artificial models to find general design rules and by real image based models to find out the wear behaviour of specific coatings. The effect of particle size, morphology, clusters, mean free path and porosity was simulated for thermal spray WC–CoCr coatings. Four main very typical mechanisms for crack initiation resulting in surface failure have been identified: brittle carbide fracture, ductile binder cracking, interface failure, and cracking from pre-existing porosities and defects. The most important coating properties having a crucial effect on coating wear resistance are defects in the coating structure as they can create detrimental stress peaks and high strain levels, particle clustering is most critical for the durability of the structure, the elasticity of the particle is of great importance as well as matrix hardness and particle morphology.

Contents

1. Introduction

About one fifth of all the energy produced worldwide is used to overcome friction. This equals to 100 million terajoule annually and results in 7000 million tonnes CO_2 emissions. Transportation represents almost one third of all the energy used globally and 208 000 million litres of fuel was used in 2009 to overcome friction only in passenger cars, according to recent calculations [1–3].

The importance of wear is equally great but no detailed information of its global impact is available. However, a general understanding is that the impact of wear in terms of energy losses, environmental impact, component lifetime and economic costs could well be of the same level as that of friction. Taking advantage of the new tribological technology

* Corresponding author. Tel.: +358 20 722 5370; fax: +358 20 722 7069.
E-mail address: kenneth.holmberg@vtt.fi (K. Holmberg).

http://dx.doi.org/10.1016/j.surfcoat.2014.02.019
0257-8972/

Symbols

C	bearing load capacity
E	modulus of elasticity
H	hardness of softer material
K_c	fracture toughness
K	constant
L	applied load
L′	equivalent bearing load
L_{10}	lifetime
M	particle mass
N	number of asperities in contact
p′	bearing load-life exponent
S	sliding distance
V	wear volume
V	velocity
α	asperity shape factor
β	material cut probability factor

for friction reduction in passenger cars can lead to the reduction of fuel consumption by 18% in the short term (5 to 10 years) which would correspond to fuel savings of 117 000 million litres annually [1]. One of the key actions identified that can be used for friction reduction is the extensive use of advanced surface coatings.

Wear, as well as friction, is taking place at the top surface of products, components and tools. The wear resistance requirements are focused especially on the surface properties. Advanced surface engineering offers many possibilities to change the properties of surfaces to become more wear resistant by surface treatments, deposition of thin layers or processing of thick surface coatings.

There has been an extensive research for the development of wear resistant, low friction thin coatings that are only few micrometres thick and are deposited by vacuum techniques such as physical vapour deposition (PVD) and chemical vapour deposition (CVD). It has been possible to reduce friction to reach a coefficient of friction as low as 0.005 and below, and to increase the wear life in various conditions by 10 to 100 times, by applying very thin, hard, ceramic, carbon-based coatings and soft, metallic layers and their combinations [4,5].

Thin coatings may be vulnerable especially in high load and at high temperature conditions due to both material and structural limitations originating from their tiny thickness. The use of thick composite coatings is another solution to tailor surface properties of the component. Typical processing methods for thick coatings are thermal spraying, laser cladding, and weld hardfacing. These methods offer a flexible route to produce unique composite-structured, rather thick wear resistant coatings, in a typical thickness range from 150 μm to 3 mm, on a substrate material selected according to other criteria, like price, extent of alloying elements and other additives, mechanical strength and low weight [6–10,64–66].

Computational modelling and simulation of modifications in a material due to surface loading, and calculations of stress and strain in loaded contacts is a research area that is rapidly evolving today. Modelling and simulation of a tribocontact helps to understand the mechanisms that result in surface cracking, wear particle formation and continuous wear. The numerical simulations can be carried out on several spatial scale levels, from nanosize to macrosize, by using software representing the material structure from atomic and even sub-atomic to continuum macro and component level [11–15].

Thin films, like the PVD and CVD deposits, can often be modelled as a surface layer system, in which both film and substrate materials are considered as homogenous and in which the interaction between the coating and the substrate material, as well as the geometrical characteristics, are crucial for the wear behaviour [4,16].

Composite coatings, like the thermal spray coatings, need to be modelled in terms of their complex composite microstructure, including grains, pores, cracks and various phases in the matrix, in order to achieve representative stress and deformation simulations that correlate with the real situations in component operation. Composite surface structures of materials such as cast iron, WC–Ni alloys, metal matrix composites and PVD nano-composites have been modelled mainly with the two-dimensional (2D) finite element method (FEM) and with analytical models [17–21]. Microstructural models are more precise representations of the material microstructure and they have been developed based on three-dimensional (3D) FEM modelling for e.g. polycrystalline, SiC–Al alloy and Ti-6Al-4V alloy surfaces [22–25].

Microstructural models developed for representing real materials have been generated by numerical techniques based on image analysis of cross section images obtained by scanning electron microscopy (SEM) or light optical microscopy [13,26,27]. A 3D microstructural representation can be generated in a similar way, by taking microscopy images of several layers below the surface [28].

The modelling of the wear process, in which the material is detached from the contact surfaces and interacts in the dynamic triboprocess between the two moving surfaces, needs other kinds of modelling techniques, such as the movable cellular automata (MCA) methods used by Österle et al. [29]. Additionally finite elements can be applied by considering cracking mechanisms like in the work by Mohd Tobi et al. [30] when applied to thick coatings, or by considering material abrasion, like in the work by Anwar et al. [31]. Discrete methods overall provide several advantages for the modelling of material failure and removal processes, as has been demonstrated in the peridynamics approach by Seleson et al. [32].

Both 2D and 3D microstructure modelling and simulation methods have been demonstrated for characterising the mechanical properties of alumina, metallic FeCrBSi and TiC/Cu coatings with pores and cracks [28,33,34]. Based on empirical experience, it is known that size, shape and spatial arrangement and orientation of pores and cracks have a strong influence on the material properties of composite thermal spray coatings [7,10]. Since the pores can improve material flexibility and stop crack growth, the porosity is not always detrimental. Other microstructural material parameters that need to be optimised in a composite coating for a favourable tribological surface behaviour, in addition to the pore-related parameters, are the size, shape, density and spacing of the grains, the interfacial bond strength and the binder mechanical properties [19,21,24].

The purpose of this work is to present a review, mainly based on our own work and experience. The goal of the review is to show how modern microstructural computational modelling and simulation techniques have been developed for better understanding of composite material behaviour under sliding loading conditions and for investigating the effect of the main coating properties on wear resistance. The developed models concern thick composite coatings, they are here adopted for thermal spray WC–CoCr coatings and optimal design of the coatings is aimed.

2. Surface coatings for wear protection

The wear resistance of a surface can be modified by changing the surface material or the surface topography. The surface material properties can be changed by thermal or chemical surface treatment and by depositing or processing a new material with new properties on the surface. The new surface layer may be a homogenous single component layer, a multilayer structure with different properties in each layer, a gradient structure with gradually changing material properties or a composite layer typically including a matrix of one material, elements like particles of some other material, phases with changed or degraded properties of the included materials, and defects of various kinds, as shown in Fig. 1.

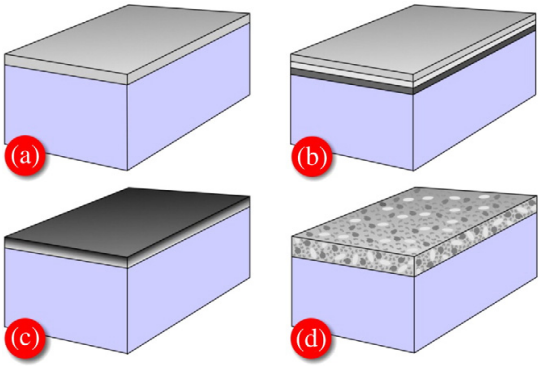

Fig. 1. Typical coating structures are a) single component coatings, b) multilayer coatings, c) gradient coatings, and d) composite coatings.

The creation of a composite coating structure is an elegant way to optimise the wear property to match completely the surface loading conditions so that the resulting stress peaks in the surface material are as low as possible and thus easier for the surface material to adapt without destruction. Composite coatings have been developed successfully for many applications but mainly using trial and error approach. In the following sections we will focus on how the wear mechanisms of composite coatings can be better understood by advanced computational modelling and simulation techniques and how the influencing parameters can be investigated and optimised with regard to wear resistance.

3. Wear prediction by equations and wear maps

The challenge to control and predict wear has been approached in three ways: by developing analytical or semi-analytical equations, by wear mapping and by computational numerical methods. The task to formulate wear equations and wear models has turned out to be not so easy. This is a very challenging task because of the complexity of the wear process. Still today we don't have any universally valid wear equation.

The large variety of different approaches to solve this problem has been shown by Meng and Ludema [35]. They found that up to 1994 there had been published more than 300 wear models and 182 of them were formulated as wear equations including more than 100 different variables and constants. This shows the large number of possible influencing variables on wear in different contact conditions.

The wear equations presented have been valid in some limited contact conditions but they all lack generality. The wear equations can be divided into three groups: 1) empirical equations formulated based on experimental data; 2) contact mechanics based equations assuming some simple contact condition relationships; and 3) material failure equations based on observations of the worn surfaces.

Table 1
Examples of basic wear equations.

Wear mechanism	Equation	Reference
Adhesive wear	$V = (k \cdot L \cdot s) / H$	Holm [38] Archard [39]
Abrasive wear, plastic deformation	$V = (\alpha \cdot \beta \cdot L \cdot s) / H$	Hutchings [36][a] Bhushan [37][a]
Abrasive wear, brittle fracture	$V = [k \cdot n \cdot (E / H) \cdot L^{9/8}] / K_c^{1/2} \cdot H^{5/8}$	Evans and Marshall [40]
Fatigue wear, rolling contacts	$L_{10} = k \cdot (C / L')^{p'}$	Zaretsky [41,42] Ioannides et al. [43]
Impact wear, erosion	$V = (k \cdot m \cdot v^2) / (2 \cdot H)$	Hutchings [36][a] Bhushan [37][a]

[a] Source where equation derivation can be found.

Some of the most commonly used and most generic wear equations related to the most common wear mechanisms and developed mainly for metallic surfaces are listed in Table 1. Their derivation is contact-mechanics based and can be found in textbooks [36,37]. In real contact conditions the prevailing wear mechanisms are very often a combination of the simplified contact mechanics based wear mechanisms analysed below [14].

The validity regime of wear equations have been shown by wear maps, or wear-mechanism maps [44–52]. In a wear map the regimes are shown as a function of two variables along the two coordinate axes. This is of course a simplified and approximate way to present wear mechanism regimes, because in a 2D wear map only two variables are included and all the other are kept constant. If, however, the two variables are those which have a dominating influence on wear in the defined contact conditions, the wear map gives a good indication of how the wear mechanisms change and where the more uncontrolled transition regimes between different wear mechanisms can be expected to appear.

Wear maps are useful as they enable implications of wear on changes in design, material and operating parameters to be assessed and allow sensible correlation to be made between laboratory-based experimental investigations and observations in the field [53].

Contact mechanics based wear equations can be further developed by analytical approaches but this route is slow due to the complexity of the contact conditions and the numerous variables involved. On the other hand, numerical methods like the computational modelling and simulation contact mechanics based approach to wear prediction is a new and very promising route.

4. Computational modelling of wear

The computational modelling approach allows consideration of several influencing variables at the same time and offers tools for systematic optimal coating design. It includes computational representations of the materials involved and of the contact conditions that are the origin for the wear process. They can be modelled very accurately and quantified into equations by new computational techniques [14].

A typical computational wear model shows how the material close to the surface responds to the loading conditions. This response can be elastic, plastic or fracture resulting in the formation of wear debris. The basic mechanisms for material detachment from the surface are related to stretching the top material due to adhesion to the countersurface, deformation by a hard countersurface or fatigue failure due to repeated loading, as shown in Fig. 2. These basic mechanisms of material detachment are basically the same as those resulting in the friction force.

Tribocorrosion is frequently listed as one basic wear mechanism but in this context it is on purpose not included here. The reason is that chemical reactions taking place on the top surface certainly have a considerable influence on wear but their role is to cause deterioration or improvement of the material properties on the top surface. After that the detachment of material is actually caused by some of the three basic wear mechanisms shown in Fig. 2.

The wear performance of a surface is depending on the contact and loading conditions and on the material properties, which are determined by the material structure, which again reflects the processing method and conditions, as shown in Fig. 3. This approach has been called the PSPP (processing–structure–properties–performance) approach to material design [11,15].

For a complete understanding and controlling of the wear behaviour of a surface we would need to cover the whole PSPP chain and know the influence of processing on structure, of structure on properties and of properties on the wear performance and manage to model them by computational techniques. This is very challenging and in most cases beyond the state-of-art. In previous works we have used FEM modelling

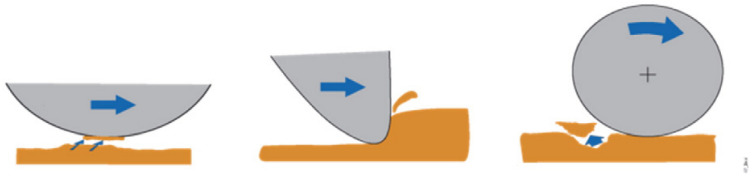

Fig. 2. Adhesive, abrasive and fatigue wear mechanisms.

for simulation of the interactions between surface properties and wear performance of thin TiN and DLC coated surfaces that could be treated as homogenous material domains [16,54–60]. Composite coatings like thick thermal spray coatings have a complex microstructure that strongly influence the wear behaviour. For an accurate wear modelling of composites it is important to model the interactions from structure over properties to performance.

Computational modelling techniques and tools for modelling the material on various length and time scale levels all from sub-atomic level to macroscale have been developed, as shown in Fig. 4. They include both discrete methods, such as first principle methods and molecular dynamics, and continuous methods, such as crystal plasticity and fracture mechanics based finite element methods.

Two different approaches may be used when developing the material models. One is to develop ideal synthetic models to find general design rules and the other to develop real image based models to find out the wear behaviour of some specific surface or coating. Examples of ideal synthetic and real image-based material models are shown in Fig. 5.

The ideal synthetic models are based on a mathematical description of the actual microstructure. They comprise the evaluation and quantification of microstructural features and their distributions such as reinforcement particle size, shape and density and further utilising the determined properties via statistical and stochastic means. Often this includes for example tessellation approaches, meaning tiling of a plane or volume using geometric shapes and controlling the degree of filling of overlap and gaps, in either two or three dimensions, in order to derive simplified aggregate-type of models, or mesoscopic sub-models for component-and-characterisation-type solutions.

Synthetic models are based on either polygonal or voxel/pixel representations of the phase geometry, or a combination of both. The most common synthetic approach is to apply various tessellation techniques for the generation of the grain geometry, as it is typically applied for materials like polycrystals. Synthetic aggregate generation methodologies based on Voronoi tessellation have been presented by e.g. Fritzen et al. [61] and Quey et al. [25] for analyses involving primarily metallic materials.

Real image based models are based on a segmentation of nano- and microstructural features directly on the basis of, for example, electron microscopy imaging. The scanning electron microscopy images are post-processed and the phase distribution is extracted for discretisation for the finite element solution. For building of the numerical finite element model, various approaches are available. They are either directly based on voxel/pixel based meshing or on the extraction of isosurfaces by way-approaches such as the marching cubes method presented by Wang [49]. The resulting surfaces and volumes are treated as geometry entities in a FEM analysis and are identical to synthetic mesoscopic models.

A representative pixel-based meshing strategy for segmented structures was presented in the OOF2 finite element analysis of microstructures [62], where a penalty approach was used in an adaptive manner to end in a representable mesh of different phase regions. Voxel based

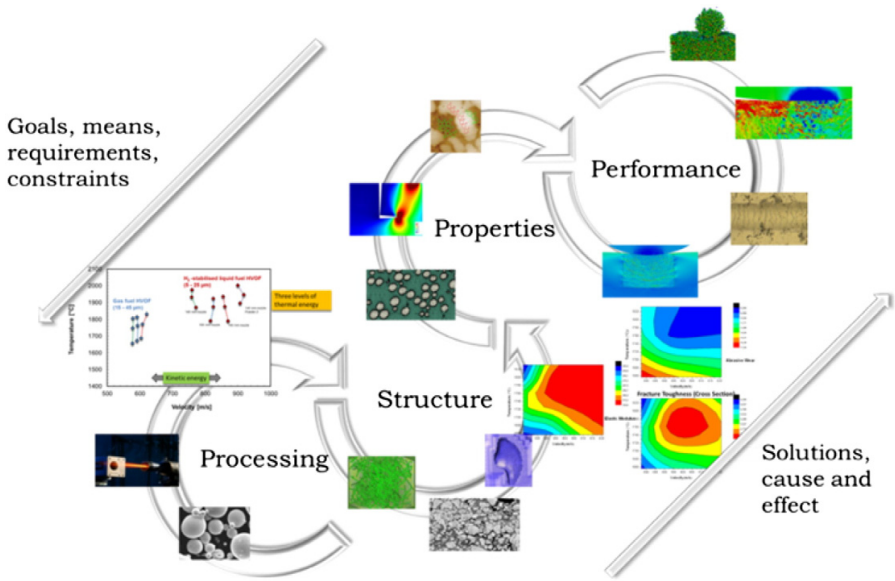

Fig. 3. In the PSPP approach to material design, the processing parameters are linked to material structures, the structures are linked to properties and the properties to material performance.

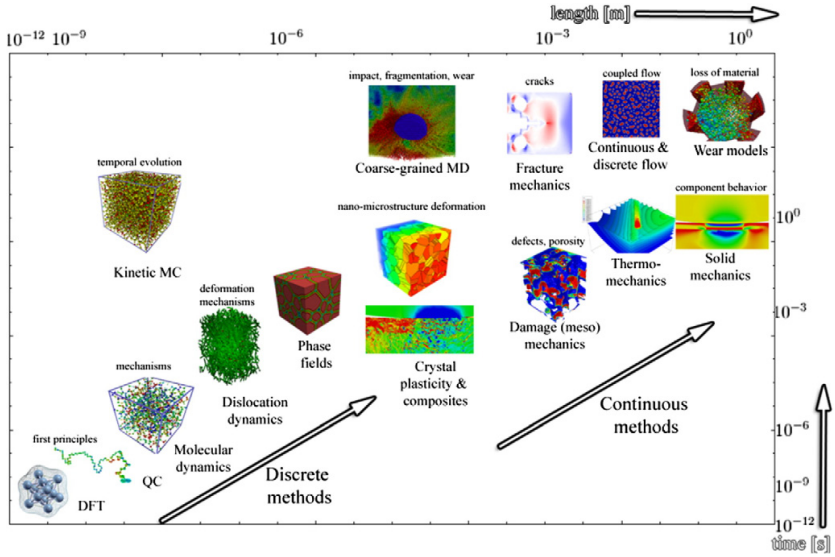

Fig. 4. Material modelling techniques on various length and time scales from sub-atomic scale to engineering macroscale.

approaches rely, for example, on the application of marching cubes like methods, in the work by Chawla et al. [23] on SiC composites, where a serial sectioning approach combined with a marching cubes algorithm was used for the extraction of the geometry of a 3D multiphase microstructure.

5. Wear models of composite coatings

Several different physical and chemical mechanisms are involved in a tribological contact when one surface is sliding over another and many of them can be separately modelled. Fig. 6 shows some of the phenomena where different modelling techniques have been applied: mechanisms of friction and wear at nanoscale, substrate structural changes at nano- and microscales, coating composite structure at nano- and microscales, nano-microstructures of interfaces, transition and gradient layers and their interfaces, effects of micro- and macroscale topography and surface texture, tribochemistry and lubrication, component scale wear and wear during component lifetime.

A traditional macroscale finite element analysis gives a general overall representation of the material response to loading, as shown in Fig. 7 on the upper countersurface image and on the lower surface left side image. However, for composite materials the microstructural features are crucial and the stress distribution as well as the stress levels, the strain and deformations can differ considerably from the macroscale figure, as shown by the microscale stress distribution in Fig. 7 on the lower surface right hand image.

When composite thermal spray coatings are used in practical applications, the loaded contact is typically on a macroscale with dimensions expressed in millimetres, while the composite material structure has a matrix including hard particles, pores, voids and cracks of micrometre scale dimensions. The relevant dimensional scales, on which these wear phenomena was studied in our work presented below, were on a macroscale for the entire counter body and on micro- and nanoscales for the composite coating structure.

6. Stress and strain simulations of thermal spray WC–CoCr coatings

In line with the approach described above we have developed a computational modelling based material design methodology and a portfolio of software modules that can be integrated to solve specific problems called VTT ProperTune™. The integrated software package is composed of in-house developed modules, modules developed by others and available free on the web, and interfaces to commercial software platforms, such as Abaqus. The VTT ProperTune™ has been applied to study the wear behaviour of composite thermal spray WC–CoCr and laser cladded WC–NiCrBSi coatings.

Three different finite element models were developed and adopted for the study of composite structured coatings. They are an ideal

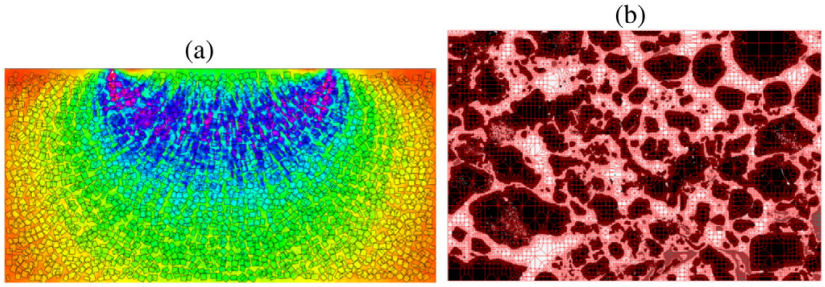

Fig. 5. Ideal synthetic (a) and real image based (b) coating models developed for a composite material microstructure.

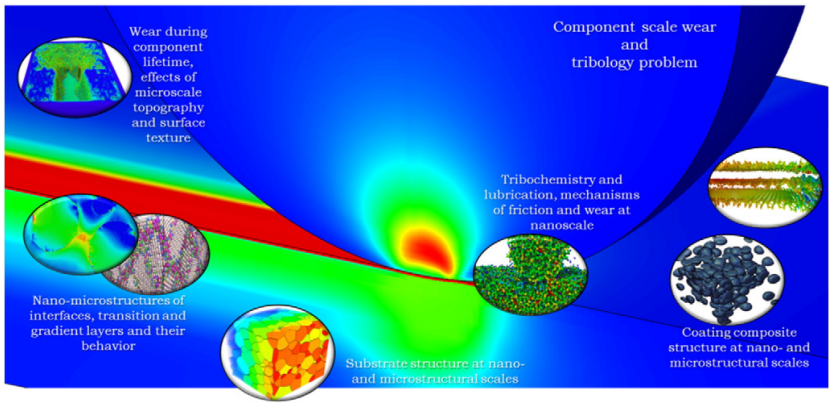

Fig. 6. Various modelling techniques have been used to model some of the complex contact and deformation mechanisms on nano-, micro- and macroscales in a tribological sliding contact.

synthetic defect-free material model, an advanced synthetic material model containing defects, and a real image based material model. We used three different models because they each gave a set of results that was complementary to the others.

The synthetic material models were used for improved understanding of the generic material behaviour under loading, and for the identification of critical and dominating parameters in relation to wear. The ideal synthetic defect-free model was used to investigate generic material parameters as they appear in ideal structures as a baseline, while the advanced synthetic model was used to investigate the effects and interactions related to defects and pores in the material. The real image based model gave a detailed and accurate insight in the material behaviour of the specific coating structures investigated, both on micro- and macroscales, and the model gave very precise information about deformations, stresses and strains as they appear in these materials under specific loading.

The ideal synthetic model is based on Monte Carlo random sampling of deterministic particle shape, distribution, aspect ratio and orientation features followed by an added statistical sampling step of particle geometry, spatial arrangement and overlap control to increase the degree of microstructural realism as seen necessary. The advanced synthetic model adds further features such as elliptic splat and substrate tessellation, strong discontinuities, smooth defects, such as pores and notches, and finally provides the ability to introduce interface features, such as secondary phases or defects. The real image based modelling approach generates microstructure segmentation from a SEM image from which finite element discretisation is carried out for the model phase interfaces. The degrees-of-freedom count for the models were typically in the range of 100 k to 1 M for the ideal synthetic model, 100 k to 4 M for the advanced synthetic model and 1 to 10 M for the real image based model. The developed software structure, the characteristics of the coatings, the experimental validation methods used as well as simulation results are in detail reported in Holmberg et al. [15].

Real image-based finite element software was used to study the deformations and the stress and strain distributions on microstructural level, the effects of carbide size, morphology, clusters, mean free path for a specific WC–CoCr coating and its cracking behaviour. In addition ideal synthetic finite element based software was used for investigating the influence of matrix elasticity and plasticity, the combined effect of particle size and mean free path as well as the effect of pores in the structure.

The detailed structure of a thermal spray WC–CoCr coated steel sample was determined by several SEM images from various regions in the coating. A typical and representative SEM image was chosen for segmentation of phases and defects, as shown in Fig. 8. The FEM meshing was done by a purpose build image based tool for the microstructure to generate the material model and a proprietary tool for the macroscopic geometries, explained in detail in [15]. The modelled material sample was loaded according to indentation test geometry and conditions, and the stress and strain distributions were simulated, as shown in Fig. 8.

A detailed study of the local stress distribution on microstructural level visualises how the stress peaks load the composite structure in different ways, as shown in Fig. 9. The quantitative colour scale goes from high tension, represented by red, over green and yellow to high

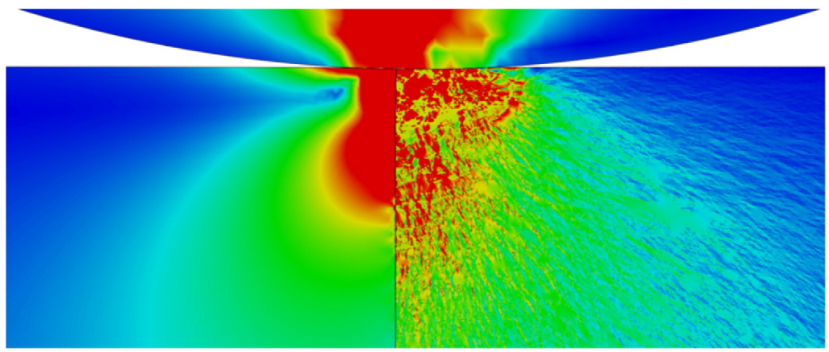

Fig. 7. Macro- (left hand side image) and microscales (right hand side image) equivalent stresses in a composite thermal spray WC–CoCr coating under the contact of a spherical sliding rigid diamond tip simulated by macrolevel and microstructural computational FEM and XFEM models.

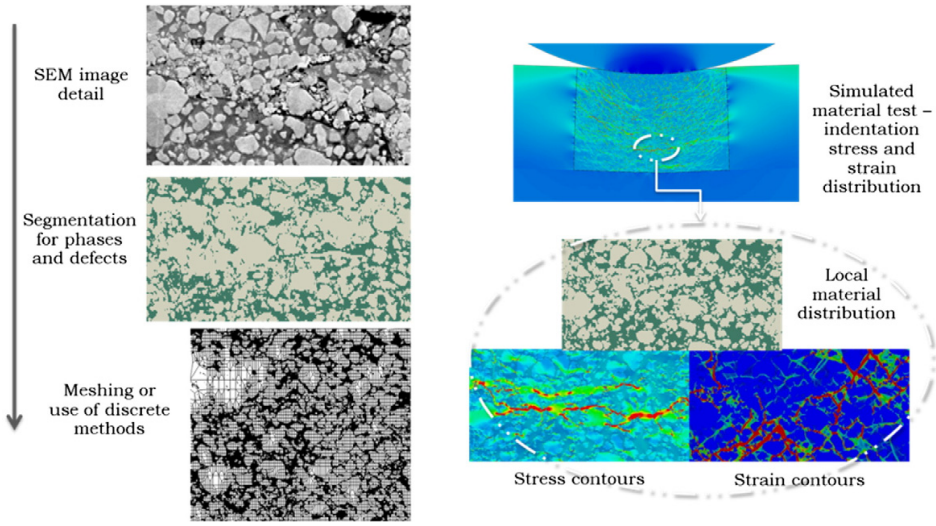

Fig. 8. The steps from SEM image microstructure over segmentation and meshing to simulation of local stresses and strain contours in a thermal spray WC–CoCr coating.

compression, represented by blue. We can observe effects of particle size, particle corners, ligament between particles, merged particles, notches and spatially and constitutively heterogeneous plasticity regions.

The detailed location of the simulated microstructural features were compared with the SEM image details, as shown in Fig. 10. Observed effects are:

a) how local carbide morphology is causing stress concentrations,
b) how a cluster of interacting carbides induce deformation during indentation,
c) how locally large mean free path and small carbide fraction result in localisation of deformation,
d) how interaction of a large and a small carbide result in stress concentration, and
e) how a large carbide strengthens the system locally and results in locally concentrated strains.

The effect of carbide size was investigated more in detail. Fig. 11 shows the real structure from SEM images, the stress distribution and the deformations for three carbide sizes. The conventional carbide size had an average particle diagonal of 3 μm, for the microscale carbide it was 1 μm and for the submicron carbide it was 0.3 μm. The model now allowed us to calculate the failure probability (P_f) in these loading conditions as a function of homogenised particle phase first principal stress for three different carbide particle sizes, as shown in Fig. 12.

The probability of failure was calculated by utilising the local segmented carbide size distribution and a carbide fracture model presented by Wallin et al. [67], which has been implemented as a fracture mechanical toughness evaluation software module by Wallin and Laukkanen

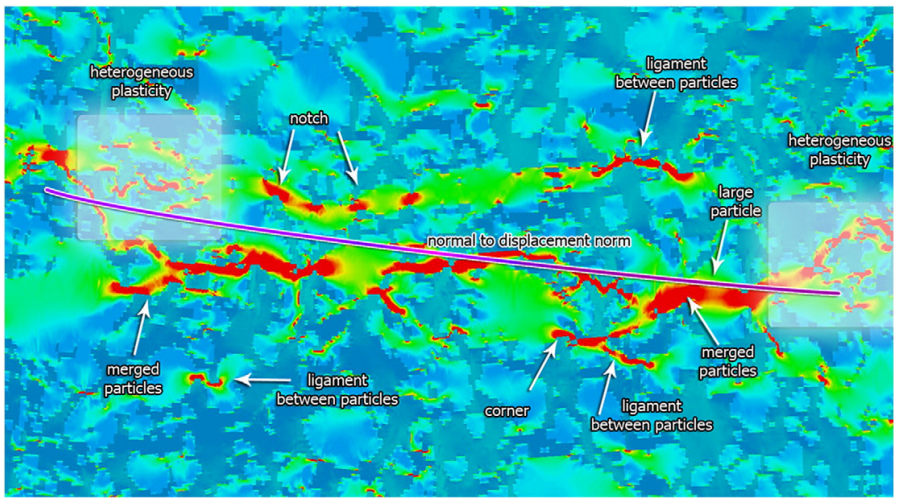

Fig. 9. Detailed image of the local stress distribution on microstructural level of the WC–CoCr thermal spray coating showing stress peaks caused by various microstructural features. In the colour scale red represents tension and blue represents compression.

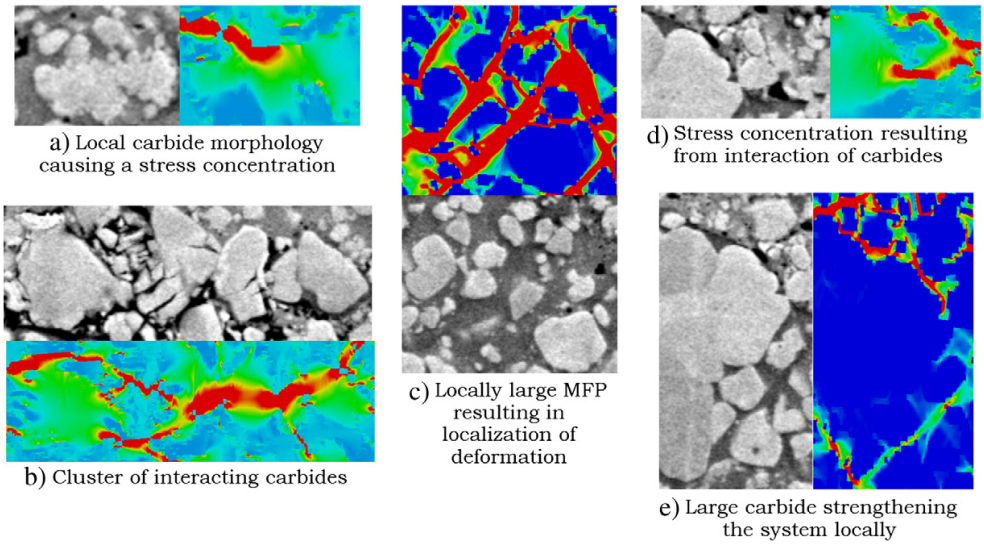

Fig. 10. Close-up of carbide size, morphology, clustering and mean free path effects in the WC–CoCr coating. The sub-images a)–e) show as comparison details from SEM images and the simulated stresses and strain in that same location.

[68]. The fracture model is based on a notion that carbide fracture is dependent on its size distribution and particle fracture probability, by assuming a Griffith like description of the initiator as well as its failure criterion. The density of the failure criterion is plotted in Fig. 11 to display the propensity of local carbides to initiate fracture, and in Fig. 12 a spatially homogenised representation is provided across the entire microstructural region in the models to display the propensity of the microstructures as a whole to initiate defects.

The results are obtained by applying a computational homogenisation procedure on identical material volumes for the results presented

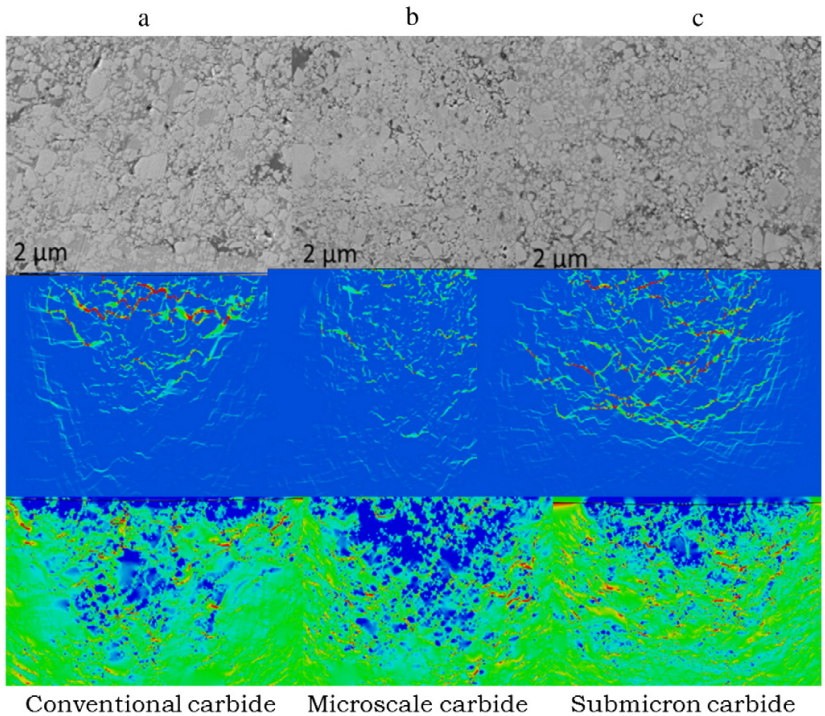

Fig. 11. The effect of particle size distribution is shown by images of microstructure, contours of the applied carbide failure criterion and local plastic strain for a) conventional size carbide particles (3 μm), b) for microscale carbide particles (1 μm), and for c) submicron size carbide particles (0.3 μm).

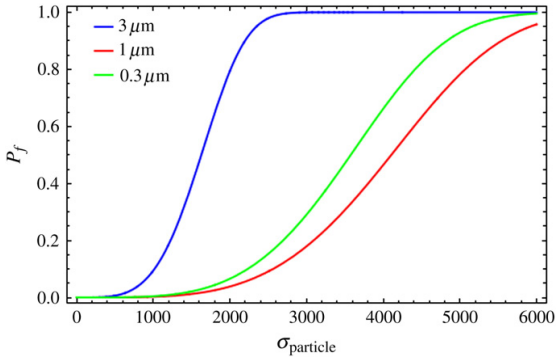

Fig. 12. The probability of failure as a function of mean particle first principal stress (in MPa) for three different carbide size distributions.

in Fig. 11. By applying a defect initiation criterion on the findings [63], cumulative failure probability of the material volume can be computed and is presented in Fig. 12. The result is a performance measure for durability of the thermal spray coating under indentation type loading, permitting a quantitative comparison between the feasibility of using such specific microstructures.

The results indicate that in the type of studied tribological contact problem the smallest grain size was not the most favoured as might be intuitively expected, but rather the micron scale carbide size scale coating displayed the most resistance to defect initiation. The causal relation for such a response can be seen in Fig. 11. The submicron carbide size coatings are spatially more clustered than the micron ones with respect to the extending stress–strain field arising from the contact via indentation.

This results locally in stronger carbide to carbide interactions increasing their stress state, and also, because of the mismatch between carbides and the binder promotes the formation of regions in the binder with locally high concentrated strain states due to the somewhat heterogeneous distribution of binder in the microstructure. This can be seen as an indication how certain microstructures are beneficial towards e.g. specific contact conditions, and that the existence of a single universally suitable microstructure is questionable, and case specific microstructural design and tailoring can yield improved properties.

The effect of porosity in the composite structure was investigated by using the ideal synthetic finite element model, as shown in Fig. 13. The first principal stress and equivalent plastic strain distributions show that there was very limited effect on the nominal mechanical response with 0.1% porosity density (f) in the structure, there appears some local stress and strain concentrations with 1% porosity density in the structure and with 5% porosity density in the structure a dominating stress–strain response can be observed on microstructural scale.

A composite material structure like the thermal spray WC–CoCr coating here investigated is very complex and the various mechanisms influencing on material response to loading is also a very complex system. Based on the observations in this study we have summarised the effects observed for the main influencing material parameters in Table 2. The trends are somewhat simplified and do not take into account all possible interacting mechanisms visible in the computational analyses, but provide a basis of linking microstructural features to material properties in thermal spray coatings on a general level. The basis for drafting Table 2 are approximately one hundred synthetic and image based numerical models on alike thermal spray coatings as presented in the current work.

Table 2 shows that defects in the coating structure are of the highest importance as they can create detrimental stress peaks and high strain levels. Secondly, the particle clustering is most critical for the durability of the structure. Thirdly, the elasticity of the particle is of great importance, and fourthly, both the matrix hardness as well as particle morphology are important to be considered. Fifthly, particle size and mean free path need to be considered. Thus, the primary emphasis is on defects and local microstructural features, and only secondarily on general coating microstructural properties such as particle size.

7. Failure process and optimal coating design

The wear process originates from local conditions in the material where the stress peaks caused by the loading conditions gets higher than the local strength of the material. A crack is formed and if the

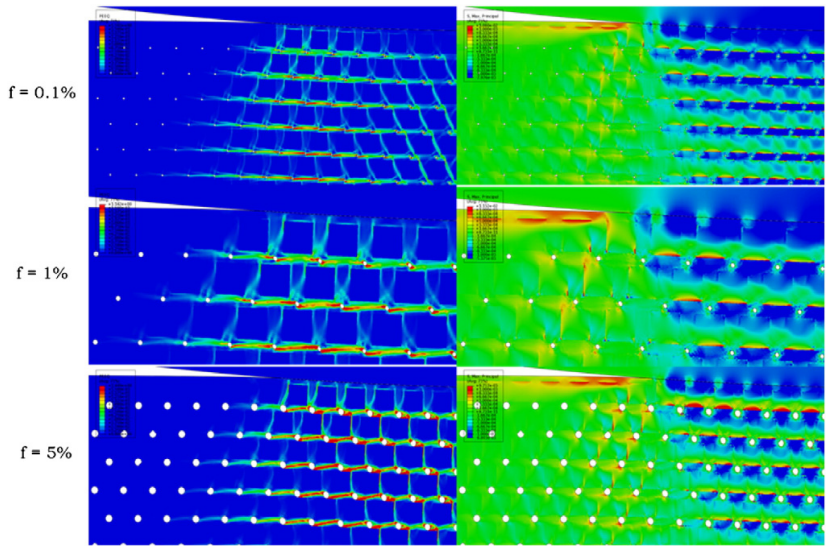

Fig. 13. The effect of coating porosity on local first principal stress and strain concentrations for three porosity levels was simulated by the ideal synthetic model for a typical thermal spray WC–CoCr structure.

Table 2
Effects of dominating coating properties on wear resistance. The "+" symbols represent the weight of each parameter with regard to material failure resulting in reduced wear resistance.

	Effect on stresses	Effect on strain	Comment
Matrix elasticity	+	+	Considering matrices able to deform
Matrix hardness	++++	+++++	Considering matrices able to deform
Particle elasticity	+++++++	+	Assuming particle elasticity greater than matrix
Particle hardness	+++	++	Assuming particle elasticity greater than matrix
Particle size	+++	+++	In the investigated range
Particle morphology	+++++	++++	Imaging derived results based conclusion
Particle clustering	++++++	++++++	Effect can be local
Mean free path	++++	++++	
Porosity*	+++++	+++++	Effect can be local
Defects*	++++++++	+++++++	Effect can be local

*Defect = crack, porosity with very high aspect ratio.

overloaded local conditions continue the crack will grow continuously and at some stage move up to the surface. A further growth of the cracks at the surface and below results in the formation of wear debris and continuous wear. In a wear resistant material this process is inhibited or limited to a level that is not disastrous for the function of the component.

The early stage of the material failure process is shown in Fig. 14, where crack initiation and subsequent crack growth are modelled and tracked leading to cracking through the surface of the thermal spray coating during a scratch test. The microstructure (a) of a thermal spray WC–CoCr coating was modelled and the stress state in a 20 × 40 × 10 μm material block for XFEM analysis is shown in image (b). The region was identified via a non-cracked body analysis. Initiation takes place as a branched crack locally at the ends of a carbide with a throat like morphology (local notch like geometry in the WC carbide) aided by locally low carbide fraction (abundance of amorphous CoCr binder) as observed in image (c). With increasing loading the crack tips grow together immediately and link (d), the crack arrests at the binder to carbide interface, and further surface scratching is required to unimpede the arrested crack (e). Further propagation to adjacent carbides results (f), and the crack follows a soft amorphous binder region (g). In images (h) and (i) the crack propagates to adjacent carbide via a throat between two carbides and a small cluster is generated by nearby WC carbides. In images (j) and (k) we can see how the crack penetrates the coating surface through a binder–carbide interface as the tensile stress region from the moving scratch test tip approaches and the local stress–strain field of the crack merges with the stress–strain field arising from the moving tip.

We have identified four typical mechanisms for crack initiation resulting in surface failure for the studied composite coatings from the analysis carried out of a large amount of material cracking and surface failure situations, as shown in Fig. 15. They are brittle carbide fracture, ductile binder cracking, interface failure, and cracking from pre-existing porosity and defects.

Based on these observations we conclude that an optimal composite coating structure, like the thermal spray coatings studied, should have the following features to result in proper wear resistance:

- Coating matrix elasticity and hardness: The most important feature of the matrix is its hardness, interpreted such that it is able to exhibit significant plastic deformation without unstable deformation mechanisms. This feature needs to be tailored relative to properties of reinforcing particles.
- Hardness of reinforcing particles: The simplest criterion is to maximise the hardness of reinforcing particles, but this is hardly optimal. Firstly, too great of a mismatch between coating matrix will promote local failure modes. Secondly, this is hardly optimal but likely an overshoot in many applications as far as coating performance and costs are concerned.
- Size distribution of particles: Particle size distribution is highly linked to MFP, i.e. these needs to be in practise considered simultaneously. With respect to size distribution in order to obtain the increase in strengthening by particle–particle interactions and wear resistance, a size distribution clearly below the characteristic spatial scales of the contact problem is adequate and necessary [15].

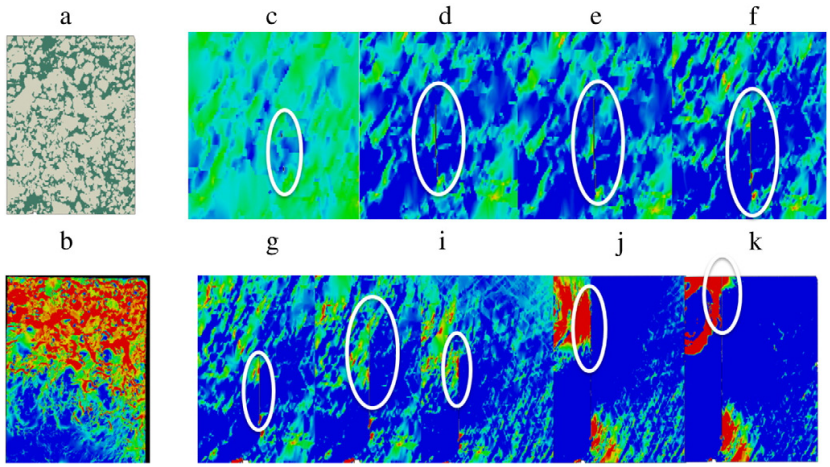

Fig. 14. The development steps from crack initiation to crack growth and crack penetration of the surface shown in the first principal local stress field of a thermal spray WC–CoCr coating (the images a)–k) are explained in the text).

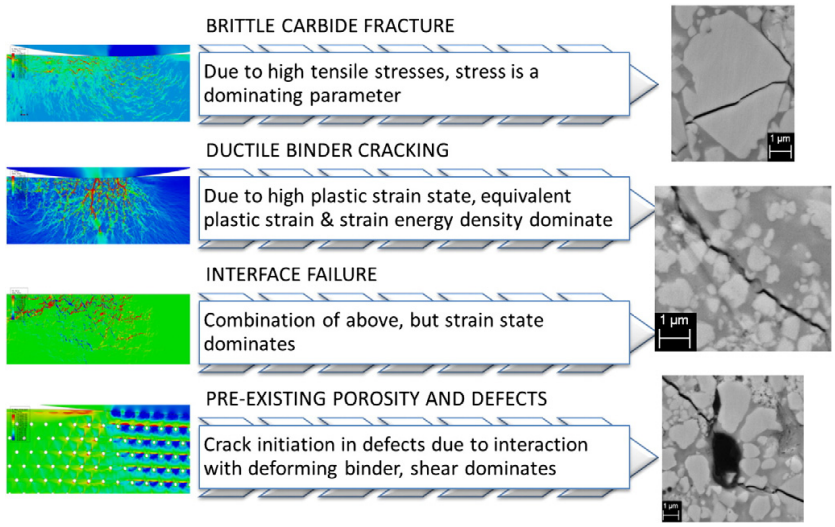

Fig. 15. Typical failure mechanisms and their dominating failure parameters in tribologically loaded thermal spray coatings.

- Morphology of particles: Well defined morphologies are recommended, since the likeliness of fracture arising from complex local morphologies promoting particle cracking is diminished. The selection of a particle shape needs to be tied to the degree of strength and wear resistance that is required, and also to the failure behaviour of the matrix and particle system. If the individual fracture toughnesses and system fracture toughness are low, "sharp" morphologies are to be even avoided, and also similarly, if the desired impact to coating properties and performance is obtained by using more lenient particles shaped such as rounded, spherical and like geometries.
- Mean free path in the matrix: Optimal MFP is to be tailored case specific to obtain the degree of strengthening and wear resistance required for a particular application, and meet the requirements of specific failure mechanisms under those conditions. The proper selection of values is one where the size scale of the problem is smaller than the characteristic length scale of the loading inducing problem, but not an extreme value in order to avoid the creation of a defect sensitive microstructure, like extremely brittle structures, and retain adequate mechanisms for deformation.
- Pores and defects: In principle pores, cracks, splat boundary defects etc. are all to be minimised. However, in some scenarios they may offer mechanisms of deformation if the affiliated behaviour does not result in defect initiation, propagation or deformation localisation. In these cases they can be beneficial, and such mechanisms require a certain degree of toughness from the individual phases and interfaces in order to yield a positive outcome.

In search of an optimal coating both with respect to performance and cost, these features are tailored in a modelling assisted manner by utilising a processing–structure–properties–performance approach, which provides the state-of-the-art manner of seeking the optimal and appropriate case specific material solution.

8. Discussion

The computational microstructural modelling approach was used to study wear resistance of composite coatings as complementary to the empirical investigations. The combination of both synthetic and real models enables one to better understand the dependencies and causal relations between microstructural features and stress–strain fields, as well as the role of different micromechanisms responsible for material properties and component performance. So far we have used this same methodology for several industrial problems related to erosive and abrasive wear of mining, sliding wear in logistic equipment, impact of elastomer coated surfaces, thin films in automotive components etc.

The adopted methodology for synthetic models can describe the statistical and morphological features of the coating microstructures. The approach is general, which means that the possibilities for controlling and tailoring the structures are numerous and primarily limited only by the available and obtainable statistical information about the microstructures in question. Numerous direct microstructure founded real models have been derived, and their use in this sense has become a commonplace routine.

The synthetic models can, for the most part, be treated with common free meshing algorithms. Some of the more complex meshing scenarios involving stochastic procedures in the generation of the microstructure can only be tackled by routines applicable to actual real microstructural models. Available solutions for generating meshes for real microstructural input were adapted, refined and further developed for the coatings under study. This was done particularly to address mesh phase boundary feature preservation issues in the thermal spray coatings.

Some steps were taken towards simulation of the behaviour of the coatings also in a performance limiting manner, focusing particularly on effects of defects. Application of homogenisation methods to extract macroscale properties is often adequate, but performance limiting micromechanisms can be approached only if the actual mechanisms themselves are modelled in the component of interest. The use of state-of-the-art finite element techniques, XFEM in particular, appears quite capable in being able to handle the numerics of the fracture mechanical problem in a case where the phase distributions are otherwise quite challenging.

One important and often time consuming part of a modelling exercise is to generate accurate input data to the models. The detailed material characterisation of the WC–CoCr coatings referred to in this article has been reported elsewhere [15]. The collecting of relevant input data for the material models turned out to be not so easy. The processing data and the structural data is fairly straight forward to measure with state-of-art techniques. In some cases, when there was a lack of suitable measuring methods, we needed to rely on data from the literature.

Validation of the models is in all modelling studies of great importance. The direct validation of the models was done by comparing material behaviour in indentation and scratch testing [15]. These contact conditions with an inert and rigid diamond tip are simplified to such a degree that a direct quantitative comparison is possible. The level of computational modelling is not yet advanced enough to allow direct quantitative validation in the more complex contact conditions, such as in abrasive rubber wheel and sliding pin-on-disc test conditions. However, these two methods were used to show the link to real tribological accumulated wear contacts.

The model validation methods applied showed good correlation between the numerical simulation results and the indentation tests with regard to the loading response of the surfaces. The corresponding correlation showed fair agreement in scratch testing. For pin-on-disc and rubber wheel abrasion test conditions there was a qualitatively explainable material behaviour supported by the quantitative results.

The modelled microstructure of the composite thermal spray WC–CoCr coating seemed to represent the real coating structure very well when using the real image based modelling tools. The simulated local stress and strain patterns correlated very well with the SEM image observations from the same locations. The big benefit with the computational modelling is that the information from the observed structure can now be complemented with quantitative information about stress pattern, stress peaks and deformations. The model and the simulations include a huge amount of new information and in this article we have only managed to make some first conclusions. The generated material about the microstructural coating behaviour offers the possibility for further analyses with regard to effects and interactions of the involved parameters and more advanced numerical optimisation of the structure and calculation of its wear resistance. This would form the basis for the development of models for prediction of accumulated wear and component lifetime.

The ideal synthetic model is interesting because of its general nature. Here a first question is naturally what would really be the correct representation of a typical thermal spray WC–CoCr coating. This study is limited in the sense that the statistical analysis of the structures is based on a small number of WC–CoCr samples that we have processed in house and this material has then been complemented by our general understanding of state-of-art WC–CoCr coatings reported in the literature. The work shows that this approach is very powerful for generating a deeper understanding of the basic mechanisms resulting in a good wear resistance and for generating general design guidelines and design rules. A systematic analysis of a much larger sample material would naturally result in a more accurate representation of the typical thermal spray WC–CoCr coating on global level.

Our conclusions in Section 6 about the four very typical mechanisms for crack initiation (Fig. 15) resulting in failure and the dominating parameters are well in agreement with observations generally done before linked to the basic characteristic of a complex composite structure, such as thermally sprayed structure, with very complex phase structure and special weak points typically causing the failure.

This modelling approach has also been applied to 2D and 3D microstructures of laser cladded WC–NiCrBSi and thermal sprayed Cr_2O_3 coatings. The former ones, including several carbide morphologies, are with respect to carbide morphology and size far more ordered and the feature size scale is of an order of magnitude greater than in the current work, while the latter is a single phase material containing a pronounced statistical distribution of pores and defects particularly at thermal spray splat boundaries at a similar spatial resolution. The results support and are in accordance with currently reported findings, and agree with the proposition that the generic features of composite coatings are captured and present in results provided in the current work.

The modelling resulted in interesting new observations not reported previously such as much deeper understanding of the role of each failure mechanism and an interaction of them related each other. Without the presented systematic modelling approach this level of understanding of the basic phenomena causing the failures would have been impossible to reach.

9. Conclusions

Computational microstructural modelling is a powerful tool as complementary to empirical investigations aiming at better understanding the wear process, optimisation of the wear resistance and tribological design of composite coated surfaces.

Ideal synthetic material models are useful for the understanding of the generic material behaviour under loading, and for the identification of critical and dominating parameters in relation to wear. Real image-based finite element models are useful for the investigation of specific material structures, both on macro- and microlevel, and the model gives very precise quantitative information about deformations, stresses and strains in real materials at specific loading conditions.

Macroscale models give an overall image of the stresses of a surface but for composite materials, such as thermal spray coatings, microstructural modelling and simulation on micro- and nanoscales is needed to get the full picture of material behaviour under loading, how cracks are initiated and the process of crack growth all the way to wear particle formation and wear.

A software package named VTT ProperTune™ was used to study in detail the effect of particle size, morphology, clusters, mean free path and porosity of thermal spray WC–CoCr coatings.

Four main very typical mechanisms for crack initiation resulting in surface failure and their dominating failure parameters were identified:

- brittle carbide fracture, with first principal stress as a dominating failure parameter,
- ductile binder cracking, with equivalent plastic strain and strain energy as dominating failure parameters,
- interface failure, with the strain state as a dominating failure parameter, and
- cracking from pre-existing porosities and defects, with shear as a dominating failure parameter.

The most important coating properties having a crucial effect on coating wear resistance were identified:

- firstly, defects in the coating structure are of highest importance as they can create detrimental stress peaks and high strain levels,
- secondly, the particle clustering is most critical for the durability of the structure,
- thirdly, the elasticity of the particle is of great importance,
- fourthly, both matrix hardness as well as particle morphology are important to be considered, and
- fifthly, particle size and mean free path need to be considered.

Acknowledgement

This study was carried out in the Matera project MOTRICOT — Model Based Tribologically Optimised Thick Multimaterial Coated Surfaces, and the VTT Frontier project IMAGO — Integrated Material Modelling for Demanding Applications. The financial support of Tekes — the Finnish Funding Agency for Technology and Innovation; the participating industrial companies Omco, Metso and Ruukki and the VTT Technical Research Centre of Finland is gratefully acknowledged.

References

[1] K. Holmberg, P. Andersson, A. Erdemir, Tribol. Int. 47 (2012) 221–234.
[2] K. Holmberg, R. Siilasto, T. Laitinen, P. Andersson, A. Jäsberg, Tribol. Int. 62 (2013) 58–77.
[3] K. Holmberg, P. Andersson, R. Siilasto, A. Erdemir, Global impact of friction on energy consumption, environment and economy, Proc. 5th World Tribology Congress, 8–13.9, AIT Associazione Italiana di Tribolgia, Turin, Italy, 2013, (Pisa, Italy, 2013b).

[4] K. Holmberg, A. Matthews, Coatings tribology: properties, mechanisms, techniques and applications in surface engineering, Elsevier Tribology and Interface Engineering Series No. 56, 2nd edition, Elsevier, Amsterdam, The Netherlands, 2009.
[5] J. Zhang, DLC coatings for friction reduction, IEA Advanced Materials for Transportation Technical Symposium, City University of Hong Kong, Hong Kong, 2.3.2013, (oral presentation).
[6] M. Cartier (Ed.), Handbook of Surface Treatments and Coatings, Tribology in Practice Series, Professional Engineering Publishing Ltd., London, UK, 2003, (412 pp.).
[7] J.R. Davis (Ed.), Handbook of Thermal Spray Technology, ASM International, Ohio, USA, 2004.
[8] B.G. Mellor (Ed.), Surface Coatings for Protection Against Wear, Woodhead Publishing in Materials, CRC Press, New York, USA, 2006.
[9] M. Jeandin, A Socratic approach to surface modification: the example of thermal spray, Proc. 24th Int. Conf. on Surface Modification Technologies, Dresden, Germany, 7–9.9.2010, pp. 3–20.
[10] A. Ghabchi, Wear resistant carbide-based thermal sprayed coatings: process, properties, mechanical degradation and wear, (PhD Thesis) Technical Research Centre of Finland, Espoo, Finland, Stony Brook University, New York, USA, 2013, (VTT Science Nr 29).
[11] G.B. Olsson, Science 288 (5468) (1997) 993–998.
[12] K. Elalem, D.Y. Li, M.J. Anderson, S. Chiovelli, Modeling abrasive wear of homogeneous and heterogeneous materials, in: G.E. Totten, D.K. Wills, D. Feldmann (Eds.), Hydraulic Failure Analysis: Fluids, Components, and Systems Effects, ASTM STP 1339, American Society for Testing Materials, West Conshohocken, PA, USA, 2001.
[13] M. Gupta, P. Nylen, Design of low thermal conductivity thermal barrier coatings by finite element modelling, in: T.S. Sudarshan, E. Beyer, L.M. Berger (Eds.), Surface Modification Technologies XXIV, Proc. 24th Int. Conf. on Surface Modification Technologies, Dresden, Germany, 7–9.9.2010, pp. 353–365.
[14] K. Holmberg, A. Laukkanen, in: R. Bruce (Ed.), Handbook on Lubrication and Tribology, vol. II. Theory and Design, 2nd edition, CRC Press, New York, USA, 2012, pp. 1–21, (Chapter 13).
[15] K. Holmberg, A. Laukkanen, A. Ghabchi, M. Rombouts, E. Turunen, R. Waudby, T. Suhonen, K. Valtonen, E. Sarlin, Tribol. Int. 72 (2013) 13–30.
[16] K. Holmberg, A. Laukkanen, H. Ronkainen, K. Wallin, S. Varjus, Wear 254 (2003) 278–291.
[17] R. Colaco, R. Vilar, Wear 245 (2003) 625–634.
[18] J. Hu, D.Y. Li, R. Llewellyn, Wear 259 (2005) 6–17.
[19] J. Hu, D.Y. Li, R. Llewellyn, Wear 263 (2007) 218–227.
[20] M. Ben Tkaya, S. Mezilin, M. El Mansori, H. Zahouani, Wear 267 (2009) 535–539.
[21] J.D. Pearson, M.A. Zikry, K. Wahl, Wear 267 (2009) 1137–1145.
[22] T. Dick, G. Cailletaud, Comput. Mater. Sci. 38 (2006) 113–125.
[23] N. Chawla, R.S. Sidhu, V.V. Ganesh, Acta Mater. 54 (2006) 1541–1548.
[24] M. Zhang, D.L. McDowell, R.W. Neu, Tribol. Int. 42 (2009) 1286–1296.
[25] R. Quey, P.R. Dawson, F. Barbe, Comput. Methods Appl. Mech. Eng. 200 (2011) 1729–1745.
[26] S.A. Lagner, E.R. Fuller, W.C. Carter, Comput. Sci. Eng. (May/June 2001) 15–23.
[27] A.C.E. Reid, S.A. Langer, R.C. Lua, V.R. Coffman, S.I. Haan, R.E. Garcia, Comput. Mater. Sci. 43 (2008) 989–999.
[28] T. Wiederkehr, B. Kluserman, B. Gies, H. Müller, B. Svendsen, Comp. Mater. Sci. 47 (2010) 881–889.
[29] W. Österle, H. Kloss, I. Urban, A.I. Dmitrievl, Wear 263 (2007) 1189–1201.
[30] A.L. Mohd Tobi, P.H. Shipway, S.B. Leen, Tribol. Int. 58 (2013) 29–39.
[31] S. Anwar, D.A. Axinte, A.A. Becker, J. Mater. Process. Technol. 213 (2013) 180–193.
[32] P. Seleson, M.L. Parks, M. Gunzburger, R.B. Lehoucq, Multiscale Model. Simul. 8 (1) (2009) 204–227.
[33] O. Amsellem, K. Madi, F. Borit, D. Jeulin, V. Guipont, M. Jeandin, E. Boller, F. Pauchet, J. Material, Science 43 (2008) 4091–4098.
[34] S. Beauvais, V. Guipont, M. Jeandin, D. Jeulin, A. Robisson, R. Saenger, Metall. Mater. Trans. 39A (2008) 2711–2724.
[35] H.C. Meng, K.C. Ludema, Wear 181–183 (1995) 443–457.
[36] I.M. Hutchings, Tribology: Friction and Wear of Engineering Materials, Butterworth Heinemann, Oxford, UK, 1992.
[37] B. Bhushan, Principles and Applications of Tribology, John Wiley & Sons, New York, USA, 1999.
[38] R. Holm, Electric Contacts, Hugo Gebers Förlag, Stockholm, Sweden, 1946.
[39] J.F. Archard, J. Appl. Phys. 25 (1953) 981–988.
[40] A.G. Evans, D.B. Marshall, Wear mechanisms in ceramics, in: D.A. Rigney (Ed.), Fundamentals of Friction and Wear of Materials, ASM Metals Park, Ohio, USA, 1981.
[41] E.V. Zaretsky, Lubr. Eng. J. STLE (Feb. 1997) 18–24.
[42] E.V. Zaretsky, Rolling bearing life prediction, theory, and application, in: G.K. Nikas (Ed.), Recent Developments in Wear Prevention, Friction and Lubrication, Research Signpost, Kerala, India, 2010, pp. 46–136.
[43] E. Ioannides, G. Bergling, A. Gabelli, An analytical formulation for the life of rolling bearings, Acta Polytechnica Scandinavia, Mechanical Engineering Series, The Finnish Academy of Technology, Espoo, Finland, 1999, (No. 137).
[44] S.C. Lim, M.F. Ashby, Acta Metall. 35 (1987) 1–24.
[45] S.C. Lim, M.F. Ashby, J.H. Brunton, Acta Metall. 35 (1987) 1343–1348.
[46] S.M. Hsu, D.S. Lim, Y.S. Wang, R.G. Munro, Lubr. Eng. J. STLE 47 (1991) 49–54.
[47] K. Adashi, K. Kato, N. Chen, Wear (1997) 203–204.
[48] S.M. Hsu, M.C. Shen, Wear mapping of materials, in: G.W. Stachowiak (Ed.), Wear: Materials, Mechanisms and Practice, John Wiley & Sons, Chichester, West Sussex, UK, 2005, pp. 367–423.
[49] Y.S. Wang, S.M. Hsu, R.G. Murno, Lubr. Eng. J. STLE 47 (1991) 63–69.
[50] D. Diao, K. Kato, K. Hayashi, The local yield map of hard coating under sliding contact, in: D. Dowson, et al., (Eds.), Thin Films in Tribology, Elsevier Science Publishers, Amsterdam, The Netherlands, 1993, pp. 419–427.
[51] K. Hokkirogawa, K. Kato, Tribol. Int. 21 (1988) 51–57.
[52] S.C. Lim, Tribol. Int. 31 (1998) 87–97.
[53] J. Williams, Tribol. Int. 38 (2005) 863–870.
[54] K. Holmberg, A. Laukkanen, H. Ronkainen, K. Wallin, Tribol. Int. 38 (2005) 1035–1049.
[55] K. Holmberg, A. Laukkanen, H. Ronkainen, K. Wallin, S. Varjus, J. Koskinen, Surf. Coat. Technol. 200 (2006) 3793–3809.
[56] K. Holmberg, A. Laukkanen, H. Ronkainen, K. Wallin, S. Varjus, J. Koskinen, Surf. Coat. Technol. 200 (2006) 3810–3823.
[57] K. Holmberg, H. Ronkainen, A. Laukkanen, K. Wallin, A. Erdemir, O. Eryilma, Wear 264 (2007) 877–884.
[58] K. Holmberg, A. Laukkanen, H. Ronkainen, K. Wallin, Tribol. Int. 42 (2009) 137–148.
[59] A. Laukkanen, K. Holmberg, J. Koskinen, H. Ronkainen, K. Wallin, S. Varjus, Surf. Coat. Technol. 200 (2006) 3824–3844.
[60] A. Laukkanen, K. Holmberg, H. Ronkainen, K. Wallin, J. ASTM Int. 8 (1) (2011) 1–21.
[61] F. Fritzen, T. Böhlke, E. Schnack, Comput. Mech. 43 (2009) 701–713.
[62] OOF2, Finite element analysis of microstructures, National Institute of Standards and Technology, http://www.ctcms.nist.gov/oof4.1.2013.
[63] K. Wallin, A. Laukkanen, Eng. Fract. Mech. 75 (2008) 3367–3377.
[64] E. Turunen, T. Varis, T. Gustafsson, J. Koskinen, T. Fält, S.-P. Hannula, Surf. Coat. Technol. 200 (2006) 4987–4994.
[65] S.-P. Hannula, E. Turunen, J. Koskinen, O. Söderberg, Curr. Appl. Phys. 9 (2009) 160–166.
[66] M. Oksa, E. Turunen, T. Suhonen, T. Varis, S.-P. Hannula, Coatings 1 (2011) 17–52.
[67] K. Wallin, T. Saario, K. Törrönen, Met. Sci. 18 (1984) 13–16.
[68] K. Wallin, A. Laukkanen, Fatigue Fract. Eng. Mater. Struct. 29 (2006) 788–798.

Publication IV

Laukkanen, A., Pinomaa, T., Holmberg, K. and Andersson, T., "Effective Interface Model for Design and Tailoring of WC-Co Microstructures," *Journal of Powder Metallurgy.*

Effective interface model for design and tailoring of WC–Co microstructures

A. Laukkanen*, T. Pinomaa, K. Holmberg and T. Andersson

Interface structures are a key feature in developing modern composite material solutions with ever improved performance. We present a nano-microstructural modelling approach for the tungsten carbide (WC)–Co system which can include the interface structures of WC–Co and various other phases present in the microstructure, utilising a methodology which combines imaging-based and synthetically generated nano-microstructures into an effective interface model for predicting the behaviour and properties of the resulting composite material. The effective model comprises of a local model of the WC/Co interface interacting with a larger-scale model of the WC–Co microstructure. The results provide a linkage between the interface character of cemented carbide microstructures and their properties, for example with respect to compressive strength, fracture toughness and wear resistance. The methodology presents a multiscale formalism for carrying out performance and application-driven evaluation and tailoring of composite interfaces and mesostructures, carried out on the basis of the emerging engineering material properties.

Keywords: Nano-microstructural modelling, Finite element modelling, Mesoscale modelling, Composites, Tungsten Carbide

Introduction

Thermal sprayed tungsten carbide (WC)–Co coatings are commonly used in industry to improve surface wear resistance. Thermal spray coatings are produced by heating and propelling tens-of-micrometres-sized powder onto a substrate, forming protective coatings. The high hardness of this metal matrix composite stems from a high content of micrometre to nano size distribution of hard WC particles. A crucial feature of these coatings, especially considering material development, is the interface structure between the WC and Co phases, and during solidification dissolution of the WCs which results e.g. in the formation of tungsten semi-carbide W_2C and complex W–C–Co phases (gamma and eta phases), which are seen detrimental to the resulting material properties and performance with respect to wear resistance of thermal spray coatings.

The ability to involve computational means in assessing the details of the interface character at the mesoscale is seen as an important tool in designing improved WC–Co-based cemented carbide materials, as well as to provide quantitative guidelines as to their use with respect to operational requirements. Subsequently, the multiscale modelling tools need to involve three stages of the processing–structure–properties–performance (PSPP) paradigm for completeness, applied for ceramic–metal composites by Holmberg *et al.*[1] First, a phase field (PF) analysis methodology is utilised to establish the interface phase distribution by assessing the dissolution of WC during thermal spraying, thereby completing the processing to structure step. Second, the resulting microstructure can be subjected to virtual testing, enabling e.g. the mechanical properties to be evaluated and the results assessed with respect to e.g. impact of the thermal history on the microstructure during the processing step. Third, the performance of the material with respect to wear behaviour can be evaluated utilising microstructure founded wear models, which are outside the scope of the current paper but the authors have carried out such multiscale analyses in the past, see, for example, Holmberg *et al.*[2]

In the current paper first the means of exploiting multiscale materials modelling and simulation in problems involving powder metallurgical (PM) materials are presented. Typical application scenarios for PSPP-centric modelling are briefly outlined and discussed. The work proceeds by presenting a methodology enabling the interfacing of PF analysis code[3] to imaging-based finite element (FE) analysis, thereby providing a methodology to cover the entire PSPP range with computational models, and enabling performance-driven material design. The PF analyses are used as an input to FE models characterising the mechanical response of the material, especially including the interface character and WC dissolution known to play a crucial role in the coating solidification, formation and cooling processes. The PF analysis results are presented in more detail in Pinomaa *et al.*[4] The interface response, e.g. the PF-derived computational FE model, is evaluated using imaging-based FEs, the results demonstrating in this extreme case the drastic changes in mechanical response due to the PF-derived interface input. The PF means and results are further

VTT Technical Research Centre of Finland, Tietotie 3, Espoo 02044, Finland

*Corresponding author, email anssi.laukkanen@vtt.fi

Published by Taylor & Francis on behalf of the Institute
Received 15 September 2015; accepted 19 November 2015
DOI 10.1080/00325899.2015.1130960

elaborated in more detail in an accompanying contribution by the authors in this conference working with the same cemented carbide system. The work focuses on specifics of thermal sprayed WC–Co microstructures where carbide dissolution (decarburisation) during the process is a key issue affecting the properties and performance of the resulting microstructure, but the methodology can be applied e.g. for sintered microstructures, in such cases including e.g. WC–WC, WC–Co, WC–gamma, gamma–gamma and gamma–Co interfaces in the models.

Computation-driven design of hard and PM materials

The mesoscale modelling concept of current work exploits the generally acknowledged PSPP approach in utilising modelling and simulation for material design problems, adapted for PM materials and presented in more detail in Holmberg *et al.*[1,2]. At the core are the linkages between material characteristics that can be systematically built and investigated by developing models between the different steps of the PSPP paradigm. The resulting correlations can be studied to quantitatively grasp the significance of nano-microstructural material features and physical phenomena giving rise to material properties and product performances. These approaches enable the effective exploitation of computation and multiscale materials modelling in design of composite materials. The implementation of these means in practice falls within the realm of integrated computational materials engineering (ICME), where computation merges with experimental, characterisation and material informatics to introduce a general and practically exploitable concept for simulation-driven material design.

For hard and PM materials in the implementation of PSPP we have identified three common steps, or specific problems typically tackled and found to be of interest, primarily due to the goal of exploiting modelling as a part of a performance-driven material design chain. These can be viewed as common use case problems on how to exploit multiscale modelling e.g. in design of PM materials, material selection or solving specific material-related problems. First, in Fig. 1, the structure–property problem is presented and case examples briefly outlined for various hard material systems and affiliated microstructures. In a structure–property problem the modelling problem is centred around the digital representation of material nano-microstructure and phenomena responsible for basic material properties, such as strength, viscoplastic strain rate, hardness, etc. As such, the key element is in possessing the capability to generate realistic enough representation of material structure, such as reinforcing constituents and defect structure, along with e.g. the underlying metallic microstructure. The most common problem types are affiliated with deformation response and following properties such as compressive strength, deciphering what features in material structure are critical for strengthening of the system and how to systematically work towards desired material properties. As such, the computation takes the form of simulating and carrying out virtual testing of common laboratory experiments such as hardness, compression and scratch testing, and the models are applied to investigate the correlation between structural morphologies, mechanisms of deformation and the resulting material properties.

The structure–property–performance problem can be viewed as the next step in exploiting computation for design of hard and PM materials, and such a concept and case example is presented in Fig. 2. Performance as a term is typically affiliated with more elaborate properties than those related to material properties, such as resistance to fatigue, wear or fracture toughness (see e.g. Holmberg *et al.*[1,2] for a more thorough discussion and further references). Subsequently, performance by the convention adopted by current authors pertains to behaviour also including component design, the use of the material in its operating conditions and environments. As such, the structure–property–performance can also be identified as an extension of the structure–property problem to more generic con"ditions. In Fig. 2, a case example of fatigue evaluation of selective laser melting

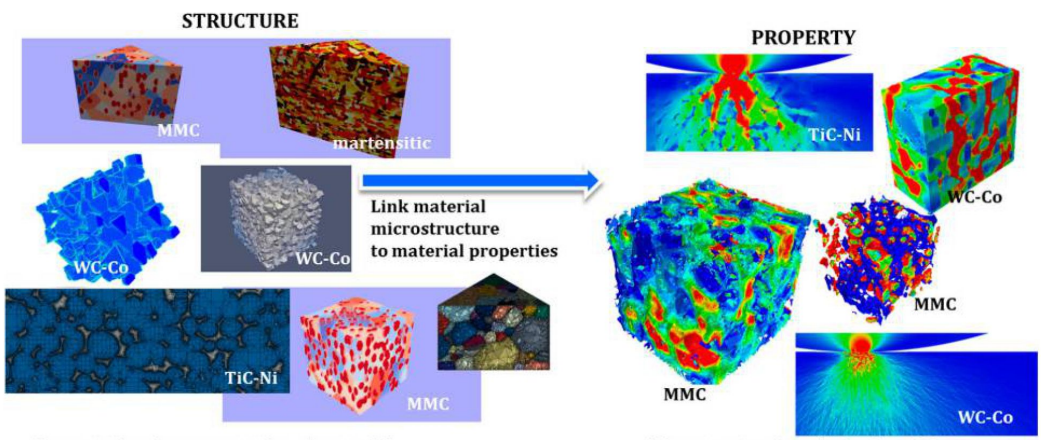

1 Modelling in solving the structure to property problem for PM materials

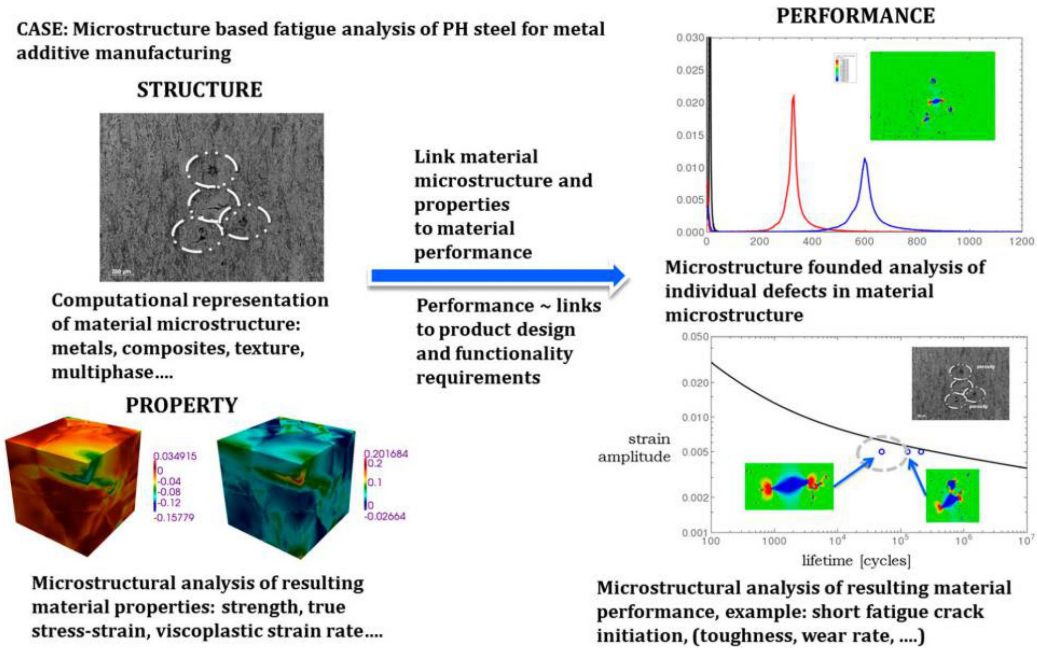

2 Modelling in solving the structure, property to performance problem for PM materials

precipitation hardened microstructure of steel is given. The differences to make note of in comparison to the structure–property problem are that material defect structure, criteria for failure micromechanisms or explicit modelling of failure processes and the conditions under which the product operates are introduced in modelling the problem. In Fig. 2, the analysis proceeds by merging a microstructural analysis of how a defect structure responds under deformation during fatigue cycling, and the subsequent stress–strain response is utilised to carry out a microstructure informed fatigue analysis. The merits of such an analysis lie in the fact that individual microstructural defects can be quantitatively linked to fatigue initiation life, enabling one to for example evaluate the significance of specific microstructural features on fatigue life, or whether certain specific defect types are at all of relevance for operational life of a component. The links to e.g. certification and developing PM parts for extreme performance environments are imminent in addition to the general notions presented for performance-driven material design.

As the third and last use case type for modelling-driven material design, the PSPP analysis type for PM materials is presented in Fig. 3. The use case can be viewed from the perspective of the structure–property–performance problem by introducing simulation of the material processing and manufacturing step, i.e. the analysis can now treat for example solidification and sintering structures directly, rather than use characterisation or like information in generating the computer-generated representation of material structure. The analysis complexity increases, but the potential impact does so as well. For example, in Fig. 3, the case depicts a PSPP analysis for additive manufacturing (AM). The process model comprises of a thermomechanical FE solver, which in current case is an example run on eight different process parameter sets to yield differing thermal histories. The output of such a thermomechanical analysis can be used in a PF analysis for alloy solidification, producing the resulting nano-microstructure. The structure–property–performance problem henceforth is carried out similarly as in other analysis scenarios. The merit of the PSPP analysis chain is in enabling the linking of material processing parameters and variables all the way to component performance. This enables the systematic investigation of causal relations accounting for all critical stages from material and component manufacturing to performance of the product, and these relations can then be systematically exploited in design of products with the required performances and also in evaluating the cost-effective means of delivering those performances and developing improved materials.

The linking of material-centric PSPP concepts, which ultimately comprise of the ICME, to other design tools to form concepts explicitly linking material and product design (i.e. computer-aided design, computer-aided engineering and topology optimisation) is presented in Fig. 4, adapted from authors' previous work inLaitinen *et al.*[5] Figure 4 is presented for AM and clarifies the role of PSPP analysis in yielding the ICME component to modelling-driven design of PM materials and processes. At the core three principal components are required in order to form a holistic design chain: the digital representations of material and the manufacturing process (i.e. PSPP), which interact with product design. Such a generic approach enables product performance-driven design, where all design variables related to material, process and product can be linked to serve the design of better performing products for specific needs and functionality profiles.

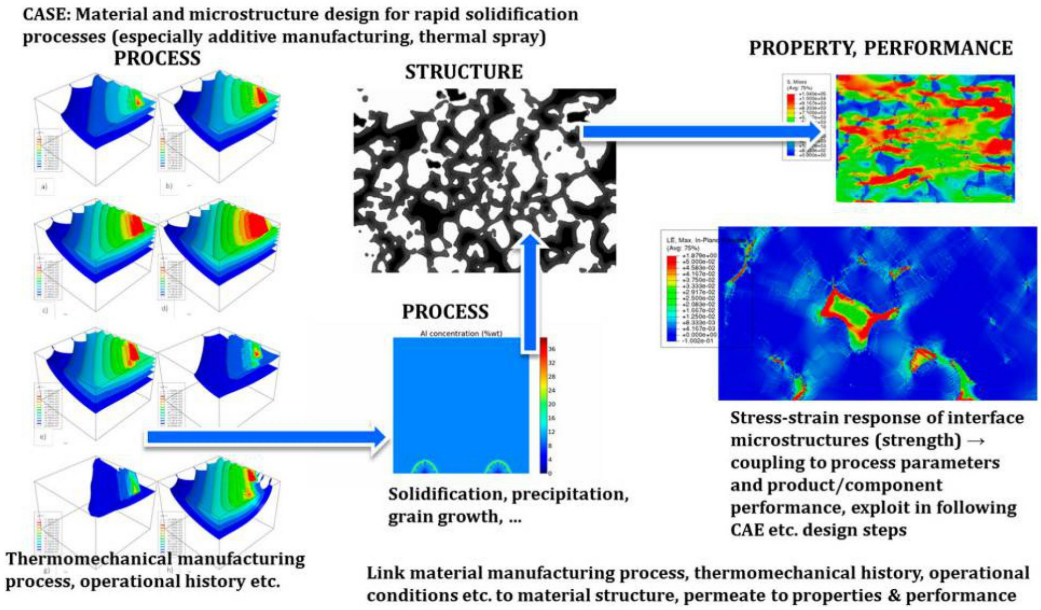

3 Modelling in solving the process, structure and property to performance problem for PM materials

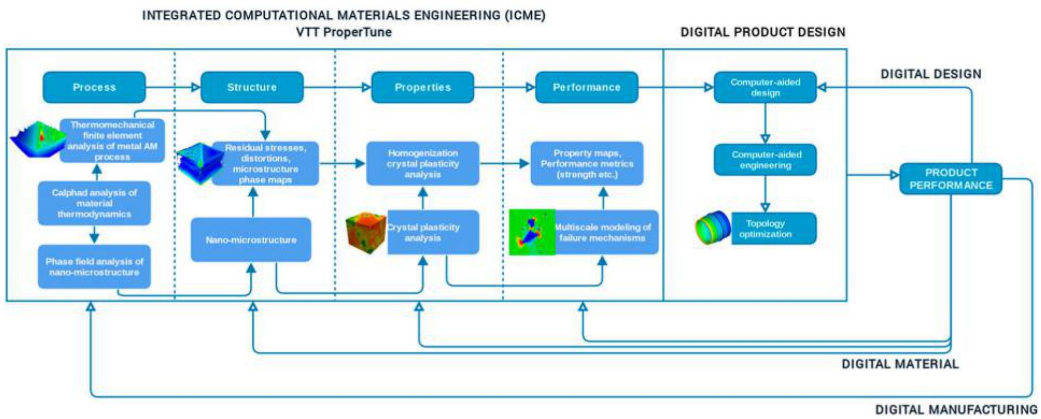

4 Integrated computational materials engineering concept linking to a digital design concept for AM, merging a digital representation of material, manufacturing process and product design and optimisation[5]

Numerical methods

An interface between two computational tools, a PF analysis code and an imaging-based FE code, is used in the current work, which is schematically presented in Fig. 5. The FE solution exploits an in-house solution, VTT ProperTune, developed by the authors and presented in more detail in Holmberg *et al.*[1,2]. The core capabilities consist of software libraries enabling the generation of 3D microstructures using imaging-based techniques, followed by creation of numerical models out of the resulting 3D images. The numerical models can then be solved e.g. for mechanical response using the FE method, solidification microstructures using PF or even more complex analysis workflows such as a wear resistance analysis involving e.g. contact and thermomechanics. When utilising the results of computational thermodynamics and kinetics as an input to a following mechanical analysis, the software interface relies on parsing input fields to the FE analysis using PF solute and orientation fields, as indicated in Fig. 5. The parsing is either local or discrete in nature, referring to the possibility of using the local PF analysis outcome to assign local phase properties with the PF governing this assignment, or the system can be discretised to a specified number of individual phases if seen as a better approach in terms of describing microstructural characteristics. In addition, thermodynamic evaluation of the resulting phases and specific properties is required. With the thermodynamics evaluation the concentration fields form the basis of model derivation by providing the phase distribution to the imaging founded FE routines.

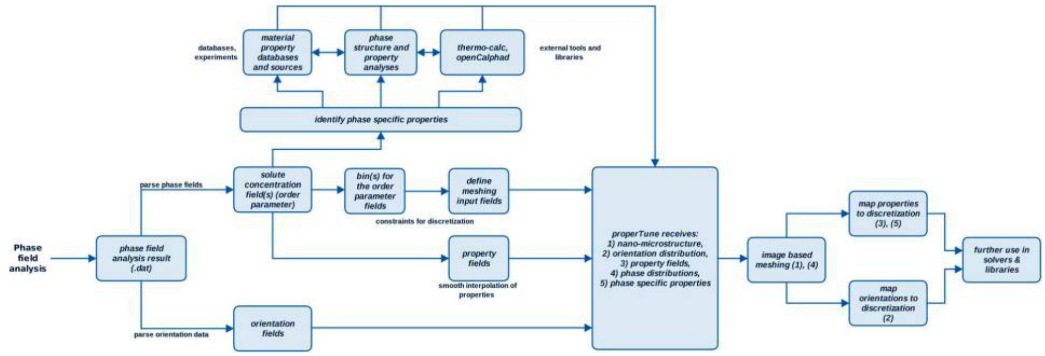

5 Phase field analysis to mesoscale microstructural FE solution

An alternative to direct use of PF input is synthetic modelling of the microstructures and interfaces, a simple example of which is presented in Fig. 6. By combining image processing and meshing routines, WC–Co microstructures can be created in their simplest cases just on the basis of WC size distribution. In this case a simple prism-like geometry is assumed to be a valid representation of a WC crystal, and its spatial size is stochastically sampled from a given size and shape distribution. The microstructure is generated via stochastic space-filling routines, with criteria producing a microstructure with specified WC to Co phase fractions. Such models form the basis for modelling with more elaborate interface characteristics. The models can contain tertiary phases and complex phase structures at interfaces, and these features can also be represented using synthetic and stochastic modelling techniques. These approaches can also be mixed, i.e. phase distribution information from a PF analysis can be merged with a synthetic model of microstructure to provide a more realistic description of the WC–WC and WC–Co interfaces.

The intermediate outcome when linking PF analysis results to microstructural FE models is presented in Fig. 7, depicting WC dissolution during thermal spray deposition of a microstructure and is the result provided by the PF analysis to the creation of the imaging-based FE model (the solidified microstructure after the thermal spray process). The carbide solute concentration field is parsed and interpolated for the image-based FE modelling mesh generation. It is noticed that within the Co binder a dendritic or epitaxial-like intermediate region is visible which is interpreted to consist of W_2C semi-carbide and its dendrite-like growth nucleating from WC–Co interfaces to the molten Co boundary being clearly visible. In Fig. 7 the PF is discretised to two levels to better visualise the epitaxial-like morphology. The region of microstructure with significant dissolution forms a carbide network within the Co phase and the WC crystals decarburise. Typical FE models of microstructure, even imaging models, are usually unable to include the resulting complex W_2C structure in the mesoscale microstructural models. However, in the current context since the PFs are meshed with very high resolution and properties assigned to the microstructure locally, the individual 'branches' and arms of the carbide network can be captured with respect to morphology and solute concentration and are input to the mechanical analysis.

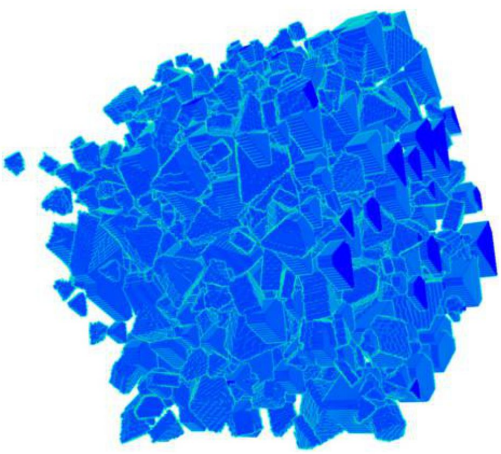

6 Synthetic WC–Co model for microstructural modelling generated using stochastic means

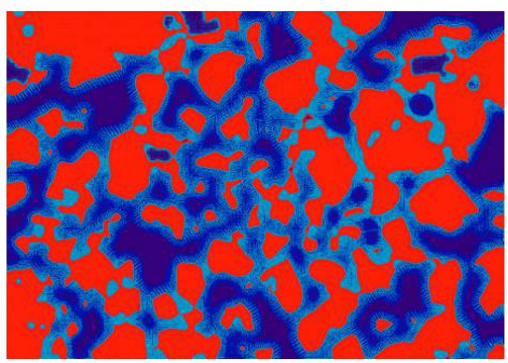

7 Interpolated W solute contours arising from carbide dissolution and resulting in a formation of a networked brittle phase within the microstructure (WC crystals in red, W_2C in shades of light blue and Co without W or C in dark blue)

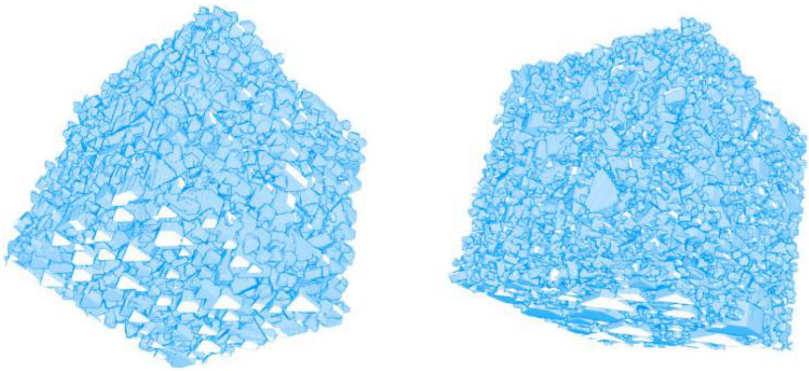

8 Synthetic 3D WC–Co microstructures generated via stochastic means: refined microstructure (left) and coarser microstructure (right)

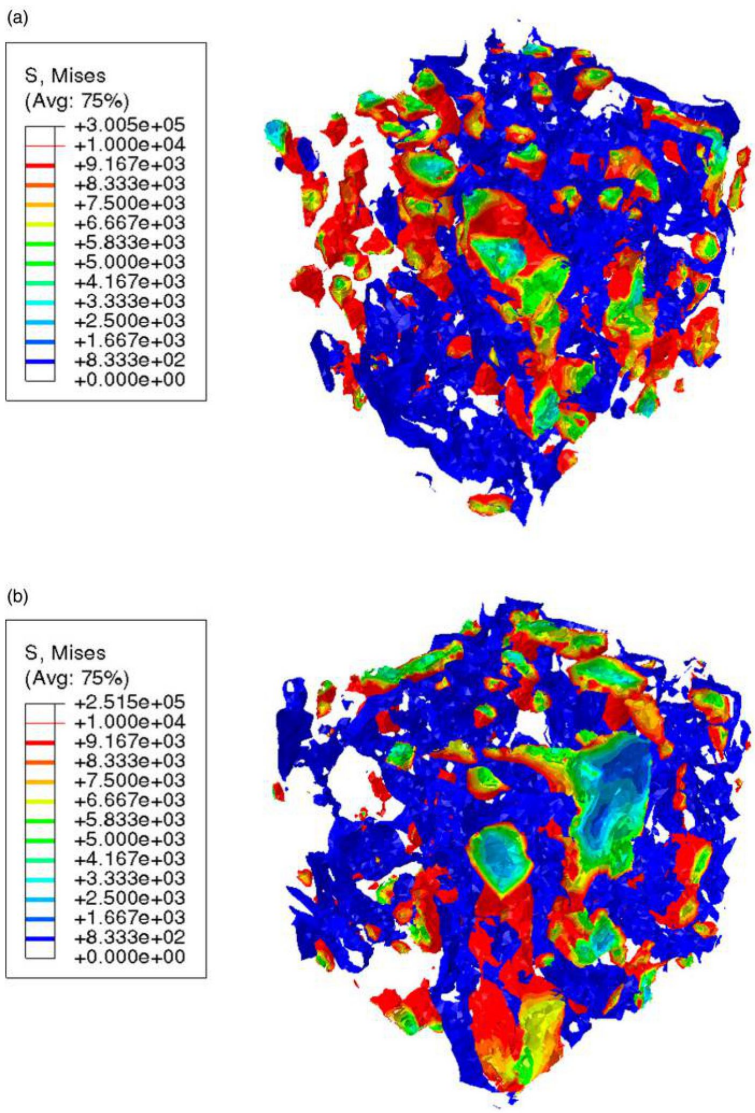

9 Equivalent stress isosurfaces of two 3D WC–Co microstructural models with identical mean crystal size: *a* refined and *b* coarser microstructure

Modelling results

Synthetic 3D microstructures and effective interface models

To demonstrate the synthetic model generation route and the linkage of interface modelling capability to typical microstructural modelling results of common WC–Co 3D microstructures, two WC–Co microstructures with differing WC size distribution were created. The 3D images of the microstructures are presented in Fig. 8. These results also form a baseline with respect to the significance of capturing specific microstructural features in the computational approach. The microstructures have identical mean crystal size, but the range of WC size distribution is flatter in one case with the maximum crystal size being 30% larger (coarser), resulting in a wider mix of smaller and larger carbides. Finite element models of these microstructures were created and subjected to tensile loading to investigate the influence of the size distribution on the analysis outcome. These results are presented in Figs. 9 and 10, respectively. The isosurface plots present the stress concentrations arising in individual WCs along with specific regions in the Co matrix which primarily deform during the simulated test, commonly as a result of carbide-free regions or due to a locally greater Co fraction. As can be expected, the overall characteristics of the analysis outcomes share many similarities, but there are certain differences in the quantitative values. Particularly, it is noted that the overall strength of the coarser microstructure is approximately 20% lower, due to greater deformations in the Co binder due to larger mean-free paths and subsequently decreased WC to WC interaction, which acts as a strengthening mechanism. The volume packing of the WC in the systems is identical with respect to WC phase fraction. However as can be expected, although these results imply that

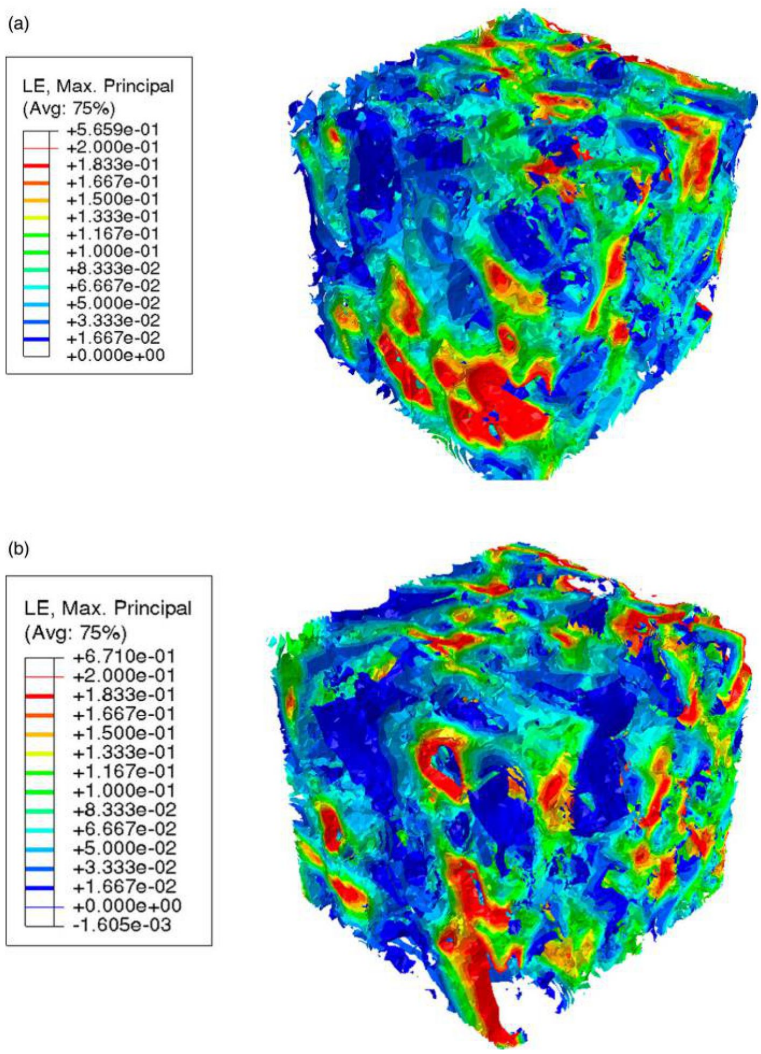

10 Principal strain isosurfaces of two 3D WC–Co microstructural models with identical mean crystal size: *a* refined and *b* coarser microstructure

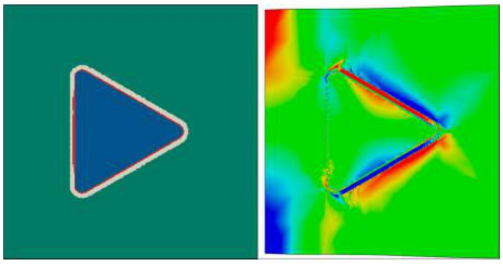

11 Phase field analysis results inspired effective interface model for WC–Co: model phase distribution (left), comprising of WC phase (blue), WC_{1-x} (red), gamma phase (light) and Co (green); and shear stress plot of the WC and interface model during horizontal compression (right)

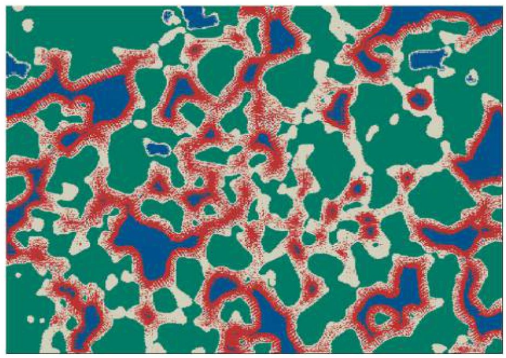

12 Microstructural FE model based on PF input fields: WC (green), Co (blue) and carbide phases (light and red)

the influence of e.g. geometric carbide features is significant, the following indicates that the influence is clearly outweighed by factors arising from the approach selected for modelling of the interface regions.

The simplest methodology to derive an effective interface model is presented in Fig. 11, along with the result of compressive loading of an individual WC crystal with the respective interface model. A simplified WC primitive is created housing the interface characteristics in a 'stacked' manner. The stacking characteristics have been extracted from a PF analysis of dissolution for formation of the interfacial gamma phase or W_2C phase (or layer), and the WC_{1-X} layer has been introduced following findings published e.g. in Lay 6 to better describe the interface

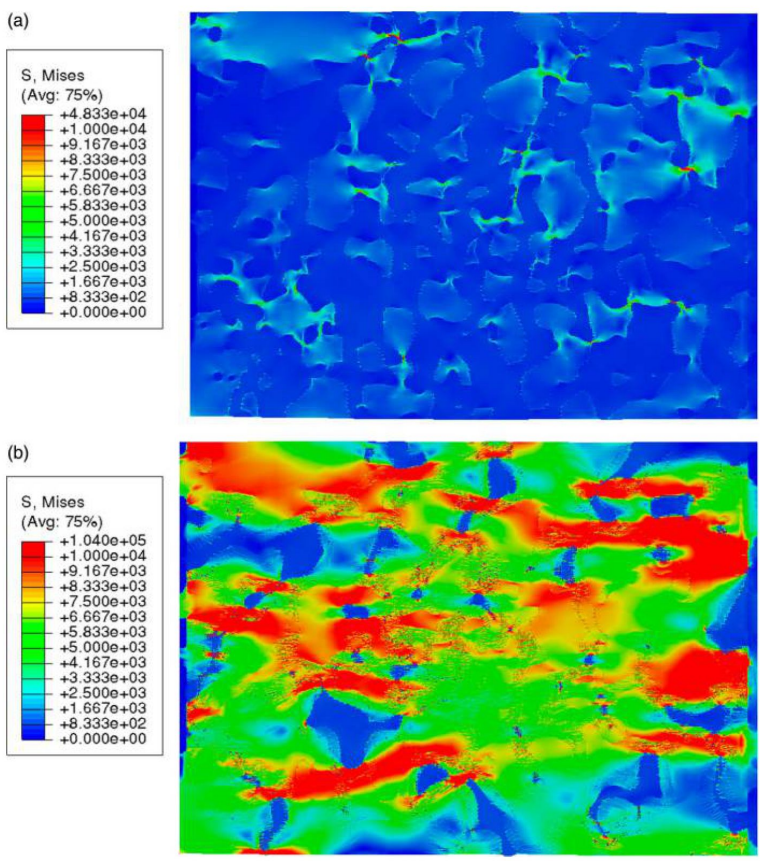

13 In-plane equivalent stress contours at WC–Co microstructure without carbide dissolution *a* and with dissolved W_2C carbide *b* during horizontal compression

structure. Although the interface is fairly simplistic, its influence on interface shear stresses is noteworthy. The mismatching properties cause a stress–strain concentration between the WC and Co phases, displaying the importance of the interface region and its potential as well as in the worst case detriment to WC–Co composite properties. In this analysis W_2C properties were used for the interfacial carbide layer. This approach can be applied generally for thermal spray or sintered WC–Co microstructures, where the microstructure itself can be created either synthetically or via use of imaging techniques.

Phase field analysis and interface models

In the analysis route exploiting PF results, FE models were created considering WC dissolution and the respective PFs to map the FE model phase distribution. The resulting model is presented in Fig. 12 where the microstructure is divided into four individual regions for clarity. In the numerical models PFs are used directly to specify phase-specific microstructural properties. The phase-specific material properties were specified following work carried out in Holmberg *et al.*[1,2] and findings of recent *ab initio* work were found to be in compliance with the specified properties for WC crystals.[7] The concentration fields are used to interpolate the properties locally. The results are purposefully drastically different due to selecting a PF analysis result where significant carbide dissolution was observed when a Co solidification analysis was carried out for thermal spray conditions. It is noted that as is expected the W_2C semi-carbide nucleation occurs on WC faces, and an epitaxial-like growth process to the Co matrix ensues, yielding a carbide network within the WC–Co microstructure that has a dendrite-like appearance to it.

In order to better display the significance of the interface structure in the mechanical response of the microstructure, analyses were carried out with and without the carbide network and results are provided in Figs. 13–15. The equivalent stress contours of the microstructures during compressive loading are shown in Fig. 13. In the analysis case without semi-carbide it is noted that individual carbides flow and rotate within the Co binder and the overall strength of the system is quite limited, especially since the Co fraction is relatively high in this particular microstructure. Carbide to carbide interactions and contact are observed yielding increased local stresses within the microstructure, and the system is seen to achieve its strength via such interactions in separated carbide clusters. When the semi-carbide is present, modelled as a linear-elastic phase embedded in an elastic–plastic Co and linear-elastic WC, the interface carbide network

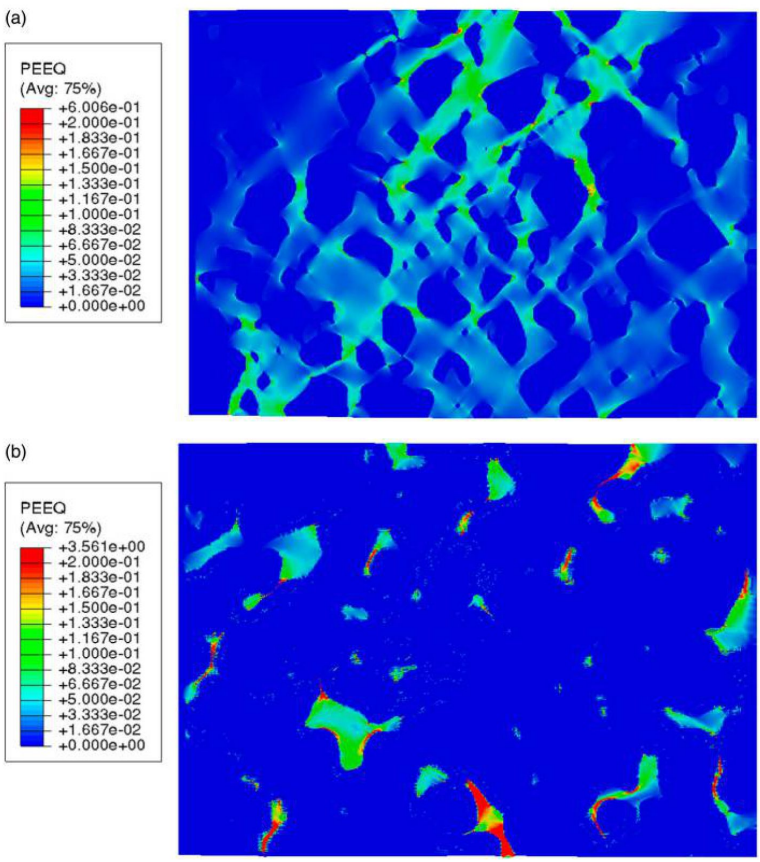

14 In-plane equivalent plastic strain contours at WC–Co microstructure without carbide dissolution *a* and with dissolved W_2C carbide *b* during horizontal compression

forms a load carrying skeleton within the microstructure, fundamentally altering the microstructural response to applied compressive loading. The introduction of the non-deforming semi-carbide phase increases the stress state significantly, and it can be expected that a fracture mechanical analysis would indicate that the toughness of the system has deteriorated as well as other properties, such as wear resistance. The dendrite structures are seen to cause actual local scatter to the analysis results due to the branches penetrating the Co matrix and the W_2C to Co interface.

The influence of the W_2C skeleton to deformation response is highlighted in Fig. 14, where equivalent plastic strain contours are plotted. In the ideal WC–Co system plastic flow throughout the microstructure is clearly visible while in the W_2C interface containing system the deformability is severely limited. Also, since Co plasticity is constrained as a means for the system to deform, far greater local strain concentrations arise in the system at W_2C to Co interfaces, the strain values at their extreme being approximately six times larger with the brittle interface phase present.

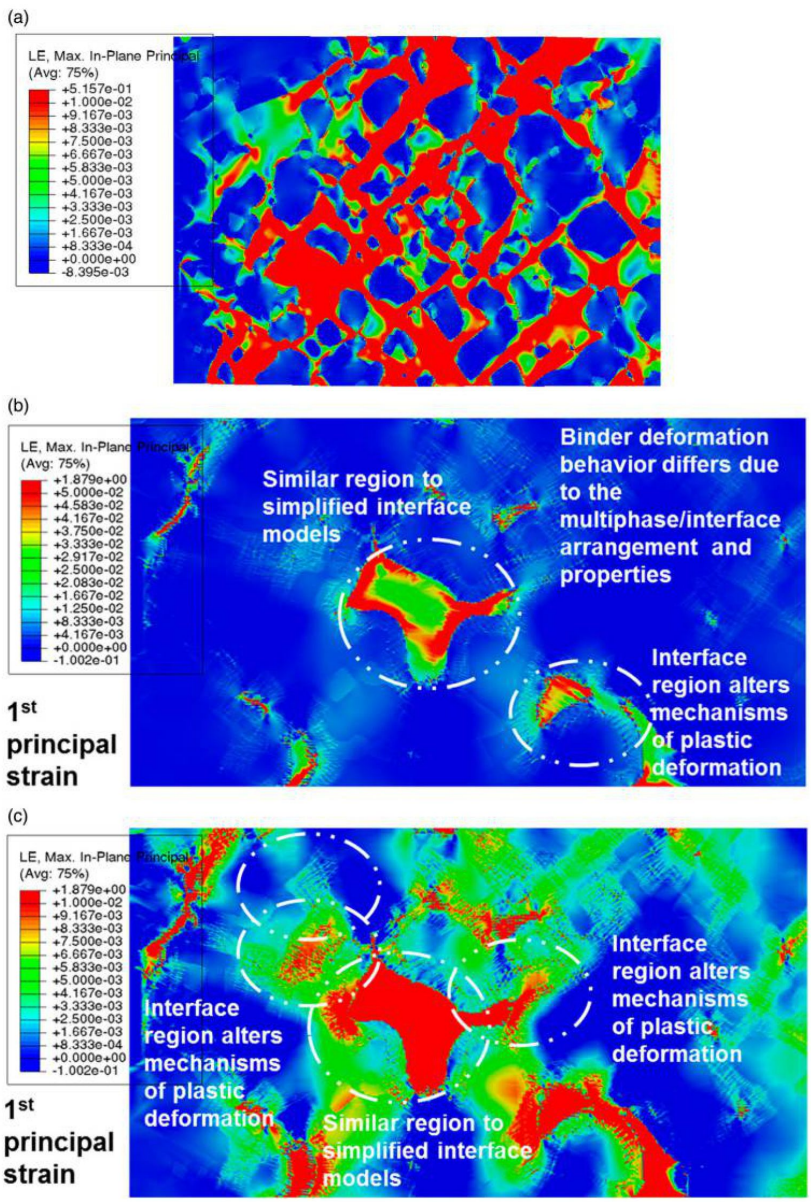

15 In-plane equivalent first principal strain contours at WC–Co microstructure without carbide dissolution *a*, with dissolved W_2C carbide *b* and in *c* detail of *b* during horizontal compression

The deformation response under compression is further highlighted in Fig. 15 by contours of first principal strain. Comparing Fig. 15*a–c*, it can be argued that the mesoscale modelling approach not including the interface characteristics is a gross simplification of the likely actual outcome and microstructural material response. With the applied imaging-based modelling techniques, the microstructural features can be resolved down to the individual dendrite morphological features of the W_2C phase, and these are seen to have an influence on the local microstructural response. In addition, it is clear that the areas of microstructure most affected are the crucial interface regions and the extreme values of the property and performance dominating stress–strain fields subsequently provide further evidence (compatible with previous understanding) of the impact of local complex and brittle phases in WC–Co microstructures.

Conclusions

Mesoscale microstructural models were created by exploiting a developed software toolset linking PF analysis results to imaging-based FE analysis, creating a methodology for deriving effective interface models for WC–Co microstructures. General observations regarding the use of multiscale materials modelling in designing composite materials were presented. Two mesoscale modelling approaches were demonstrated, one focusing on synthetic modelling and the other using imaging-based microstructural information supplemented with PF analysis results to parse more realistic information on the WC–Co microstructure. The solute concentrations and PFs of the PF results were utilised in deriving an interface phase distribution to microstructural FE models, subsequently enabling the evaluation of effects of carbide dissolution and complex phase structures on properties and performance of the resulting microstructure during applied compressive loading. Although the focal area of this current work was the study of interface modelling means for WC–Co on the mesoscale, the means can be applied in evaluation of material performance e.g. with respect to fracture characteristics or wear resistance by coupling them to suitable experimental, characterisation and modelling work.

The results of the work can be summarised as follows:

(i) The PF to FE analysis route provides a modelling framework which covers the entire mesoscale materials modelling range in a PSPP context, enabling systematic computation-driven design of cemented carbide material systems.

(ii) The interface morphology and incorporation of the semi-carbide phase drastically altered the deformation response and strength of the WC–Co system due to the presence of a carbide network and skeleton within the microstructure, often ignored in materials modelling and its impact on material properties is principally difficult to approach via only experimental means.

(iii) The interface with carbide dissolution and dendritic distribution of solute acts as a mismatching finite thickness layer around the cemented carbides. In the detrimental case it promotes the concentration of shear, limiting deformation ability and is considered an enabler towards mechanisms increasing the propensity of material failure. In the beneficial scenario it offers a means to improve upon these material properties.

(iv) The PF analyses of carbide dissolution can be utilised to define interface phase characteristics and its spatial morphology. When linked to microstructural FE it provides a methodology for quantifying the significance of specific interface phases and structures, and increases greatly the realism in modelling the WC–Co system and in deriving multiscale modelling solutions to that effect.

Acknowledgements

The work has been in part carried out within the FIMECC HYBRIDS (Hybrid Materials) programme. We gratefully acknowledge the financial support from the Finnish Funding Agency for Innovation (Tekes) and the participating companies. The collaborative efforts of Prof. N. Provatas (McGill University) and Dr N. Ofori-Opoku (Northwestern University) are gratefully acknowledged.

References

1. K. Holmberg, A. Laukkanen, A. Ghabchi, M. Rombouts, E. Turunen, R. Waudby, T. Suhonen, K. Valtonen and E. Sarlin: 'Computational modeling based wear resistance analysis of thick composite coatings', *Tribol. Int.*, 2014, **72**, 13–30.
2. K. Holmberg, A. Laukkanen, E. Turunen and T. Laitinen: 'Wear resistance optimization of composite coatings by computational microstructural modeling', *Surf. Coat. Tech.*, 2014, **247**, 1–13.
3. N. Ofori-Opoku and N. Provatas: 'A quantitative multi-phase field model of polycrystalline alloy solidification', *Acta Mater.*, 2010, **58**, 2155–2164.
4. T. Pinomaa, A. Laukkanen, S. Gurevich and N. Provatas: 'Phase field analysis of solidification structures and interface composition in WC–Co hard metals', EuroPM proceedings, Reims, France, 2015, 6.
5. T. Laitinen, P. Julkunen, A. Laukkanen, P. Puukko and E. Turunen: 'Additive manufacturing of spare part supported by digital design concept', AMPM2015 proceedings, San Diego, USA, 2015, 15.
6. S. Lay, C. H. Allibert, M. Christensen and G. Wahnstrom: 'Morphology of WC grains in WC–Co alloys', *Mater. Sci. Eng. A*, 2008, **486**, 253–261.
7. Y. Liu, Y. Jiang, R. Zhou and J. Feng: 'Mechanical properties and chemical bonding characteristics of WC and W_2C compounds', *Ceram. Int.*, 2014, 40, 2891–2899.

Publication V

Laukkanen, A., Holmberg, K., Ronkainen, H., Stachowiak, G., Podsiadlo, P., Wolski, M., Gee, M., Gachot, C. and Li, L., "Topographical Orientation Effects on Surface Stresses Influencing on Wear in Sliding DLC Contacts, Part 2: Modeling and Simulations," *Wear*.

Wear 388-389 (2017) 18–28

Contents lists available at ScienceDirect

Wear

journal homepage: www.elsevier.com/locate/wear

Topographical orientation effects on surface stresses influencing on wear in sliding DLC contacts, Part 2: Modelling and simulations

A. Laukkanen [a], K. Holmberg [a,*], H. Ronkainen [a], G. Stachowiak [b], P. Podsiadlo [b], M. Wolski [b], M. Gee [c], C. Gachot [d], L. Li [e]

[a] VTT Technical Research Centre of Finland, Espoo, Finland
[b] Curtin University, Perth, Australia
[c] NPL, Teddington, UK
[d] Saarland University, Saarbuecken, Germany
[e] City University of Hong Kong, Hong Kong

ARTICLE INFO

Article history:
Received 12 October 2016
Accepted 28 March 2017
Available online 31 March 2017

Keywords:
Friction
Wear
Topography
FEM modeling
DLC

ABSTRACT

The effects of surface roughness and topographical orientation on surface stresses influencing wear have been investigated for diamond like carbon (DLC) coated steel surfaces with three levels of surface roughness in the range of 0.004–0.11 μm R_a values, and with topographical groove orientations of 0°, 45° and 90°. A novel multiscale numerical finite element method (FEM) model was developed to integrate the layered and microstructural material features with the grooved topography. Fractal geometry and a surface voxelisation based approach were utilised to derive 3D surface topography. The surface texture representation includes: fractal signatures, which are sets of fractal dimensions calculated at individual scales in different directions, texture aspect ratio describing surface anisotropy, and texture direction signatures calculated by the variance orientation transform (VOT) method. The simulations show details of the main topographical orientation effects on local stresses affecting wear as they appear at a single scratch test with a spherical diamond ball and in a self-mated sliding situation of two rough surfaces. The 45° sliding direction in relation to grooves resulted in a mixed state of surface loading in the scratch test contact. In the complex state of stress-strain within the roughness peaks the overall tensile stress decreased, leading to greater surface resistance to cracking as compared to 0° and 90° directions. Model based calculations showed that the surface structure was about four times more rigid in the direction of grooves as compared to the more flexible behaviour in the perpendicular direction. This behaviour was empirically confirmed. The numerical calculations of rough vs rough sliding surface include real surface topographical features at various scales, material microstructural features down to nano-scale and topographical-microstructural interaction features. This approximation is thus more comprehensive than the classical approach. The real area of contact was 15–30% of the apparent contact area. The macro-topography dominated the tendency for surface cracking and plastic deformation, which is influencing on both wear and friction, while the micro-topographical features contributed to cracking and deformation by less than 40%.

1. Introduction

The impact of friction, wear and lubrication on society was for the first time systematically analysed in the so-called Jost report [1]. They reported that 515 million UK pounds could be saved by implementing better tribological solutions in machines, engines and mechanical systems. Today, fifty years later after the report's publication, the impact of friction and wear is of equal or even higher importance. This can be concluded from recent studies on impact of friction on energy consumption, emissions and economical losses worldwide [2–5]. The studies estimate that one fifth of all energy consumed today is used to overcome friction while the impact of wear can be assumed to be less but of the same order of magnitude.

Over the last fifty years, wear has been studied intensively and the main wear mechanisms have been identified and described [6,7]. However, the influence of surface roughness and topography was for long not much considered in tribological studies and has only more recently received more attention. Our understanding of how surface roughness affects wear is based mainly on observations

* Corresponding author.
E-mail address: Kenneth.holmberg@vtt.fi (K. Holmberg).

http://dx.doi.org/10.1016/j.wear.2017.03.026
0043-1648/

gathered from tribological experiments. When one or both mating surfaces are coated, the effect of surface roughness on wear is even more complex [8]. The surface topography of both surfaces in contact has often a crucial influence on both friction and wear in dry and lubricated tribological contacts.

In wear studies, surface topography is typically characterized by standard 2D roughness parameters such as R_a and R_q values. These parameters tend to work well with isotropic surfaces but they are not able to provide full information about surface anisotropy and roughness at different scales of measurement [6,9]. This limitation of standard parameters is crucial since most real engineering surfaces are anisotropic and multi-scale objects. To address these problems new techniques have been developed [10–13] and alternative topography parameters and both statistical and deterministic approaches has been analysed and suggested [23,24].

The influence of surface roundness in tribological contacts was early recognised and modelled by simple analytical models by Greenwood and Williamson [25] and Halling [26,27]. The development of sophisticated topographical measurement techniques and analysis methods has made it possible to approach the surface roughness influence on friction and wear in detail both experimentally and by modelling [28–30] on microscale and even on nanoscale [31], and also including topographical orientational effects [32–35]. The effect of substrate surface roughness on the wear of DLC coated surfaces has been demonstrated [36,37]. Most of the studies are investigating tribological contacts in dry conditions but the importance of this topic in automotive and industrial machinery applications have resulted in a growing interest to also study lubricated contacts both as real rough surfaces and artificially patterned [30,32,35,38-40].

Advanced computational modelling and simulation of changes in a material due to surface loading, and calculations of stress and strain in loaded contacts are a research area that is rapidly evolving today. Modelling and simulation of a tribocontact help to understand the mechanisms that result in surface cracking, wear particle formation and continuous wear. Numerical simulations can be carried out on several spatial scale levels, from nano to macro size, by using software representing the material structure from atomic and even sub-atomic to continuum macro and component level [14–17].

In a recent paper Holmberg et al. [18] carried out an extended empirical study on the influence of roughness and surface topographical orientation effects on friction and wear in sliding diamond-like carbon (DLC) and steel contacts. It has been concluded that the topographical orientation had considerable effects on both friction and wear in DLC vs DLC contacts while these effects were minor and sometimes not even observable in steel vs steel contacts. A higher surface strengthening effect for smooth DLC surfaces was reported. Micro-cracking and micro-delamination on asperity tips at low loads for rougher surfaces observed.

The present study is a continuation of the empirical Holmberg's et al. [18] investigation. The same materials and characterisation data of topographies and mechanical properties described in [18] are used. The aim of the second part of this study is to build a computational integrated material model including both multiscale topographical and subsurface microstructural features of the materials and to study friction and wear behaviour by means of numerical simulations.

2. Methodology

The methodology used in this study is based on the so-called PSPP (process-structure-properties-performance) approach to material investigation presented in details by Holmberg et al. [16,17]. It includes a description of the materials and coating deposition processing, detailed characterisation of microstructural and micro-topographic scale of the samples and surfaces and tribological experiments by three complementary techniques: scratch testing, linear reciprocating pin-on-plate sliding and rotational pin-on-disc testing, as previously reported in Holmberg et al. [18]. In the present work we report the modelling part, which is an integration of structural modelling carried out by finite element methods and the multiscale surface topography characterisation based on the variance orientation transform (VOT) method.

3. Materials and their mechanical properties

The samples used in this investigation are steel discs with three different surface roughness, and coated with a DLC coating. The steel samples were manufactured from bearing steel (AISI52100) and heat treated to 6.3 GPa hardness. On the steel discs the coatings were deposited by magnetron sputtering technique [18]. The DLC coating had a multilayer structure, as shown in Fig. 1.

Three surface finishes for the disc substrates were produced by polishing the ground discs with two polishing media of different grades. The ground surface was considered as rough (R) surface and the two polished surfaces as average (A) and smooth (S). The three dimensional (3D) surface topography of the discs was measured using a chromatic confocal surface profilometer.

The individual coating layers were analysed by scanning electron microscopy (SEM) and their thickness was measured from the focused ion beam (FIB) cross-section, as shown in Fig. 1, using a dual beam SEM/FIB facility. The layer structure was practically homogenous, i.e. virtually free from microstructural features, defects, pores and the like on a sub-micron scale. Some randomly distributed coating heterogeneity or impurity was observed on the micro to macroscale. Indentation testing was performed both at the macro and nano scales, in order to assess the plastic and elastic behaviour of the coated system and its constituent components. The most important mechanical properties used in the modelling are shown in Table 1. The total coefficient of friction has been measured to be in the range of 0.12 – 0.18 with 15 N load for these surfaces. Based on these and previous measurements we estimate that the adhesive component of the coefficient of friction, needed for the model, was about 0.1 [18–20].

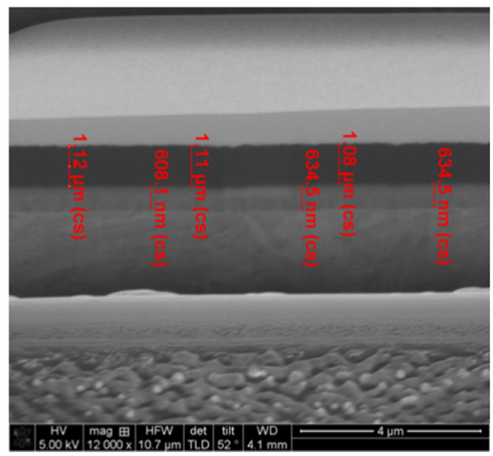

Fig. 1. Section of the smooth DLC coating showing from top the thicknesses of the DLC, CrCx gradient, and Cr buffer layers and the substrate.

Table 1
Mechanical properties of the used samples.

Properties	Symbol (unit)	DLC coated steel disc	Steel substrate, AISI52100 (100Cr6)
Flat surface			
Total coating thickness	h (μm)	1.76 ± 0.04	–
Hardness (nano)	H (GPa)	18 ± .3	–
Elastic modulus (nano)	E (GPa)	205 ± 10	220
Poisson's ratio	v (-)	0.202[a]	0.3[a]
Surface roughness			
– smooth	Ra (μm)	0.005	0.004
– average	Ra (μm)	0.01	0.01
– rough	Ra (μm)	0.11	0.1
Surface topography	VOT	See table 4 in [18]	See table 4 in [18]
Yield strength	MPa	–	2100
Tensile strength	MPa	–	2200
Tangent modulus	(GPa)	–	22.0
Spherical countersurface		**Diamond tip**	
Diameter	μm	200	
Roughness		ideally smooth	
Hardness	H (GPa)	80	
Elastic modulus	E (GPa)	1140	
Poisson's ratio	v (-)	0.07	
Adhesive friction coefficient	μ (-)	0.1	

[a] From literature.

4. Surface topography characterisation

The specifications of the directions used in topographical surface characterisation correspond to the direction of grinding marks on the discs, marked as 0°, 45° and 90°, as shown in Fig. 2. Range-images of the surfaces scanned were obtained by encoding the 3D surface elevation data obtained from the profilometer into 256 grey-scale images. In these images, the brightest and the darkest pixels represent the highest and the lowest elevation points on a surface, respectively.

The range-images of DLC-coated steel surfaces were characterized by the VOT method. In this method, log-log data points of variances of grey-scale differences between pixel distances are divided into overlapping 5-data point subsets with a line fitted to each subset. For each line the slope and the between-pixel distance corresponding to the central log–log data point are recorded. The distance represents the length scale and the slope of the line is a Hurst coefficient (H). Using the Hurst coefficient, a fractal dimension is calculated as FD = 3 - H. It should be noted that the FD is a measure of surface roughness at the scale; as opposed to traditional FDs that measure the roughness over more than an order of magnitude in scale range. The Hurst coefficients were calculated in different directions and at nine length scales [11]. Five surface parameters were calculated:

Table 2
Surface topography data obtained on four scales.

Scale	Direction and length scales	Data from
1	Groove directions: 0°, 45°, 90°	Optical observations
2	1–10 mm	Profilometer
3	100–1000 μm	Fractal VOT1, 360–840 μm
4	10–100 μm	Fractal VOT2, 30–70 μm

- **Fractal signatures** in 0° (FS_0), 45° (FS_{45}) and 90° (FS_{90}) directions. These signatures are defined as sets of FDs calculated at individual scales in the direction of 0°, 45° and 90° degrees to the grinding marks on the steel discs, as shown in Fig. 2. The range of scales is listed in Table 2.
- **Texture aspect ratio signature** (*StrS*). The parameter is defined as the set of texture ratios of the minor axes to the major axes of the ellipses. The StrS measures surface anisotropy at different scales. For perfectly isotropic surfaces (i.e. surfaces exhibiting the same FDs in all directions), StrS values are equal to one. For anisotropic surfaces, they are less than one.
- **Texture direction signature** (*StdS*). This parameter is defined as set of angles between the major axes of the ellipses fitted and the vertical image axis. The axis corresponds to the directions of grinding marks on surface (0° direction). The parameter indicates a dominating surface direction (anisotropy direction).

Range images and values of the parameters FS_0, FS_{45}, FS_{90}, *StrS* and *StdS* obtained are found in Holmberg et al. [18]. The surface topography data used in the modelling was obtained at four scales by optical observations and by profilometer measurements. VOT analysis was conducted at two different surface roughness ranges, in between 360–840 μm (VOT1) and between 30–70 μm (VOT2), as shown in Table 2. An example of the profile of the rough surface obtained from profilometer measurements is shown in Fig. 3.

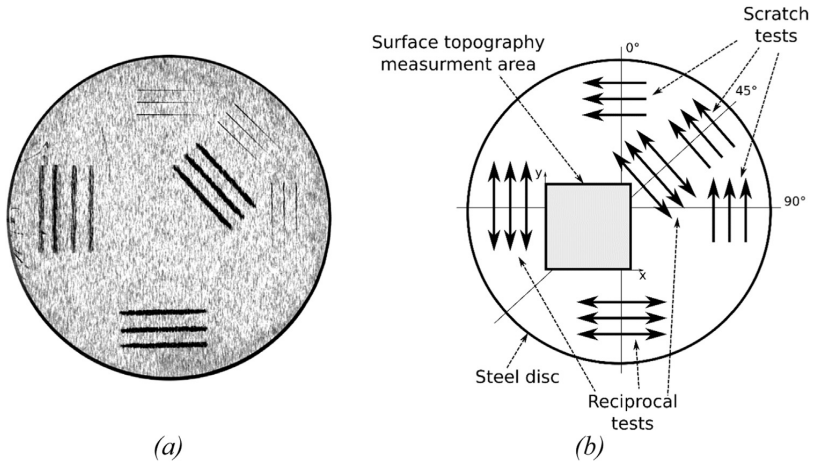

Fig. 2. (a) Example image of a steel disc and (b) its schematic illustration with marked locations of scratched and linear reciprocating tests, surface topography measurement area and tests directions. Area for surface topography measurement was 10.72 × 10.72 mm^2.

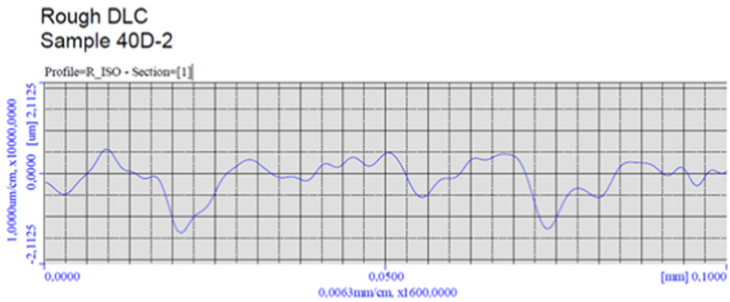

Fig. 3. Example of the surface profile of the rough surface. Note that the ratio of the horizontal vs vertical length scale is 1:20.

5. Material and surface modelling

A digital FEM computer model of the samples was created. In the model the topographical features on fractal scales from 30 to 840 μm and 3D profilometry data from 1 to 10 mm are linked to the microstructural features on scales down to about one nanometre, as shown in Fig. 4.

The models of the three surface topographies studied, i.e. smooth, average and rough, are shown in Fig. 5. The grooves direction is visible in all three topographies. Note, that the original surface was rough (Fig. 5c) while the average (Fig. 5b) and smooth (Fig. 5a) surfaces were generated by polishing the rough surface.

To produce computational models with various surface topographies, a software toolset implementing different means to describe surface structure was developed and incorporated as a module of the in-house multiscale modelling solution, VTT ProperTune [21]. The primary functionalities are presented in Fig. 6. As a first step, the form of topography data is provided to the solution. This data can be given as a measured surface topography, a fractal surface or at its simplest solely as a R_a roughness value. Thus, different means are applicable to describe and generate the surface structure.

Firstly, a methodology utilising Fourier series and power spectra was implemented to describe the surface topography and the expression fitted to available experimental data. Secondly, a methodology generating the surface via a random walk process was used, i.e. the stochastic method utilising for example R_a values or their distribution to produce a representative isotropic rough surface. Thirdly, a fractal surface was included. Methods such as midpoint displacement were used to generate isotropic and anisotropic fractal surfaces of given roughness (i.e., fractal dimension). Fourthly, the surface was generated directly to match a measured surface topography with a given resolution, overlaying the experimentally obtained data on a computational model surface.

Following the inclusion of surface topography which is typically carried out by introducing a polygonal mesh on top of the features of interest, a 3D image is generated by voxelisation operations. The 3D image can be further operated upon, i.e. the different means can be linked to tools of nano-microstructural modelling, e.g. including the interactions of microstructure, coating defect structures. For example coating cracking and damage can be investigated as steps of modelling cumulative wear. Meshing of the 3D image generates the final computational grid, which can subsequently be input and solved typically by a separate finite element or particle methods solver.

In the current work the goal was to establish a consistent description of surface topography in order to make general observations on the correlation between surface character and its stress-strain state under contact loading. As such, direct generation of a numerical model based on measured surface topography was not considered, but rather, the topography was fitted to a particular methodology of describing the surface profile. Since the empirical work relied on a fractal description of the surface, this was selected also for generating the surfaces in numerical models.

The multiscale fractal characterization of surface topographies was employed for two scale description. First, an anisotropic fractal surface that contains primary grooves was generated. This can be considered a coarse description of the surface. Second, the anisotropic description was imposed with the smallest length scale measurement data to describe the isotropic fractal nature of the surface. This can be viewed as a compromise since a resolution is inherently build in the methodology, but on the other hand, it makes best use of the available experimental data.

Selection of the scales depends on the desired outcome, i.e. the characteristic length scales pertinent to the phenomena being modelled; typically found through a sensitivity study. In the current work, since the coating thickness scale features are of significance, the highest available resolution in the fractal data was used. Two different types of contacts were studied. The

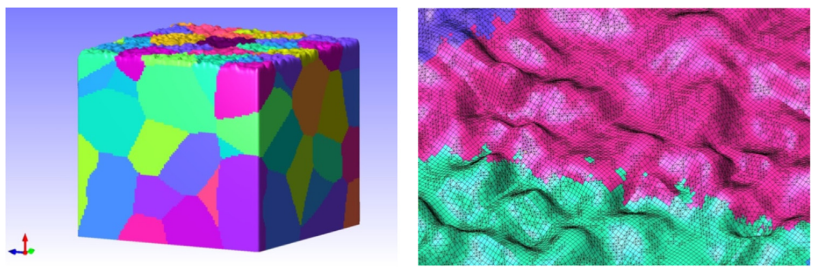

(a) (b)

Fig. 4. (a) The integrated topographical surface and microstructural material model, and (b) a close up image of the surface topography with FEM mesh. The dimension of the modelled cube in (a) is $60 \times 60 \times 60$ μm.

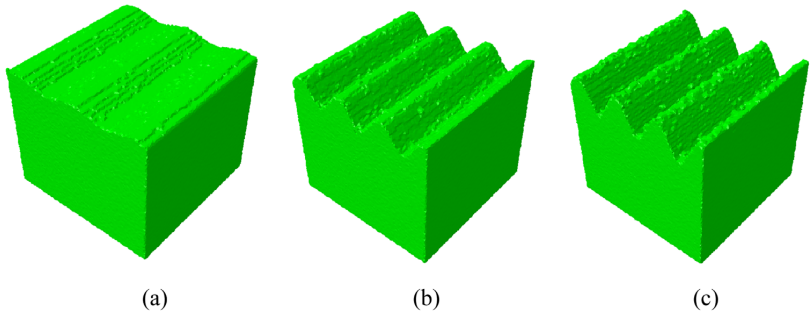

Fig. 5. Topography and material models of the (a) smooth, (b) average, and (c) rough surfaces. The modelled cube dimension is approximately 100 × 100x100 μm. The roughness profile is exaggerated by 10 fold for visualization purpose.

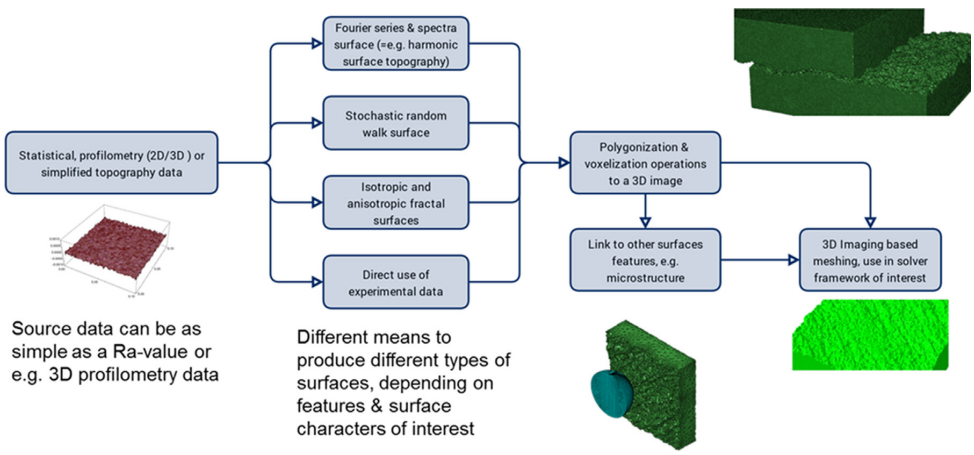

Fig. 6. The developed computational material model introduces topographical features in tribological multiscale models.

experimental findings were matched with those of the anisotropic two scale fractal surfaces against an ideally smooth surface. Also, the surfaces with identical characteristics in rough on rough contacts were modelled.

6. Sliding tribocontact stress simulations

6.1. Diamond ball sliding on flat surface with topographies

The scratch test contact was computer simulated for a rigid diamond ball with perfectly smooth surface that slides with increasing load over a DLC coated steel surface with various topographies. Local topographical ridges in the contact zone create regions of increased stresses and residual stresses behind the contact, as shown in Fig. 7.

The patterns of the first principal stresses under the sliding ball at a load of 12 N are shown in Figs. 8–10. When the ball moves in the direction of the grooves (0°) over the smooth surface (Fig. 8a) long and narrow regions of high tensile stresses up to about 1100 MPa and locally even greater values are observed in the valleys. Even if the surface is smooth the surface machining leaves characteristics grooves that were present before the polishing process. Elongated regions under compressive stresses up to

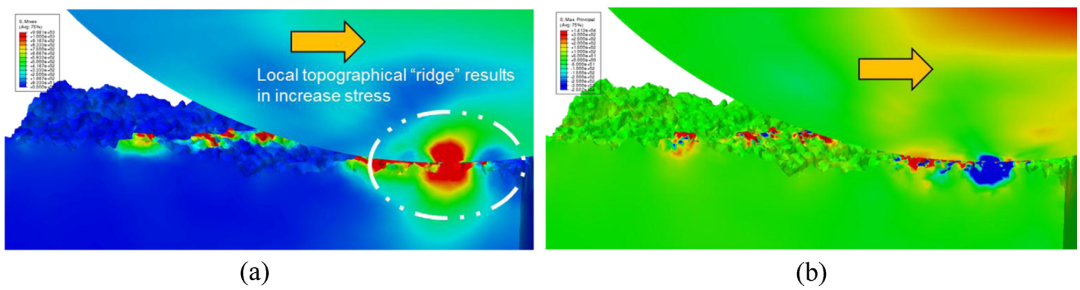

Fig. 7. A perfectly smooth and rigid diamond ball slides over the rough DLC coated steel surface creating regions of increased stresses in the contact zone and regions of residual stresses behind the contact. (a) the equivalent stress contours and (b) the first principal stress contours.

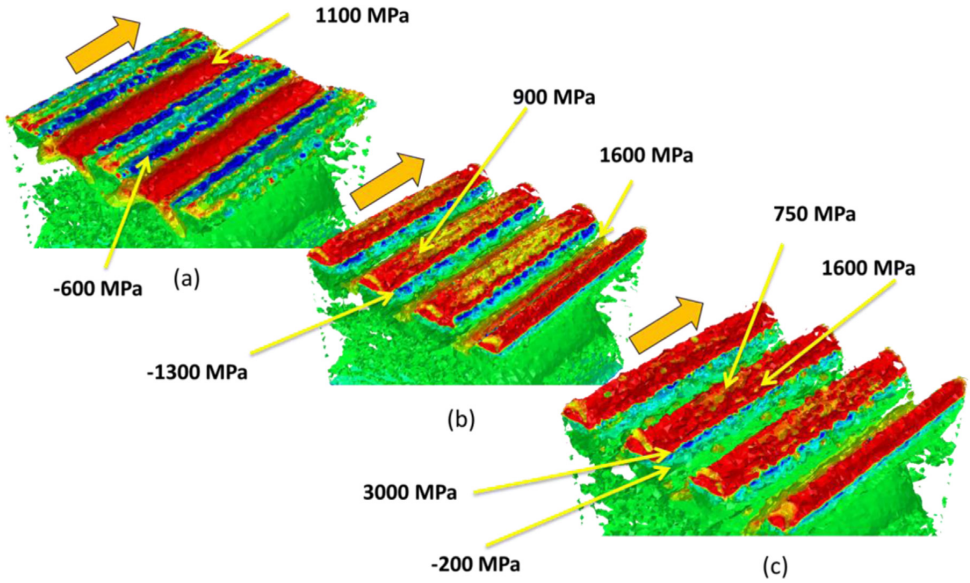

Fig. 8. First principal stresses on the surface of (a) **smooth,** (b) **average,** and (c) **rough topographies** created when the sliding ball moves in the direction of the grooves at 0° degrees orientation over the DLC coated steels surface. The ball moves in the direction indicated by the arrow. The cube dimensions are approximately 100 × 100 x 100 μm. The roughness profile is magnified by 10 fold.

600 MPa are found on the slopes while the flat top regions of the ridges are in an almost stress-free state. With increasing roughness the stress field changes, as shown in Fig. 8b and c. With high roughness the valleys are more in a stress-free state. The highest tensile stresses are found in a plane section cutting the ridges horizontally at about two thirds of their height while lower tensile stresses are generated in the top regions of the ridges. This behaviour is believed to be due to the higher stiffness of the more bulk like structure of the smooth surface. On the other hand higher ridges result in more flexible contact areas that allow for elastic and plastic deformations and thus decrease the stresses in these areas. It must be noted that this behaviour is to some extend

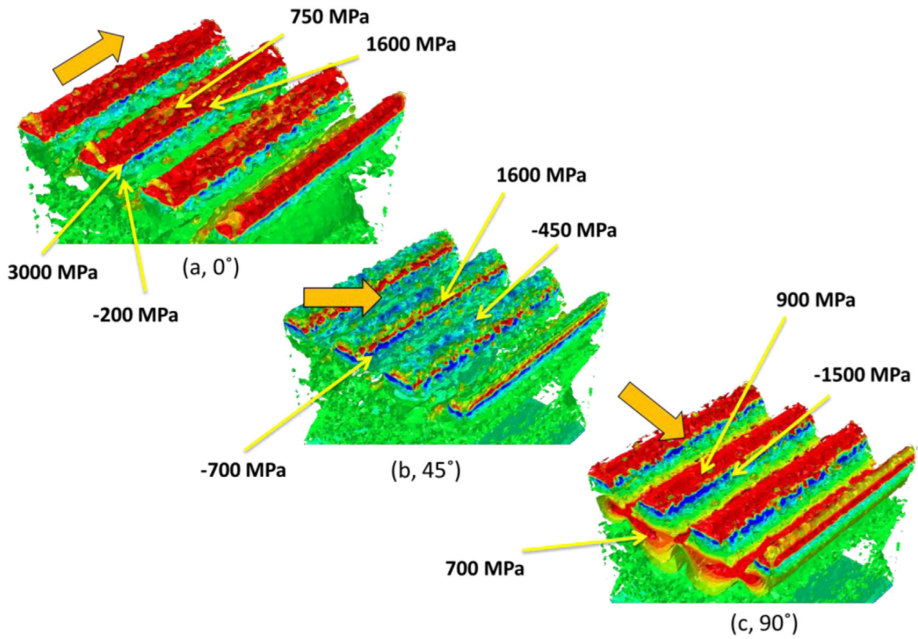

Fig. 9. First principal stresses in the surface with **rough topography** when the smooth diamond ball is sliding in (a) 0°, (b) 45°, and (c) 90° directions in relation to the grooves over the DLC coated steels surface. The ball moves in the direction indicated by the arrow. The modelled cube dimensions are approximately 100 × 100x100 μm. The roughness profile is magnified by 10 fold.

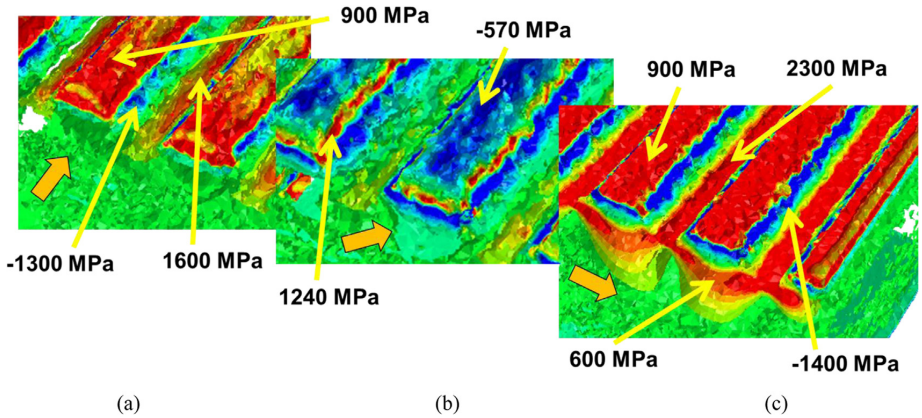

Fig. 10. First principal stresses in the surface with **average roughness** when the smooth diamond ball is sliding in (a) 0°, (b) 45°, and (c) 90° directions in relation to the grooves over the DLC coated steels surface. The ball moves in the direction indicated by the arrow. The modelled cube dimensions are approximately 100 × 100 x 100 μm. The roughness profile is magnified by 10 fold.

limited to loads where failure and plastic deformation mechanisms are not yet truly prevalent, and as such, the very top of the coated system is most active in carrying the load.

The surface stress patterns as the ball slides in the 0°, 45° and 90° directions in relation to the grooves with **rough topographies** are shown in Fig. 9. In surfaces with rough topography and sliding direction (Fig. 9a) along the grooves there are high tensile stress peaks close to the middle height of the ridges, even up to 3000 MPa. The maximum tensile stress is about 750 MPa on the top of the ridges while the valleys are in an almost stress-free state. When sliding perpendicular to the grooves tensile stresses of 900 MPa are found on top of the ridges and of 700 MPa below the ridges with a high compressive stress plane at half height of the ridges, as shown in Fig. 9c. Greatest compression with respect to the top of the ridges is within the material and near the transition where the bending of the asperity tip takes place. Thus, at the top surface of the coating at 0° and 90° sliding directions the tensile stress state dominates.

It is interesting to observe that when the ball slides in 45° direction with reference to the grooves, as shown in Fig. 9b, only a small region of higher tensile stresses, up to 1600 MPa, is observed at the slopes and the valleys are close to a stress-free state. There are compressive stresses of about 450 MPa in the top region of the ridges.

A closer view of the **average roughness surface** stress pattern, when sliding in 0°, 45° and 90° directions, is shown in Fig. 10. When sliding in the direction of the groove (Fig. 10a) there are high tensile stresses of 1600 MPa in the valleys and also high tensile stresses in the top region of the ridges of 900 MPa. When sliding in the perpendicular direction in relation to the grooves there are again high tensile stresses up to 900 MPa on the top of the ridges and a second region of very high stresses is observed both in the valleys, 2300 MPa, and also under the ridges with values of 600 MPa. Right under upper high tensile stress region at the top of the ridges there is a horizontal plane region with high compressive stresses up to 1400 MPa. This stress pattern is explained by tilting of the surface roughness peaks during sliding. The peaks exhibit both bending and tension. On the side of the roughness peaks outside the region of contact both the tensile and bending loads strain the surface, yielding a stress maxima.

It is again interesting to observe that when sliding in 45° direction no large regions of high tensile stresses are observed. Half way up the slopes there is now a horizontal plane section going through the ridges of tensile stresses of 1240 MPa. Both above and below there are regions of compressive stresses in the order of 570 MPa. This is explained by examining again the deformation state resulting from the contact. At both 0° and 90° sliding directions the deformation state exhibited by the roughness peaks is either aligned or perpendicular to the roughness peaks, resulting in a tensile like loading state at the roughness peaks or at the flats between the peaks. On the other hand, when the loading is at a 45° angle to the main axis of surface anisotropy, neither of these states can be reached and a mixed state of surface loading and stress results. As such, it can be argued that the complex state of stress-strain within the roughness peaks decreases the overall tensile stress state, which might indicate a propensity for greater surface resistance to cracking.

In the experimental part of this work we reported previously an unusual cracking behaviour that appeared during scratch tests when sliding with the diamond ball in 45° direction to the surface grooving for both rough and average surfaces [18]. To the best of our knowledge this has not been previously reported in the literature. A normal angular cracking pattern appeared on the left hand side of the grooving by the groove edge but no cracking at all was observed on the right hand side all along the 8 mm scratch length, as illustrated in Fig. 11a. The developed computational model was used for calculating the tensile stress fields on both sides of the scratch groove and for the average roughness it showed high tensile stress peaks of 3690 MPa on the left hand side while they were only 940 MPa on the right hand side, as shown in Fig. 11b. These values correspond to the maximum of tensile stresses at local peaks of surface roughness. On average, it can be stated that the ratio of tensile stresses on the left hand side vs right hand side when averaged over the size scale of the roughness peaks is close to zero for the smooth surface, it is approximately 4 for the average roughness and 4.4 for the roughest cases.

This can be explained as follows. When sliding along a surface in 45° direction from the surface grooving with a counter surface, such as the smooth diamond ball used as counter surface in a scratch surface, such tensional stresses will occur on the ridges on one side of the generated groove where the tensile pulling direction is in line with the grooving and about four times lower tensile stresses occur when the pulling direction is perpendicular to the grooving. The reason is that the surface structure is more rigid in the direction of grooving and more flexible in the direction perpendicular to the grooving. The behaviour is expected to be dependent on applied loading and material response as they influence the deformations of the surface topography.

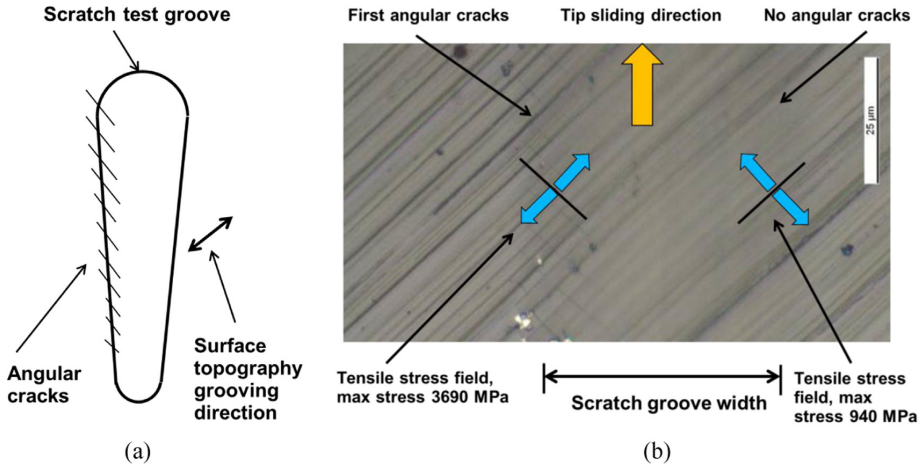

Fig. 11. Schematic illustration of scratch test groove (a) showing how the angular cracks appearing only on the left hand side of the groove edge and (b) picture showing the stress fields on the groove edges close to the first angular cracks.

6.2. Rough on rough surface sliding

The contact between two rough DLC coated surfaces was created by copying a rough anisotropic surface model and rotating it twice by 180°, first so that it is turned up-side-down and then once more in the horizontal plane and making it slide over the first surface. The contact is shown in Fig. 12 where Fig. 12a illustrates the local equivalent stress field while Fig. 12b illustrates the first principal stresses generated as the upper surface moves from left to right. Equivalent stresses provide an overall measure of stress at the contact surface, while 1st principal stresses provide an indication as to the compressive and tensile nature of surface loading.

High tensile stress peaks up to 2000 MPa and above are observed. This shows that the local stress state seems to be dominated by local rough on rough asperity contacts. Due to the overall smaller contact area, in addition to the sharp features of surface topography, greater stress values are generated. These results are in line with the classical concept of rough-on-rough surface contacts originally introduced by Bowden and Tabor [22]. They showed that the load is carried by a very small real area of contact that is only a fraction of the apparent area of contact. Our calculations show that the real area of contact, which contributes to the load carrying process, is only 15–30% of the apparent area of contact, in the contacts studied.

The calculations conducted in this work including the integrated multiscale material model are considered as more precise than calculations carried out with the classical approach. The classical analytical calculations consider the surface materials as homogenous. Our computational calculations include real topographical surface characteristics on fractal scales, material microstructural features down to nanometre scale and interactions of these features in the stress and strain generation process. As such, classical approaches are only approximate and include the effects of materials deformation behaviour and microstructure, only in an average sense. Considering the characteristics of layered structures, e.g. the anisotropic plasticity of the substrate microstructure, it can be argued that many of the local details critical for crack initiation and subsequent evolution of wear can be properly captured only with a numerical methodology, such as the one used in this work.

The stress pattern over the whole contact area is shown in Fig. 13. A contact depicted in Fig. 12 is shown in the way that the whole stress field in the contact area and also in sections at the sample wall are visible, providing a contact surface scale view of the stress state. Features that can be observed are the differences between micro-scale contacts associated with isotropic fractal roughness and the macro-scale anisotropic fractal features that are affiliated with longer wavelength surface characteristics. With respect to longer wavelengths, it seems that some parts of the system are primarily under compression, while certain regions predominantly exhibit tensile stresses. This is seen as an indication of the effect of longer wavelengths of surface roughness, if the topography is considered with respect to its different fractal characteristics.

Locally, with respect to the tensile stress areas, the local isotropic fractal characteristics including the peaks and valleys of the

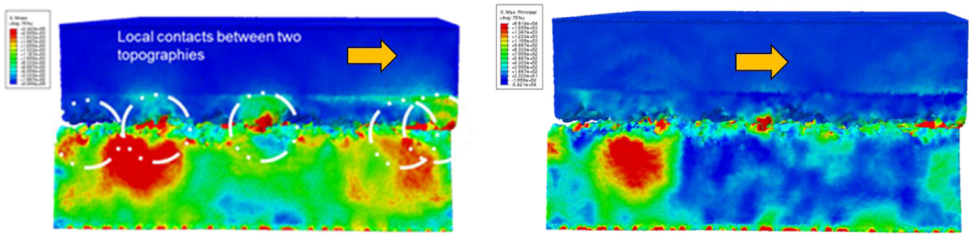

Fig. 12. (a) Equivalent and (b) first principal stresses in the rough surface and in the microstructure below as one rough DLC coated steel surface slides over a similar surface. The sliding direction is indicated by the arrow.

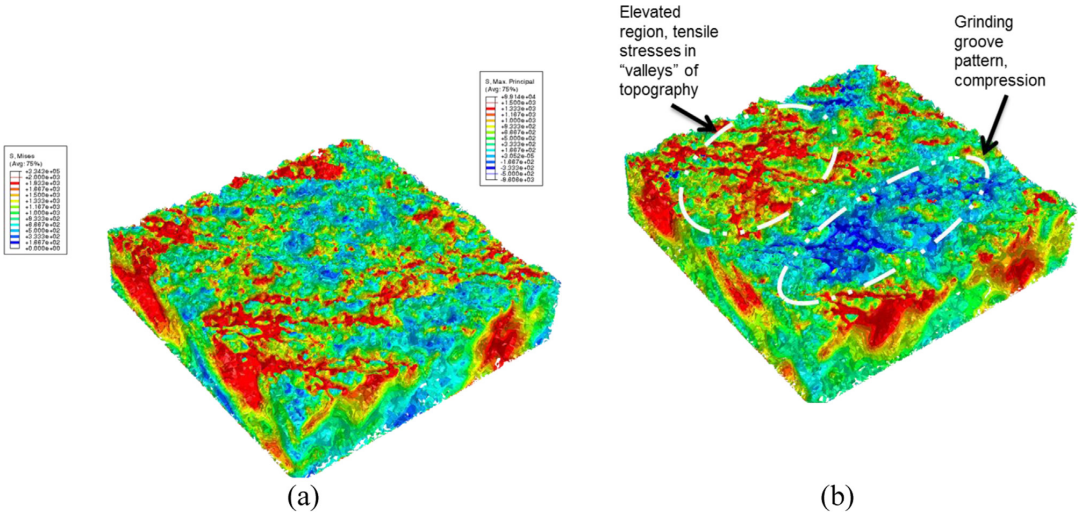

Fig. 13. The stress pattern in the rough surfaces from the contact shown in Fig. 11. (a) Equivalent von Mises stress contours and (b) 1st principal stress contours. The modelled cube dimensions are approximately 100 × 100x25 μm. The roughness profile is magnified by 10 fold.

surface topography are seen to play a crucial role especially with respect to extreme values, such as maximum stresses. It can then be argued that the role of both characteristics is significant in realistic rough-on-rough contacts. The greater wavelengths influence the overall contact surface and contact area. However, with respect to the coating characteristics and, e.g. cracking behaviour, the local features are seen to have a clear influence on the stress field, implying that the smaller scale morphology is ultimately crucial with respect to engineering material properties and wear resistance of the tribological system. Also the interactions leading to surface failure can be quite intricately related to the scale size of the coating thickness and as such are influenced by surface topography, contact conditions, contact loading, friction and also the material's microstructure.

When surface mean stresses are compared to local stresses and fractal character of the surface is considered then we can gain an overall estimate how surface stresses are influenced by the two scale topographical features. The macro-topographical features dominate the cracking and plastic deformation behaviour of the surface, resulting in friction and wear, while the micro-topographical features contribute to surface cracking and deformation with less than 40%, in the contacts and specific topographies studied.

7. Discussion

7.1. Model development

Modelling of surface topographies and rough surface contacts can be simplified if effective roughness models or 2D models are used. The primary reason for this simplification is computational. In current work a novel methodology for generating surface topographical models is presented. The methodology allows for importing the experimental or computer generated surface topographies and converting measured data to a numerical 3D model. This approach can provide a high-resolution description of the contact conditions and integrate the effects of surface topography with coating and substrate properties. These features are critical for a better understanding of tribological material systems and an improvement of the systems performance. The methodology can be expanded by including nano-microstructure and defect structure within the coating.

7.2. Comparison with empirical results and model validation

A strong correlation was found between the empirical and computer simulation results obtained from the scratch test in which the ball slides over the average rough or the rough surface in the direction of 45° to the grooves. Specifically, the angular crack pattern was identified on the left hand side of the scratch groove (Fig. 11). The simulation showed (Fig. 11) that the tensile stresses calculated on the left side are four times higher as compared to those on the other side.

Another relevant comparison of the simulations conducted is associated with the scratch test results previously reported in [18]. Correlation with the experimental results and the calculated stress profiles was found as shown in Fig. 8.

For the sliding of the smooth diamond ball over the average roughness surface (Fig. 10), the lowest stress levels were found along 45° directions. This agrees with the highest critical load of 11.8 N measured during the experiments. The results indicated that a high critical load value is needed to generate the first crack. This is clear evidence of a good resistance to surface cracking and wear. For the stress profiles shown in Figs. 8 and 9 we did not find such correlation.

7.3. Influence of topographical orientation on friction and wear

Both the experimental modelling parts clearly demonstrate that the topographical orientation of a surface directly affects surface cracking and hence have a crucial influence on both friction and wear. Significant changes in the stress field were observed when sliding over a grooved surface in 0°, 45° and 90° directions. For the 45° direction this effect was the weakest. This finding could be of practical importance, i.e. wear can be reduced by rotating the grooves with respect to the sliding direction. Similar effects on the topographical ploughing component of friction and thus its an impact on friction are also expected.

7.4. Surface parameters to indicate wear behaviour

Correlation between the surface topography and the modelling results obtained would be of interest to those who design wear resistant material systems and surfaces. The surface fractal signatures, texture aspect and direction signatures had a strong influence on the macroscale contact response. The signatures were found responsible for the observed experimental and computer simulated orientation effect, including the overall stress state of the rough surfaces. The results indicate that the texture parameters have a fundamental influence on the macroscale contact response, essentially providing a measure of the anisotropic character of the topography. These measures were found to be responsible for the observed experimental and modelled orientation effects, as well as the overall stress state of the rough surface contacts investigated. As such, much of the contribution to friction, with limited ploughing and plastic deformation, and surface cracking can be linked to the surface texture features (described by these parameters). It was found that the fractal signatures were best correlated with the local stress-strain state of the coated surface. The results indicate that local features contribute to the top surface stress state in general by less than 40%. This difference is considered significant in terms of surface failure, especially due to the fact that the size scale of the local stresses is in the of order of coating thickness. It can be argued that due to this difference, local cracking and defect initiation are dependent on the topography features, described by fractal signatures. However, further propagation and development of extensive surface damage will depend upon the texture parameters and mean fractal signature measured over larger range of scales.

8. Conclusions

A computational integrated topographical-microstructural 3D model was developed to investigate the influence of surface roughness and topography on friction and wear. The model contains a full 3D multiscale representation of the surface topography, which is derived using an anisotropic fractal model. The data resolution equal to the spatial scale of the coated system allowed for an investigation of the system's property and a control of its performance. The model was solved in a fully explicit manner, i.e. no effective roughness or similar type model is employed.

Fractal and texture signatures were identified and used in the modelling to give a better understanding of how the surface topography correlates with the numerical modelling results. It was found that the initiation of defects and wear correlates with the signatures. In the material damage beyond crack fields, the ranges of scales over which the signatures were calculated played an important role.

The model was used in the simulation of the contact between DLC coated steel samples that have three levels of surface roughness in the range of 0.004–0.11 μm R_a. In the model, the topographical features on fractal scales from 30 to 840 μm and 3D profilometry data from 1 to 10 mm are linked to the microstructural features on scales down to about one nanometre. The topographical data on three scale levels, the groove directions identified through optical observations, the roughness features on macro level obtained from the profilometer measurements and on micro and nanoscales obtained from the fractal VOT analysis were used.

The scratch test simulation conducted for the rigid smooth ball sliding over the DLC coated surfaces in the 0°, 45°, and 90° directions with respect to the surface grooves showed that:

1. Sliding in the direction of grooves, results in high, more than 1100 MPa, tensile stress acting in the valleys of the smooth surface while the valleys of the rough surface are more in a stress free state, with compressive stresses of about 200 MPa. Local peak stress values are the greatest at the surface's small scale topographical features, and larger than, for example, in the smooth larger spatial scale surface impressions.
2. When sliding over the surface with average roughness in 45° direction to the surface grooves the tensile surface stresses generated are much lower (1240 MPa) in a small region compared with the higher tensile stresses (1600 MPa and 2300 MPa) in large regions of the surface when sliding along the grooves or perpendicular to it. A similar effect for the rough surface was observed. This is explained by the deformation state resulting from the contact. At both 0° and 90° directions of sliding the deformation state exhibited by the roughness peaks are either aligned or perpendicular to the roughness peaks, resulting in a tensile like loading state either at the roughness peaks or at the flats between the peaks. When the loading form sliding is at a 45° to the main axis of surface anisotropy, neither of these states can be reached and a mixed state of surface loading and stress results. The more complex state of stress-strain within the roughness peaks decreases the overall tensile stress state and indicates a greater surface resistance to cracking.
3. When sliding at 45° direction to the surface grooves against a smooth counter surface, such as the diamond ball during the scratch test, tensile stresses will occur at the groove ridges on both sides. On one side of the groove, where the tensile pulling direction is in line with the grooves, high tensile stresses of about 3700 MPa appear while on the other side where the pulling direction is perpendicular to the grooves much lower stresses of only 950 MPa occurs. The reason is that the surface structure is roughly four times more rigid in the direction of grooves while it is more flexible in the direction perpendicular to the grooves.

Simulations of a DLC coated rough surface sliding on a similar DLC coated rough surface revealed the following observations:

4. In the contact between two rough DLC coated surfaces the total real area of contact was only 15–30% of the apparent contact area. This is in line with the classical theory of rough vs rough sliding contacts. However, the calculation results found in this work appear to be more comprehensive since they also include real surface topographical features at different scales, material microstructural features down to nanoscale and topographical-microstructural interaction influencing on the real stress and strain state.
5. The macro-topography in the studied rough DLC coated contacts dominates the tendency for crack development and deformation that is influencing both wear and friction while the micro-topographical features contribute to cracking and plastic deformation by about 40%.

The integrated topographical-microstructural computational model developed shows to be a good representation of the contacts between real surfaces studied and it can be used for detailed investigations of surface and material response to moving mechanical loading and subsequently to friction and wear.

Acknowledgements

In this study the DLC coating deposition was carried out by City University of Hong Kong, material characterisation by Saarland University in Germany, topographical characterisation by Curtin University in Australia, nanoindentation and micro tribology testing by National Physical Laboratory in UK and characterisation, indentation, scratch testing, linear reciprocating pin-on-plate and

rotational pin-on-disc testing by VTT Technical Research Centre of Finland.

The authors acknowledge the contributions of Lauri Kilpi and Simo Varjus for carrying out tribotesting at VTT tribology laboratory.

The study was conducted as part of the Implementing Agreement on Advanced Material for Transportation Applications, Annex IX Model based design of tribological coating systems. The Implementing agreement functions within a framework created by the International Energy Agency (IEA). The views, findings, and publications of the AMT IA do not necessarily represent the views or policies of the IEA or of all of its individual member countries.

In Finland the study was carried out as part of the Finnish joint industrial consortium strategic research action coordinated by FIMECC Ltd within the program on Breakthrough Materials called HYBRIDS in the Fundamentals and Modelling project. We gratefully acknowledge the financial support of Tekes - the Finnish Funding Agency for Innovation, the participating companies, and VTT Technical Research Centre of Finland.

References

[1] P. Jost (ed), Lubrication (Tribology) education and research, A Report on the Present Position and Industry's Needs, Department of Education and Science, Her Majesty's Stationary Office, UK, 1966.
[2] K. Holmberg, P. Andersson, A. Erdemir, Global energy consumption due to friction in passenger cars, Tribol. Int. 47 (2012) 221–234.
[3] K. Holmberg, R. Siilasto, T. Laitinen, P. Andersson, A. Jäsberg, Global energy consumption due to friction in paper machines, Tribol. Int. 62 (2013) 58–77.
[4] K. Holmberg, P. Andersson, N.-O. Nylund, K. Mäkelä, A. Erdemir, Global energy consumption due to friction in trucks and buses, Tribol. Int. 78 (2014) 94–114.
[5] A. Erdemir, K. Holmberg, Energy consumption due to friction in motored vehicles and low-friction coatings to reduce it, in: S.C. Cha, A. Erdemir (Eds.), Coating Technology for Vehicle Applications, Springer, Heidelberg, Germany, 2015, pp. 1–23.
[6] G.W. Stachowiak, A.W. Batchelor, Engineering Tribology, 4th ed., Butterworth-Heinemann, 2013.
[7] R. Bruce (ed.), Handbook on Lubrication and Tribology (2nd ed.), vols. I and II, CRC press, New York, USA, 2012.
[8] K. Holmberg, A. Matthews, Coatings Tribology: Properties, Mechanisms, Techniques and Applications in Surface Engineering, Elsevier Tribology and Interface Engineering Series No. 56, Elsevier, Amsterdam, The Netherlands, 2009.
[9] W.K. Kubin, M. Pletz, W. Daves, S. Scheriau, A new roughness parameter to evaluate the near-surface deformation in dry rolling/sliding contact, Tribol. Int. 67 (2013) 132–139.
[10] M. Wolski, P. Podsiadlo, G.W. Stachowiak, Directional fractal signature analysis of trabecular bone: evaluation of different methods to detect early osteoarthritis in knee radiographs, J. Eng. Med. Proc. IMechE Pt H 223 (2009) 211–236.
[11] M. Wolski, P. Podsiadlo, G.W. Stachowiak, Applications of the variance orientation transform method to the multi-scale characterization of surface roughness and anisotropy, Tribol. Int. 43 (2010) 2203–2215.
[12] M. Wolski, P. Podsiadlo, G.W. Stachowiak, Directional fractal signature analysis of self-structured surface textures, Tribol. Lett. 47 (3) (2012) 323–340.
[13] P.G. Podsiadlo, G.W. Stachowiak, Directional multiscale analysis and optimization for surface textures, Tribol. Lett. 49 (1) (2013) 179–191.
[14] G.B. Olsson, Designing a new material world, Science 288 (5468) (1997) 993–998.
[15] K. Holmberg, A. Laukkanen Wear models, in: R. Bruce (ed.), Handbook on Lubrication and Tribology, Vol II Theory and Design (2nd ed.), vol. 13, 2012, pp. 1–21, CRC Press New York.
[16] K. Holmberg, A. Laukkanen, A. Ghabchi, M. Rombouts, E. Turunen, R. Waudby, T. Suhonen, K. Valtonen, E. Sarlin, Computational modelling based wear resistance analysis of thick composite coatings, Tribol. Int. 72 (2014) 13–30.
[17] K. Holmberg, A. Laukkanen, E. Turunen, T. Laitinen, Wear resistance optimisation of composite coatings by computational microstructural modelling and simulation, Surf. Coat. Technol. 247 (2014) 1–13.
[18] K. Holmberg, A. Laukkanen, H. Ronkainen, R. Waudby, G. Stachowiak, M. Wolski, P. Podsiadlo, M. Gee, J. Nunn, C. Gachot, L. Li, Topographical orientation effects on friction and wear in sliding DLC and steel contacts, Exp. Wear 330–331 (part 1) (2015) 3–22.
[19] K. Holmberg, A. Laukkanen, H. Ronkainen, K. Wallin, S. Varjus, A model for stresses, crack generation and fracture toughness calculation in scratched TiN-coated steel surfaces, Wear 254 (2003) 278–291.
[20] H. Ronkainen, A. Laukkanen, K. Holmberg, Friction in a coated surface deformed by a sliding sphere, WoM 2007 – Wear of Materials 16th International Conference, 15-19.4. 2007, Montreal, Canada.
[21] V. ProperTune, 23.6.2016. Available online: ⟨http://www.vttresearch.com/propertune⟩.
[22] F.P. Bowden, D. Tabor, The Friction and Lubrication of Solids, Oxford University Press, Oxford, UK, 1950.
[23] F.M. Borodich, A. Pepelyshev, O. Savencu, Statistical approaches to description of rough engineering surfaces at nano and microscales, Tribology International 103 (2016) 197–207.
[24] M. Kalin, A. Pogacnik, I. Etsion, B. Reaymaekers, Comparing surface topography parameters of rough surfaces obtained with spectral moments and deterministic methods, Tribology International 93 (2016) 137–141.
[25] J.A. Greewood, J.B.P. Williamson, Contact of nominally flat surfaces, Proc. R. Soc. Lond. A 295 (1966) 300–319.
[26] J. Halling, A contribution to the theory of mechanical wear, Wear 34 (1975) 239–249.
[27] J. Halling, Toward a Mechanical Wear Equation, J. Lubrication Technology, Trans. ASME 105 (1983) 212–219.
[28] M. Kalin, A. Pogacnik, Criteria and properties of the asperity peaks on 3D engineering surfaces, Wear 308 (2013) 95–104.
[29] S. Kucharski, G. Starzynski, Study of contact of rough surfaces: Modeling and experiment, Wear 311 (2014) 167–179.
[30] S. Reichert, B. Lorentz, S. Heldmaier, A. Albers, Wear simulation in non-lubricated and mixed lubricated contacts taking into account the microscale roughness, Tribology International 100 (2016) 272–279.
[31] V. Westlund, J. Heinrichs, M. Olsson, S. Jacobson, Investigation of material transfer in sliding friction-topography or surface chemistry? Tribology International 100 (2016) 213–223.
[32] C. Gachot, A. Rosenkratnz, L. Reinert, E. Ramos-Moore, N. Souza, M.H. Muser, F. Mucklich, Dry friction between laser-patterned surfaces: Role of alignment, structural wavelength and surface chemistry, Tribology Letters 49 (2013) 193–202.
[33] N. Prodanov, C. Gachot, A. Rosenkrantz, F. Mucklich, M.H. Muser, Contact mechanics of laser-textured surfaces – Correlating contact area and friction, Tribology Letters 50 (2013) 41–48.
[34] A. Rosenkrantz, L. Reinert, C. Gachot, F. Mucklich, Alignement and wear debris effects between laser-patterned steel surfaces under dry sliding conditions, Wear 318 (2014) 49–61.
[35] C. Cachot, A. Rosenkrantz, S.M. Hsu, H.L. Costa, A critical assessment of surface texturing for friction and wear improvement, Wear 372-373 (2017) 21–41.
[36] J. Jiang, R.D. Arnell, The effect of substrate surface roughness on the wear of DLC coatings, Wear 239 (2000) 1–9.
[37] Y. Xiao, W. Shi, Z. Han, J. Luo, L. Xu, Residual stress and its effect on failure in a DLC coating on a steel substrate with rough surfaces, Diamond and Related Materials 66 (2016) 23–35.
[38] I. Etsion, E. Sher, Improving fuel efficiency with laser surface textured piston rings, Tribology International 42 (2009) 542–547.
[39] I. Etsion, Modelling of surface texturing in hydrodynamic lubrication, Friction 1 (2013) 195–209.
[40] C. Wu, L. Zhang, S. Li, Z. Jiang, P. Qu, A unified method for characterizing multiple lubrication regimes involving plastic deformation of surface asperities, Tribology International 100 (2016) 70–83.

Tampereen teknillinen yliopisto
PL 527
33101 Tampere

Tampere University of Technology
P.O.B. 527
FI-33101 Tampere, Finland

ISBN 978-952-15-4257-2
ISSN 1459-2045